

UC Santa Cruz

UC Santa Cruz Electronic Theses and Dissertations

Title

Co-Binding Bis-Pocket Iron Porphyrins: Towards the Development of a CO Poisoning Antidote

Permalink

<https://escholarship.org/uc/item/3wb7b8cr>

Author

Droege, Daniel G

Publication Date

2023

Peer reviewed|Thesis/dissertation

UNIVERSITY OF CALIFORNIA
SANTA CRUZ

**CO-BINDING BIS-POCKET IRON PORPHYRINS: TOWARDS THE
DEVELOPMENT OF A CO POISONING ANTIDOTE**

A dissertation submitted in partial satisfaction
of the requirements for the degree of

DOCTOR OF PHILOSOPHY

in

CHEMISTRY

By

Daniel G. Droege

December 2023

The Dissertation of Daniel G. Droege is
approved:

Professor Timothy Johnstone, chair

Professor Pradip Mascharak

Professor Scott Lokey

Peter Biehl
Vice Provost and Dean of Graduate Studies

Copyright © by
Daniel G. Droege
2023

Table of Contents

	Page
Title Page	i
Copyright Notice	ii
Table of Contents	iii
List of Figures	vi
List of Schemes	x
List of Tables	xi
Abstract	xii
Dedication	xiv
Acknowledgments	xv
Chapter 1. Carbon Monoxide Poisoning and a Path Towards a Carbon Monoxide Poisoning Antidote	1
1.1 CO Poisoning	2
1.2 Iron Porphyrin Based CO Binding Molecules	4
1.3 Current Progress Towards a CO Poisoning Antidote	7
1.4 Synthesis of <i>meso</i> -Substituted Porphyrins	10
1.5 Conclusion	14
1.6 References	15

Chapter 2. Design and Synthesis of Water-Soluble Iron-Porphyrin Complexes Capable of Binding CO	19
2.1. Introduction	20
2.2. Results and Discussion	22
2.3. Conclusions	34
2.4. Experimental Methods	35
2.5. References	53
Chapter 3: Synthesis and Functionalization of <i>meso</i>-Aryl Bis-pocket Porphyrins	56
2.1. Introduction	57
2.2. Results and Discussion	59
2.3. Conclusions	77
2.4. Experimental Methods	77
2.5. References	98
Chapter 4. Derivatives of a Modular Water-Soluble Iron-Porphyrin Complex for the Sequestration of Carbon Monoxide	101
2.1. Introduction	102
2.2. Results and Discussion	103
2.3. Conclusions	117
2.4. Experimental Methods	118

2.5. References	138
Appendix A: Supplementary Experimental Data for Chapter 2	140
Appendix B: Supplementary Experimental Data for Chapter 3	153
Appendix C: Supplementary Experimental Data for Chapter 4	198
Bibliography	212

List of Figures

	Page
Chapter 1	
Figure 1.1. Routes of oxidation of an Fe(II) porphyrin with O ₂ .	4
Figure 1.2. Select heme model complexes.	5
Figure 1.3. Graphical representation of hemoglobin's O ₂ /CO binding site.	8
Figure 1.4. Structure of oxy-HemoCD1.	9
Figure 1.5. Numbering and nomenclature of porphine.	10
Figure 1.16. UV-vis spectra of 2.10 . Depicting the Soret band and Q-bands.	11
Figure 1.7. Cartoon representation of the HOMOs (a _{2u} , a _{1u}) and LUMOs (e _{gx} , e _{gy}) of free base porphyrins.	11
Figure 1.8. Adler method for TPP synthesis.	12
Figure 1.9. Lindsey method for TPP synthesis.	13
Figure 1.10. Functional groups that impart water solubility in porphyrins.	14
Chapter 2	
Figure 2.1. Collman's picket fence iron porphyrin and Suslick's bis-pocket porphyrin.	20
Figure 2.2. Proposed mechanism of CO scavenging from a red blood cell.	21
Figure 2.3. Electronic absorption spectra of 2.5 , reduced 2.5 , and 2.6 .	23
Figure 2.4. UV-vis of COHb-saturated RBCs treated with compound 2.5 .	24

Figure 2.5. Schematic overview of the proposed small-molecule for CO sequestration.	25
Figure 2.6. Unit cell contents of the crystal structure of 2.10 ·2MeCN.	27
Figure 2.7. Thermal ellipsoid plots of 2.11 ·DCM and the anion obtained upon slow recrystallization of 2.12 from DMSO/CHCl ₃ .	28
Figure 2.8. Reaction of 2.12 with CO under reducing conditions and electronic absorption spectra of 2.12 , reduced 2.12 , and 2.13 .	29
Figure 2.9. IR spectra of 2.12 and the precipitate from 2.13 and (PPh ₄)Cl.	30
Figure 2.10. Titration of bovine COHb with 2.12 in PBS.	31
Figure 2.11. Hemolysis by 2.12 or 1.5 M NH ₄ Cl.	32
Figure 2.12. Titration of CO-treated bovine RBCs with reduced 2.12 .	33
Figure 2.13. Decrease in COHb following addition of reduced 2.12 to CO-treated RBCs.	34
Figure 2.14. Stability of reduced 2.12 following exposure to air.	46
Figure 2.15. Stability of 2.13 in PBS (pH 7.4) containing 5.7 mM dithionite following exposure to air.	48
Figure 2.16. Ball-and-stick representation of 2.12 .	49
Figure 2.17. Titration of bovine COHb with 1 equiv Fe(II)TPPS.	50
Figure 2.18. Titration of Hb and reduced 2.12 with CO-saturated water.	51
 Chapter 3	
Figure 3.1. Examples of bis-pocket porphyrin syntheses.	58

Figure 3.2. Exploration of the scope of groups that can be coupled to the porphyrin framework according to the depicted reaction.	64
Figure 3.3. Metal insertion into bulky bis-pocket porphyrins.	68
Figure 3.4. Thermal ellipsoid plots of 3.4a , 3.4b , 3.4e , and 3.4f .	70
Figure 3.5. Sulfonation of bulky bis-pocket porphyrins and thermal ellipsoid plot of 3.3b .	73
Figure 3.6. Pockets of 3.2c , 3.2d , 3.2f , 3.2k , 3.2q , and 3.2i .	76
 Chapter 4	
Figure 4.1. Diagram of a SAR cycle.	102
Figure 4.2. Metalation of the target derivatives.	104
Figure 4.3. Sulfonation of the target derivatives.	105
Figure 4.4. Suzuki coupling with 4.1 and various boronic acids.	108
Figure 4.5. Metalation of sulfonated derivatives.	109
Figure 4.6. RT and approximate solubilities of target derivatives.	111
Figure 4.7. Electronic absorption spectra of Fe(III), Fe(II), and Fe(II)CO derivatives of 4.4h .	112
Figure 4.8. CO stretching frequencies for the Fe(II)CO species of each derivative.	114
Figure 4.9. Stability of the Fe(II)CO complex of 4.4c in PBS (pH 7.4).	115
Figure 4.10. Diagram of steric bulk inhibiting oxidation.	116
Figure 4.11. Titration of bovine COHb with 4.4h in PBS.	117

Appendix A	140
Figures A.1-A.18. NMR spectra.	141
Figure A.19. HPLC chromatogram of 2.12 .	150
Appendix B	
Figures B.1-B.48. NMR spectra.	154
Figures B.49-B.52. HPLC chromatograms.	178
Figures B.53-B.72. Thermal ellipsoid plots of crystal structures.	187
Appendix C	
Figures C.1-C.10. NMR spectra.	199
Figures C.11-C.17. Electronic absorption spectra.	204
Figures C.18-C.25. HPLC chromatograms.	207

List of Schemes

	Page
Chapter 2	
Scheme 2.1. Synthesis of 2.5 .	22
Scheme 2.2. Synthesis of reduced 2.5 and 2.6 .	23
Scheme 2.3. Synthesis of 2.12 .	26
Chapter 3	
Scheme 3.1. Overview of the coupling reaction.	58
Chapter 4	
Scheme 4.1. Sulfonation of 4.1 .	106
Scheme 4.2. Generation of the Fe(II)CO species.	112

List of Tables

	Page
Chapter 3	
Table 3.1. Optimization of Catalyst Loading for Coupling.	61
Table 3.2. Optimization of Coupling with PhB(OH) ₂ .	62
Appendix A	
Table A.1. Refinement Details for High-Resolution Crystal Structures.	151
Table A.2. Crystallographic Parameters for Low-Resolution Crystal Structure of 2.12 .	152
Appendix B	
Tables B.1-B.7. Crystallographic Refinement Details.	180
Table B.8. Pocket Volumes.	187

Abstract

CO-binding Bis-Pocket Iron Porphyrins: Towards the Development of a CO

Poisoning Antidote

By

Daniel G. Droege

A dissertation submitted in partial satisfaction of the requirements for the degree of

Doctor of Philosophy in Chemistry

Carbon monoxide (CO) poisoning results in over 50,000 emergency department visits every year in the US and is one of the most common forms of poisoning worldwide. Oxygen is still the accepted treatment for CO poisoning but, depending on the amount of CO inhaled and the time it takes to receive treatment, O₂ treatment may not be enough to prevent death or long-term damage. Despite the great need, there is no established antidote for CO poisoning. The toxicity of CO is derived from its interaction with diverse biological targets, and development of a treatment capable of addressing the myriad of symptoms that arise would be difficult. Instead, if the concentration of CO in the body can be lowered fast enough, the negative short-term and long-term effects of CO poisoning can be avoided. Presented here is the initial phase of the investigation of a novel *meso*-substituted porphyrin scaffold to discover an antidote for CO poisoning. The Lindsey method was used to generate an aryl *meso*-substituted porphyrin core. Arylaldehydes featuring a 2,6-substitution pattern permit modulation of the bulk of the CO binding pocket either early in the

synthesis or at a later stage via Pd-catalyzed $C_{aryl}-C_{aryl}$ coupling. Optimization of the coupling reaction was undertaken to facilitate derivatization. Installation of four sulfonate groups imparted water solubility at physiological pH and also inhibited membrane permeability. The modular nature of this scaffold allowed for the derivatization of multiple complexes. The solubility, CO binding ability, and oxidative stability of the complexes were investigated using UV-vis spectroscopy, IR spectroscopy, and X-ray crystallography. A preliminary demonstration of efficacy was performed using purified red blood cells (RBCs). A suspension of the cells was treated with sodium dithionite and then sparged with CO, generating carboxyhemoglobin (COHb). The COHb-containing RBCs were then washed with PBS and centrifuged to remove any excess dissolved CO. The COHb-containing RBCs were dosed with one of our iron(II) porphyrin compounds. UV-vis spectroscopy of the suspension confirmed the presence of the CO-bound form of the iron(II) porphyrin and the loss of CO from hemoglobin. Using the knowledge gained from the first set of derivatives of this scaffold, new complexes will be targeted. This work will prove useful in the rapid advancement of novel porphyrin derivatives to uncover a small molecule CO poisoning antidote.

To Amberly and Alora Droege

Acknowledgements

First and foremost, I acknowledge my research supervisor, Professor Timothy Johnstone. Upon entering graduate school, I made it my goal to step out of my comfort zone and join a research group that would force me to learn new skills and grow as a scientist. Tim welcomed me to his lab without hesitation, or so I like to think, where I was not only allowed to gain new skill sets, but also confidence in myself. Tim will forever remain one of the most influential people in my continued scientific growth and future research careers.

Thanks also goes out to all my fellow Johnstone Lab members and other friends from the chemistry department I met along the way. Through the ups and downs I knew I could rely on them to help me and always put a smile on my face.

I acknowledge the ARCS foundation for selecting me as an ARCS Scholar in 2021-2022 and awarding me a scholarship that allowed me to focus on my research.

Finally, I acknowledge the support of my family. Thanks to my parents for always supporting me and pushing me towards science. Thanks to my amazing wife Jess. Without her support and motivation, I would not have been able to pursue graduate school.

In my brief time at UCSC, I have been blessed with two daughters. Fortunately, Tim and the whole lab have been very supportive as my wife and I navigate this exciting new time in our lives. As a new family, balancing family time, work time, and teaching time, plus worrying about finances, has been challenging. However, even with all the challenges, my daughters have made my time at UCSC

even better. Their light on my life has doubled my commitment to excelling in my continued scientific growth and future research careers, not just for myself, but so I can be a good role model for them. To them I dedicate this Thesis.

Chapter 1

**Carbon Monoxide Poisoning and a Path Towards a Carbon Monoxide Poisoning
Antidote**

1.1 CO Poisoning

The toxic effects of gases released during combustion have been documented since the time of Aristotle.¹ It is now well established that the incomplete combustion of carbonaceous matter produces carbon monoxide (CO), but it is widely accepted that the first intentional synthesis of CO was conducted by Joseph Priestly in the 18th century. To synthesize CO, he heated chalk to produce CO₂, which was then passed over hot iron to generate CO.² While he successfully synthesized CO, its correct atomic formula was not uncovered until 1800 by William Cruickshank.³ It was not until the end of the 19th century that seminal work from Haldane showed CO to be the major source of toxicity from combustion gases.⁴ Experiments from Haldane and Douglas detailed the interaction of CO and oxygen (O₂) with hemoglobin (Hb) and the dissociation curves of both.⁵ These experiments showed that O₂ could be used to remove CO from carboxyhemoglobin (COHb), demonstrating the first treatment for CO poisoning. These results led Haldane to propose that the toxicity of CO stemmed from interruption of the O₂-binding ability of hemoglobin leading to hypoxemic hypoxia. Much of Haldane's work still holds true. However, many experiments have consistently shown that the toxicity of CO is the result of more than just hypoxemic hypoxia. For example, dogs given a transfusion of CO-treated blood suffer no ill effects, but dogs inhaling CO did.⁶

CO is produced endogenously primarily by heme oxygenase enzymatically catabolizing heme, and like nitric oxide (NO) and hydrogen sulfide (H₂S), CO is classified as a gasotransmitter. In mammals, unlike NO and H₂S, CO is not

metabolized, and is primarily removed via exhalation.⁷ The first experiments to confirm CO as a gasotransmitter were in 1987 where Brune and Ullrich demonstrated that CO could activate soluble guanylate cyclase, an important receptor for nitric oxide, which plays a part in vasorelaxation.⁸ Since then, CO has also been shown to be involved in the regulation of ion channels, cell proliferation, apoptosis, and anti-inflammatory effects.⁷

Due to an abundance of biological targets, CO has also been investigated for its therapeutic potential. To date, work on the preclinical efficacy of CO is extensive.⁹ The most common form of delivery of CO is inhalation or the administration of CO releasing molecules (CORMs). Both inhalation and CORMs have shown potential therapeutic benefits for decreasing graft and organ transplant rejection, anti-inflammation properties, and the ability to prevent organ failure during severe bacterial infection.⁹ CORMs have also been used in the targeted treatment of cancer.¹⁰⁻¹¹ Even with all the native biochemistry and medicinal potential, high doses of CO are unequivocally toxic. CO poisoning results in over 50,000 emergency department visits every year in the US and is one of the most common forms of poisoning worldwide.¹² High concentration of CO has shown to increase the formation of reactive oxygen species (ROS) in the brain, increase the amount of nitric oxide (NO) produced and released in blood, and affect regulated ion channels in both the heart and brain.⁵ All these interactions lead to several sequelae that cannot be treated with oxygen alone. Despite the great need, there is no established antidote for CO poisoning.

1.2 Iron Porphyrin Based CO Binding Molecules

Due to the biological relevance of iron porphyrins, much research has been devoted to the synthesis of model complexes that reproduce the reactivity of heme containing proteins, such as hemoglobin and cytochrome P450. Out of the many iron porphyrin complexes that have been synthesized and shown to bind CO, a select few will be described here as they are closely related to the work described in the following chapters. One challenge in synthesizing a model complex is designing a

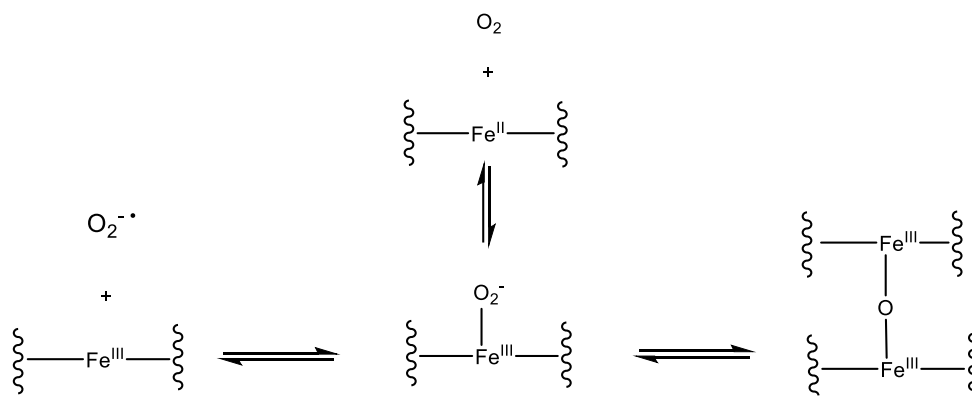


Figure 1.1. Routes of oxidation of an Fe(II) porphyrin with O_2 .

molecule that is not prone to oxidation (Figure 1.1). In the Fe(II) state, the electron-rich iron center readily binds O_2 and CO. Upon the binding of O_2 , the iron oxyporphyrin complex can interact with another Fe(II) porphyrin to generate a μ -oxo Fe(III) species that can no longer bind O_2 or CO. The Fe(II) species can also be oxidized to the Fe(III) complex via an autooxidation mechanism, in which superoxide can dissociate to give the oxidized Fe(III) complex (Figure 1.1 left). A common method to prevent this oxidation, and thereby more accurately model biology, is to add steric bulk to an iron porphyrin complex.

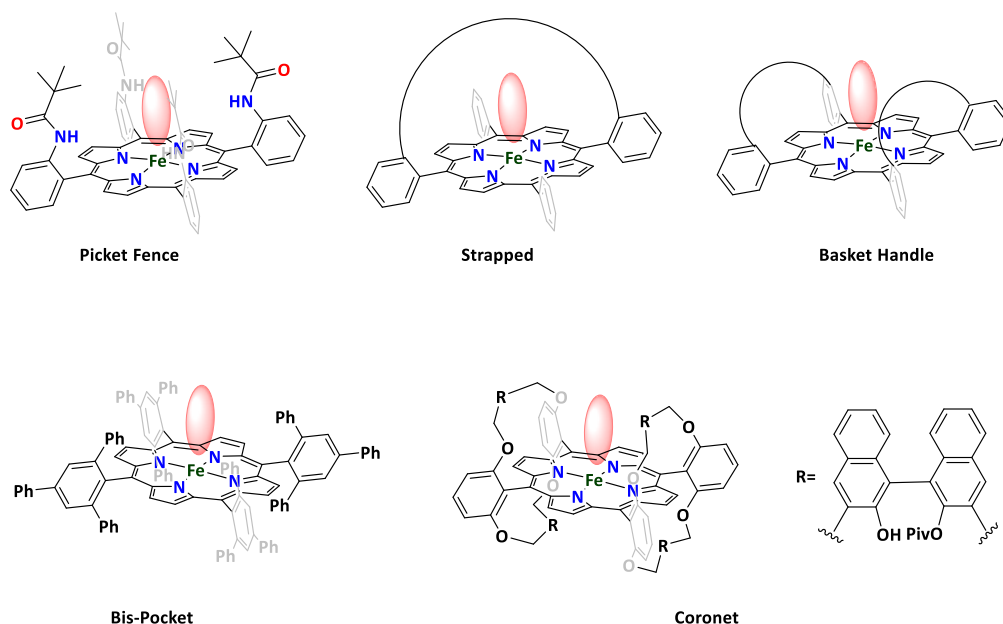


Figure 1.2. Select heme model complexes, red disk depicts CO binding pocket.

One of the seminal hemoglobin model complexes is Collman's *picket fence porphyrin*. Depicted in Figure 1.2, this compound relies on a pocket formed on one face of the porphyrin core. On the other face of the porphyrin there is usually a nitrogen containing heterocycle, such as imidazole, acting as an axial ligand (not depicted in the figure). Collman's picket fence porphyrin was one of the first hemoglobin model compounds to reversibly bind O_2 and it showed a strong affinity for CO.¹³ Stemming from the idea of creating a pocket on one face of a porphyrin, a multitude of research groups synthesized porphyrins with a fully enclosed pocket on one face. This type of structure was given the *capped porphyrin* moniker. Work from the Hoffman group demonstrated that the capped porphyrin also had a strong affinity for CO, greater than that of hemoglobin.¹⁴ By connecting opposing *meso* aryl rings with an alkyl chain, the so called *strapped porphyrin* has also demonstrated its

usefulness as a myoglobin model complex with an ability to bind O₂ and CO, while also being water soluble.¹⁵ By introducing a second “strap”, either one or two hydrophobic pockets can be created. This porphyrin, known as the *basket handle porphyrin* has also demonstrated the ability to bind O₂ and CO.¹⁶ Unfortunately the aforementioned model complexes require elaborate synthesis to maintain a pocket on one face of the porphyrin.

Expanding on the idea of creating pockets around the face of a porphyrin to mimic biology, the Suslick group created a porphyrin with mirroring pockets above and below of the porphyrin plane, describing it as a *bis-pocket porphyrin*. With this complex, Suslick demonstrated an increase in oxidative stability under normal atmospheric conditions and studied the effects of a non-polar pocket, solvent polarity, and axial ligand on the binding of CO.¹⁷ Despite having a more symmetric design, the yield of the bis-pocket porphyrin was still very low. In a similar vein, the Naruta group synthesized an iron porphyrin with a hydrophobic bis-pocket motif that was composed of binaphthalene bridges.¹⁸ They were able to decorate their bis-pocket architecture with alcohol groups pointed at the iron center to test the effect hydrogen bonding would play on the binding of O₂ and CO. These model complexes were synthesized to probe structurally and spectroscopically the binding of O₂ to heme containing proteins. The binding of CO was generally used for spectroscopic comparison since it is the more stable complex for these models.

Two more compounds, Ngb-H64Q-CCC and HemoCD, have also demonstrated the capability to bind CO.¹⁹⁻²⁰ These will be discussed in more detail in

the next section as they are currently being tested for their ability to act as CO poisoning antidotes.

1.3 Current Progress Towards a CO Poisoning Antidote

Currently, oxygen is the accepted treatment for CO poisoning. Generally, treatment consists of giving the patient O₂ via a nonrebreathing mask.²¹ COHb has a half-life of 320 min under normal atmospheric conditions and 71 min when breathing 100% O₂ at atmospheric pressure. If there is an O₂ hyperbaric chamber at the treatment facility, O₂ can be administered at 1.5 atm to reduce the half-life of COHb to 21 min.⁵ However, depending on the amount of CO inhaled and the time it takes to eliminate CO, O₂ treatment may not be enough to prevent casualty or long-term damage.²²

The toxicity of CO is derived from its interaction with diverse biological targets, and development of a treatment capable of addressing the myriad of symptoms that arise would be difficult. Instead, if the concentration of CO in the body can be lowered fast enough, the negative short-term and long-term effects of CO poisoning can be avoided.²¹ To quickly remove CO from the body, the ability of hemoglobin to bind CO needs to be overcome. Deoxyhemoglobin contains a high-spin Fe(II) porphyrin that can bind CO, a bonding interaction that is greatly stabilized through back-bonding generating a low-spin Fe(II)-CO complex. Model complexes of the hemoglobin binding site bind CO 1500 times stronger than O₂.²³ This discrepancy

in binding affinity arises from a distal histidine residue present in the binding site of hemoglobin. That histidine interferes with the ability of CO to bind to the iron in a linear fashion and lowers the binding affinity (Figure

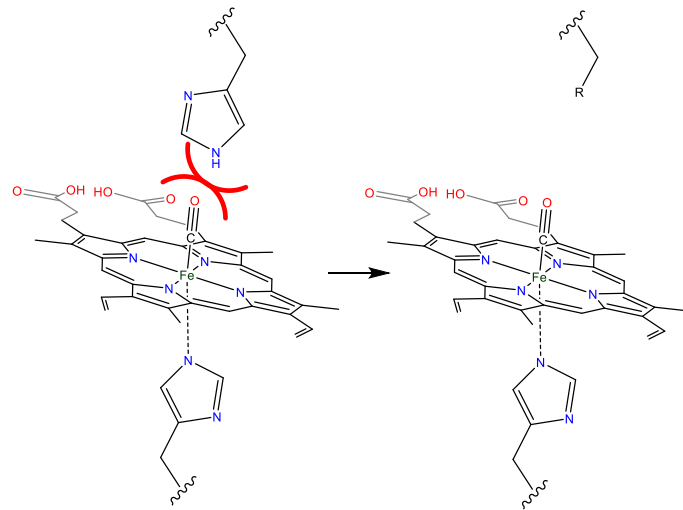


Figure 1.3. Graphical representation of hemoglobin's O₂/CO binding site. Red lines represent steric clash. Removal of the distal histidine gives more space for CO.

1.3). Researchers have begun to use this idea to synthesize mutated proteins and small molecule compounds that could act as CO poisoning antidotes.

One route currently being explored is using hemoprotein-based scavengers. The Gladwin group mutated human neuroglobin to replace histidine 64 with a glutamine residue and three surface thiol residues (C46G/C55S/C120S). This mutated neuroglobin (Ngb-H64Q-CCC) platform has demonstrated the potential to act as a CO poisoning antidote and the researchers have founded a company, Globin Solutions, to pursue the therapeutic potential of this protein. They have shown that their mutated protein has a picomolar affinity for CO and binds CO 300-400 times stronger than hemoglobin. To demonstrate its efficacy as an antidote, mice were subjected to a lethal dose of CO followed by an infusion of 250 mL of 9 to 12 mM Ngb-H64Q-CCC. Injection of the antidote resulted in a drop in the levels of COHb in

mice by 35% in 5 min, leading to an increase in survival. Ngb-H46Q-CCC led to 87% of the mice surviving whereas a control injection of phosphate buffered saline solution (PBS) resulted in only 10% of the mice surviving.²⁴

Another compound under current investigation as a CO poisoning antidote is

HemoCD from the

Kitagishi group. HemoCD

is a family of water-

soluble supramolecular

complexes of a sulfonated

iron porphyrin. One

specific example is

HemoCD1, which is encapsulated by two beta-cyclodextrins linked together by a

pyridine unit to act as an axial ligand for iron (Figure 1.4).²⁵ This compound has

demonstrated a picomolar affinity for CO, slow oxidation, and high selectivity for CO

over O₂. Their most recent work is on a system called *HemoCD-Twins*, which is a

mixture of HemoCD compounds that can sequester both CO and CN⁻. The CO is

bound by a HemoCD construct with Fe in the +2 oxidation state and CN⁻ is

sequestered by a different HemoCD construct with Fe in the +3 oxidation state. This

antidote was tested in mice and rats that had been poisoned with combustion gas. The

Kitagishi group demonstrated that a 200 μ L injection of a 14 mM solution of the

antidote mixture is almost completely excreted within 120 min as the CO bound

species. HemoCD Twins also shows an 80% survival rate for the rats poisoned with

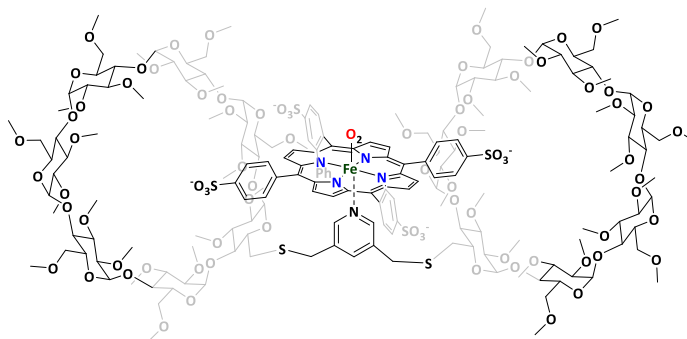


Figure 1.4. Structure of oxy-HemoCD1.

combustion gas, compared to 40% for the control group injected with saline. Also, preliminary safety of the molecule has been demonstrated by measuring biochemical makers that assess renal and liver function. Histological stains revealed no cytotoxicity, and this compound did not elicit any other toxic effects in healthy mice injected with a therapeutic dose.²⁶

1.4 Synthesis of *meso*-Substituted Porphyrins

Porphyrins hold an important role in biology and chemistry. Ubiquitous in nature, porphyrin-based cofactors play essential roles in photosynthetic light-harvesting, oxidative metabolism, and O₂ transport. Due to their biological and chemical importance, much work has gone into the isolation, characterization, and

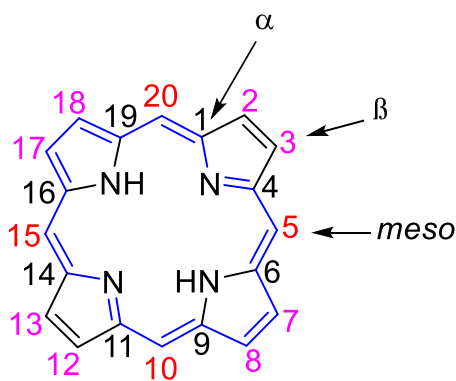


Figure 1.5. Numbering and nomenclature of porphine.

synthesis of both natural and synthetic porphyrins.²⁷ Porphyrins, or derivatives of porphine (Figure 1.5), are aromatic heterocyclic macrocycles that comprise four pyrroles attached together by methine bridges (Figure 1.5) and are vibrant purple in color. The methine bridges are numbered 5, 10, 15, 20 around the macrocycle and are also called the *meso* positions. Of the 22 π electrons, 18 are in conjugation and

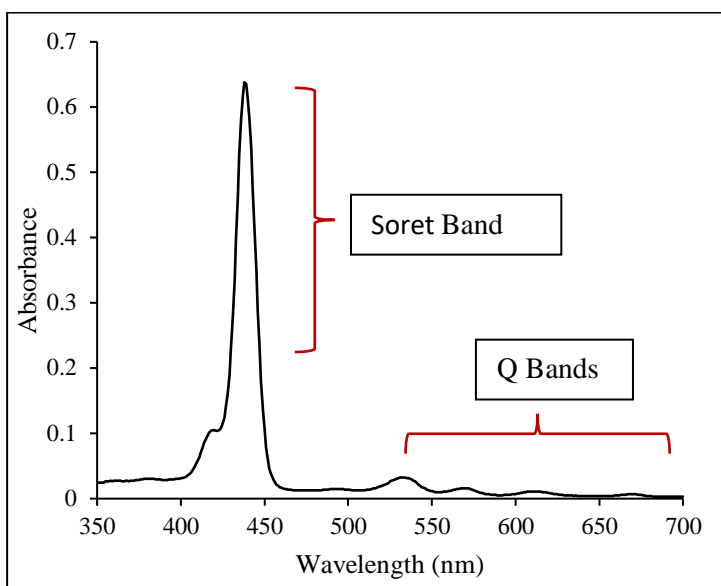


Figure 1.6. UV-vis spectra of **2.10**. Depicting the Soret band and Q-bands.

delocalized following Huckel's rule (Figure 1.5 in blue). This conjugation gives the porphyrin its intense color and very characteristic UV-vis spectrum (Figure 1.6). The characteristic absorption spectra of

porphyrins were first explained using the four-orbital model, two π -symmetry HOMOs and two π^* -symmetry LUMOs, by Martin Gouterman (Figure 1.7).²⁸ The general absorption spectra for porphyrins consists of two regions. There is a strong absorption band in the 300-500 nm range called the Soret band and a second region consisting of weaker absorption signals in the 500-750 nm range called Q bands (Figure 1.6). The number and relative intensities of these Q bands can provide information such as symmetry and substitution pattern around the porphyrin ring.

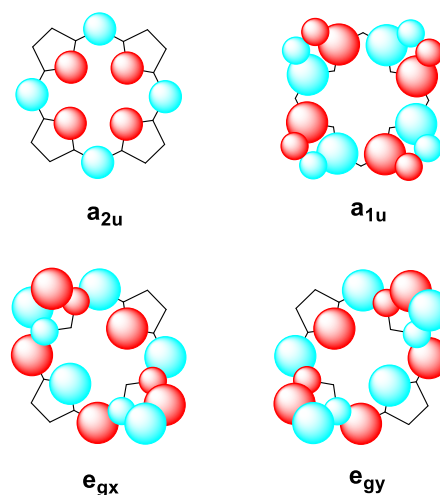


Figure 1.7. Cartoon representation of the HOMOs (a_{2u} , a_{1u}) and LUMOs (e_{gx} , e_{gy}) of free base porphyrins.

One of the first substituted synthetic porphyrins was the *meso*-substituted porphyrin with aryl

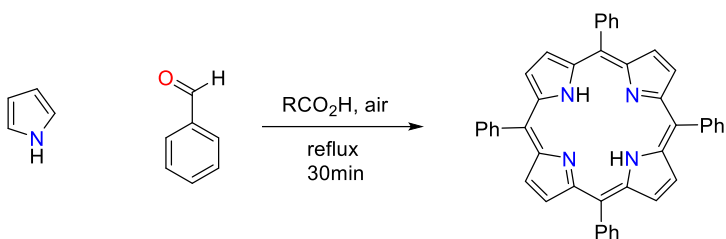
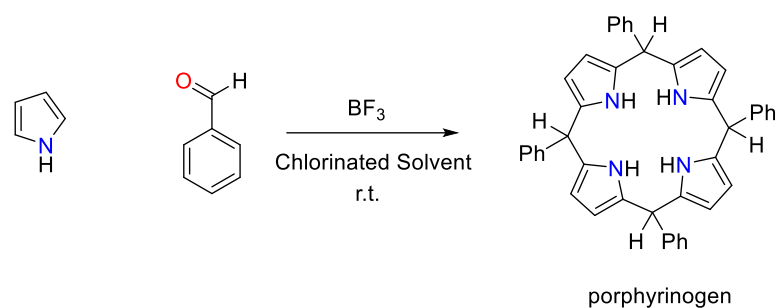


Figure 1.8. Adler method for TPP synthesis.

groups are attached to the 5, 10, 15, and 20 positions of porphine (Figure 1.5).

Rothmund first reported the synthesis of 5,10,15,20-tetraphenylporphyrin (TPP) by heating benzaldehyde and pyrrole at 150 °C for 24 h.²⁹ This method gave low yields, and the harsh conditions were not amenable for many aryl aldehydes. Following this work, Adler demonstrated that benzaldehyde and pyrrole could be refluxed in propionic acid open to air for 30 min to give TPP (Figure 1.8). This method gave higher yields, up to 30-40%, and allowed for a greater number of aryl aldehydes to be employed.³⁰ These porphyrin syntheses proceed via two steps. First the condensation of pyrrole and benzaldehyde to generate a porphyrinogen (Figure 1.9). Followed by in situ aerial oxidation to form the desired porphyrin. To further broaden the scope of *meso*-substituted porphyrins and provide mild reactions conditions, Lindsey separated the two steps and utilized a chemical oxidant to create a method that could be performed at room temperature. Pyrrole and an aryl aldehyde were condensed utilizing BF₃ as a Lewis acid to generate the corresponding porphyrinogen. This was performed under very dilute conditions to promote macrocyclization over linear polymerization. This intermediate could then be oxidized to the desired porphyrin using 2,3-dichloro-5,6-dicyano-1,4-benzoquinone (DDQ) Figure 1.9.³¹ This method

1. Condensation



2. Oxidation

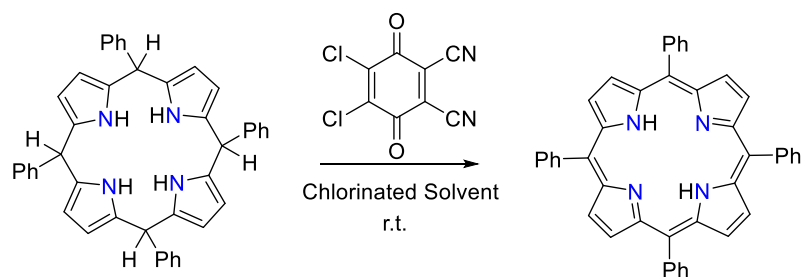


Figure 1.9. Lindsey method for TPP synthesis.

also proved useful in the synthesis of porphyrins utilizing sterically hindered aryl aldehydes, such as mesitaldehyde. These porphyrins tend to have low solubility, even in organic solvents. Chlorinated solvents like chloroform tend to give the best solubility for these porphyrins.

Because of the biological importance of porphyrins, their use as model compounds has been heavily explored. However, the *meso*-substituted porphyrins described above have minimal solubility in water. So, to create model compounds that can be studied in biologically relevant conditions, much research has been done to synthesize water-soluble synthetic porphyrins.³² The most common way to impart water solubility in synthetic porphyrins is via the incorporation of functional groups

that are charged at physiological pH, or to incorporate functional groups that contain enough polarity

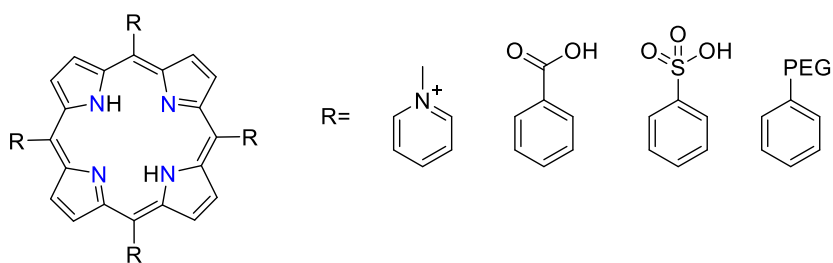


Figure 1.10. Functional groups that impart water solubility in porphyrins (PEG = polyethylene glycol).

and hydrogen bonding capacity to promote dissolution such as chains of polyethylene glycol (PEG) Examples of *meso* substituents included to achieve this goal are depicted in Figure 1.10.

1.5 Conclusion

CO poisoning affects many people yearly and there is an unmet need for a CO poisoning antidote. Recent research into CO scavengers has produced some promising possibilities for CO poisoning antidotes. However, the current compounds suffer from the requirement of large doses, biosynthesis of large-scale quantities, or lack of synthetic modularity to facilitate the drug discovery process. In the following chapters, the synthesis of a modular novel bis-pocket porphyrin and its ability to bind CO in a biologically relevant system will be explored. Chapter 2 will investigate the potential to use small molecule bis-pocket porphyrins as CO scavengers. This will progress into the investigation of a novel bis-pocket scaffold that demonstrates the ability to sequester CO from COHb. Chapter 3 will expand on the synthesis of the novel scaffold from Chapter 2 and investigate an improved synthesis and the scope of

derivatives this methodology can facilitate. Chapter 3 will also explore metalations of this scaffold and improve on the metalation from Chapter 2, as well as observe changes in structure due to subtle changes in the bis-pocket architecture. Finally, Chapter 4 will exploit the results of Chapters 2 and 3 to generate a small library of compounds to investigate as CO scavengers. The capability of these molecules to bind CO, as well as their solubility and oxidation stability, will be studied to determine if any trends arise across the derivatives. These are the first steps into providing the insight needed to design a molecule with this scaffold capable of acting as a CO poisoning antidote.

1.6 References

1. Varma, D. R.; Mulay, S.; Chemtob, S., Carbon Monoxide: From Public Health Risk to Painless Killer. In *Handbook of Toxicology of Chemical Warfare Agents*, **2009**; pp 271-292.
2. Priestley, J., XIX. Observations on different kinds of air. *Phil. Trans. R. Soc.* **1772**, *62*, 147-264.
3. Hopper, C. P.; Zambrana, P. N.; Goebel, U.; Wollborn, J., A brief history of carbon monoxide and its therapeutic origins. *Nitric Oxide* **2021**, *111-112*, 45-63.
4. Haldane, J., The Relation of the Action of Carbonic Oxide to Oxygen Tension. *J Physiol.* **1895**, *18*, 201-217.
5. Roderique, J. D.; Josef, C. S.; Feldman, M. J.; Spiess, B. D., A modern literature review of carbon monoxide poisoning theories, therapies, and potential targets for therapy advancement. *Toxicology* **2015**, *334*, 45-58.
6. Goldbaum, L. R.; Ramirez, R. G.; Absalon, K. B., What is the mechanism of carbon monoxide toxicity? *Aviat. Space. Environ. Med.* **1975**, *46*, 1289-91.

7. Untereiner, A. A.; Wu, L.; Wang, R., The Role of Carbon Monoxide as a Gasotransmitter in Cardiovascular and Metabolic Regulation. In *Gasotransmitters: Physiology and Pathophysiology*, **2012**; pp 37-70.
8. Brune, B.; Ullrich, V., Inhibition of platelet aggregation by carbon monoxide is mediated by activation of guanylate cyclase. *Mol. Pharmacol.* **1987**, *32*, 497-504.
9. Motterlini, R.; Otterbein, L. E., The therapeutic potential of carbon monoxide. *Nat. Rev. Drug Discov.* **2010**, *9*, 728-743.
10. Chakraborty, I.; Carrington, S. J.; Roseman, G.; Mascharak, P. K., Synthesis, Structures, and CO Release Capacity of a Family of Water-Soluble PhotoCORMs: Assessment of the Biocompatibility and Their Phototoxicity toward Human Breast Cancer Cells. *Inorg. Chem.* **2017**, *56*, 1534-1545.
11. Chakraborty, I.; Carrington, S. J.; Mascharak, P. K., Design Strategies To Improve the Sensitivity of Photoactive Metal Carbonyl Complexes (photoCORMs) to Visible Light and Their Potential as CO-Donors to Biological Targets. *Acc. Chem. Res.* **2014**, *47*, 2603-2611.
12. Sircar, K.; Clower, J.; Shin, M. k.; Bailey, C.; King, M.; Yip, F., Carbon monoxide poisoning deaths in the United States, 1999 to 2012. *Am. J. Emerg. Med.* **2015**, *33*, 1140-1145.
13. Collman, J. P.; Gagne, R. R.; Halbert, T. R.; Marchon, J.-C.; Reed, C. A., Reversible oxygen adduct formation in ferrous complexes derived from a "picket fence" porphyrin. A model for oxymyoglobin. *J. Am. Chem. Soc.* **1973**, *95*, 7868-7870.
14. Rose, E. J.; Venkatasubramanian, P. N.; Swartz, J. C.; Jones, R. D.; Basolo, F.; Hoffman, B. M., Carbon monoxide binding kinetics in "capped" porphyrin compounds. *Proc. Natl. Acad. Sci. U.S.A.* **1982**, *79*, 5742-5745.
15. Mao, Q.; Das, P. K.; Le Gac, S.; Boitrel, B.; Dorcet, V.; Oohora, K.; Hayashi, T.; Kitagishi, H., Functional Myoglobin Model Composed of a Strapped Porphyrin/Cyclodextrin Supramolecular Complex with an Overhanging COOH That Increases O₂/CO Binding Selectivity in Aqueous Solution. *Inorg. Chem.* **2021**, *60*, 12392-12404.
16. Momenteau, M.; Loock, B., 'Basket handle' porphyrins: new synthetic iron(II) complexes for oxygen binding. *J. Mol. Catal.* **1980**, *7*, 315-320.
17. Suslick, K. S.; Fox, M. M.; Reinert, T. R., Influences on carbon monoxide and dioxygen binding to iron(II) porphyrins. *J. Am. Chem. Soc.* **1984**, *106*, 4522-4525.

18. Matsu-ura, M.; Tani, F.; Naruta, Y., Formation and Characterization of Carbon Monoxide Adducts of Iron “Twin Coronet” Porphyrins. Extremely Low CO Affinity and a Strong Negative Polar Effect on Bound CO. *J. Am. Chem. Soc.* **2002**, *124*, 1941-1950.
19. Kano, K.; Kitagishi, H.; Kodera, M.; Hirota, S., Dioxygen Binding to a Simple Myoglobin Model in Aqueous Solution. *Angew. Chem., Int. Ed.* **2005**, *44*, 435-438.
20. Dewilde, S.; Kiger, L.; Burmester, T.; Hankeln, T.; Baudin-Creuzat, V.; Aerts, T.; Marden, M. C.; Caubergs, R.; Moens, L., Biochemical characterization and ligand binding properties of neuroglobin, a novel member of the globin family. *J. Biol. Chem.* **2001**, *276*, 38949-55.
21. Weaver, L. K., Clinical practice. Carbon monoxide poisoning. *N. Engl. J. Med.* **2009**, *360*, 1217-25.
22. Hampson, N. B.; Piantadosi, C. A.; Thom, S. R.; Weaver, L. K., Practice Recommendations in the Diagnosis, Management, and Prevention of Carbon Monoxide Poisoning. *Am. J. Respir. Crit. Care Med.* **2012**, *186*, 1095-1101.
23. Collman, J. P.; Brauman, J. I.; Doxsee, K. M., Carbon monoxide binding to iron porphyrins. *Proc. Natl. Acad. Sci. U.S.A.* **1979**, *76*, 6035-6039.
24. Azarov, I.; Wang, L.; Rose, J. J.; Xu, Q.; Huang, X. N.; Belanger, A.; Wang, Y.; Guo, L.; Liu, C.; Ucer, K. B.; McTiernan, C. F.; O'Donnell, C. P.; Shiva, S.; Tejero, J.; Kim-Shapiro, D. B.; Gladwin, M. T., Five-coordinate H64Q neuroglobin as a ligand-trap antidote for carbon monoxide poisoning. *Sci. Transl. Med.* **2016**, *8*, 368ra173.
25. Kitagishi, H.; Mao, Q.; Kitamura, N.; Kita, T., HemoCD as a Totally Synthetic Artificial Oxygen Carrier: Improvements in the Synthesis and O₂/CO Discrimination. *Artif. Organs* **2017**, *41*, 372-380.
26. Mao, Q.; Zhao, X.; Kiriyama, A.; Negi, S.; Fukuda, Y.; Yoshioka, H.; Kawaguchi, A. T.; Motterlini, R.; Foresti, R.; Kitagishi, H., A synthetic porphyrin as an effective dual antidote against carbon monoxide and cyanide poisoning. *Proc. Natl. Acad. Sci. U.S.A.* **2023**, *120*, 9.
27. Motterlini, R.; Foresti, R., Biological signaling by carbon monoxide and carbon monoxide-releasing molecules. *Am. J. Physiol.: Cell Physiol.* **2017**, *312*, C302-C313.
28. Gouterman, M., Study of the Effects of Substitution on the Absorption Spectra of Porphin. *J. Chem. Phys.* **1959**, *30*, 1139-1161.

29. Rothemund, P., Formation of Porphyrins from Pyrrole and Aldehydes. *J. Am. Chem. Soc.* **1935**, *57*, 2010-2011.
30. Adler, A. D.; Longo, F. R.; Finarelli, J. D.; Goldmacher, J.; Assour, J.; Korsakoff, L., A Simplified Synthesis for *meso*-Tetraphenylporphine. *J. Org. Chem.* **1967**, *32*, 476-476.
31. Lindsey, J. S.; Wagner, R. W., Investigation of the Synthesis of Ortho-Substituted Tetraphenylporphyrins. *J. Org. Chem.* **1989**, *54*, 828-836.
32. Pisarek, S.; Maximova, K.; Gryko, D., Strategies toward the synthesis of amphiphilic porphyrins. *Tetrahedron* **2014**, *70*, 6685-6715.

Chapter 2

Design and Synthesis of Water-Soluble Iron-Porphyrin Complexes Capable of

Binding CO

Published in part Droege, D. G.; Johnstone, T. C. *Chem. Commun.* **2022**, 58, 2722–
2725

2.1 Introduction

Porphyrins are a class of flat aromatic molecules that can be readily metalated to form iron porphyrin complexes. In the Fe(II) state, the electron-rich iron center in such complexes readily binds π -accepting ligands like O₂ and CO. The iron oxy porphyrin complex that results from the binding of O₂ can interact with another Fe(II) porphyrin to generate a μ -oxo Fe(III) species that can no longer bind O₂ or CO. In heme model complex work from Collman and Suslick, installation of steric bulk around the iron center inhibits this oxidation of the iron.¹⁻² Collman's picket fence porphyrin (Figure 2.1, left) was one of the first hemoglobin model compounds to reversibly bind O₂. However, the synthesis requires the separation of atropisomers leading to low yields and difficult purifications. The Fe(II) half-life of Suslick's bis-pocket porphyrin (Figure 2.1, right), which can be synthesized more readily, is more than 30 h at 25 °C in toluene with a P_{1/2}(O₂) (partial pressure of O₂ required to convert half of the complex to the O₂ bound form) value of 508 torr in toluene and a P_{1/2}(CO) of 0.0091 torr in toluene.³ This molecule also has a significantly stronger binding affinity for CO than hemoglobin, which has a P_{1/2}(CO) of 0.035 torr at pH 7 in water.⁴ As described in Chapter 1, this discrepancy in binding affinity is attributed to the distal histidine

residue in the binding pocket of hemoglobin.

This residue can engage in a hydrogen bonding

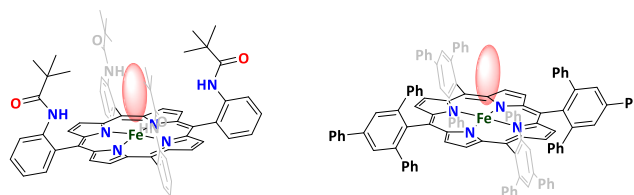


Figure 2.1. *Left:* Collman's picket fence iron porphyrin, red disk depicts CO binding pocket. *Right:* Suslick's bis-pocket porphyrin.

interaction with O₂ to stabilize the Fe-O₂ adduct. Its location in the pocket, however, also provides steric bulk that hinders the linear binding of CO. The hemoglobin model compounds do not have this histidine residue, so CO can bind to the iron without interference leading to a higher binding affinity. The bis-pocket porphyrin also binds CO stronger than hemoglobin because of the hydrophobic nature of its CO binding pocket, as demonstrated by the Suslick group using their bis-pocket porphyrin.³

Using the knowledge gained from previous heme model compounds, I targeted a sulfonated symmetrical bis-pocket porphyrin. The pockets would help prevent oxidation of the Fe(II) complex. Sulfonation of the complex would impart water solubility at physiological pH. This complex could then be tested against carboxyhemoglobin as a potential antidote for CO poisoning. If the complex has a CO affinity sufficiently greater than that of Hb, transfer will proceed as shown in Figure 2.2. It is noteworthy that this mechanism implies that the antidote does not need to pull the CO off of the metalated protein, nor does it need to enter into cells. The kinetic lability of the Fe complexes and membrane permeability of CO are exploited.

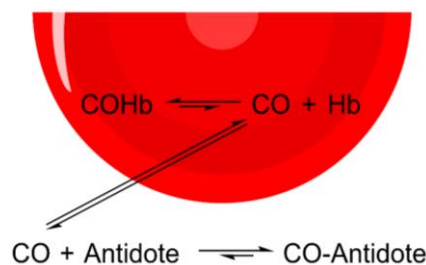


Figure 2.2. Proposed mechanism of CO scavenging from a red blood cell.

2.2 Results and Discussion

Initial Proof of Concept

As an initial target, a known water-soluble bis-pocket porphyrin was chosen to test if it could have the potential to be a CO poisoning antidote.

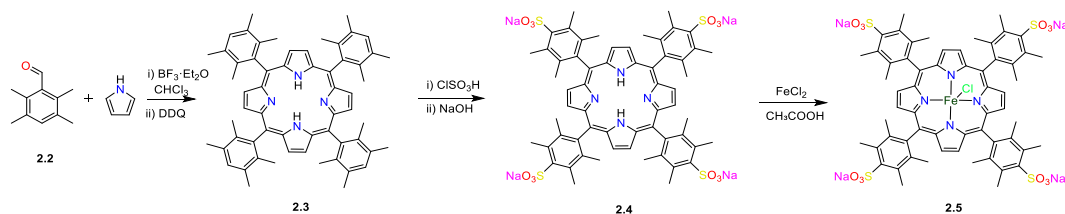
Synthesis of the known porphyrin followed literature precedent (Scheme 2.1).⁵

2,3,4,5-Tetramethylbenzaldehyde **2.2** was prepared from 2,3,4,5-

tetramethylbromobenzene via sequential reaction with *n*-BuLi and DMF. BF₃·OEt₂-catalyzed condensation of **2.2** and pyrrole proceeded readily to give the

tetradurylporphyrin **2.3**. Reaction of **2.3** with chlorosulfonic acid and subsequent hydrolysis with 3 M NaOH, gives the now water-soluble sulfonated porphyrin **2.4**.

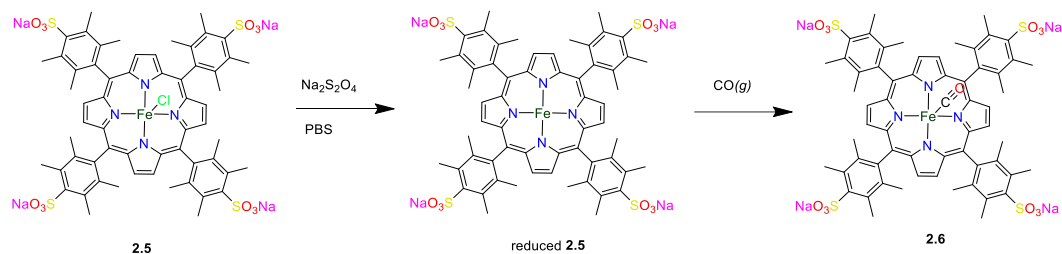
Refluxing **2.4** with ferrous chloride and sodium acetate in acetic acid gave the desired metalated porphyrin **2.5**.



Scheme 2.1. Synthesis of **2.5**.

The methyl substitution pattern was implemented to generate the bulk of the CO binding pocket (Scheme 2.2) and inhibit μ -oxo formation. The methyl groups at the *meta* positions of the *meso* substituents directed sulfonation, using chlorosulfonic acid, at the *para* position.⁵ Symmetrical substitution facilitated purification and characterization. Installation of four sulfonate groups imparted water solubility at physiological pH.⁶ The high negative charge was designed to inhibit membrane

permeability, which would ultimately help to ensure that the antidote remained in the blood stream rather than entering into cells.⁷



Scheme 2.2. Synthesis of reduced **2.5** and **2.6**.

To confirm that **2.5** could be reduced and bind CO, sodium dithionite was added to a solution of **2.5** ($\lambda_{\text{max}} = 417 \text{ nm}$ in PBS, pH 7.4), which reduced it to afford an Fe(II) complex (Figure 2.3). The Soret band red shifts to 429 nm upon reduction of **2.5** (Figure 2.3). A red shift in the Soret is consistent with literature reductions of iron porphyrins to an Fe(II) porphyrin.⁸ CO was added to solutions of reduced **2.5** to produce the CO adduct **2.6** (Figure 2.3). UV-vis of **2.6** shows a Soret band at 418 nm in PBS (Figure 2.3); this

blue shift is consistent with formation of an Fe(II)CO complex.⁸ Changes in the Q-band region of the spectrum also occurs as expected.

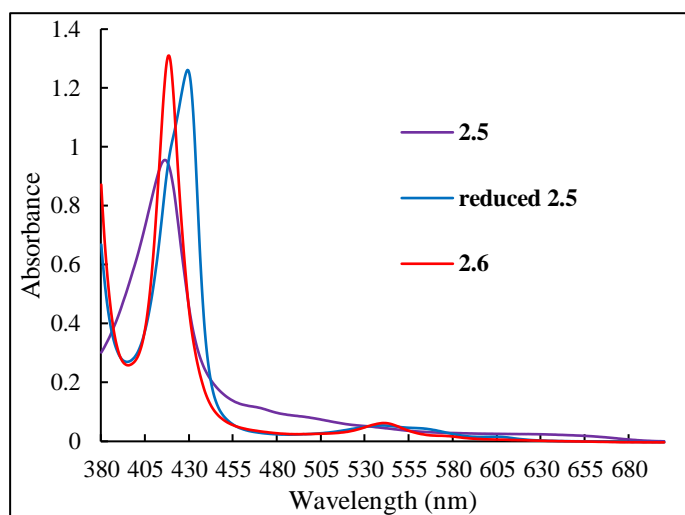


Figure 2.3. Electronic absorption spectra of **2.5**, reduced **2.5**, and **2.6**, 4 μM in PBS (pH 7.4).

Efficacy of the Duryl Derivative

To demonstrate the efficacy of this potential antidote, the ability of reduced **2.5** to extract CO from red blood cells was explored. Purified human red blood cells (RBCs) were treated with a 10 mM solution of sodium dithionite in PBS. The sodium dithionite reduced any methemoglobin (metHb) to deoxyhemoglobin, and any oxyhemoglobin was converted to COHb when CO was introduced. These conversions were monitored by UV-vis spectroscopy after lysing the cells. Bubbling CO through the solution generated COHb, determined by the generation of a Soret band at 419 nm, consistent with the literature.⁹ The COHb-containing RBCs were washed

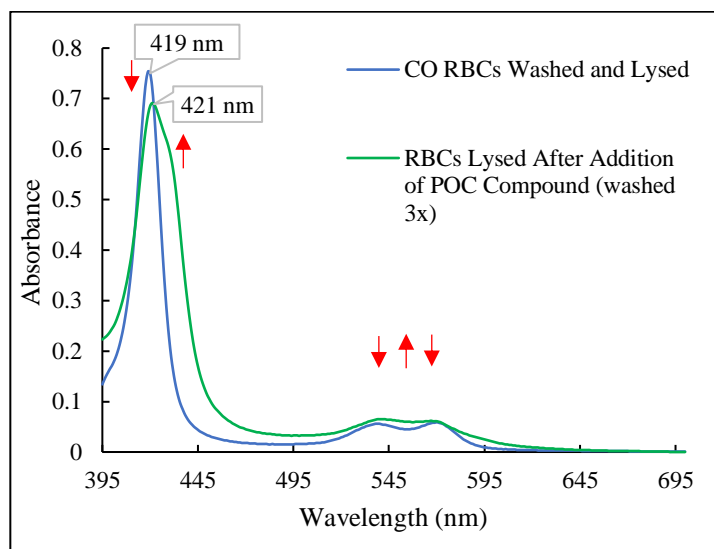


Figure 2.4. UV-vis spectrum of COHb (1 μ M) saturated RBCs treated with compound **2.5**. 0.25 equivalents of **2.5** calculated on a per heme basis.

with PBS and centrifuged to remove any excess dissolved CO. The COHb-containing RBCs were then dosed with reduced **2.5**. After letting the solution rest for 1 min, the RBCs were centrifuged. UV-vis spectroscopy of the supernatant confirmed the presence of Fe(II)CO porphyrin antidotes (**2.6**). The RBCs were washed three-fold with PBS and lysed. UV-vis of the

with PBS and centrifuged to remove any excess dissolved CO. The COHb-containing RBCs were then dosed with reduced **2.5**. After letting the solution rest for 1 min, the RBCs were centrifuged. UV-

lysate confirmed partial loss of CO from hemoglobin with a shift in the Soret band and a change in the number of Q-bands (Figure 2.4, red arrows highlighting changes).

These experiments demonstrated the ability of compounds like this to act like a CO poisoning antidote. However, this iteration had very limited stability. After reduction of **2.5** with sodium dithionite to generate the Fe(II) complex, the solution was opened to air. Once opened to air, this complex is oxidized to the Fe(III) complex within seconds as determined by UV-vis. This rate of oxidation is much too rapid for this compound to act as a CO antidote under biological conditions. As described next, to combat the rapid oxidation, I decided to add more bulk around the iron center. The bulkier pocket should help protect the iron from oxidation and create a hydrophobic pocket to increase the CO affinity.

Improved Antidote Platform Design

The design continued to be influenced by the work done by the Suslick group. I wanted to maintain a bis-pocket architecture but increase the bulk. Due to the redox stability of the bis-pocket porphyrin synthesized by the Suslick group, I modified our target compound's bis-pocket motif to also be comprised of phenyl groups. I envisioned the synthesis of an iron-porphyrin complex with 2,6-diphenyl-4-sulfophenyl *meso* substituents (Figure 2.5; R = Ph, Y = SO₃⁻). The *ortho*-phenyl groups will prevent μ -oxo dimer

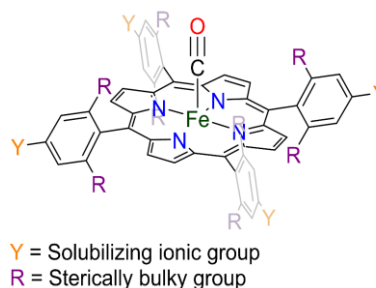
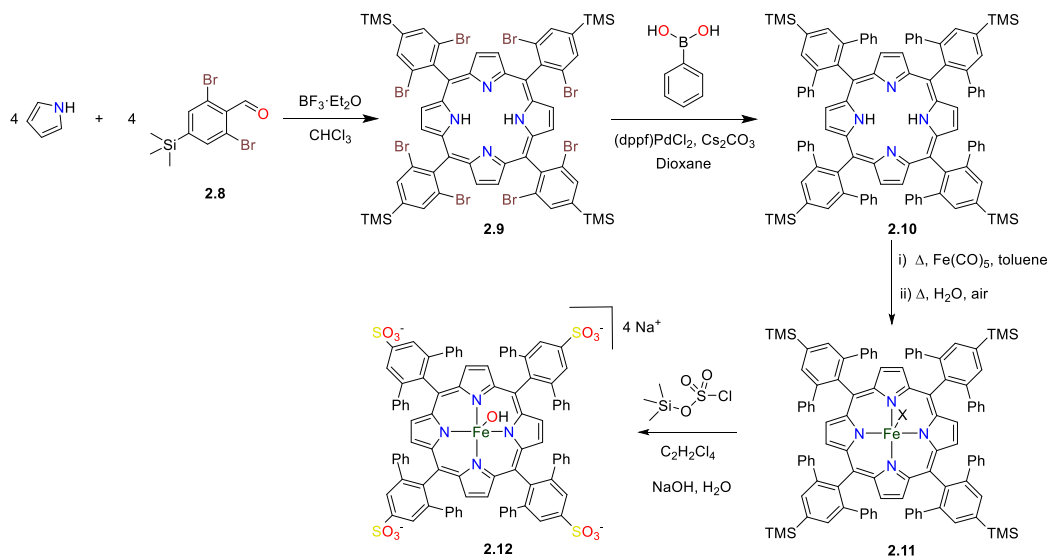


Figure 2.5. Schematic overview of the proposed small-molecule for CO sequestration.

formation, create a hydrophobic CO-binding pocket, and increase aerobic stability. The *para*-sulfonate groups will remain charged at physiological pH and ensure water solubility. The Suslik bis-pocket porphyrin with 2,4,6-triphenylphenyl *meso* substituents was previously accessed from pyrrole and 2,4,6-triphenylbenzaldehyde using a standard Adler synthesis, but macrocyclization was limited by the extreme steric congestion in the product; the final yield was 1%.² To avoid poor macrocyclization from steric bulk, I instead targeted 2,6-dibromophenyl-containing *meso* substituents (Scheme 2.3). The smaller bromines would allow for macrocyclization and permit the addition of steric bulk that can be incorporated via Pd-catalyzed cross-coupling reactions after macrocyclization. In the water solubilization step, I avoided the complications associated with harsh electrophilic aromatic sulfonation by incorporating a trimethylsilyl group that can undergo facile early or late-stage conversion to a sulfonyl chloride, which can then be hydrolyzed to a sulfonate.¹⁰



Scheme 2.3. Synthesis of **2.12**.

Synthesis

(3,5-Dibromophenyl)trimethylsilane (**2.7**) was prepared from 1,3,5-tribromobenzene via sequential reaction with *n*-BuLi and Me₃SiCl. Conversion to aldehyde **2.8** was achieved via deprotonation with LDA and carbonylation with DMF. BF₃·OEt₂-catalyzed condensation of **2.8** and pyrrole proceeded readily to give brominated porphyrin **2.9**, which is sparingly soluble in MeCN. Washing the crude product with MeCN until the filtrate is colorless afforded analytically pure material in 48% yield. Eight phenyl rings were installed on the porphyrin via Suzuki-Miyaura coupling in 20:1 1,4-dioxane/water using a three-fold excess of PhB(OH)₂ (per Ar–Br bond), Cs₂CO₃ as a base, and 12.5 mol% (1,1'-bis(diphenylphosphino)ferrocene)palladium(II) dichloride ((dppf)PdCl₂) (per Ar–Br bond). Silica gel chromatography afforded bulky porphyrin **2.10** as a deep purple solid in 86% yield. An X-ray

quality crystal was grown by layering MeCN over the product dissolved in chloroform. Single-crystal X-ray diffraction confirms the formation of the hydrophobic bis-pocket motif (Figure 2.6). The free base porphyrin was metalated by refluxing it with Fe(CO)₅ and a catalytic amount of I₂ in toluene

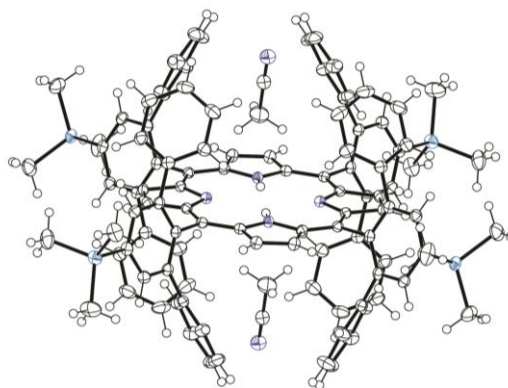


Figure 2.6. Unit cell contents (50% ellipsoids, H atoms as spheres of arbitrary radius) of the crystal structure of **2.10**·2MeCN. Disordered H atoms omitted for clarity. Color code: Si teal, N blue, C grey.

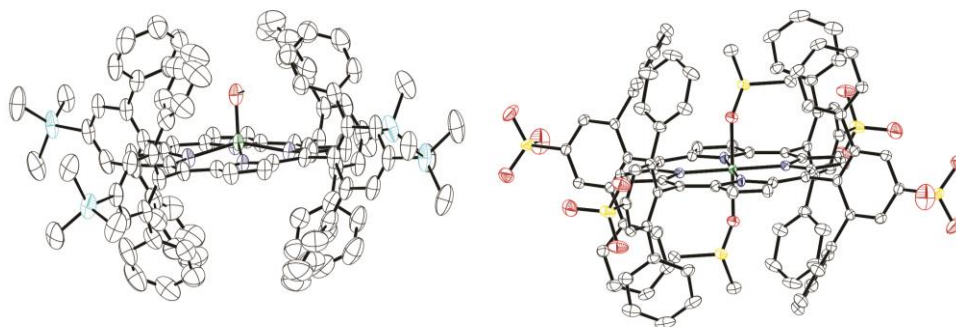


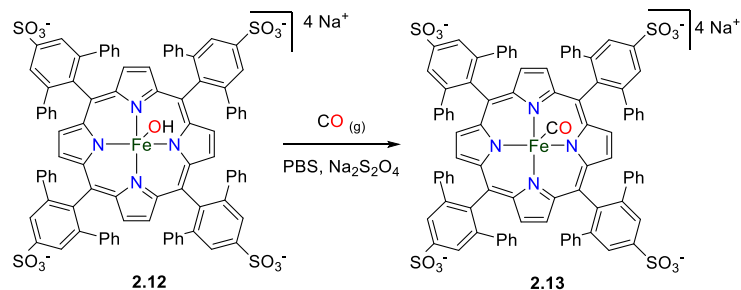
Figure 2.7. Thermal ellipsoid plots of **2.11**·DCM (50% ellipsoids, H atoms as spheres of arbitrary radius) and the anion obtained upon slow recrystallization of **2.12** from DMSO/CHCl₃. C-bound H atoms, solvent, and counterions omitted for clarity. Color code: Fe green, Si teal, O red, S yellow, N blue, C grey.

under N₂ for 4 h. This gave numerous iron porphyrin species, but an additional hour of reflux in open air followed by an alkaline aqueous work-up ensured oxidation to the Fe(III) state resulting in a green material. ¹H NMR spectroscopy in CDCl₃ showed broadened phenyl resonances appearing in the 15-20 ppm range and the β-pyrrole protons characteristically resonating at 82.16 ppm confirming that product **2.11** is paramagnetic.¹¹ Crystals of the reaction product grown from MeCN confirmed the proposed connectivity and the presence of an apical hydroxide ligand (Figure 2.7). Compound **2.11** was treated with Me₃SiOSO₂Cl in CCl₄ followed by hydrolysis with 1 M NaOH(aq). The intensely colored, now water soluble, porphyrin complex was extracted from the reaction mixture with water and subsequently purified by reverse-phase chromatography. The final tetrasodium salt **2.12** was isolated as a very dark purple solid in 40% yield. The purity of the product was established using analytical HPLC (Figure A.20). Weakly diffracting crystals confirmed the proposed connectivity, including the apical hydroxide ligand (Figure 2.16). High-quality

crystals were grown from DMSO/CHCl₃ permitted refinement that confirmed the proposed structure; however, an axial ligand substitution with the solvent took place. (Figure 2.7).

Reduction and CO binding of the New Derivative

Adding sodium dithionite to a solution of **2.12** ($\lambda_{\text{max}} = 431 \text{ nm}$ in PBS, pH 7.4) reduces the compound to afford an Fe(II) complex (Figure 2.8). The Soret band red



shifts to 448 nm upon reduction of **2.12** (Figure 2.8). A red shift in the Soret is

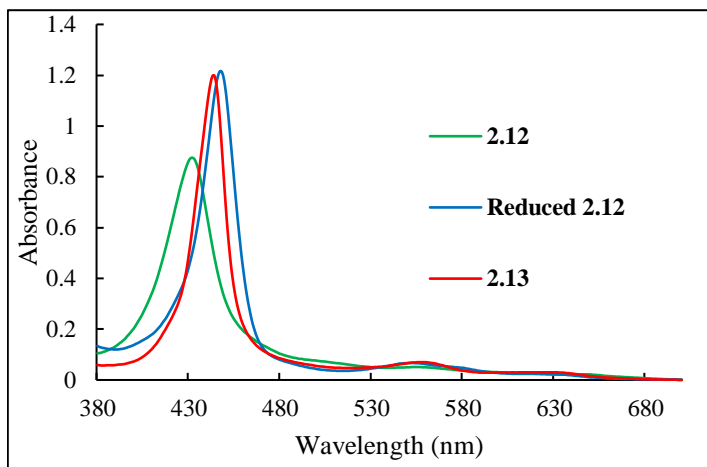


Figure 2.8. (Top) Reaction of **2.12** with CO under reducing conditions to produce **2.13**. (Bottom) Electronic absorption spectra of 10 μM solutions of **2.12**, reduced **2.12**, and **2.13** in PBS (pH 7.4). For reduced **2.12** and **2.13**, the solutions also contain 5.7 mM Na₂S₂O₄.

consistent with literature reductions of iron porphyrins to an Fe(II) porphyrin.⁸ *In situ* generated reduction product in deuterated PBS (PBS-*d*) gives a ¹H NMR spectrum that exhibits a signal at – 3.63 ppm, which I tentatively assign as the

β -pyrrole protons, and Evans' method measurements return a μ_{eff} of $3.69 \mu_{\text{B}}$ (Figure A.18). These data are consistent with the formation of a four-coordinate intermediate-spin ($S = 1$) Fe(II) complex.¹²⁻¹⁴ Solutions of the Fe(II) form of **2.12** in PBS containing excess $\text{Na}_2\text{S}_2\text{O}_4$, under a nitrogen atmosphere are stable for days. When the solutions are opened to air, the complex reverts to the Fe(III) complex **2.12** ($t_{1/2} \approx 30$ min) following aerial oxidation of the dithionite (Figure 2.14). CO can be added to solutions of reduced **2.12** to produce the CO adduct **2.13** (Figure 2.8). UV-

vis of **2.13** shows a Soret band at 444 nm in PBS (Figure 8); this blue shift is consistent with formation of an Fe(II)CO complex.⁸

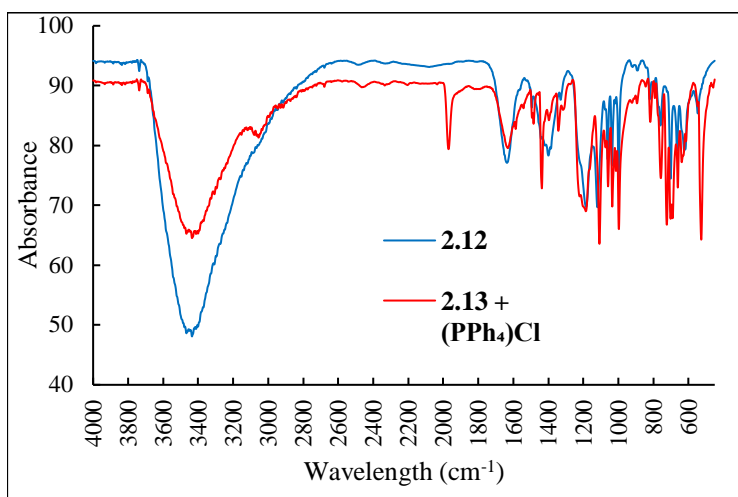


Figure 2.9. IR spectra (KBr pellet) of **2.12** and the precipitate formed from **2.13** and $(\text{PPh}_4)\text{Cl}$.

In PBS, solutions of **2.13** that have been

opened to air oxidize to **2.12** with $t_{1/2} \approx 120$ min (Figure 2.15). If the reduction of **2.12** under a CO atmosphere is performed in $\text{PBS-}d$, ^1H NMR spectroscopy shows **2.13** to be diamagnetic and Evans' method measurements return a μ_{eff} of $0 \mu_{\text{B}}$ (Figure A.19). Upon complexation of CO, the formation of a low-spin Fe(II) complex is expected, and these results are consistent with this electronic configuration. In order to obtain an IR spectrum of the CO bound species, tetraphenylphosphonium chloride was

added to a solution of **2.13** resulting in rapid precipitation of a red solid. IR spectroscopic analysis of this solid revealed a ν_{CO} of 1970 cm^{-1} (Figure 2.9). The higher value of ν_{CO} for **2.13** as compared to COHb (1951 cm^{-1})¹⁵ suggests that the small-molecule porphyrin complex will bind CO more strongly than Hb.¹⁶

Sequestration of CO from COHb

To test whether our compound could sequester CO from COHb, I titrated COHb with **2.12** in PBS under reducing conditions (5.7 mM $\text{Na}_2\text{S}_2\text{O}_4$). I observed

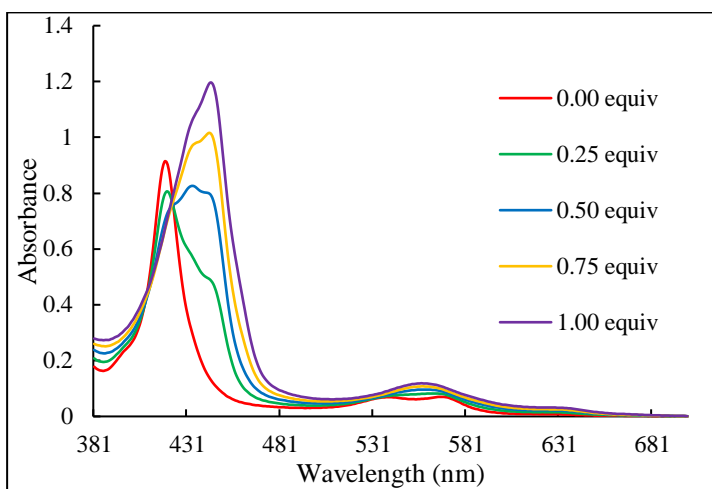


Figure 2.10. Titration of bovine COHb ($2.5 \mu\text{M}$) with **2.12** in PBS (pH 7.4, 5.7 mM $\text{Na}_2\text{S}_2\text{O}_4$).

clean transition from COHb to (deoxyHb + **2.13**) (Figure 2.10) with tight isobestic points, which demonstrated a rapid dose-dependent and stoichiometric transfer of CO to form **2.13** and

deoxyHb, which occurs between time of mixing and spectral acquisition. The apparent stoichiometric transfer of CO as aliquots are added indicates that the CO binding constant of reduced **2.12** is appreciably greater than that of Hb ($P_{1/2}(\text{CO}) < 0.004 \text{ torr}$).¹⁶ It is worth noting that performing the same experiment with 5,10,15,20-tetrakis(4-sulfonatophenyl)porphyrinatochloroiron(III), which has no

pocket motif, yielded no sequestration of CO (Figure 2.17). To further demonstrate the preference of CO binding of reduced **2.12** over COHb, I also titrated a solution of deoxyHb and **2.12** in 5.7 mM Na₂S₂O₄ with CO-saturated water. As aliquots of CO-saturated water were added, UV-Vis showed reduced **2.12** convert to **2.13** but the Soret band of deoxyHb was unchanged. Addition of more aliquots of CO results in conversion of deoxyHb to COHb (Figure 2.18). These experiments confirm that reduced **2.12** can bind CO preferentially in the presence of Hb and sequester CO from COHb.

Sequestration of CO from CO poisoned RBCs

The last experiment to show the capabilities of this proof-of-concept CO poisoning antidote, was to demonstrate its effectiveness with CO-poisoned RBCs.

First it was demonstrated that the compound does not lyse RBCs as compared to a

known lysing buffer of

NH₄Cl. As seen in Figure

2.11, no significant lysing

was observed over 15 min as

compared to suspensions of

RBCs treated with NH₄Cl,

which quickly became clear.

For the sequestration of CO,

I performed the

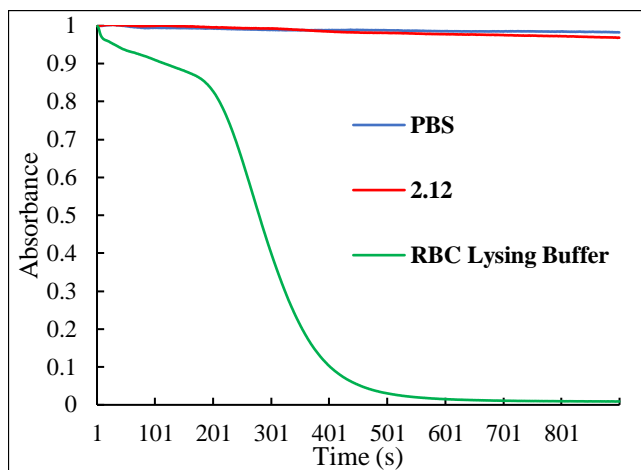


Figure 2.11. Hemolysis as assessed by measuring OD₇₀₀ over time of a suspension of RBCs in PBS (pH 7.4, 5.7 mM Na₂S₂O₄) containing no further additives, an equimolar (on the basis of porphyrin centers) amount of **2.12**, or 1.5 M NH₄Cl.

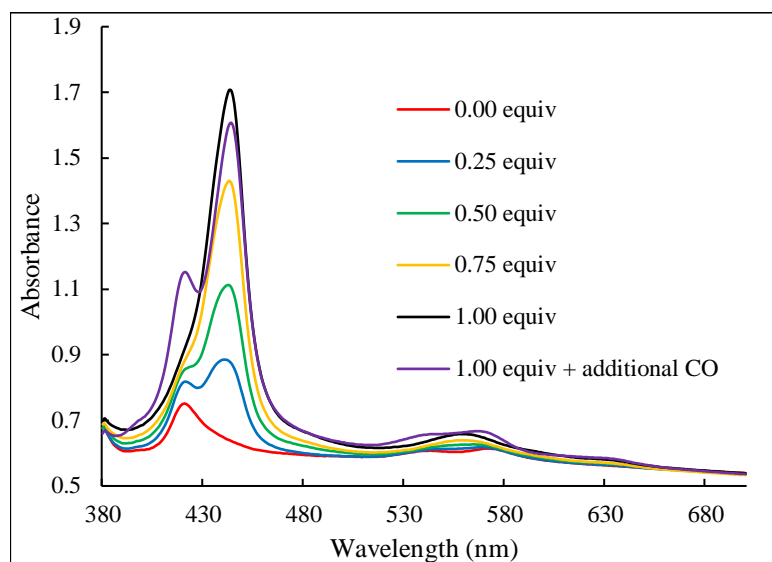


Figure 2.12. Titration of a PBS suspension (pH 7.4, 5.7 mM $\text{Na}_2\text{S}_2\text{O}_4$) of CO-treated bovine RBCs with **2.12** (reduced *in situ*). Final trace obtained after bubbling CO through the suspension treated with 1.00 equiv of **2.12**.

spectroscopic
 titrations directly
 on suspensions of
 CO-treated RBCs
 in PBS containing
 5.7 mM
 dithionite. Due to
 an inner filter
 effect, the
 intensity of the
 Soret band of

COHb ($\lambda_{\text{max}} = 420 \text{ nm}$) is decreased from the concentration-predicted absorbance. To accurately obtain concentrations of COHb, aliquots from a stock solution of CO poisoned RBCs were lysed. CO poisoned RBCs were then titrated with **2.12**, which is reduced *in situ*, this resulted in a dose-dependent decrease in the intensity of the COHb signal, and an increase of the signal for **2.13** ($\lambda_{\text{max}} = 444 \text{ nm}$) (Figure 2.12). To confirm that CO had indeed been abstracted from Hb and the Soret band was not just being obscured by **2.13**, additional CO was bubbled through the suspension of RBCs that had been treated with 1 equiv of **2.12**; the COHb signal was regenerated. To obtain an estimate of the rate of CO sequestration, I monitored absorbance at 420 nm

of a suspension of CO-poisoned RBCs in a buffered dithionite solution following addition of 1 equiv of **2.12**. After 3 min, no further change was observed at 420 nm, indicating that CO is removed from RBCs in less than 3 min, which is significantly faster than treatment with oxygen (Figure 2.13).

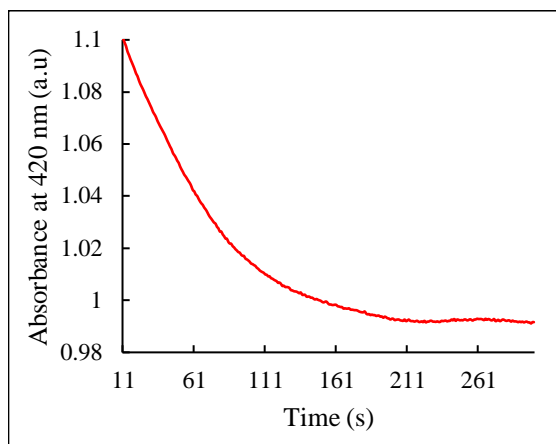


Figure 2.13. Decrease in COHb ($\lambda_{\max} = 420$ nm) over time following addition of reduced **2.12** to a PBS suspension (pH 7.4, 5.7 mM $\text{Na}_2\text{S}_2\text{O}_4$) of CO-treated RBCs at an equimolar amount on the basis of porphyrin centers.

2.3 Conclusions

In summary, I have shown that a simple water soluble *meso*-substituted porphyrin, **2.5**, can bind CO following *in situ* reduction. Reduced **2.5** also showed promise in the ability to remove CO from COHb. From this information, a novel small-molecule platform has been developed for CO sequestration that could have applications in the development of a CO-poisoning antidote. The synthesis of proof-of-principle compound **2.12** has demonstrated not only the viability of the synthetic strategy to access sterically encumbered bis-pocket porphyrin complexes, but the potential for rapid derivatization that this scaffold presents. Without damage to RBCs, reduced **2.12** was able to sequester CO from a solution of COHb and from CO poisoned RBCs. I hypothesize that the increased affinity of reduced **2.12** for CO as

compared to Hb comes from a combination of increased electron density at the metal center, increased hydrophobicity of the CO-binding pocket, and decreased steric hinderance to linear binding. Chapter 4 will explore the derivatives that can be readily accessed from **2.9** to test the relative importance of these factors. Chapter 4 will also investigate derivatives of **2.12** to uncover compounds with the greater stability, selectivity, and O₂ tolerance needed to function as CO-poisoning antidotes.

2.4 Experimental Methods

General considerations. All reactions were performed under N₂ unless otherwise stated. Glassware was oven dried prior to use. All solvents and reagents were commercially available and used as received unless stated otherwise. Pyrrole was distilled under N₂ and 1,3,5-tribromobenzene was purified by silica gel chromatography (eluted with hexanes). 5,10,15,20-Tetrakis(4-sulfonatophenyl)porphyrinatochloroiron(III), Fe(III)TPPS, was synthesized as previously reported.¹⁷⁻¹⁹ THF, diethyl ether, and chloroform were dried using 3-Å molecular sieves. For the purification of **2.12**, an Isolera Prime Biotage fitted with a Sfär C18 column was employed. Analytical HPLC was performed on a Shimadzu Prominence-I LC-2030 Plus fitted with a Shimadzu Nexcol C18 5 µm column (50 × 3.0 mm). CDCl₃ was purchased from Cambridge Isotope Laboratories and used as received. ¹H, ¹³C{¹H}, and ²⁹Si{¹H} NMR spectra were recorded on a Bruker Avance III HD 500 NMR spectrometer equipped with a multinuclear Smart Probe. Signals in the ¹H, ¹³C, and ²⁹Si NMR spectra are reported in ppm as chemical shifts from

tetramethylsilane and were referenced using the CHCl_3 (^1H , 7.26 ppm) or H_2O (^1H , 4.79 ppm) or CDCl_3 (^{13}C , 77.0 ppm) solvent signals or TMS in CDCl_3 (^{29}Si , 0.0 ppm). Deuterated phosphate-buffered saline (PBS-*d*) was obtained by lyophilizing an aliquot of proteo-PBS and redissolving the solid in an equivalent volume of D_2O . The following abbreviations were used to explain the multiplicities: s = singlet, d = doublet, t = triplet, q = quartet, m = multiplet. Glass background was removed from the ^{29}Si NMR spectra via backwards linear prediction of the first 100 points of the FID. UV-visible absorption spectra were measured on a Shimadzu UV-2401PC dual-beam spectrophotometer. IR spectra were recorded on a PerkinElmer Spectrum One FT-IR spectrometer. ESI mass spectra were obtained using a ThermoFisher LTQ Orbitrap Velos Pro. MALDI mass spectra were acquired using timsControl v 1.1.19 on a timsTOF fleX mass spectrometer (Bruker Scientific, Billerica, MA) over the mass range 100–2000 Da. In positive reflectron mode, laser power was set to 12%, and laser application was set to MS Dried Droplet. Compounds were dissolved in DCM and 1 μl was mixed with 1 μl of matrix (50:50 α -cyano-4-hydroxycinnamic acid: 2,5-dihydroxybenzoic acid in a solution of 70:30 ACN: H_2O with 0.1% trifluoroacetic acid). Samples were spotted on a stainless steel MSP 96 spot target plate and allowed to air dry. For each compound, 1000 laser shots at 2000 Hz were delivered in a random walk across the spot. Data were subsequently analyzed in DataAnalysis v 5.3 (Bruker Scientific, Billerica, MA). Elemental analysis was performed by Midwest Microlabs (Indianapolis, IN) using an Exeter CE440 analyzer. Melting point data were collected using an electrothermal Mel-Temp apparatus with a

Fluke 52 II thermocouple probe and temperatures are uncorrected. Solution phase magnetic moments were measured using a modified Evans method.²⁰

Synthesis of 2.2 2,3,5,6-methylbenzaldehyde. To a THF solution (25 mL) of 1-bromo-2,3,5,6-tetramethylbenzene (0.50g, 2.30 mmol) was added a hexane solution of n-butyllithium (2.5 M, 1.04 mL, 2.59 mmol) dropwise at -78°C. This mixture was stirred at -78 °C for 1 hour. To this was added dropwise a solution of DMF (11.8 mmol) at -78 °C. The mixture was stirred for 48 h, allowing the cold bath to come to room temperature. The reaction was quenched with 1M HCl and the product extracted with diethyl ether. The organic layer was dried with sodium sulfate and concentrated to give a crude pale yellow oil. The crude oil was purified by column chromatography (silica gel, hexanes:diethyl ether, 95:5) yielding 2,3,5,6-tetramethylbenzaldehyde as a clear colorless oil after concentration (155 mg, 40%).
¹H NMR (500 MHz, CDCl₃) δ 10.68 (s, 1H), 7.15 (s, 1H), 2.42 (s, 6H), 2.29 (s, 6H).

Synthesis of 2.3 5,10,15,20-tetrakis(2,3,5,6-tetramethylphenyl)porphyrin. A mixture of 2,3,5,6-methylbenzaldehyde (2.98 mmol) and pyrrole (2.98 mmol) dissolved in CHCl₃ (300 mL) and ethanol (2.2 mL) was placed into a 500 mL round bottom flask fitted with magnetic stirrer. The reaction mixture was flushed with nitrogen for 5 min followed by the addition of BF₃ etherate (0.98 mmol, 0.122 mL). The solution became yellow and slowly darkened to red and then to brown. After 1 h of stirring in the dark at room temperature, DDQ (2.98 mmol) was added in one

portion. This solution was allowed to stir for 30 min. The reaction was concentrated to dryness under reduced pressure. The crude product was filtered through a pad of silica gel with a solution of DCM:Hexanes (1:1). Yielding product **2.3** as a purple solid. This was recrystallized by layering ethanol over the product dissolved in CHCl₃ (101 mg, 16%). ¹H NMR (500 MHz, CDCl₃) δ 8.59 (s, 8H), 7.41 (s, 4H), 2.50 (s, 24H), 1.76 (s, 24H), -2.33 (s, 2H).

Synthesis of 2.4 Sodium 5,10,15,20-tetrakis(2,3,5,6-tetramethyl-4-(sulfonate)phenyl)porphyrin. Compound **2.3** (100 mg, 0.12 mmol) was dissolved in 6 mL of chlorosulfonic acid and stirred at room temperature for 1 hour. The mixture was added dropwise to ice (be careful, will splatter during quench) and extracted with chloroform. The organic layer was washed with a saturated sodium bicarbonate solution and a brine solution. This resulted in a dark purple solid after concentration (132 mg, 94.9%). The solid (115 mg, 0.09 mmol) was dissolved in water and refluxed overnight. The pH was made basic with 3 M NaOH and the solution was concentrated under reduced pressure. This was redissolved in methanol and passed through a pad of silica gel with methanol yielding a dark purple solid **2.4** after concentration (99 mg, 93%). ¹H NMR (500 MHz, DMSO-d₆) δ 8.52 (s, 8H), 2.75 (s, 24H), 1.68 (s, 24H), -2.45 (s, 2H).

Synthesis of 2.5 Sodium 5,10,15,20-tetrakis(2,3,5,6-tetramethyl-4-(sulfonate)phenyl)porphyrinatochloroiron(III). Compound **2.4** (90 mg, 0.076 mmol), sodium acetate (19 mg, 0.22 mmol), and FeCl₂ (45 mg, 0.22 mmol) were dissolved in acetic acid (25 mL) and stirred at reflux for 3 hours. The reaction mixture was concentrated under reduced pressure and purified by filtering through a pad of silica with methanol. After concentration, the resulting solid was dissolved in water and desalted via dialysis. Lyophilization yielded a fluffy brown/purple solid **2.5** (65 mg, 67%).

***In situ* reduction of 2.5.** For UV-vis characterization, compound **2.5** was dissolved in PBS and diluted to 4 μM. A minimal amount of sodium dithionite was added to effect reduction of **2.5**, which resulted in an immediate change in the electronic absorption spectrum.

***In situ* formation of 2.6.** For UV-vis characterization, compound **2.5** was dissolved in PBS. A minimal amount of sodium dithionite was added to effect reduction of **2.5**. CO was bubbled through for 5 s to generate compound **2.6**, which resulted in an immediate change in the electronic absorption spectrum.

Synthesis of 2.7 (3,5-dibromophenyl)trimethylsilane. A previously reported procedure was modified.²¹ 1,3,5-Tribromobenzene (13 g, 41.8 mmol) was dissolved in Et₂O (250 mL, 0.17 M) and sparged with N₂ for 10 min. This solution was cooled

to $-78\text{ }^{\circ}\text{C}$. *n*-BuLi (17.56 mL, 43.89 mmol) was added in a dropwise manner over 30 min using a syringe pump. The reaction was allowed to stir at $-78\text{ }^{\circ}\text{C}$ for an additional 30 min. Chlorotrimethylsilane (5.8 mL, 45.98 mmol) was added in a dropwise manner over 10 min. The solution was warmed to $0\text{ }^{\circ}\text{C}$ over approximately 20 min. The $0\text{ }^{\circ}\text{C}$ reaction mixture was filtered through a pad of silica, which was then washed with ether. The filtrates were combined and solvent was removed under reduced pressure to give crude (3,5-dibromophenyl)trimethylsilane as a yellow oil (12.457 g, 97% yield) that solidified upon standing at room temperature. This crude product was dissolved in hexanes and passed through a pad of silica. Solvent was removed from the eluent under reduced pressure to give an off-white solid (11.825 g, 93% yield). Recrystallization from cold ethanol afforded the pure product as colorless needles (9.925 g, 78% yield). ^1H NMR (500 MHz, CDCl_3) δ 7.66-7.62 (m, 1H), 7.51 (s, 2H), 0.27 (s, 9H); $^{13}\text{C}\{^1\text{H}\}$ NMR (126 MHz, CDCl_3) δ 146.19, 134.62, 134.32, 123.34, -1.21 ; $^{29}\text{Si}\{^1\text{H}\}$ NMR (99 MHz, CDCl_3) δ -2.16 ; Melting point: $41.2\text{ }^{\circ}\text{C}$; Anal. Calcd for $\text{C}_9\text{H}_{12}\text{Br}_2\text{Si}$: C, 35.09; H, 3.93. Found: C, 34.61; H, 3.65.

Synthesis of 2.8 2,6-dibromo-4-trimethylsilylbenzaldehyde. A procedure previously used to prepare aryl aldehydes was modified.²² (3,5-Dibromophenyl)trimethylsilane (7 g, 22.9 mmol) was dissolved in THF (225 mL, 0.1 M), cooled to $-78\text{ }^{\circ}\text{C}$, and sparged with N_2 for 10 min. Lithium diisopropylamide (2.0 M in THF/heptane/ethylbenzene, 45.8 mL, 91.8 mmol) was added in a dropwise manner over 30 min such that the reaction temperature, monitored with a

thermocouple probe, did not exceed $-75\text{ }^{\circ}\text{C}$. The reaction was stirred at this temperature for 1.5 h. DMF (7.9 mL, 103.28 mmol) was added in a dropwise manner and the reaction was stirred for an additional 1.5 h. Aqueous 1 M H_2SO_4 (100 mL) was added and the product was extracted with ether (100 mL). The organic layer was dried over sodium sulfate and filtered. The crude product was dry-loaded onto silica gel and purified by column chromatography (silica gel, hexanes:ether 95:5) yielding 2,6-dibromo-4-trimethylsilylbenzaldehyde as a pale-yellow oil that solidified while drying under vacuum (6.20 g, 80% yield). This crude product was then recrystallized from hot ethanol and the pale-yellow needles were collected by filtration. Two crops were collected (first crop 4.562 g, second crop 1.072 g, 73% combined yield). ^1H NMR (500 MHz, CDCl_3) δ 10.25 (s, 1H), 7.69 (s, 2H), 0.31 (s, 9H); $^{13}\text{C}\{^1\text{H}\}$ NMR (126 MHz, CDCl_3) δ 191.39, 150.50, 138.11, 132.71, 124.81, -1.41 ; Melting point: $89.8\text{ }^{\circ}\text{C}$; Anal. Calcd for $\text{C}_{10}\text{H}_{12}\text{Br}_2\text{OSi}$: C, 35.74; H, 3.60. Found: C, 35.28; H, 3.53.

Synthesis of 2.9 5,10,15,20-tetrakis(2,6-dibromo-4-

(trimethylsilyl)phenyl)porphyrin. A published procedure was modified.²³ A mixture of 2,6-dibromo-4-trimethylsilylbenzaldehyde (1.754 g, 5.22 mmol), and pyrrole (350 mg, 5.22 mmol) in CHCl_3 (350 mL) and EtOH (0.2 mL) was added to a 1 L oven-dried round bottom flask. The reaction mixture was sparged with N_2 for 20 min, followed by the addition of BF_3 etherate (185 mg, 1.3 mmol). The solution became yellow and slowly darkened to wine red. After stirring for 16 h in the dark at room temperature, DDQ (2.371 g, 10.4 mmol) was added in one portion, turning the

solution black. This solution was allowed to stir for 2 h. The crude mixture was filtered through a pad of silica gel, which was then washed with CHCl_3 . The combined filtrates yielded a purple solid after concentration under reduced pressure. This solid was washed with MeCN to give 5,10,15,20-tetrakis(2,6-dibromo-4-(trimethylsilyl)phenyl)porphyrin **2.9** as a purple solid after drying (957 mg, 48% yield). X-ray quality crystals were grown by layering MeCN over the product in CHCl_3 to give purple plates. ^1H NMR (500 MHz, CDCl_3) δ 8.65 (s, 8H), 8.09 (s, 8H), 0.53 (s, 36H), -2.42 (s, 2H); $^{13}\text{C}\{^1\text{H}\}$ NMR (126 MHz, CDCl_3) δ 146.06, 142.97, 136.01, 128.76, 118.76, -0.89; Melting point: >400 °C; Anal. Calcd for $\text{C}_{56}\text{H}_{54}\text{Br}_8\text{N}_4\text{Si}_4$: C, 43.83; H, 3.55; N, 3.65. Found: C, 43.36; H, 3.52; N, 3.60; UV/Vis (CHCl_3) λ_{abs} (log ϵ): 406 (sh), 424 (4.64), 518 (3.35), 593 (2.86).

Synthesis of 2.10 5,10,15,20-tetrakis(2,6-diphenyl-4-

(trimethylsilyl)phenyl)porphyrin. Compound **2.9** (300 mg, 0.1967 mmol), (dppf) PdCl_2 (144 mg, 0.1967 mmol), phenylboronic acid (576 mg, 4.7213 mmol), and Cs_2CO_3 (2.061 g, 6.251 mmol) were dissolved in a mixture of dioxane (20 mL) and H_2O (1 mL). The solution was sparged with N_2 for 5 min. The reaction was sealed with a septum and stirred at 100 °C for 14 h. The crude reaction mixture was stripped of solvent under reduced pressure, taken up in CHCl_3 (50 mL) and passed through a pad of silica gel. The filtrate was dried to give a purple solid that was washed with MeCN. The washed solid was dissolved in CHCl_3 , dry loaded onto silica gel, and purified by column chromatography (silica, hexanes: CHCl_3 1:1). The eluted

product was concentrated to give **2.10** as a purple solid (256 mg, 86% yield). X-ray quality purple plates were grown by layering MeCN over the product in CHCl₃. ¹H NMR (500 MHz, CDCl₃) δ 8.38 (s, 8H), 7.77 (s, 8H), 6.56 (d, J = 7.7 Hz, 16H), 6.40 (t, J = 7.2 Hz, 8H), 6.22 (t, J = 7.4 Hz, 16H), 0.51 (s, 36H), -3.40 (s, 2H); ¹³C{¹H} NMR (126 MHz, CDCl₃) δ 144.80, 142.44, 140.75, 139.39, 133.66, 129.44, 126.67, 125.22, 116.12, -0.62; ²⁹Si{¹H} NMR (99 MHz, CDCl₃) δ -3.44; Melting point: >400 °C; HRMS (MALDI) *m/z*: [M+H]⁺ Calcd for C₁₀₄H₉₅N₄Si₄⁺ 1512.6662; Found 1512.6650; UV/Vis (CHCl₃) λ_{abs} (log ε): 419 (sh), 439 (4.54), 495 (2.62), 533 (3.17), 570 (2.93), 610 (2.79), 670 nm (2.34).

Synthesis of 2.11 5,10,15,20-tetrakis(2,6-diphenyl-4-

(trimethylsilyl)phenyl)porphyrinatohydroxoiron(III). A procedure previously used for inserting iron into sterically hindered porphyrins was modified.² Compound **2.10** (200 mg, 0.1325 mmol), Fe(CO)₅ (2.589 g, 13.2 mmol, 1.786 mL), and I₂ (101 mg, 0.397 mmol) were dissolved in toluene (30 mL) and refluxed for 5 h under N₂. This solution was then refluxed another 1 h under ambient conditions. The solution was concentrated under reduced pressure, taken up in CHCl₃ and filtered through a pad of Celite. The filtrate was washed with 1 M NaOH_(aq). The organic layer was dried with anhydrous sodium sulfate, filtered, and concentrated under reduced pressure to give **2.11** as a green solid (183 mg, 88% yield). X-ray quality dark purple plates were grown by layering MeCN over a solution of the product in CHCl₃. ¹H NMR (500 MHz, CDCl₃; paramagnetic) δ 82.16 (β-pyrrole); Melting point: >400 °C;

HRMS (MALDI) m/z : $[M-OH]^+$ Calcd for $C_{104}H_{92}FeN_4Si_4^+$ 1565.5777; Found 1565.5786. $[M+H]^+$ Calcd for $C_{104}H_{94}FeN_4OSi_4^+$ 1583.5883; Found 1583.5887; UV/Vis ($CHCl_3$) λ_{abs} ($\log \epsilon$): 360 (sh), 379 (4.52), 443 (5.14), 524 (4.07), 596 (sh); μ_{eff} (Evans', $CDCl_3$): 5.49 μ_B ; Anal. Calcd for $C_{104}H_{93}FeN_4OSi_4 \cdot CH_2Cl_2 \cdot C_2H_3N$: C, 75.20; H, 5.78; N, 4.10. Found: C, 74.95; H, 5.70; N, 3.97, Solvents added to the calculated elemental analysis are corroborated by the diffraction data. See Table A.1.

Synthesis of 2.12 Sodium 5,10,15,20-tetrakis(2,6-diphenyl-4-(sulfonate)phenyl)-porphyrinatohydroxoiron(III). A procedure previously used to convert aryl TMS groups into chlorosulfonates was modified.¹⁰ Compound **2.11** (50 mg, 0.0316 mmol) was dissolved in CCl_4 (4 mL). To this solution was added trimethylsilyl chlorosulfonate (72 mg, 0.38 mmol, 0.058 mL). The solution was stirred at reflux for 60 min under N_2 . After cooling to room temperature, 1 M $NaOH_{(aq)}$ (5 mL) was added and the reaction was stirred vigorously for 10 min. This solution was diluted with DI water (50 mL), washed with chloroform (50 mL), and stripped of solvent under reduced pressure. The resulting green solid was dry-loaded onto C18-functionalized silica gel and eluted across 25 g of stationary phase (6.35 cm) with a gradient of $H_2O/MeCN$ containing 0.01% TFA (5-95% MeCN over 15 min). The first colored fraction was collected and dialyzed against DI water for 3 d (changing dialysate every 12 h). The retentate was lyophilized yielding the tetrasodium salt **2.12** as a dark purple/black solid (22 mg 40% yield). Weakly diffracting crystals of **2.12** were grown from $CHCl_3/DMSO$. Higher-quality crystals (**2.12**_{DMSO}) were grown slowly by slowly

layering CHCl_3 over the product in DMSO. ^1H NMR (500 MHz, $\text{PBS-}d$, 10% $^t\text{BuOH}$; paramagnetic) δ 78.65 (β -pyrrole); HRMS (ESI) m/z : $[\text{M}-4\text{Na}-\text{OH}+\text{H}]^{3-}$ Calcd for $\text{C}_{92}\text{H}_{57}\text{FeN}_4\text{O}_{12}\text{S}_4^{3-}$ 531.0740; Found 531.0711. $[\text{M}-3\text{Na}-\text{OH}+\text{H}]^{2-}$ Calcd for $\text{C}_{92}\text{H}_{57}\text{FeN}_4\text{NaO}_{12}\text{S}_4^{2-}$ 808.1057; Found 808.1004. $[\text{M}-4\text{Na}-\text{OH}+\text{H}+\text{MeOH}]^{3-}$ Calcd for $\text{C}_{93}\text{H}_{61}\text{FeN}_4\text{O}_{13}\text{S}_4^{3-}$ 541.7494; Found 541.7454. $[\text{M}-\text{OH}-4\text{Na}]^{4-}$ Calcd for $\text{C}_{92}\text{H}_{56}\text{FeN}_4\text{O}_{12}\text{S}_4^{4-}$ 398.3046; Found 398.3028; HPLC ($\text{H}_2\text{O}/\text{MeCN}$): $t_r = 1.10$ min; UV/Vis (PBS) λ_{abs} ($\log \epsilon$): 333 (3.19), 431 (3.82), 509 (sh), 545 (sh); μ_{eff} (Evans', $\text{PBS-}d$): 5.22 μB .

***In situ* reduction of 2.12.** For NMR spectroscopic characterization, compound **2.12** (6 mg) was dissolved in $\text{PBS-}d$ (1.5 mL) containing 10% $^t\text{BuOH}$. The alcohol was included for the Evans' Method μ_{eff} determination. The alcohol also increases the solubility of the compound allowing highly concentrated solutions to be used to compensate for the decrease in the signal-to-noise ratio from paramagnetic broadening. Attempts to run the NMR reaction at equivalent concentrations in the absence of the $^t\text{BuOH}$ resulted in precipitation over the course of minutes. The same situation held for the following reaction with CO. Note that the UV-vis experiments (*vide infra*), which are performed at lower concentrations, confirm that this and the subsequent reaction proceed without the added $^t\text{BuOH}$. The solution was sparged with N_2 for 5 min and an ^1H NMR spectrum was acquired (Figure A.17). Sodium dithionite (1 mg) was added and an ^1H NMR spectrum was acquired (Figure A.18).

^1H NMR (500 MHz, $\text{PBS-}d$, 10% $^t\text{BuOH}$; paramagnetic) δ -3.63 (β -pyrrole)¹²; μ_{eff} (Evans', $\text{PBS-}d$, 10% $^t\text{BuOH}$): $3.69 \mu_{\text{B}}$.

For UV-vis characterization, compound **2.12** was dissolved in PBS and diluted to 0.02 mM. A minimal amount of sodium dithionite was added to effect

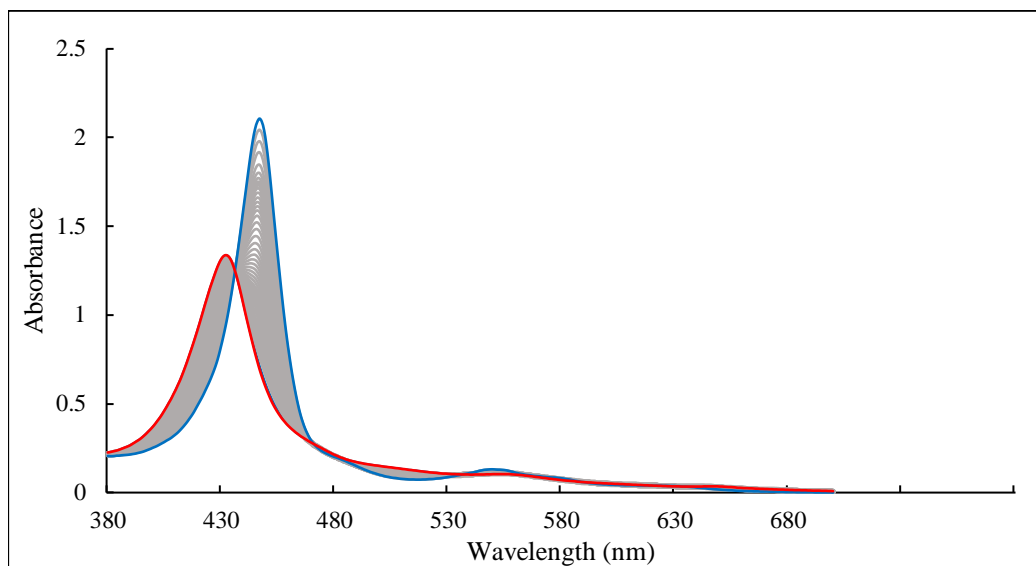


Figure 2.14. Stability of reduced **2.12** in PBS (pH 7.4) containing 5.7 mM dithionite following exposure to air. Spectra were acquired at 90 s intervals once dithionite consumption was complete.

reduction of **2.12**, which resulted in an immediate change in the electronic absorption spectrum. UV/Vis (PBS) λ_{abs} ($\log \epsilon$): 448 (5.08), 551 (3.81), 578 (sh), 625 (3.38). Air was bubbled through the solution to remove any excess sodium dithionite as assessed by reduction in intensity of the absorption at 315 nm. Once all of the dithionite had been consumed, the quiescent solution was left open to air and electronic absorption spectra were acquired at 90 s intervals (Figure 2.14).

***In situ* formation of 2.13.** For NMR spectroscopic characterization, compound **2.12** (6 mg) was dissolved in PBS-*d* containing 10% ¹BuOH (1.5 mL). The solution was sparged with N₂ for 5 min and sodium dithionite (1 mg) was added to the NMR tube. Then, CO was bubbled through the solution for approximately 5 s. The NMR tube was sealed and an ¹H NMR spectrum was acquired (Figure A.19). ¹H NMR (500 MHz, PBS-*d*, 10% ¹BuOH) δ 8.09 (s, 8H), 7.98 (s, 8H), 6.35 (d, J = 7.2 Hz, 16H), 6.01 (s, 8H), 5.95-5.87 (m, 16H); μ_{eff} (Evans', PBS-*d*, 10% ¹BuOH): 0 μ_B.

For UV-vis characterization, compound **2.12** was dissolved in PBS and diluted to 0.02 mM. A minimal amount of sodium dithionite was added to effect reduction of **2.12**. CO was bubbled through for 5 s to generate compound **2.13**, which resulted in an immediate change in the electronic absorption spectrum. UV/Vis (PBS) λ_{abs} (log ε): 444 (5.08), 557 (3.85), 624 (3.48). Air was bubbled through the solution to remove any excess sodium dithionite as assessed by reduction in intensity of the absorption at 315 nm. Once all of the dithionite had been consumed, the quiescent solution was left open to air and electronic absorption spectra were acquired at 600 s intervals (Figure 2.15).

To collect IR data, compound **2.12** (5 mg) was dissolved in DI water (5 mL). The solution was sparged with nitrogen and excess sodium dithionite was added (1 mg). CO was bubbled through the solution for 5 s. To this solution was added an excess of tetraphenylphosphonium chloride (5 mg). The resulting precipitate was collected, washed with DI water, and dried under a stream of N₂ for 5 min. The

resulting solid was used to prepare a KBr pellet for IR spectroscopic measurement (Figure 2.9).

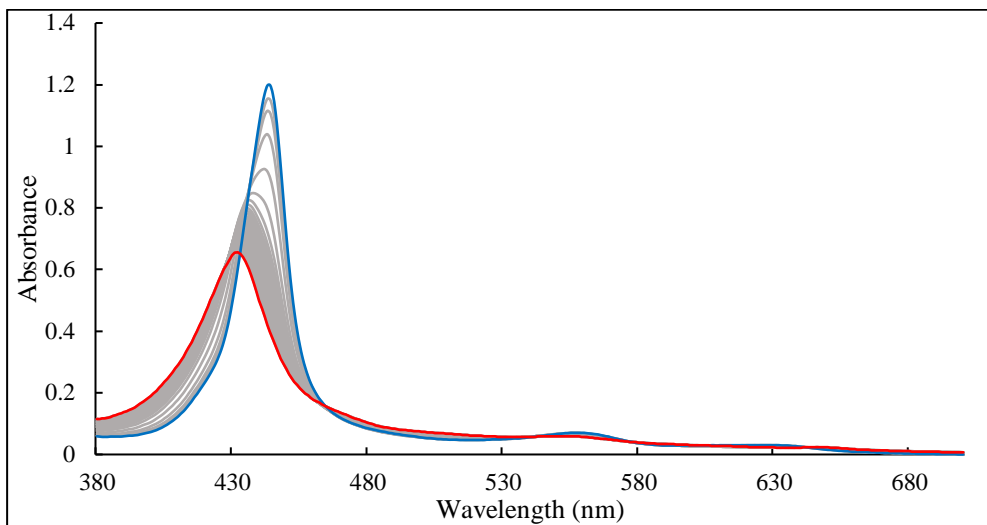


Figure 2.15. Stability of **2.13** in PBS (pH 7.4) containing 5.7 mM dithionite following exposure to air. Spectra were acquired at 600 s intervals once dithionite consumption was complete.

X-ray crystallography. Crystals of **2.10**·2MeCN, **2.11**·DCM·MeCN, **2.12**, and **2.12**_{DMSO}·4DCM were grown as described above, selected under a microscope, loaded onto a nylon fiber loop using Paratone-N, and mounted onto a Rigaku XtaLAB Synergy-S single-crystal diffractometer. Each crystal was cooled to 100 K under a stream of nitrogen. Diffraction of Cu K α radiation from a PhotonJet-S microfocus source was detected using a HyPix-6000HE hybrid photon counting detector. Screening, indexing, data collection, and data processing were performed with CrysAlis^{Pro}.²⁴ The structures were solved using SHELXT and refined using SHELXL as implemented in OLEX2 following established strategies.²⁵⁻²⁸ The contents of the unit cell of **2.10**·2MeCN are depicted in Figure 2.6. The contents of

the unit cell of **2.11**·MeCN are depicted in

Figure 2.7. The crystals of **2.12** were

twinned and diffracted weakly. The

diffraction data allowed the proposed

connectivity of the iron complex to be

confirmed (Figure 2.16) but were not

suitable for detailed analysis of bond

metrics. Notably, in **2.12**, the apical ligand

is located 1.9 Å from the Fe center and exhibited an electron density consistent with

an O atom. The contents of the unit cell of **2.12**_{DMSO} are depicted in Figure 2.7. For

the atomic-resolution crystal structures of **2.10**·2MeCN, **2.11**·DCM·MeCN, and

2.12_{DMSO}·4DCM, all non-H atoms were refined anisotropically and carbon-bound H

atoms were placed at calculated positions and refined with a riding model and

coupled isotropic displacement parameters ($1.2 \times U_{eq}$ for aryl groups and $1.5 \times U_{eq}$

for methyl groups). For **2.11**·DCM·MeCN, the oxygen-bound H atom was placed at a

calculated position and refined using a riding model that additionally allowed

refinement of the torsional setting of the H and the O–H bond length, the latter

restrained to 0.84(2) Å. Refinement parameters for **2.10**·2MeCN, **2.11**·DCM·MeCN,

and **2.12**_{DMSO}·4DCM are collected in Table A.1. The unit cell parameters for **2.12** are

collected in Table A.2.

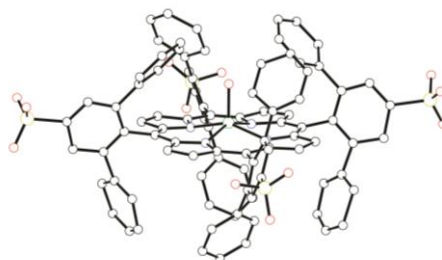


Figure 2.16. Ball-and-stick representation of **2.12** from low-quality diffraction data confirming connectivity. Color code: Fe green, O red, S yellow, N blue, C grey.

CO abstraction from COHb. A stock solution of COHb was created by dissolving bovine Hb (5 mg) in 1 mL of PBS containing 5.7 mM sodium dithionite that had been sparged with N₂. CO was bubbled through this solution for 5 s. N₂ was slowly bubbled through this solution for 20 min to remove excess CO. Working solutions were prepared from this stock by dilution with PBS containing 5.7 mM sodium dithionite. Concentrations

were determined with the mass of Hb used to prepare the stock solution and a molecular weight of 64,500 g/mol. For CO abstraction, a 2.5 μM

PBS solution of COHb was prepared and titrated with a PBS solution of **2.12** or Fe(III)TPPS.

Equivalents of **2.12** and Fe(III)TPPS were calculated per heme unit of Hb (i.e., 4 × molar quantity of protein). Spectra are presented in Figures 2.10 and 2.17.

Reduced 2.12 protects Hb from CO. A stock solution of bovine hemoglobin was prepared by dissolving 5 mg in 1 mL of N₂-sparged PBS containing 5.7 mM sodium dithionite. Working solutions were prepared from this stock by dilution with PBS

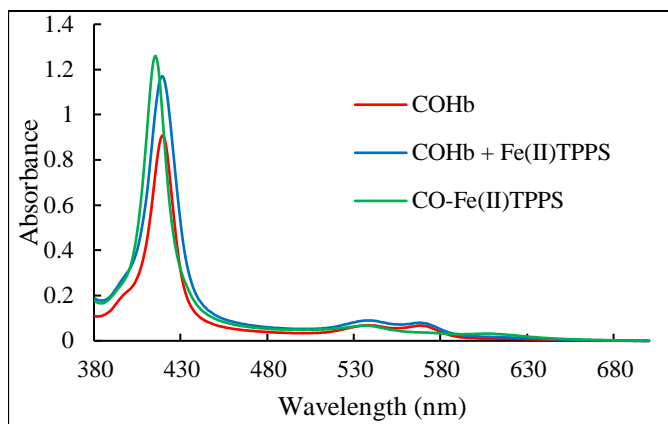


Figure 2.17. Titration of bovine COHb (2.5 μM) with 1 equiv Fe(II)TPPS (produced in situ from reduction of Fe(III)TPPS) in PBS (pH 7.4, 5.7 mM Na₂S₂O₄). Also shown is the spectrum obtained when CO is bubbled through a solution of Fe(II)TPPS to form CO-Fe(II)TPPS.

containing 5.7 mM sodium dithionite. Concentrations were determined with the mass of Hb used to prepare the stock solution and a molecular weight of 64,500 g/mol. From this stock, a working

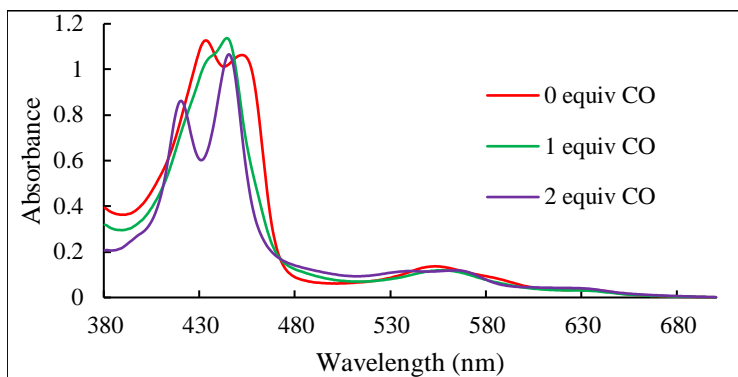


Figure 2.18. Titration of an equimolar (on the basis of porphyrin centers) mixture of Hb and **2.12** in PBS (pH 7.4, 5.7 mM Na₂S₂O₄) with CO-saturated water. At 0 equiv CO, the mixture contains deoxyHb and reduced **2.12**. At 1 equiv CO, the mixture contains deoxyHb and **2.13**. At 2 equiv CO, the mixture contains COHb and **2.13**.

solution containing 2.5 μ M Hb and 10 μ M reduced **2.12** (prepared from *in situ* reduction of **2.12**) was prepared and titrated with CO-saturated water (approx. 1 mM CO_(aq)). UV-vis spectra were acquired after addition of 1 and 2 equivalents (with respect to **2.12**) of CO (Figure 2.18).

Hemolytic potential of reduced 2.12. Defibrinated bovine blood (Hemostat Laboratories) was diluted with PBS containing 5.7 mM sodium dithionite. This mixture was centrifuged for 30 s at 760 \times g. The supernatant was discarded, and the pellet was washed with PBS containing 5.7 mM sodium dithionite. The pellet was suspended in PBS containing 5.7 mM sodium dithionite to give a suspension with $A_{700} = 1.0$. An aliquot of this suspension was lysed and the absorbance at 420 nm was used to quantify the amount of COHb ($\epsilon = 10^{5.63}$). Based on this concentration, 1

equiv of compound **2.12**, which was reduced immediately, was added to the suspension of cells. After the addition, turbidity was monitored continuously at 700 nm. This process was repeated both in the absence of any added species (negative control) and upon addition of a RBC-lysing solution (1.5 M NH₄Cl) (Figure 2.11).

CO abstraction from CO-treated RBCs. Defibrinated bovine blood (Hemostat Laboratories) was diluted with PBS containing 5.7 mM sodium dithionite. CO was bubbled through this suspension for 5 s. This mixture was centrifuged for 30 s at 760 × g. The supernatant was discarded, and the pellet was washed with PBS containing 5.7 mM sodium dithionite. This washing was repeated three more times to remove excess CO. An aliquot of the stock suspension of CO-treated RBCs was added to a quartz cuvette containing 1 mL of DI water to lyse the cells. The concentration of COHb was assessed by measuring the absorbance at 420 nm ($\epsilon = 10^{5.63}$) of this lysate. For abstraction studies, an aliquot of the stock suspension of CO-treated RBCs was diluted to 1 mL with PBS containing 5.7 mM sodium dithionite. Compound **2.12**, which is reduced *in situ*, was added in increments based on the concentration of COHb determined in the lysate. A UV-vis spectrum was acquired after each addition (Figure 2.12).

Time-course CO removal from CO-treated RBCs. Defibrinated bovine blood (Hemostat Laboratories) was diluted with PBS containing 5.7 mM sodium dithionite. CO was bubbled through this suspension for 5 s. This mixture was centrifuged for 30

s at $760 \times g$. The supernatant was discarded, and the pellet was washed with PBS containing 5.7 mM sodium dithionite. This washing was repeated three more times to remove excess CO. An aliquot of the stock suspension of CO-treated RBCs was added to a quartz cuvette containing 1 mL of DI water to lyse the cells. The concentration of COHb was assessed by measuring the absorbance at 420 nm ($\epsilon = 10^{5.63}$) of this lysate. For time-course CO removal, an aliquot of the stock suspension of CO-treated RBCs was diluted to 1 mL with PBS containing 5.7 mM sodium dithionite. A full equivalent of compound **2.12** (which is reduced *in situ*) was added, the suspension was rapidly mixed, and absorbance at 420 nm was monitored continuously (Figure 2.13).

2.5 References

1. Collman, J. P.; Gagne, R. R.; Reed, C.; Halbert, T. R.; Lang, G.; Robinson, W. T., "Picket fence porphyrins." Synthetic models for oxygen binding hemoproteins. *J. Am. Chem. Soc.* **1975**, *97*, 1427-1439.
2. Suslick, K. S.; Fox, M. M., A Bis-Pocket Porphyrin. *J. Am. Chem. Soc.* **1983**, *105*, 3507-3510.
3. Suslick, K. S.; Fox, M. M.; Reinert, T. R., Influences on carbon monoxide and dioxygen binding to iron(II) porphyrins. *J. Am. Chem. Soc.* **1984**, *106*, 4522-4525.
4. Collman, J. P., Synthetic models for the oxygen-binding hemoproteins. *Acc. Chem. Res.* **1977**, *10*, 265-272.
5. Boaz, N. C.; Bell, S. R.; Groves, J. T., Ferryl Protonation in Oxoiron(IV) Porphyrins and Its Role in Oxygen Transfer. *J. Am. Chem. Soc.* **2015**, *137*, 2875-2885.
6. Luciano, M.; Brückner, C., Modifications of Porphyrins and Hydroporphyrins for Their Solubilization in Aqueous Media. *Molecules* **2017**, *22*, 980.

7. Yang, N. J.; Hinner, M. J., Getting Across the Cell Membrane: An Overview for Small Molecules, Peptides, and Proteins. In *Site-Specific Protein Labeling*, 2015; pp 29-53.
8. Kano, K.; Kitagishi, H.; Kodera, M.; Hirota, S., Dioxygen Binding to a Simple Myoglobin Model in Aqueous Solution. *Angew. Chem., Int. Ed.* **2005**, *44*, 435-438.
9. Azarov, I.; Wang, L.; Rose, J. J.; Xu, Q.; Huang, X. N.; Belanger, A.; Wang, Y.; Guo, L.; Liu, C.; Ucer, K. B.; McTiernan, C. F.; O'Donnell, C. P.; Shiva, S.; Tejero, J.; Kim-Shapiro, D. B.; Gladwin, M. T., Five-coordinate H64Q neuroglobin as a ligand-trap antidote for carbon monoxide poisoning. *Sci. Transl. Med.* **2016**, *8*, 368ra173.
10. Ye, B.-H.; Naruta, Y., A novel method for the synthesis of regiospecifically sulfonated porphyrin monomers and dimers. *Tetrahedron* **2003**, *59*, 3593-3601.
11. La Mar, G. N.; Walker, F. A., Dynamics of Axial Ligation in Metalloporphyrins. I. Imidazole Exchange in Low-Spin Ferric Porphyrins. *J. Am. Chem. Soc.* **1972**, *94*, 8607-8608.
12. Walker, F. A., NMR and EPR Spectroscopy of Paramagnetic Metalloporphyrins and Heme Proteins. In *Handbook of Porphyrin Science (Volume 6)*, 2010; pp 1-337.
13. Collman, J. P.; Hoard, J. L.; Kim, N.; Lang, G.; Reed, C. A., Synthesis, Stereochemistry, and Structure-Related Properties of $\alpha,\beta,\gamma,\delta$ -Tetraphenylporphinatoiron(II). *J. Am. Chem. Soc.* **1975**, *97*, 2676-2681.
14. Hu, C.; Noll, B. C.; Schulz, C. E.; Scheidt, W. R., Four-Coordinate Iron(II) Porphyrinates: Electronic Configuration Change by Intermolecular Interaction. *Inorg. Chem.* **2007**, *46*, 619-621.
15. Moore, J. N.; Hansen, P. A.; Hochstrasser, R. M., Iron-carbonyl bond geometries of carboxymyoglobin and carboxyhemoglobin in solution determined by picosecond time-resolved infrared spectroscopy. *Proc. Natl. Acad. Sci. U.S.A.* **1988**, *85*, 5062-5066.
16. Collman, J. P.; Brauman, J. I.; Halbert, T. R.; Suslick, K. S., Nature of O₂ and CO binding to metalloporphyrins and heme proteins. *Proc. Natl. Acad. Sci. U.S.A.* **1976**, *73*, 3333-3337.
17. Adler, A. D.; Longo, F. R.; Finarelli, J. D.; Goldmacher, J.; Assour, J.; Korsakoff, L., A Simplified Synthesis for *meso*-Tetraphenylporphine. *J. Org. Chem.* **1967**, *32*, 476-476.

18. Fleischer, E. B.; Palmer, J. M.; Srivastava, T. S.; Chatterjee, A., Thermodynamic and Kinetic Properties of an Iron-Porphyrin System. *J. Am. Chem. Soc.* **1971**, *93*, 3162-3167.
19. Esfandiari bayat, Z.; Rahiminezhad, H.; Zakavi, S., Solvent effects on catalytic activity of manganese porphyrins with cationic, anionic and uncharged *meso* substituents: Indirect evidence on the nature of active oxidant species. *Appl. Organomet. Chem.* **2019**, *33*, e4678.
20. Schubert, E. M., Utilizing the Evans method with a superconducting NMR spectrometer in the undergraduate laboratory. *J. Chem. Educ.* **1992**, *69*, 62.
21. Lin, C.-H.; Tour, J., Hydrogen-Bond-Assisted π -Stacking of Shape-Persistent Cyclophanes. *J. Org. Chem.* **2002**, *67*, 7761-7768.
22. Guillermin, V.; Weseliński, Ł. J.; Alkordi, M.; Mohideen, M. I. H.; Belmabkhout, Y.; Cairns, A. J.; Eddaoudi, M., Porous organic polymers with anchored aldehydes: a new platform for post-synthetic amine functionalization en route for enhanced CO₂ adsorption properties. *Chem. Commun.* **2014**, *50*, 1937-1940.
23. Lindsey, J. S.; Wagner, R. W., Investigation of the Synthesis of Ortho-Substituted Tetraphenylporphyrins. *J. Org. Chem.* **1989**, *54*, 828-836.
24. Rigaku Oxford Diffraction *CrysAlis^{Pro} software system*, version 1.171.40.78a; Rigaku Corporation: Wroclaw, Poland, 2020.
25. Sheldrick, G. M., *SHELXT* – Integrated space-group and crystal-structure determination. *Acta Crystallogr. Sect. A* **2015**, *71*, 3-8.
26. Sheldrick, G. M., Crystal structure refinement with *SHELXL*. *Acta Crystallogr. Sect. C* **2015**, *71*, 3-8.
27. Dolomanov, O. V.; Bourhis, L. J.; Gildea, R. J.; Howard, J. A. K.; Puschmann, H., *OLEX2*: a complete structure solution, refinement and analysis program. *J. Appl. Crystallogr.* **2009**, *42*, 339-341.
28. Müller, P., Practical suggestions for better crystal structures. *Crystallogr. Rev.* **2009**, *15*, 57-83.

Chapter 3

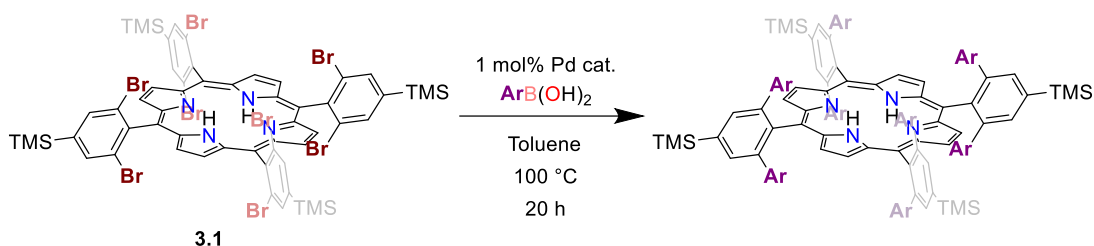
Synthesis and Functionalization of *meso*-Aryl Bis-pocket Porphyrins

Published in part Daniel G. Droege, A. Leila Parker, Griffin M. Milligan, Robert Jenkins, and Timothy C. Johnstone, *J. Org. Chem.* **2022**, 87, 17, 11783–11795

3.1 Introduction

As discussed in Chapter 1, the porphyrin scaffold is important in both biology and chemistry. Significant contributions to the synthesis of porphyrins, including those from Rothemund, Adler, and Lindsey, have led to an explosion of porphyrin synthesis throughout biological and chemical research.¹⁻³ Nevertheless, a thorough search of the literature on bis-pocket porphyrins with non-polar pockets revealed a lack of synthetic methodologies to achieve a modular bis-pocket porphyrin, where the pockets have hydrophobic properties and the molecule could eventually be made water soluble. The influential work by Suslick on the bis-pocket porphyrin⁵ prompted me to develop methodologies that would circumvent the low yields afforded by using bulky aldehydes during porphyrin macrocyclization.

In the previous chapter, I described the coupling of PhB(OH)_2 to 5,10,15,20-tetrakis(2,6-dibromo-4-(trimethylsilyl)phenyl)porphyrin (**3.1**) to give 5,10,15,20-tetrakis(2,6-diphenyl-4-(trimethylsilyl)phenyl)porphyrin (**3.2a**). This methodology permitted me to synthesize the desired bulky bis-pocket architecture with functional yields. However, that methodology required improvement for a number of reasons. The original method used a high loading of palladium catalyst which was likely more than was required. Also, that method only demonstrated the coupling of one particular arylboronic acid. To prove useful, the scope of coupling needed to be demonstrated. Furthermore, the original metalation of that scaffold gave multiple products and needed to be improved.



Scheme 3.1. Overview of the coupling reaction.

In this chapter, I will discuss an optimization of this coupling reaction (Scheme 3.1), which was achieved by varying the catalyst, catalyst loading, base, stoichiometry, solvent, and temperature. It will be demonstrated that the method allows a significant variety of groups to be coupled to the scaffold, varying in sterics, electronics, and functional groups. To further demonstrate the synthetic flexibility of this scaffold, I will discuss an optimization of the originally reported sulfonation reaction (Figure 3.1). This allows for modular use of the TMS groups on the porphyrin derivatives, which provide excellent organic solubility. In this reaction, the ipso-directing TMS groups direct the sulfonation reaction and allow for facile

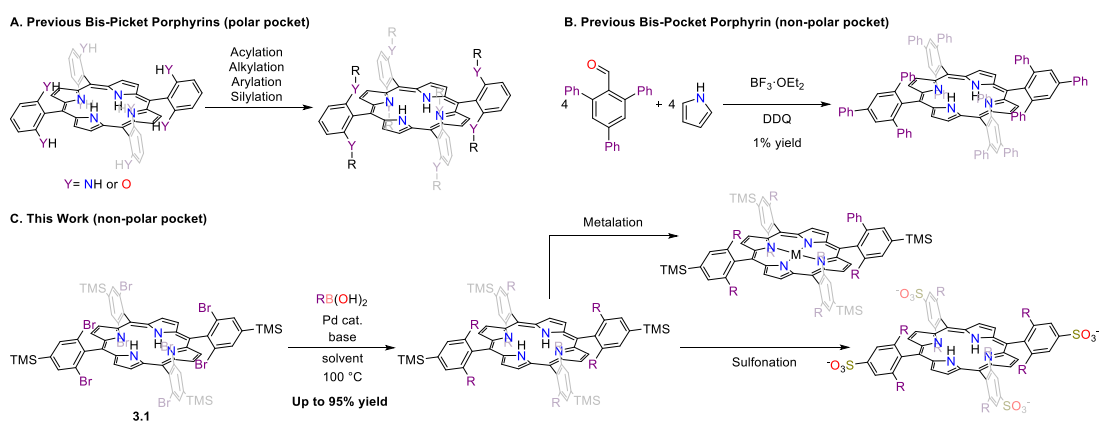


Figure 3.1. Examples of bis-pocket porphyrin syntheses.

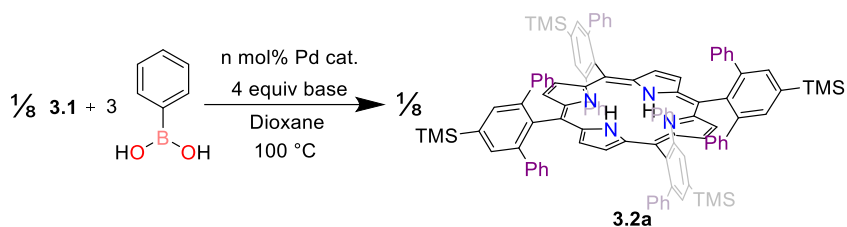
synthesis of water soluble bis-pocket porphyrins. Due to the importance of metalloporphyrins, this chapter will also discuss improvements made to the metalation of these bulky bis-pocket porphyrins. Although the bulky substituents can inhibit the insertion of some metals into these porphyrins, refluxing a metal halide, 2,6-lutidine, and the free-base ligand in 1,2,4-trichlorobenzene (1,2,4-TCB) allows for clean and rapid metalation. Not only will these synthetic methods allow for the derivatization of CO-poisoning antidotes, but these reactions could also prove useful in the preparation of porphyrin compounds intended for a range of fundamental and applied studies. Finally, this chapter will briefly discuss the structural outcomes of the bis-pocket architecture that occur by varying the coupling partners in this reaction. This would give future researchers looking to utilize this scaffold the ability to fine tune the pocket shape and size.

3.2 Results and Discussion

Synthesis Optimization

To further optimize the reaction, a series of palladium catalysts known to facilitate sterically demanding coupling reactions were screened at a catalyst loading of 1 mol% (Table 3.2).⁶ Pd(PPh₃)₄ performed comparably to (dppf)PdCl₂ (Table 3.2, entry 1). Pd supported by bidentate ligands such as Xantphos and rac-BINAP, afforded greater yields than catalysts with the monodentate ligands SPhos and DavePhos (Table 3.2, entries 2-5). The precatalyst alone afforded no product (Table 3.2, entry 6). Using the set of reaction conditions from Chapter 2, (dppf)PdCl₂ and

$\text{Pd}(\text{PPh}_3)_4$ were the only catalysts tested that allowed the reaction to reach completion; all others gave mixtures of the desired product and various partially functionalized intermediates with fewer than eight of the aryl bromides having reacted. Purification of the reactions where completion of coupling did not occur proved difficult. These partially substituted intermediates were poorly resolved from the product by silica gel column chromatography, even after extensive optimization. When evaluating the different reaction conditions (Table 3.2), the product and all partially substituted intermediates were collected together and, using NMR spectroscopy, the fraction of the porphyrinic material corresponding to the desired product could be determined. In the ^1H NMR spectra, the aromatic resonances of these species overlap, but due to the position of the pyrrolic H atoms in the center of the porphyrin's ring current, the N-H signals are characteristically shifted upfield ($\delta < -2$ ppm). Fortunately, these N-H signals are well separated for the desired reaction product and the partially substituted intermediates. The progress of the reaction could be followed by monitoring the progressive growth and disappearance of the N-H signal(s) of each intermediate. The yields of the reactions (Table 3.2) could be calculated by multiplying the mass of the total isolated porphyrinic material by the quotient of the integral of the N-H resonance of the desired product and the integral of all N-H resonances in the isolated material. $\text{Pd}(\text{PPh}_3)_4$ and $(\text{dppf})\text{PdCl}_2$ afforded comparable yields. Optimization was continued with $(\text{dppf})\text{PdCl}_2$ due to its relatively low cost, ease of use, and benchtop stability.

Table 3.1. Optimization of Catalyst Loading for Coupling ^a.

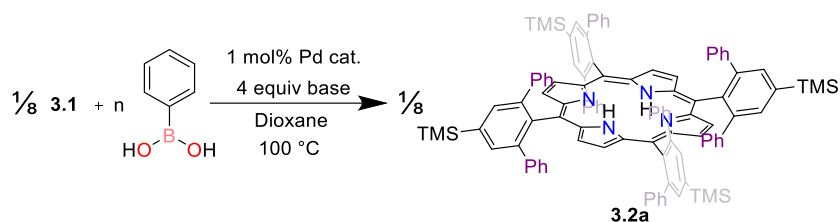
Entry	Catalyst	mol% cat	Yield	Time (h)
1	(dppf)PdCl ₂	12.5	76%	16
2	(dppf)PdCl ₂	5	77%	16
3	(dppf)PdCl ₂	1	73%	16
4	(dppf)PdCl ₂	0.5	60%	16
5	(dppf)PdCl ₂	0.5	72%	20
6	(dppf)PdCl ₂	0.1	0%	20
7	None	0	0%	20

^a mol% of catalyst, equiv PhB(OH)₂, and equiv base are provided with respect to Ar–Br bonds.

From the initially reported coupling reaction (Chapter 2), another factor to be addressed was the amount of palladium catalyst that was being used. The initial reaction used a significant amount of palladium, 12.5 mol% per C–Br bond, to ensure reaction completion, however the literature of Suzuki reactions reveals this is much more catalyst than what is generally used.⁷ To probe the amount of catalyst needed, I iteratively decreased the amount of Pd catalyst (Table 3.1, entry 1-4). The desired product was observed down to 0.5 mol%, however a decrease in yield was observed. Increasing the reaction time to 20 h at 0.5 mol% catalyst regained the initial yield

(Table 3.1, entry 5). A loading of 0.1 mol% resulted in no formation of desired product, even at the longer reaction time (Table 3.1, entry 6).

Table 3.2. Optimization of Coupling with PhB(OH)₂^a.



Entry	Catalyst	Equiv PhB(OH) ₂	Base	Solvent	Yield
1	Pd(PPh ₃) ₄	3	Cs ₂ CO ₃	Dioxane	79%
2	Pd ₂ (DBA) ₃ /Xantphos ^b	3	Cs ₂ CO ₃	Dioxane	57%
3	Pd ₂ (DBA) ₃ /rac-BINAP ^b	3	Cs ₂ CO ₃	Dioxane	70%
4	Pd ₂ (DBA) ₃ /Sphos ^b	3	Cs ₂ CO ₃	Dioxane	8%
5	Pd ₂ (DBA) ₃ /DavePhos ^b	3	Cs ₂ CO ₃	Dioxane	3%
6	Pd ₂ (DBA) ₃ ^c	3	Cs ₂ CO ₃	Dioxane	0%
7	(dppf)PdCl ₂	3	KOH	Dioxane	0%
8	(dppf)PdCl ₂	3	KOAc	Dioxane	51%
9	(dppf)PdCl ₂	3	K ₃ PO ₄	Dioxane	57%
10	(dppf)PdCl ₂	3	K ₂ CO ₃	Dioxane	36%
11	(dppf)PdCl ₂	3	Cs ₂ CO ₃	DMF	0%
12	(dppf)PdCl ₂	3	Cs ₂ CO ₃	Diglyme	70%
13	(dppf)PdCl ₂	3	Cs ₂ CO ₃	Toluene	89%
14	(dppf)PdCl ₂	4	Cs ₂ CO ₃	Toluene	93%
15	(dppf)PdCl ₂	2	Cs ₂ CO ₃	Toluene	6%
16	(dppf)PdCl ₂	3	Cs ₂ CO ₃ ^d	Toluene	77%

^a mol% of catalyst, equiv PhB(OH)₂, and equiv base are provided with respect to Ar–Br bonds. ^b 1 mol% Pd₂(DBA)₃ (per Pd atom) and 2 mol% of specified ligand were precomplexed prior to the start of the reaction. ^c No ligand added. ^d 3 equiv.

Base plays an important role in the catalytic cycle of the Suzuki coupling, so a series of bases demonstrated to be successful in previous Suzuki couplings was screened to further optimize the reaction.⁸ While there was no clear trend in pK_b , using a base with a significantly lower pK_b like KOH completely halted product formation. All other bases, while not as detrimental, significantly decreased yield and afforded inseparable mixtures of porphyrinic material (Table 3.2, entries 7-10).

With Cs_2CO_3 being the only viable base of those tested, the influence of solvent was tested next (Table 3.2, entries 11-13). Due to the limited solubility of the starting porphyrin, the choice of solvents was limited. For example, even at 100 °C, the starting porphyrin minimally dissolved in DMF. Unsurprisingly, no product was formed in the reaction utilizing DMF as the solvent. The starting material exhibited a solubility in diglyme similar to that which it had in dioxane; the reaction performed in diglyme and gave comparable results to the one performed in dioxane (Table 3.2, entry 12). Toluene appeared to solubilize the starting material the best, and in turn gave the best results, increasing the yield to 89% (Table 3.2, entry 13). Increasing the amount of $PhB(OH)_2$ in the reaction (for a total of 4 equiv) improved the yield slightly to 93% (Table 3.2, entry 14). Importantly, this increased yield represents isolated and recrystallized product. Finally, decreasing the amount of boronic acid or base proved detrimental to the reaction yield (Table 3.2, entries 15-16).

Reaction Scope

With a set of optimized reaction conditions for coupling **3.1** to $\text{PhB}(\text{OH})_2$ in hand, the versatility of groups that could be installed on the porphyrin framework in this way was tested (Scheme 3.1). From the crystal structure of **3.2a** (Figure 2.6), which was described in Chapter 2, the pocket is shaped in such a way that the 3 and 5 positions of the phenyl rings point at each other.⁹ Since the bis-pocket architecture is

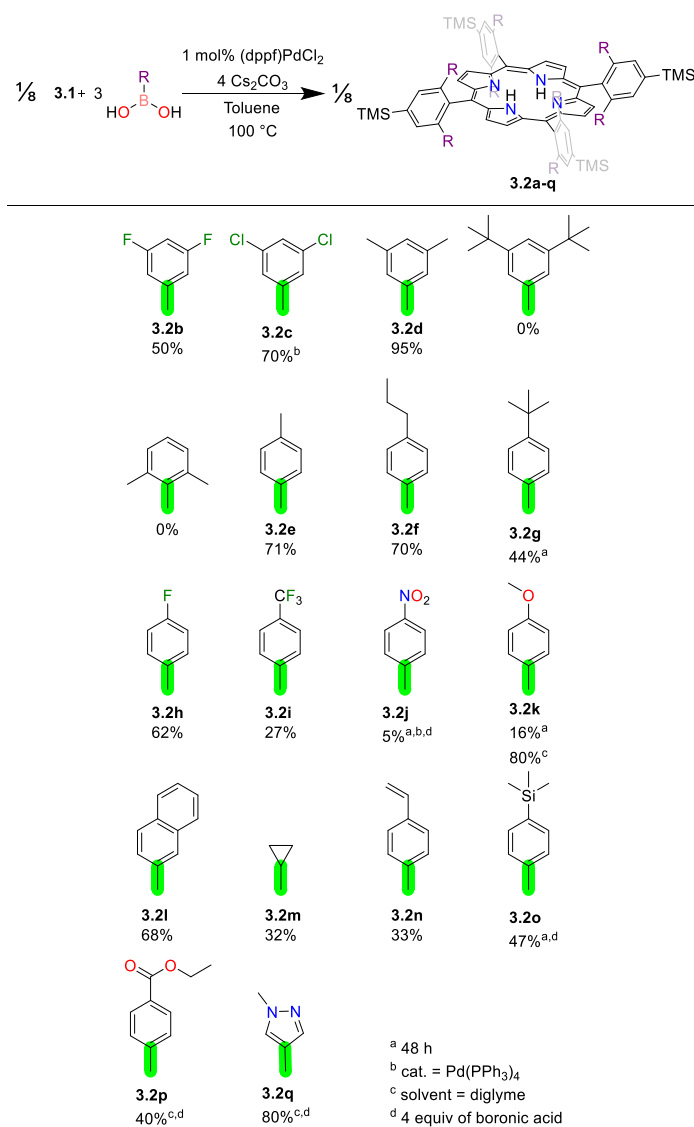


Figure 3.2. Exploration of the scope of groups that can be coupled to the porphyrin framework according to the depicted reaction. Yields are isolated yields.

already inherently sterically congested, it was first tested whether more steric hindrance at the 3 and 5 positions could be tolerated. The 3,5-difluoro-, -dichloro-, and -dimethyl derivatives of phenylboronic acid were tolerated in the coupling, however, a further increase in size to 3,5-di-*tert*-butylphenylboronic acid afforded no product. As expected, steric bulk at the 2 and 6 positions was detrimental and 2,6-dimethylphenylboronic acid afforded no product. Much more tolerance was afforded for the 4 position of phenylboronic acid; with methyl, *n*-propyl, or *tert*-butyl groups at this position, the coupling could be successfully performed. While the size increase at the 4 position was tolerated, in the case of the 4-*tert*-butylphenylboronic acid, there was a noticeable decrease in reaction rate, and the reaction time was increased to 48 h.

The influence of the electronic properties of the substituents on the coupling of phenylboronic acid derivatives was also explored. Aromatic rings functionalized with electron-withdrawing halogen substituents, such as 3,5-difluorophenyl and 4-fluorophenyl, could be installed with moderately high yields.

The reaction could also be scaled up to 1 mmol of 4-fluorophenyl-substituted boronic acid, and the product **3.2h** could successfully be obtained in 71% isolated yield (154 mg). While exploring the electronic effects of different boronic acids on this reaction, a trend in increasing electronegativity was noted. 4-Fluorophenyl-, 4-trifluoromethylphenyl-, and 4-nitrophenyl-substituted products were obtained in systematically decreased yield, consistent with their respective Hammett *para* substituent constant (σ_p) values of 0.06, 0.54, and 0.78. Increased reaction time of

48 h, an extra equivalent of boronic acid, and using Pd(PPh₃)₄ was required to obtain even a 5% yield of the 4-nitrophenyl-coupled product. Coupling of the electron-donating 4-methoxyphenyl group was similarly inhibited under the standard reaction conditions. While electronic changes in the boronic acids varied the success of the reaction, the Suzuki coupling reaction allows for facile optimization of the yield of any particular product with simple changes to the reaction parameters. Without changing the standard reaction conditions, 2-naphthylboronic acid and cyclopropylboronic acid were also able to couple to **3.1**. The latter example demonstrates that the strategy is not restricted to forming sp²-sp² C-C bonds.

The first attempt to couple 3,5-dichlorophenyl boronic acid gave surprisingly low yields; better yields were obtained with groups that were both larger and smaller as well as with groups that were more or less electron-withdrawing. Although (dppf)PdCl₂ is not generally used in Suzuki couplings featuring aryl chlorides, it is possible that the low yield came from over-derivatization, such that 3,5-dichlorophenyl groups were coupled to 3,5-dichlorophenyl groups that had already added to the porphyrin scaffold.¹⁰ Mass spectrometric analysis of the crude reaction confirmed this hypothesis; prominent signals were observed for over-coupling (*m/z* = 2172.58, 2285.54, 2394.58). To prevent this over-derivatization, a catalyst that does not easily undergo oxidative addition to aryl chlorides needed to be used.¹¹ Ph(PPh₃)₄ was chosen since it was already established that it worked well for our desired coupling. Indeed, using 1 mol% Pd(PPh₃)₄ as the catalyst afforded the desired product in 70% yield without any further change to the reaction conditions (Figure 3.2).

To further demonstrate this reaction's usefulness, precursors suitable for further functionalization were prepared. In addition to the 4-nitrophenyl derivative described above, which can be reduced to afford reactive amine units, we were also able to successfully install 4-vinylphenyl groups, which are amenable to further functionalization via alkene metathesis. 4-Trimethylsilylphenyl groups could be installed similarly to the *tert*-butyl derivative, but the reaction proceeded more slowly than many of the others. Increasing the reaction time to 48 h and including an extra equivalent of boronic acid allowed the product to be obtained in 47% yield.

Esters were another functional group of interest to couple onto the porphyrin platform, because they would be able to undergo either transesterification or saponification. Unfortunately, coupling of **3.1** and 4-ethoxycarbonylphenylboronic acid was unsuccessful using the standard conditions. Fortunately, simple substitution of the solvent for diglyme and inclusion of an extra equivalent of boronic acid provided the desired product in 40% yield. This example highlights how the modular nature of the synthetic protocol allows for rapid and efficient screening of solvent, catalyst, base, temperature, and reaction time to allow for ready incorporation of a given group. To further demonstrate flexibility of the method, two more derivatives were shown to benefit from simple solvent change. The standard reaction conditions did not permit the coupling of **3.1** and 1-methylpyrazole-4-boronic acid, but this product formed in 80% yield using the same toluene-to-diglyme solvent substitution described above and an extra equivalent of boronic acid, but no further optimization of reaction conditions. The other example is 4-methoxyphenylboronic acid. The

coupling was successful using our standard reaction conditions, however, changing the solvent to diglyme increased the yield 5-fold (Figure 3.2). This work highlights the capability of this strategy for preparing bis-pocket porphyrins with a variety of different substituents.

Metalation

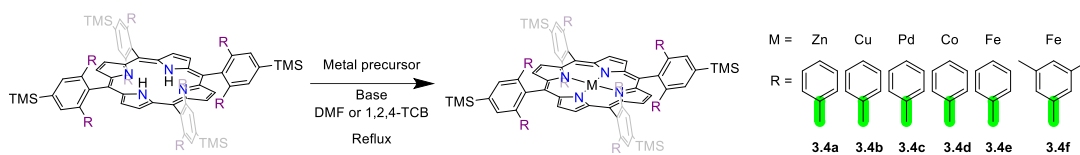


Figure 3.3. Metal insertion into bulky bis-pocket porphyrins.

Free-base porphyrins have a variety of valuable properties and reactivities, however, these molecules are perhaps most widely investigated as ligands for transition metals. Typically, porphyrin metalations are performed by heating the free-base ligand with a metal halide and a base in DMF. Unfortunately, due to the significant steric bulk of the bis-pocket motif, these classic conditions do not work with the framework described in this chapter. In the original bis-pocket porphyrin report, the ligand, $\text{Fe}(\text{CO})_5$ and I_2 were heated, followed by an aqueous aerobic work up.⁵ In the previous chapter, it was confirmed that this approach affords the Fe(III) complex of **3.2a**. This section aims to explore whether a more streamlined metalation strategy could be developed (Figure 3.3). Using standard reaction conditions, refluxing the free-base and excess pyridine in DMF with excess $\text{Zn}(\text{OAc})_2 \cdot 2\text{H}_2\text{O}$ and $\text{CuCl}_2 \cdot 2\text{H}_2\text{O}$, afforded the Zn(II) and Cu(II) complexes of **3.2a** respectively. The ^1H

NMR spectrum of the diamagnetic Zn(II) product **3.4a** shows the loss of the upfield N-H resonances, as compared to the spectrum of the free ligand, and subtle shifts in the aromatic signals. Additionally, the spectrum features a new singlet of 2H integration at -1.29 ppm. Since square-planar coordination is disfavored for Zn(II), there is a strong driving force to coordinate even trace amounts of water giving rise to the new singlet, and due to that water ligand's position relative to the strong ring current of the porphyrin, its signal is strongly shifted upfield. The presence of the aqua ligand was confirmed crystallographically (Figure 3.4) with a Zn–O bond length of $2.194(5)$ Å. The crystal structure also revealed the Zn center to lie $0.3196(6)$ Å above the plane of the porphyrin. Due to the paramagnetic nature of the Cu(II) complex **3.4b**, NMR spectroscopic characterization was not possible, but single-crystal X-ray diffraction from the red plates of the product confirmed insertion of the metal (Figure 3.4). The Cu assumes a square-planar geometry with no axial ligand coordination.

Attempts to use the previous method to form the Pd(II) complex with Pd(OAc)₂ were unsuccessful. Refluxing an excess of Pd(OAc)₂ with ligand **3.2a** in 1,2,4-tetrachlorobenzene (1,2,4-TCB), however, resulted in insertion into the macrocycle, as indicated by mass spectrometric analysis. Due to the higher boiling point of 1,2,4-TCB (213.5 °C) to that of DMF (153 °C) it is likely that the increase in reflux temperature provided the greater activation energy needed to metalate the bulky porphyrin. The mass spectrometric analysis of the reaction mixture revealed, however, that side-products featuring loss of TMS groups formed during the reaction,

in addition to the desired product. Refluxing **3.2a** alone is not sufficient to induce desilylation of the starting porphyrin and it is therefore likely that the Pd itself is effecting this transformation. By using only 1 equiv of Pd(OAc)₂, the desilylation was

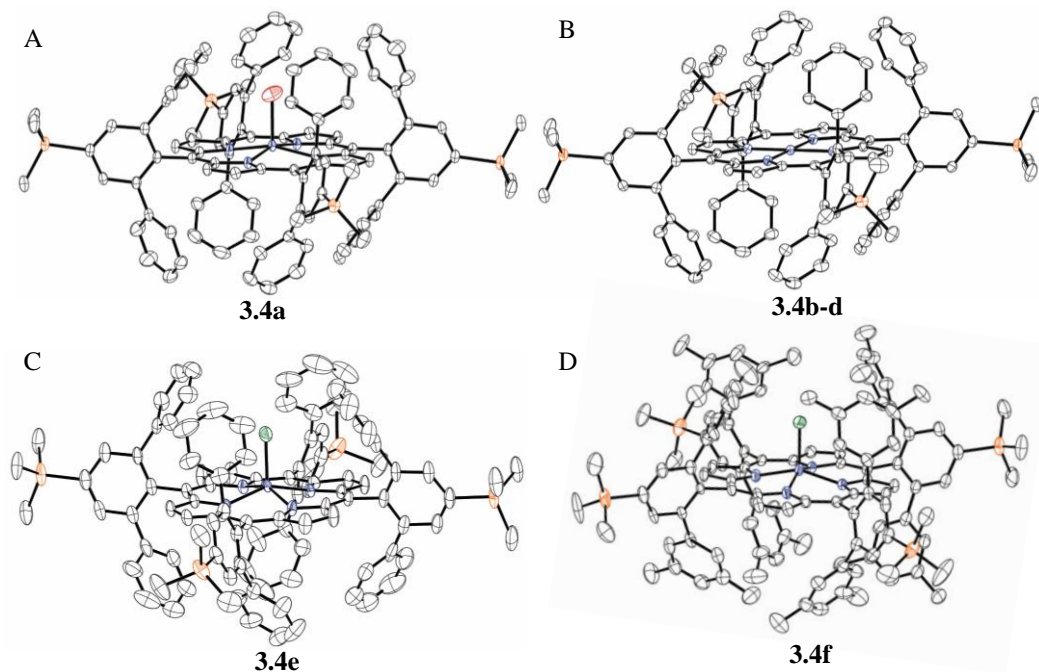


Figure 3.4. Thermal ellipsoid plots (50% probability level) of (A) the Zn-aqua complex **3.4a**, (B) the Cu complex **3.4b** (note that Pd complex **3.4c** and the Co complex **3.4d** are isomorphous), (C) the Fe-chloro complex **3.4e**, and (D) the Fe-chloro complex **3.4f**. H atoms, disorder, and solvent molecules are omitted for clarity. Color code: C grey, Si orange, O red, N blue, Cl green, Metal purple.

decreased enough so that the Pd(II) complex could be isolated in 25% yield. The complex is diamagnetic and features all of the expected resonances. Unlike the Zn(II) complex, there are no additional features to the spectrum, consistent with the square-planar geometry expected for a Pd(II) complex. Single-crystal X-ray diffraction revealed the Pd(II) complex to be isostructural with the Cu(II) complex.

Refluxing metal halide, lutidine, and **3.2a** in 1,2,4-TCB also permitted insertion of Co(II). The reaction proceeded smoothly and the resulting paramagnetic Co(II) complex, **3.4d**, was isolated in 91% yield. X-ray crystallography confirmed the formation of a square-planar complex that is isostructural with the Pd(II) and Cu(II) complexes.

Using the knowledge gained from the insertion of Pd, it was investigated whether Fe could be inserted into **3.2a** directly using a metal halide as opposed to the circuitous route involving Fe(CO)₅ described in Chapter 2. Refluxing the porphyrin ligand with an excess of FeCl₂ and lutidine in DMF afforded no product. However, refluxing with the higher boiling 1,2,4-TCB cleanly produced 5,10,15,20-tetrakis(2,6-diphenyl-4-(trimethylsilyl)phenyl)porphyrinatochloroiron(III), **3.4e**. Due to the complex being paramagnetic, the ¹H NMR spectrum suffers from severe broadening, however, it clearly shows the characteristic β-pyrrole signal at 80.42 ppm. A suitable crystal was grown by layering MeCN over the compound dissolved in CHCl₃, and X-ray diffraction confirms formation of the desired complex (Figure 3.4). The Fe center is displaced 0.492(3) Å from the plane of the porphyrin, which adopts a flat configuration (RMSD = 0.069 Å). Unlike the Fe(CO)₅/I₂/alkaline hydrolysis procedure, which affords an Fe(III) hydroxide complex, this reaction affords an Fe(III) chloride complex with an Fe–Cl bond length of 2.203(5) Å. The magnetic moment of **3.4e** was measured using the Evans method, which returned a value of 5.65 μ_B. This value compares favorably with the value of 5.49 μ_B, which was previously obtained for the hydroxoiron(III) complex of this same porphyrin in

Chapter 2, and also agrees with the spin-only magnetic moment prediction for a tetragonal high-spin d^5 center ($\mu_{s.o.} = 5.92 \mu_B$). This metalation protocol is also capable of producing the Fe(III) chloride derivative of **3.2d**, which bears the even more sterically encumbered 2,6-bis(3,5-dimethylphenyl)-4-(trimethylsilyl)phenyl *meso* substituents, demonstrating the increased usefulness of this new metalation method. With this ligand, the $\text{Fe}(\text{CO})_5/\text{I}_2$ /alkaline hydrolysis method was unsuccessful, whereas refluxing **3.2d** with excess FeCl_2 and 2,6-lutidine in 1,2,4-TCB affords the product **3.4f** in 71% yield. As before, crystallographic analysis (Figure 3.4) reveals that the Fe was successfully inserted and is displaced from the plane of the porphyrin ($0.4993(15) \text{ \AA}$) and that the axial ligand is a chloride ($\text{Fe}-\text{Cl} = 2.213(2) \text{ \AA}$). As with **3.4e**, the magnetic moment of **3.4f** ($\mu_{s.o.} = 6.59 \mu_B$) again agrees best with a high-spin Fe(III) complex.

Sulfonation

The TMS groups present in the porphyrin starting material serve a number of functions. In addition to providing additional ^1H , ^{13}C , and ^{29}Si NMR spectroscopic handles, they impart increased organic solubility to **3.1**, facilitating the coupling reaction. More importantly for the work presented here, the TMS groups also provide a means of performing regioselective sulfonation.¹² Sulfonation of these porphyrins can confer upon them greater solubility in polar organic solvents or, in some cases, aqueous solubility. The previous chapter discussed that 5,10,15,20-tetrakis(2,6-diphenyl-4-(trimethylsilyl)phenyl)porphyrinatohydroxoiron(III) could be converted to

the corresponding tetrasulfonate salt in 40% yield by treatment with trimethylsilyl chlorosulfonate in refluxing CCl_4 for 1 h, followed by aqueous alkaline work up.⁹ While evidence was discussed that this low yield arose from desilylation of the starting material, the 40% yield was sufficient to obtain the amount of material needed to test the CO-sequestering properties of this metalloporphyrin.

To improve the yield and decrease desilylation, the sulfonation of the free-base **3.2a** was performed with fewer equivalents of sulfonating agent (1.2 equiv). The tetrasulfonated product **3.3a** was obtained in 60% yield by performing the reaction at

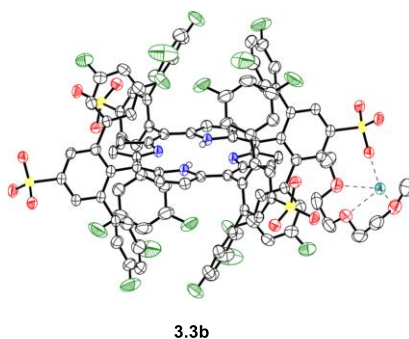
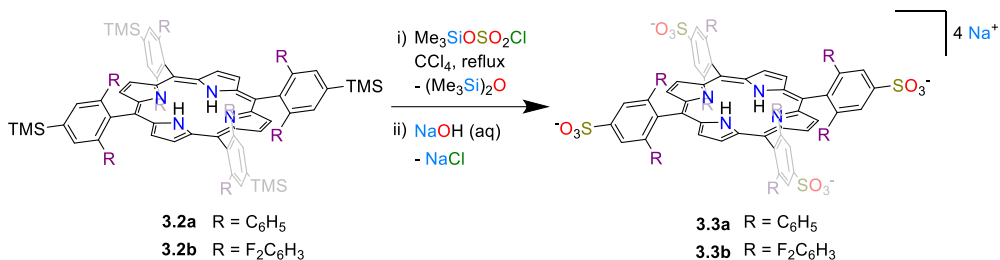


Figure 3.5. Sulfonation of bulky bis-pocket porphyrins. Bottom: thermal ellipsoid plot (50% probability level) of **3.3b** with non-polar H atoms and three of the four Na^+ -diglyme complexes omitted for clarity. Color code: O red, N blue, Cl green, Na teal, C grey, and H white spheres of arbitrary radius.

75°C for 1 h. To demonstrate applicability to other substrates, the tetrasulfonated derivative of **3.2b**, was obtained in an 84% yield (Figure 3.5). This mild reaction

provides a simple means of altering the solubility of the porphyrin. While the starting molecules **3.2a** and **3.2b** are completely insoluble in water and methanol, **3.3a** and **3.3b** can be easily dissolved in these solvents. Saturated aqueous solutions of **3.3a** and **3.3b** have concentrations of 9.5 mM and 5.8 mM, respectively, and the UV-vis spectra of **3.3a** and **3.3b** remain the same as their non-sulfonated counterparts.

Bis-pocket Porphyrin Architecture

The aryl substituents introduced at the 2 and 6 positions of the *meso* phenyl groups create pockets above and below the plane of the porphyrin, giving rise to the “bis-pocket” moniker introduced by Suslick and coworkers.⁵ By changing the electronics and structure of the aryl rings, the pockets can be sculpted. Thirteen of the free-base TMS-functionalized porphyrin compounds derived from **3.1** were successfully crystallized, in addition to **3.2a**, the crystal structure of which was previously discussed in Chapter 2. The diffraction data confirm, in all cases, the connectivity of the desired products. In many cases, the porphyrin resides on an inversion center, but in no case is the planarity of the entire porphyrin core crystallographically required. Nevertheless, the porphyrins exhibit little distortion from planarity, with the greatest deviation (RMSD = 0.091 Å) observed for **3.2c**, R = 3,5-dichlorophenyl.

Since the shapes and volumes of the pockets are impacted significantly by torsion angles, the shallow potential energy profiles of which allow them to be readily deformed by crystal packing forces, there is not expected to be well-defined

relationships between molecular structure and pocket volume. The structures do, however, highlight the variety of pocket shapes and sizes that can be accessed when the substituents are varied. The structures of a number of the compounds (**3.2b**, **3.2e**, **3.2f**, **3.2h**, **3.2k**, **3.2l**, **3.2o**) feature a pocket on either side of the plane of the porphyrin and both pockets contain solvent molecules. The structure of **3.2i** also features two pockets, one above and one below the plane of the porphyrin, but neither contains a solvent molecule. In the structures of **3.2c** and **3.2d**, one pocket contains a solvent molecule, and the other does not. Interestingly, these are two of the most sterically congested porphyrins prepared in this study. This is possibly because the internal motions that open one pocket sufficiently to accommodate a solvent molecule cause the other pocket to collapse.

To quantify these variations in pocket volume, a tool developed to measure the volumes of protein pockets, POVME2, was used (Figure 3.6, Table B.8).¹³ Consistent with the analysis above, the volume estimates for **3.2c**, **3.2d**, and **3.2q** reflect the differences in the volumes of the two pockets; whereas **3.2b**, **3.2e**, **3.2f**, **3.2h**, **3.2i**, **3.2k**, **3.2l**, and **3.2o** each feature pockets with similar or identical volumes (the latter arising in the case of crystallographic equivalence). The volume estimates also highlight the variation in pocket shape from one molecule to the next. For

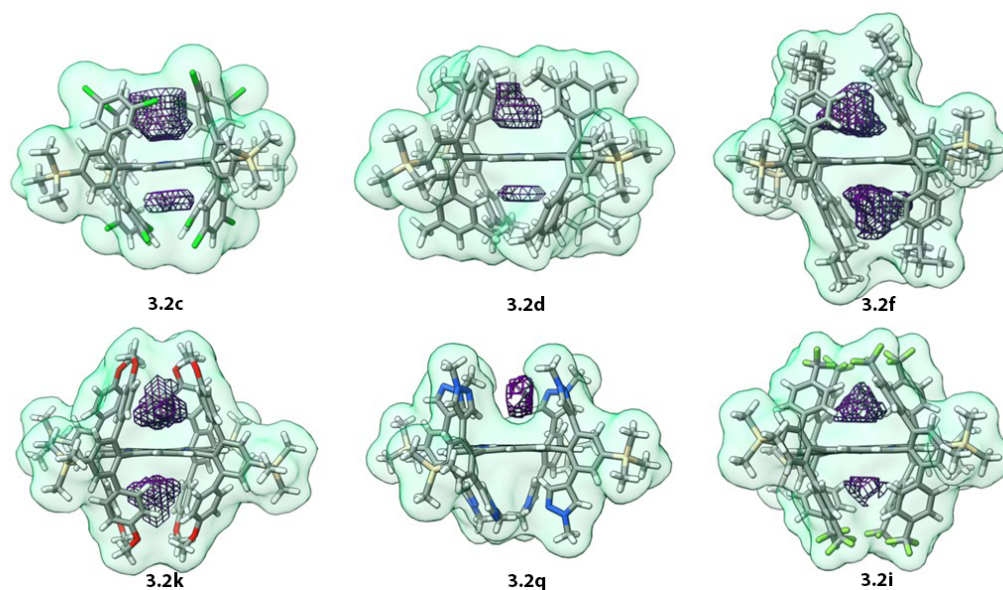


Figure 3.6. Pockets of **3.2c**, **3.2d**, **3.2f**, **3.2k**, **3.2q**, and **3.2i** as calculated with POVME2 using atomic coordinates from single-crystal X-ray diffraction data. The molecules are shown as sticks with a green surface at the van der Waals distance. The pockets are depicted as purple mesh. Atomic color code: C grey, H white, O red, N blue, Si tan, Cl green, F light green. Molecular graphics and analyses performed with UCSF ChimeraX.⁴

example, the volumes of the pockets for **3.2a** and **3.2i** are approximately equal despite the fact that **3.2a** features phenyl substituents and **3.2i** features the taller naphthyl substituents. The increase in pocket height for **3.2i** is offset by a narrowing of the pocket width. While the torsionally defined pockets present in these crystal structures are undoubtedly influenced by crystal packing forces in many instances, they highlight the variability in pocket size/shape that is accessible with this scaffold. This diversity is demonstrated in Figure **3.6**.

3.3 Conclusion

This chapter demonstrates that Pd-catalyzed Suzuki-Miyaura cross-coupling can be readily performed with an easily synthesized free-base porphyrin to access a range of novel porphyrins. This reaction proved versatile in tuning the steric, as shown with the crystallographic data, and electronic properties of the resulting porphyrins. Broad synthetic usefulness was demonstrated by coupling substituents featuring a variety of synthetic handles, rendering the bis-pocket porphyrin products amenable to further modification. The strategically placed TMS groups of the precursor **3.1** and products **3.2** impart organic solubility and can be readily converted to aqueous solubility upon sulfonation with trimethylsilyl chlorosulfonate. Metalation could be readily achieved using standard protocols for some metals, or refluxing 1,2,4-TCB when necessary, generated metaloporphyrins previously unobtainable. This tunable porphyrin platform offers a widely applicable scaffold for research seeking to study or exploit the properties of these molecules.

3.4 Experimental Methods

General considerations. All reactions were performed under N₂ unless otherwise specified. Glassware was oven dried prior to use. All solvents and reagents are commercially available and used as received unless otherwise stated. Compound **3.1** was prepared as previously described.⁹ Suzuki-Miyaura reactions were performed in Chemglass 20-mL reaction vials fitted with pressure relief caps and heated on a hot plate fitted with a Chemglass 4-place pie wedge for 20-mL scintillation vials. For the

purification of **3.3a** and **3.3b**, an Isolera Prime Biotage fitted with a Sfar C18 column was employed. A solution of 1% triethylammonium bicarbonate in water was generated by dissolving 40 mL of triethylamine in 4 L of ultra-pure (UP) water (>18 MΩ cm) followed by the addition of 150 g of dry ice. Analytical HPLC was performed on a Shimadzu Prominence-I LC-2030 Plus fitted with a Phenomenex Luna silica 5 μm 100 Å column (250 × 10 mm). Organic solutions were concentrated under reduced pressure on a Buchi Rotavapor R-100. CDCl₃ and DMSO-*d*6 were purchased from Cambridge Isotope Laboratories and used as received. ¹H, ¹³C{¹H}, and ¹⁹F{¹H} NMR spectra were recorded on a Bruker Avance III HD 500 NMR spectrometer equipped with a multinuclear Smart Probe. Signals in the ¹H and ¹³C NMR spectra are reported in ppm as chemical shifts from tetramethylsilane; ¹⁹F NMR signals are reported in ppm as chemical shifts from CFCl₃. NMR signals were referenced using the CHCl₃ (¹H, 7.26 ppm), DMSO-*d*5 (¹H, 2.50 ppm), or CDCl₃ (¹³C, 77.0 ppm) solvent signals. The following abbreviations were used to explain the multiplicities: s = singlet, d = doublet, t = triplet, q = quartet, m = multiplet, sext = sextet. Solution phase magnetic moments were measured using a modified Evans method.¹⁴ UV-visible absorption spectra were measured on a VWR UV-6300PC dual-beam spectrophotometer. MALDI mass spectra were acquired using timsControl v 1.1.19 on a timsTOF fleX mass spectrometer (Bruker Scientific, Billerica, MA) over the mass range 1000–2500 Da. In positive reflectron mode, laser power was set to 20%, and laser application was set to MS Dried Droplet. In negative reflectron mode, laser power was set to 30%, and laser application was set to MS Dried Droplet.

Compounds were dissolved in DCM or MeOH and 1 μL was mixed with 1 μL of matrix (50:50 α -cyano-4-hydroxycinnamic acid:2,5-dihydroxybenzoic acid in a solution of 70:30 MeCN:H₂O with 0.1% trifluoroacetic acid). Samples were spotted on a stainless steel MSP 96 spot target plate and allowed to air dry. For each compound, 1000 laser shots at 2000 Hz were delivered in a random walk across the spot. Data were subsequently analyzed in DataAnalysis v 5.3 (Bruker Scientific, Billerica, MA). The aqueous solubility of **3.3a** and **3.3b** was assessed by adding sufficient solid to a minimal volume of water such that a portion of solid remained undissolved at room temperature, centrifuging the mixture, removing an aliquot from the supernatant, and determining the concentration of the compound in the aliquot using UV-vis spectroscopy.

X-ray crystallography. Crystals of **3.2b**, **3.2c**, **3.2d**, **3.2e**, **3.2f**, **3.2h**, **3.2i**, **3.2k**, **3.2l**, **3.2m**, **3.2o**, **3.2p**, **3.2q**, **3.3b**, **3.4a**, **3.4b**, **3.4c**, **3.4d**, **3.4e**, and **3.4f** were grown as described in the Experimental Section of this chapter. Single crystals suitable for X-ray diffraction were selected under a microscope, loaded onto a nylon fiber loop using Paratone-N, and mounted onto a Rigaku XtaLAB Synergy-S single-crystal diffractometer. Each crystal was cooled to 100 K under a stream of nitrogen. Diffraction of Cu K α radiation from a PhotonJet-S microfocus source was detected using a HyPix-6000HE hybrid photon counting detector. Screening, indexing, data collection, and data processing were performed with CrysAlis^{Pro}.¹⁵ The structures were solved using SHELXT and refined using SHELXL as implemented in OLEX2

following established strategies.¹⁶⁻¹⁹ Unless otherwise specified in the CIF, all non-H atoms were refined anisotropically and H atoms were placed at calculated positions and refined with a riding model and coupled isotropic displacement parameters. As noted in the appropriate CIFs, a number of the structures featured pockets of disordered solvent that could not be satisfactorily modeled. In these instances, the contribution of the electron density in those pockets to the observed structure factors was masked using Olex2. Refinement parameters are collected in Tables B.1-B.7.

Pocket volume estimation. Pocket volumes were calculated using POVME2.¹³ PDB files of each porphyrin were generated from the corresponding X-ray diffraction coordinates. The grid spacing was set to 0.5 Å and a points-inclusion sphere of 10-Å radius was generated at the center of each porphyrin. A contiguous pocket-seed sphere of 4-Å radius was generated at the center of each porphyrin and a contiguous points criterion of 5 was employed (criteria of 3 and 7 were used for **3.2b** and **3.2m**, respectively). Molecular graphics were generated with UCSF ChimeraX.⁴ Pocket volumes are collected in Table B.8.

General method for Suzuki-Miyaura coupling. Compound **3.1** (100 mg, 0.0656 mmol), 1 mol% per carbon-bromine bond of palladium catalyst (0.0052 mmol), 3 equiv of boronic acid (1.574 mmol), and 4 equiv of cesium carbonate (2.09 mmol) were dissolved in a mixture of toluene (5 mL) and DI water (0.2 mL) in a 20-mL reaction vial fitted with a pressure relief cap. The mixture was sparged with N₂ for 5

min, then sealed and brought to 100 °C on a hot plate and stirred for 20 h. The crude reaction mixture was dry loaded onto silica and purified by normal phase flash chromatography. The eluted product was concentrated under reduced pressure, then redissolved in a minimal amount of chloroform and recrystallized overnight via layering with MeCN. The resulting purple crystals were isolated via vacuum filtration.

Synthesis of 3.2a 5,10,15,20-tetrakis(2,6-diphenyl-4-(trimethylsilyl)phenyl)porphyrin. Synthesized using the general method for Suzuki-Miyaura couplings. Column chromatography run as a ramp to 50% CHCl₃ in hexanes. **3.2a** was isolated as purple crystals (88 mg, 89%). Characterization was consistent with previously reported data (chapter 2, **2.10**). ¹H NMR (500 MHz, CDCl₃) δ 8.38 (s, 8H), 7.77 (s, 8H), 6.55 (d, J = 7.9 Hz, 16H), 6.40 (t, J = 7.2 Hz, 8H), 6.22 (t, J = 7.5 Hz, 16H), 0.50 (s, 36H), -3.46 (s, 2H). ¹³C{¹H} NMR (126 MHz, CDCl₃) δ 144.8, 142.4, 140.8, 139.3, 133.6, 129.4, 126.7, 125.3, 116.1, -0.6; HRMS (MALDI) *m/z*: [M+H]⁺ Calcd for C₁₀₄H₉₅N₄Si₄⁺ 1512.6662; Found 1512.6669; UV/Vis (CHCl₃) λ_{abs} (log ε): 420 (sh), 439 (5.67), 533 (4.32), 570 (4.01), 611 (3.42), 669 (3.48).

Synthesis of 3.2b 5,10,15,20-tetrakis(2,6-di(3,5-difluorophenyl)-4-(trimethylsilyl)phenyl)porphyrin. Synthesized using the general method for Suzuki-Miyaura couplings. Column chromatography run as a ramp to 40% CHCl₃ in hexanes. **3.2b** was isolated as purple crystals (59 mg, 50%). X-ray quality crystals were grown

by layering MeCN over a solution of the product in CHCl₃. ¹H NMR (500 MHz, CDCl₃) δ 8.42 (s, 8H), 7.80 (s, 8H), 6.06 (d, J = 4.4 Hz, 16H), 5.87 – 5.79 (m, 8H), 0.54 (s, 36H), -3.16 (s, 2H). ¹³C{¹H} NMR (126 MHz, CDCl₃) δ 162.6, 162.5, 160.6, 160.5, 144.6, 143.2, 142.3, 138.7, 134.0, 115.7, 112.3, 112.1, 101.8, 101.6, 101.4, -0.7. ¹⁹F{¹H} NMR (470 MHz, CDCl₃) δ -111.49. HRMS (MALDI) *m/z*: [M+H]⁺ Calcd for C₁₀₄H₇₉F₁₆N₄Si⁺ 1800.5155; Found 1800.5142; UV/Vis (CHCl₃) λ_{abs} (log ε): 417 (sh), 435 (5.66), 430 (4.32), 565 (3.98), 608 (3.79), 667 (3.47).

Synthesis of 3.2c 5,10,15,20-tetrakis(2,6-di(3,5-dichlorophenyl)-4-

(trimethylsilyl)phenyl)porphyrin. Synthesized using the general method for Suzuki-Miyaura couplings, but with Pd(PPh₃)₄ as the catalyst. Column chromatography run as a ramp to 10% toluene in pentane. **3.2c** was isolated as purple crystals (74 mg, 70%). X-ray quality crystals were grown by layering MeCN over a solution of the product in CHCl₃. ¹H NMR (500 MHz, CDCl₃) δ 8.47 (s, 8H), 7.76 (s, 8H), 6.45 (d, J = 1.8 Hz, 16H), 6.39 (t, J = 1.8 Hz, 8H), 0.54 (s, 36H), -2.93 (s, 2H). ¹³C{¹H} NMR (126 MHz, CDCl₃) δ 144.3, 142.7, 142.4, 138.2, 134.9, 133.5, 127.5, 126.3, 115.6, -0.7. HRMS (MALDI) *m/z*: [M+H]⁺ Calcd for C₁₀₄H₇₉Cl₁₆N₄Si⁺ 2064.0309; Found 2064.0280; UV/Vis (CHCl₃) λ_{abs} (log ε): 419 (sh), 438 (5.58), 490 (4.06), 530 (4.26), 567 (3.91), 608 (3.72), 668 (3.41)

Synthesis of 3.2d 5,10,15,20-tetrakis(2,6-di(3,5-dimethylphenyl)-4-

(trimethylsilyl)phenyl)porphyrin. Synthesized using the general method for Suzuki-

Miyaura couplings. Column chromatography was performed as a ramp to 30% chloroform in hexanes. **3.2d** was isolated as purple crystals (108 mg, 95%). X-ray quality crystals were grown by layering MeCN over the product in 1,2,4-TCB to give purple plates. ^1H NMR (500 MHz, CDCl_3) δ 8.51 (s, 8H), 7.71 (s, 8H), 6.20 (s, 16H), 5.92 (s, 8H), 1.15 (s, 48H), 0.49 (s, 36H), -3.04 (s, 2H). $^{13}\text{C}\{^1\text{H}\}$ NMR (126 MHz, CDCl_3) δ 145.1, 142.5, 140.3, 138.7, 135.7, 134.6, 127.5, 127.3, 116.7, 20.7, -0.6. HRMS (MALDI) m/z : $[\text{M}+\text{H}]^+$ Calcd for $\text{C}_{120}\text{H}_{127}\text{N}_4\text{Si}_4^+$ 1736.9166; Found 1736.9185; UV/Vis (CHCl_3) λ_{abs} (log ϵ): 418 (sh), 437 (5.66), 532 (4.28), 567 (3.99), 609 (3.74), 669 (3.44).

Synthesis of 3.2e 5,10,15,20-tetrakis(2,6-di(4-methylphenyl)-4-(trimethylsilyl)phenyl)porphyrin. Synthesized using the general method for Suzuki-Miyaura couplings. Column chromatography was performed as a ramp to 40% chloroform in hexanes. **3.2f** was isolated as purple crystals (76 mg, 71%). X-ray quality crystals were grown by layering MeCN over the product in toluene to give purple plates. ^1H NMR (500 MHz, CDCl_3) δ 8.43 (s, 8H), 7.72 (s, 8H), 6.51 (d, $J = 8.1$ Hz, 16H), 6.05 (d, $J = 8.1$ Hz, 16H), 1.70 (s, 24H), 0.50 (s, 36H), -3.31 (s, 2H). $^{13}\text{C}\{^1\text{H}\}$ NMR (126 MHz, CDCl_3) δ 144.7, 140.5, 139.8, 139.3, 134.3, 133.7, 129.3, 127.5, 116.33, 20.8, -0.6. HRMS (MALDI) m/z : $[\text{M}+\text{H}]^+$ Calcd for $\text{C}_{112}\text{H}_{111}\text{N}_4\text{Si}_4^+$ 1624.7914; Found 1624.7885; UV/Vis (CHCl_3) λ_{abs} (log ϵ): 420 (sh), 439 (5.64), 533 (4.28), 569 (3.95), 610 (3.75), 671 (3.39).

Synthesis of 3.2f 5,10,15,20-tetrakis(2,6-di(4-*n*-propylphenyl)-4-

(trimethylsilyl)phenyl)porphyrin. Synthesized using the general method for Suzuki-Miyaura couplings. Column chromatography was performed as a ramp to 20% diethyl ether in hexanes. **3.2f** was not recrystallized and was isolated as a purple solid (85 mg, 70%). X-ray quality crystals were grown by layering a one-to-one mixture of EtOH and MeCN over the product in CHCl₃ to give purple needles. ¹H NMR (500 MHz, CDCl₃) δ 8.38 (s, 8H), 7.74 (s, 8H), 6.46 (d, J = 7.5 Hz, 16H), 6.03 (d, J = 8.2 Hz, 16H), 1.94 – 1.82 (m, 16H), 1.11 (sext, J = 7.4 Hz, 16H), 0.53 – 0.45 (m, 60H), -3.28 (s, 2H). ¹³C{¹H} NMR (126 MHz, CDCl₃) δ 140.0, 139.1, 133.8, 129.3, 126.7, 37.7, 24.4, 13.8, -0.6. HRMS (MALDI) *m/z*: [M+H]⁺ Calcd for C₁₂₈H₁₄₃N₄Si₄⁺ 1849.0417; Found 1849.0427; UV/Vis (CHCl₃) λ_{abs} (log ε): 420 (sh), 440 (5.63), 534 (4.27), 570 (3.95), 611 (3.74), 671 (3.37).

Synthesis of 3.2g 5,10,15,20-tetrakis(2,6-di(4-*tert*-butylphenyl)-4-

(trimethylsilyl)phenyl)porphyrin. Synthesized using the general method for Suzuki-Miyaura couplings but with the reaction time extended to 48 h. Column chromatography was performed as a ramp to 5% chloroform in hexanes. **3.2g** was not recrystallized and was isolated as a purple solid (57 mg, 44%). ¹H NMR (500 MHz, CDCl₃) δ 8.38 (s, 8H), 7.82 (s, 8H), 6.42 – 6.30 (m, 32H), 0.77 (s, 72H), 0.52 (s, 36H), -2.97 (s, 2H). ¹³C{¹H} NMR (126 MHz, CDCl₃) δ 147.7, 145.1, 140.5, 140.0, 138.7, 135.3, 129.5, 124.0, 116.1, 33.9, 31.3, -0.6. HRMS (MALDI) *m/z*: [M+H]⁺

Calcd for $C_{136}H_{159}N_4Si_4^+$ 1961.1669; Found 1961.1690; UV/Vis ($CHCl_3$) λ_{abs} (log ϵ): 422 (sh), 443 (5.68), 537 (4.30), 573 (4.07), 612 (3.79), 672 (3.43).

Synthesis of 3.2h 5,10,15,20-tetrakis(2,6-di(4-fluorophenyl)-4-

(trimethylsilyl)phenyl)porphyrin. Synthesized using the general method for Suzuki-Miyaura couplings. Column chromatography was performed as a ramp to 30% chloroform in hexanes. **3.2h** was isolated as purple crystals (67 mg, 62%). X-ray quality crystals were grown by layering MeCN over the product in toluene at $-20\text{ }^\circ\text{C}$ to give purple plates. ^1H NMR (500 MHz, $CDCl_3$) δ 8.38 (s, 8H), 7.75 (s, 8H), 6.52 (dd, $J = 8.7, 5.4$ Hz, 16H), 5.95 (t, $J = 8.7$ Hz, 16H), 0.52 (s, 36H), -3.35 (s, 2H). $^{13}\text{C}\{^1\text{H}\}$ NMR (126 MHz, $CDCl_3$) δ 161.6, 159.7, 143.9, 141.4, 139.2, 138.2, 138.2, 133.8, 130.9, 130.8, 116.3, 113.7, 113.5, -0.7. $^{19}\text{F}\{^1\text{H}\}$ NMR (470 MHz, $CDCl_3$) δ -116.48. HRMS (MALDI) m/z : $[M+H]^+$ Calcd for $C_{104}H_{87}F_8N_4Si_4^+$ 1656.5909; Found 1656.5879; UV/Vis ($CHCl_3$) λ_{abs} (log ϵ): 419 (sh), 439 (5.66), 533 (4.30), 569, (3.99), 611 (3.76), 670 (3.45).

Synthesis of 3.2i 5,10,15,20-tetrakis(2,6-di(4-trifluoromethylphenyl)-4-

(trimethylsilyl)phenyl)porphyrin. Synthesized using the general method for Suzuki-Miyaura couplings. Column chromatography was performed as a ramp to 10% chloroform in hexanes. **3.2i** was not recrystallized and was isolated as a purple solid (37 mg, 27%). X-ray quality purple needles were grown by layering MeCN over a solution of the product in $CHCl_3$. ^1H NMR (500 MHz, $CDCl_3$) δ 8.40 (s, 8H), 7.80 (s,

8H), 6.59 (d, J = 8.1 Hz, 16H), 6.47 (d, J = 8.2 Hz, 16H), 0.52 (s, 36H), -3.33 (s, 2H). $^{19}\text{F}\{^1\text{H}\}$ NMR (470 MHz, CDCl_3) δ -63.27. $^{13}\text{C}\{^1\text{H}\}$ NMR (126 MHz, CDCl_3) δ 145.5, 143.8, 142.2, 138.5, 134.5, 129.5, 128.2, 128.0, 126.7, 126.5, 124.5, 123.6, 122.3, 120.2, 115.9, -0.7. HRMS (MALDI) m/z : $[\text{M}+\text{H}]^+$ Calcd for $\text{C}_{112}\text{H}_{87}\text{F}_{24}\text{N}_4\text{Si}_4^+$ 2056.5652; Found 2056.5643; UV/Vis (CHCl_3) λ_{abs} (log ϵ): 418 (sh), 437 (5.61), 495 (3.65), 531 (4.26), 567 (3.96), 608 (3.79), 668 (3.48), 700 (2.98).

Synthesis of 3.2j 5,10,15,20-tetrakis(2,6-di(4-nitrophenyl)-4-

(trimethylsilyl)phenyl)porphyrin. Synthesized using the general method for Suzuki-Miyaura couplings, but with $\text{Pd}(\text{PPh}_3)_4$ as the catalyst, 4 equiv of boronic acid, and 48 h reaction time. Column chromatography was performed as a slow ramp from 100% hexanes to 100% chloroform. **3.2j** was not recrystallized and isolated as a purple solid (5.7 mg, 5%). ^1H NMR (500 MHz, CDCl_3) δ 8.38 (s, 8H), 7.84 (s, 8H), 7.11 (d, J = 8.9 Hz, 16H), 6.58 (d, J = 8.9 Hz, 16H), 0.54 (s, 36H), -3.33 (s, 2H). $^{13}\text{C}\{^1\text{H}\}$ NMR (126 MHz, CDCl_3) δ 148.2, 145.9, 143.3, 137.9, 135.0, 130.1, 122.1, 115.9, -0.8. HRMS (MALDI) m/z : $[\text{M}+\text{H}]^+$ Calcd for $\text{C}_{104}\text{H}_{87}\text{N}_{12}\text{O}_{16}\text{Si}_4^+$ 1872.5468; Found 1872.5437; UV/Vis (CHCl_3) λ_{abs} (log ϵ): 423 (sh), 445 (5.42), 536 (4.14), 573 (3.85), 612 (3.60), 671 (3.21).

Synthesis of 3.2k 5,10,15,20-tetrakis(2,6-di(4-methoxyphenyl)-4-

(trimethylsilyl)phenyl)porphyrin. Synthesized using the general method for Suzuki-Miyaura couplings, but with diglyme as the solvent. After reaction completion, the

crude mixture was diluted with hexanes (50 mL) and loaded onto a silica column. The loaded column was washed with hexanes, then 100 mL of 1:1 chloroform/hexanes and then 100 mL of 100% chloroform. The product was then eluted by ramping to 15% methanol in chloroform. **3.2j** was not recrystallized and was isolated as a purple solid (92 mg, 80%). X-ray quality crystals were grown by layering MeCN over the product in CHCl₃ to give purple needles. ¹H NMR (500 MHz, CDCl₃) δ 8.40 (s, 8H), 7.72 (s, 8H), 6.46 (d, J = 8.8 Hz, 16H), 5.78 (d, J = 8.9 Hz, 16H), 3.17 (s, 24H), 0.50 (s, 36H), -3.27 (s, 2H). ¹³C{¹H} NMR (126 MHz, CDCl₃) δ 157.2, 144.5, 140.5, 139.6, 135.0, 133.5, 130.4, 116.5, 112.2, 54.6, -0.6. HRMS (MALDI) *m/z*: [M+H]⁺ Calcd for C₁₁₂H₁₁₁N₄O₈Si₄⁺ 1752.7507; Found 1752.7490; UV/Vis (CHCl₃) λ_{abs} (log ε): 422 (sh), 442 (5.57), 497 (3.76), 535 (4.23), 572 (3.97), 612 (3.74), 671 (3.45).

Synthesis of 3.2l 5,10,15,20-tetrakis(2,6-di(2-naphthyl)-4-

(trimethylsilyl)phenyl)porphyrin. Synthesized using the general method for Suzuki-Miyaura couplings. Column chromatography was performed as a ramp to 50% chloroform in hexanes. **3.2l** was isolated as purple crystals (85.3 mg, 68%). X-ray quality crystals were grown by layering MeCN over a solution of the product in CHCl₃. ¹H NMR (500 MHz, CDCl₃) δ 8.47 (s, 8H), 7.79 (s, 8H), 7.32 (s, 8H), 7.13 – 7.06 (m, 16H), 6.94 (t, J = 7.3 Hz, 8H), 6.81 (d, J = 8.3 Hz, 8H), 5.94 (d, J = 8.3 Hz, 8H), 5.26 (d, J = 8.6 Hz, 8H), 0.51 (s, 36H), -3.56 (s, 2H). ¹³C{¹H} NMR (126 MHz, CDCl₃) δ 144.8, 140.9, 140.1, 139.6, 134.1, 132.4, 131.0, 127.8, 127.5, 127.2, 126.9, 125.3, 125.1, 116.0, -0.6. HRMS (MALDI) *m/z*: [M+H]⁺ Calcd for C₁₃₆H₁₁₁N₄Si₄⁺

1912.7913; Found 1912.7938; UV/Vis (CHCl₃) λ_{abs} (log ϵ): 423 (sh), 444 (5.58), 536 (4.24), 571 (3.93), 611 (3.72), 671 (3.38).

Synthesis of 3.2m 5,10,15,20-tetrakis(2,6-dicyclopropyl-4-

(trimethylsilyl)phenyl)porphyrin. Synthesized using the general method for Suzuki-Miyaura couplings. Column chromatography was performed as a ramp to 50% chloroform in hexanes. **3.2m** was not recrystallized and was isolated as a purple solid (26 mg, 32%). X-ray quality crystals were grown by layering MeCN over the product in CHCl₃ to give purple needles. ¹H NMR (500 MHz, CDCl₃) δ 8.66 (s, 8H), 7.22 (s, 8H), 1.15 – 1.09 (m, 8H), 0.67 – 0.61 (m, 16H), 0.46 (s, 36H), 0.05 – -0.03 (m, 16H), -2.29 (s, 2H). ¹³C{¹H} NMR (126 MHz, CDCl₃) δ 143.4, 143.3, 140.5, 125.2, 117.3, 15.8, 8.7, -0.6. HRMS (MALDI) m/z : [M+H]⁺ Calcd for C₈₀H₉₅N₄Si₄⁺ 1223.6628; Found 1223.6599; UV/Vis (CHCl₃) λ_{abs} (log ϵ): 404 (sh), 422 (5.55), 516 (4.16), 550 (3.62), 591 (3.63), 646 (3.26).

Synthesis of 3.2n 5,10,15,20-tetrakis(2,6-di(4-vinylphenyl)-4-

(trimethylsilyl)phenyl)porphyrin. Synthesized using the general method for Suzuki-Miyaura couplings. Column chromatography was performed as a ramp to 30% chloroform in hexanes. **3.2n** was not recrystallized and was isolated as a purple solid (37 mg, 33%). ¹H NMR (500 MHz, CDCl₃) δ 8.42 (s, 8H), 7.76 (s, 8H), 6.49 (d, J = 8.2 Hz, 16H), 6.27 (d, J = 8.3 Hz, 16H), 6.03 (dd, J = 17.6, 10.9 Hz, 8H), 5.14 (d, J = 17.5 Hz, 8H), 4.77 (d, J = 11.3 Hz, 8H), 0.51 (s, 36H), -3.27 (s, 2H). ¹³C{¹H} NMR

(126 MHz, CDCl₃) δ 144.7, 142.1, 140.9, 139.2, 136.3, 134.4, 133.8, 129.6, 124.8, 116.2, 113.1, -0.7. HRMS (MALDI) m/z : [M+H]⁺ Calcd for C₁₂₀H₁₁₁N₄Si₄⁺ 1720.7914; Found 1720.7893; UV/Vis (CHCl₃) λ_{abs} (log ϵ): 422 (sh), 443 (5.38), 536 (4.05), 571 (3.76), 612 (3.55), 672 (3.25).

Synthesis of 3.2o 5,10,15,20-tetrakis(2,6-di(4-trimethylsilylphenyl)-4-

(trimethylsilyl)phenyl)porphyrin. Synthesized using the general method for Suzuki-Miyaura couplings, but with 4 equiv of boronic acid. Column chromatography was performed as a ramp to 5% toluene in hexanes. **3.2o** was not recrystallized and was isolated as a purple solid (64 mg, 47%). X-ray quality crystals were grown by layering a one-to-one mixture of EtOH and MeCN over the product in CHCl₃ to give purple needles. ¹H NMR (500 MHz, CDCl₃) δ 8.38 (s, 8H), 7.79 (s, 8H), 6.52 (d, J = 7.6 Hz, 16H), 6.42 (d, J = 7.4 Hz, 16H), 0.50 (s, 36H), -0.26 (s, 72H), -3.05 (s, 2H). ¹³C{¹H} NMR (126 MHz, CDCl₃) δ 145.4, 143.5, 140.6, 138.5, 136.5, 135.7, 132.3, 129.3, 115.7, -0.6, -0.9. HRMS (MALDI) m/z : [M+H]⁺ Calcd for C₁₂₈H₁₅₉N₄Si₁₂⁺ 2088.9824; Found 2088.9763; UV/Vis (CHCl₃) λ_{abs} (log ϵ): 424 (sh), 444 (5.63), 538 (4.31), 574 (4.07), 612 (3.85), 671 (3.52).

Synthesis of 3.2p 5,10,15,20-tetrakis(2,6-di(4-ethoxycarbonylphenyl)-4-

(trimethylsilyl)phenyl)porphyrin. Synthesized using the general method for Suzuki-Miyaura couplings, but with diglyme as the solvent and 4 equiv of boronic acid. After reaction completion, the crude mixture was diluted with hexanes (50 mL) and loaded

onto a silica column. The loaded column was washed with hexanes, then 100 mL of 1:1 chloroform/hexanes, and then 100 mL of 100% chloroform. The product was then eluted by ramping to 15% methanol in chloroform. **3.2p** was not recrystallized and was isolated as a purple solid (55 mg, 40%). X-ray quality crystals were grown by layering MeCN over the product in toluene at $-20\text{ }^{\circ}\text{C}$ to give purple plates. ^1H NMR (500 MHz, CDCl_3) δ 8.30 (s, 8H), 7.80 (s, 8H), 6.95 (d, $J = 8.0$ Hz, 16H), 6.47 (d, $J = 7.9$ Hz, 16H), 3.92 (q, $J = 7.0$ Hz, 16H), 0.96 (t, $J = 7.0$ Hz, 24H), 0.53 (s, 36H), -3.31 (s, 2H). $^{13}\text{C}\{^1\text{H}\}$ NMR (126 MHz, CDCl_3) δ 165.7, 146.8, 144.5, 141.6, 138.6, 134.8, 129.6, 128.1, 127.8, 115.6, 60.5, 14.1, -0.7. HRMS (MALDI) m/z : $[\text{M}+\text{H}]^+$ Calcd for $\text{C}_{128}\text{H}_{127}\text{N}_4\text{O}_{16}\text{Si}_4^+$ 2088.8353; Found 2088.8318; UV/Vis (CHCl_3) λ_{abs} (log ϵ): 424 (sh), 444 (5.64), 537 (4.31), 574 (4.09), 613 (3.83), 672 (3.61).

Synthesis of 3.2q 5,10,15,20-tetrakis(2,6-di(*N*-methylpyrazolyl)-4-

(trimethylsilyl)phenyl)porphyrin. Synthesized using the general method for Suzuki-Miyaura couplings, but with diglyme as the solvent and 4 equiv of boronic acid. After reaction completion, the crude mixture was diluted with hexanes (50 mL) and loaded onto a silica column. The loaded column was washed with hexanes, then 100 mL of 1:1 chloroform/hexanes, and then 100 mL of 100% chloroform. The product was then eluted by ramping to 15% methanol in chloroform. **3.2q** was not recrystallized and was isolated as a purple solid (81 mg, 80%). X-ray quality crystals were grown by layering diethyl ether over the product in CHCl_3 to give purple plates. ^1H NMR (500 MHz, CDCl_3) δ 8.51 (s, 8H), 7.79 (s, 8H), 6.29 (s, 8H), 5.73 (s, 8H), 2.88 (s, 24H),

0.51 (s, 36H), -2.64 (s, 2H). $^{13}\text{C}\{^1\text{H}\}$ NMR (126 MHz, CDCl_3) δ 141.4, 138.0, 137.6, 135.6, 131.7, 128.6, 123.0, 118.0, 38.2, -0.7. HRMS (MALDI) m/z : $[\text{M}+\text{H}]^+$ Calcd for $\text{C}_{88}\text{H}_{95}\text{N}_{20}\text{Si}_4^+$ 1543.7120; Found 1543.7139; UV/Vis (CHCl_3) λ_{abs} (log ϵ): 412 (sh), 431 (5.57), 524 (4.27), 559 (3.71), 598 (3.78), 656 (3.4).

Larger Scale Synthesis of 3.2h 5,10,15,20-tetrakis(2,6-di(4-fluorophenyl)-4-(trimethylsilyl)phenyl)porphyrin. This procedure demonstrates that the coupling can be performed on a scale such that 1 mmol of arylboronic acid is coupled to the porphyrin framework. Compound **3.1** (200 mg, 0.1311 mmol), 1 mol% per carbon-bromine bond of (dppf) PdCl_2 (0.0105 mmol), 3 equiv of 4-fluorophenylboronic acid (3.1455 mmol), and 4 equiv of cesium carbonate (4.1940 mmol) were dissolved in a mixture of toluene (10 mL) and DI water (0.4 mL) in a 20-mL reaction vial fitted with a pressure relief cap. The mixture was sparged with N_2 for 5 min, then sealed and brought to 100 °C and stirred for 20 h. The crude reaction mixture was dry loaded onto silica and purified by normal phase flash chromatography. Column chromatography was performed as a ramp to 30% chloroform in hexanes. The eluted product was concentrated under reduced pressure, then redissolved in a minimal amount of chloroform and recrystallized overnight via layering with MeCN. The resulting purple crystals were isolated via vacuum filtration. **3.2h** was isolated as purple crystals (154 mg, 71%).

Sulfonations

Synthesis of 3.3a sodium 5,10,15,20-tetrakis(2,6-diphenyl-4-(sulfonato)phenyl)porphyrin. Compound **3.2a** (50 mg, 0.0331 mmol) and 4.8 equiv of trimethylsilyl chlorosulfonate (24 μ L, 0.1589 mmol) were dissolved in carbon tetrachloride (5 mL) in a 20-mL reaction vial fitted with a pressure release cap. The reaction was sealed and incubated at 75 °C for 2 h. The reaction was removed from heat and quenched with 5 mL of 1 M NaOH_(aq) and stirred vigorously for 30 min. The crude mixture was concentrated under reduced pressure and purified by reverse phase flash column chromatography using a ramp to 95% acetonitrile in water with 1% triethylammonium bicarbonate. The eluted product was diluted with 20 mL of brine and dialyzed overnight against DI water through a 3.5 kDa MWCO membrane. The solution was concentrated under reduced pressure and **3.3a** was isolated as a purple solid (32 mg, 60%). ¹H NMR (500 MHz, DMSO-*d*₆) δ 8.41 (s, 8H), 7.87 (s, 8H), 6.50 (d, J = 7.7 Hz, 16H), 6.42 (t, J = 7.2 Hz, 8H), 6.28 (t, J = 7.5 Hz, 16H), -3.69 (s, 2H). ¹³C{¹H} NMR (126 MHz, DMSO-*d*₆) δ 148.2, 144.4, 141.1, 137.7, 128.5, 126.8, 125.7, 125.6, 115.5; HRMS (MALDI) *m/z*: [M-4Na+3H]⁻ Calcd for C₉₂H₆₁N₄O₁₂S₄⁻ 1541.3174; Found 1541.3159; UV/Vis (H₂O) λ_{abs} (log ϵ): 416 (sh), 435 (5.29), 529 (3.94), 565 (3.48), 606 (3.40), 665 (2.96)

Synthesis of 3.3b sodium 5,10,15,20-tetrakis(2,6-di(3,5-difluorophenyl)-4-(sulfonato)phenyl)porphyrin. Compound **3.2b** (50 mg, 0.0278 mmol) and 12 equiv of trimethylsilyl chlorosulfonate (51 μ L, 0.334 mmol) were dissolved in carbon tetrachloride (5 mL) in a 20-mL reaction vial fitted with a pressure release cap. The

reaction was sealed and incubated at 75 °C for 1 h. The reaction was taken off heat and quenched with 5 mL of 1M NaOH (aq) and stirred vigorously for 30 min. The crude mixture was concentrated under reduced pressure and purified by reverse phase flash column chromatography using a ramp to 95% acetonitrile in water with 1% triethylammonium bicarbonate. The eluted product was diluted with 20 mL of brine and dialyzed overnight against DI water through a 3.5 kDa MWCO membrane. The solution was concentrated under reduced pressure and **3.3b** was isolated as a purple solid (45 mg, 84%). X-ray quality crystals were grown by vapor diffusion of diethyl ether into a solution of the product in 1:1 methanol/diglyme to give purple plates.

HRMS (MALDI) m/z : $[M-4Na+3H]^-$ Calcd for $C_{92}H_{45}F_{16}N_4O_{12}S_4^-$ 1829.1667; Found 1829.1639; 1H NMR (500 MHz, DMSO- d_6) δ 8.58 (s, 8H), 7.96 (s, 8H), 6.29 – 6.01 (m, 24H), -3.44 (s, 2H). $^{19}F\{^1H\}$ NMR (470 MHz, DMSO- d_6) δ -110.91. $^{13}C\{^1H\}$ NMR (126 MHz, DMSO- d_6) δ 161.9, 161.8, 159.9, 159.8, 148.9, 143.9, 142.5, 137.3, 126.3, 114.8, 111.7, 111.5, 101.9, 101.7, 101.5; UV/Vis (H₂O) λ_{abs} (log ϵ): 414 (sh), 432 (5.29), 527 (3.94), 568 (3.48), 607 (3.40), 665 (3.36)

Synthesis of 3.4a 5,10,15,20-tetrakis(2,6-diphenyl-4-

(trimethylsilyl)phenyl)porphyrinatoaquazinc(II). Compound **3.2a** (50 mg, 0.033 mmol), zinc(II) acetate dihydrate (700 mg, 3.20 mmol), pyridine (0.1 mL), DMF (5 mL), and a stir bar were added to a 15-mL round bottom flask outfitted with a reflux condenser under a stream of nitrogen. The reaction was heated to reflux in an oil bath and allowed to stir overnight (16 h). UV-vis spectroscopy was used to confirm

product formation. The reaction was diluted with water and the resulting precipitate was collected by vacuum filtration. The solid was purified by column chromatography (silica gel, chloroform:hexanes 1:1). The product fractions were concentrated under reduced pressure to give the product as a blue-purple solid (40 mg, 76%). X-ray quality crystals were grown by layering MeCN over the product dissolved in CHCl_3 . ^1H NMR (500 MHz, CDCl_3) δ 8.48 (s, 8H), 7.76 (s, 8H), 6.62 (d, $J = 7.1$ Hz, 16H), 6.37 (t, $J = 7.1$ Hz, 8H), 6.20 (t, $J = 7.2$ Hz, 16H), 0.51 (s, 36H), -1.29 (s, 2H). $^{13}\text{C}\{^1\text{H}\}$ NMR (126 MHz, CDCl_3) δ 149.8, 144.6, 142.9, 140.3, 133.4, 131.5, 129.5, 126.4, 125.1, 116.7, -0.6; HRMS (MALDI) m/z : $[\text{M}+\text{H}-\text{OH}]^+$ Calcd for $\text{C}_{104}\text{H}_{93}\text{N}_4\text{Si}_4^+$ 1574.5796; Found 1574.5760; UV/Vis (CHCl_3) λ_{abs} (log ϵ): 422 (sh), 444 (5.58), 572 (4.22), 613 (3.50).

Synthesis of 3.4b 5,10,15,20-tetrakis(2,6-diphenyl-4-

(trimethylsilyl)phenyl)porphyrinatocopper(II). Compound **3.2a** (50 mg, 0.033 mmol), copper(II) chloride dihydrate (563 mg, 3.30 mmol), pyridine (0.1 mL), DMF (5 mL), and a stir bar were added to a 15-mL round bottom flask outfitted with a reflux condenser under a stream of nitrogen. The reaction was heated to reflux in an oil bath and allowed to stir overnight (16 h). UV-vis spectroscopy was used to confirm product formation. The reaction was diluted with water and the resulting precipitate was collected by vacuum filtration. The solid was purified by column chromatography (silica gel, chloroform:hexanes 1:1). The product fractions were concentrated under reduced pressure to give the product as a red solid (51 mg, 98%).

X-ray quality crystals were grown by layering MeCN over the product dissolved in CHCl₃. HRMS (MALDI) *m/z*: [M+H]⁺ Calcd for C₁₀₄H₉₃CuN₄Si₄⁺ 1573.5801; Found 1573.5765; μ_{eff} (Evans', CDCl₃): 1.94 μ_{B} ; UV/Vis (CHCl₃) λ_{abs} (log ϵ): 414 (sh), 436 (5.49), 557 (4.25). HPLC (Silica, hexane/DCM = ramp to 100% DCM, flow rate = 3.0 mL/min, λ = 400 nm) t_{R} = 11.7 min (96%)

Synthesis of 3.4c 5,10,15,20-tetrakis(2,6-diphenyl-4-

(trimethylsilyl)phenyl)porphyrinatopalladium(II). Compound **3.2a** (52 mg, 0.034 mmol), palladium(II) acetate (5.7 mg, 0.033 mmol), 2,6-lutidine (0.1 mL), 1,2,4-TCB (5 mL), and a stir bar were added to a 15-mL round bottom flask outfitted with a reflux condenser under a stream of nitrogen. The reaction was heated to reflux in an oil bath and allowed to stir overnight (16 h). UV-vis spectroscopy was used to confirm product formation. The reaction was diluted with water and the resulting precipitate was collected by vacuum filtration. The solid was purified by column chromatography (silica gel, chloroform:hexanes, ramp chloroform to 1:1). The product fractions were concentrated under reduced pressure to give the product as a red-purple solid (13 mg, 25%). X-ray quality crystals were grown by layering MeCN over the product dissolved in CHCl₃. ¹H NMR (500 MHz, CDCl₃) δ 8.33 (s, 8H), 7.76 (s, 8H), 6.50 (d, *J* = 7.8 Hz, 16H), 6.40 (t, *J* = 7.3 Hz, 8H), 6.21 (t, *J* = 7.6 Hz, 16H), 0.49 (s, 36H). ¹³C{¹H} NMR (126 MHz, CDCl₃) δ 144.5, 142.3, 141.4, 133.6, 130.6, 129.3, 126.6, 125.2, 117.9, -0.6; HRMS (MALDI) *m/z*: [M+H]⁺ Calcd for

$C_{104}H_{93}N_4PdSi_4^+$ 1616.5544; Found 1616.5521; UV/Vis ($CHCl_3$) λ_{abs} (log ϵ): 437 (5.2), 532 (sh), 541 (4.11), 573 (2.94).

Synthesis of 3.4d 5,10,15,20-tetrakis(2,6-diphenyl-4-

(trimethylsilyl)phenyl)porphyrinatocobalt(II). Compound **3.2a** (100 mg, 0.0662 mmol), 10 equiv of 2,6-lutidine (0.662 mmol), and 100 equiv of $CoCl_2$ hexahydrate (6.62 mmol) were dissolved in 1,2,4-TCB (5 mL) in a 20-mL reaction vial fitted with a pressure relief cap. The reaction mixture was heated at 213 °C without the cap for 30 min to remove water. The reaction was then sealed and allowed to stir at 213 °C for 2 h on a hot plate fitted with a Chemglass 4-place pie wedge for 20-mL scintillation vials. The crude reaction mixture was diluted with hexanes (50 mL), wet loaded onto a silica column, and purified by normal phase flash chromatography. The product was eluted in a 1:1 solvent mixture of hexanes:chloroform and concentrated under reduced pressure to yield the isolated product as a red solid (96 mg, 91%). X-ray quality crystals were grown by layering MeCN over the product in $CHCl_3$ to give red plates. HRMS (MALDI) m/z : $[M+H]^+$ Calcd for $C_{104}H_{93}CoN_4Si_4^+$ 1569.5838; Found 1569.5807; μ_{eff} (Evans', $CDCl_3$): 1.99 μ_B ; UV/Vis ($CHCl_3$) λ_{abs} (log ϵ): 432 (5.29), 546 (4.15). HPLC (Silica, hexane/DCM = ramp to 100% DCM, flow rate = 3.0 mL/min, λ = 400 nm) t_R = 11.1 min (97%)

Synthesis of 3.4e 5,10,15,20-tetrakis(2,6-diphenyl-4-

(trimethylsilyl)phenyl)porphyrinatochloroiron(III). Compound **3.2a** (73 mg,

0.0483 mmol), 10 equiv of 2,6-lutidine (0.483 mmol), and 100 equiv of FeCl₂ (4.83 mmol) were dissolved in 1,2,4-TCB (5 mL) under an aerobic atmosphere in a 20-mL reaction vial fitted with a pressure relief cap. The reaction mixture was sealed and heated to 213 °C for 1 h on a hot plate fitted with a Chemglass 4-place pie wedge for 20-mL scintillation vials. The crude reaction mixture was diluted with hexanes, loaded onto a silica column, and purified by normal phase flash chromatography. The product was eluted in a 1:1 solvent mixture of hexanes:chloroform and concentrated under reduced pressure to yield the isolated product as deep purple crystals (63 mg, 82%). X-ray quality crystals were grown by layering MeCN over the product dissolved in chloroform. ¹H NMR (500 MHz, CDCl₃; paramagnetic) δ 80.42 (β-pyrrole); μ_{eff} (Evans', CDCl₃): 5.65 μ_B; UV/Vis (CHCl₃) λ_{abs} (log ε): 361 (4.56), 372 (sh), 444 (5.17), 552 (3.86), 579 (3.72), 593 (sh), 678 (sh), 707 (3.61); HRMS (MALDI) *m/z*: [M+H]⁺ Calcd for C₁₀₄H₉₃ClFeN₄Si₄⁺ 1601.5543; Found 1601.5447; [M-Cl]⁺ Calcd for C₁₀₄H₉₂FeN₄Si₄⁺ 1565.5776; Found 1565.5761. HPLC (Silica, hexane/DCM = ramp to 100% DCM, flow rate = 3.0 mL/min, λ = 440 nm) t_R = 8.7 min (99%)

Synthesis of 3.4f 5,10,15,20-tetrakis(2,6-di(3,5-dimethylphenyl)-4-(trimethylsilyl)phenyl)porphyrinatochloroiron(III). Compound **3.2d** (49 mg, 0.0281 mmol), 10 equiv of 2,6-lutidine (0.281 mmol), and 100 equiv of iron(II) chloride (1.40 mmol) were dissolved in 1,2,4-TCB (5 mL) under an aerobic atmosphere in a 20 mL reaction vial fitted with a pressure relief cap. The reaction

mixture was sealed and heated to 213 °C for 6 h on a hot plate fitted with a Chemglass 4-place pie wedge for 20-mL scintillation vials. The crude reaction mixture was diluted with hexanes, wet loaded onto a silica column, and purified by normal phase flash chromatography. The product was eluted in a 1:1 solvent mixture of hexanes: chloroform and concentrated under reduced pressure to yield the isolated product as deep purple crystals (36 mg, 71%). X-ray quality crystals were grown by layering MeCN over the product dissolved in toluene. HRMS (MALDI) m/z : $[M+H]^+$ Calcd for $C_{120}H_{125}ClFeN_4Si_4^+$ 1825.8047; Found 1825.8016; $[M-Cl]^+$ Calcd for $C_{120}H_{124}FeN_4Si_4^+$ 1789.8280; Found 1789.8306; UV/Vis ($CHCl_3$) λ_{abs} (log ϵ): 379 (4.45), 442 (5.03), 520 (4.13), 588 (3.62), 707 (3.61). 1H NMR (500 MHz, $CDCl_3$; paramagnetic) δ 81.06 (β -pyrrole); μ_{eff} (Evans', $CDCl_3$): 6.59 μ_B . HPLC (Silica, hexane/DCM = ramp to 100% DCM, flow rate = 3.0 mL/min, λ = 440 nm) t_R = 9.2 min (98%)

1.5 References

1. Rothemund, P., Formation of Porphyrins from Pyrrole and Aldehydes. *J. Am. Chem. Soc.* **1935**, *57*, 2010-2011.
2. Adler, A. D.; Longo, F. R.; Finarelli, J. D.; Goldmacher, J.; Assour, J.; Korsakoff, L., A Simplified Synthesis for *meso*-Tetraphenylporphine. *J. Org. Chem.* **1967**, *32*, 476-476.
3. Lindsey, J. S.; Wagner, R. W., Investigation of the Synthesis of Ortho-Substituted Tetraphenylporphyrins. *J. Org. Chem.* **1989**, *54*, 828-836.
4. Pettersen, E. F.; Goddard, T. D.; Huang, C. C.; Meng, E. C.; Couch, G. S.; Croll, T. I.; Morris, J. H.; Ferrin, T. E., UCSF ChimeraX: Structure visualization for researchers, educators, and developers. *Protein Sci.* **2020**, *30*, 70-82.

5. Suslick, K. S.; Fox, M. M., A Bis-Pocket Porphyrin. *J. Am. Chem. Soc.* **1983**, *105*, 3507-3510.
6. Maluenda, I.; Navarro, O., Recent Developments in the Suzuki-Miyaura Reaction: 2010–2014. *Molecules* **2015**, *20*, 7528-7557.
7. Farhang, M.; Akbarzadeh, A. R.; Rabbani, M.; Ghadiri, A. M., A retrospective-prospective review of Suzuki–Miyaura reaction: From cross-coupling reaction to pharmaceutical industry applications. *Polyhedron* **2022**, *227*, 116124.
8. Lima, C. F. R. A. C.; Rodrigues, A. S. M. C.; Silva, V. L. M.; Silva, A. M. S.; Santos, L. M. N. B. F., Role of the Base and Control of Selectivity in the Suzuki-Miyaura Cross-Coupling Reaction. *ChemCatChem* **2014**, 1291-1302.
9. Droege, D. G.; Johnstone, T. C., A water-soluble iron-porphyrin complex capable of rescuing CO-poisoned red blood cells. *Chem. Commun.* **2022**, *58*, 2722-2725.
10. Littke, A. F.; Fu, G. C., Palladium-Catalyzed Coupling Reactions of Aryl Chlorides. *Angew. Chem., Int. Ed.* **2002**, *41*, 4176-4211.
11. Miyaura, N.; Yanagi, T.; Suzuki, A., The Palladium-Catalyzed Cross-Coupling Reaction of Phenylboronic Acid with Haloarenes in the Presence of Bases. *Synth. Commun.* **2006**, *11*, 513-519.
12. Ye, B.-H.; Naruta, Y., A novel method for the synthesis of regiospecifically sulfonated porphyrin monomers and dimers. *Tetrahedron* **2003**, *59*, 3593-3601.
13. Durrant, J. D.; Votapka, L.; Sørensen, J.; Amaro, R. E., POVME 2.0: An Enhanced Tool for Determining Pocket Shape and Volume Characteristics. *J. Chem. Theory Comput.* **2014**, *10*, 5047-5056.
14. Schubert, E. M., Utilizing the Evans method with a superconducting NMR spectrometer in the undergraduate laboratory. *J. Chem. Educ.* **1992**, *69*.
15. Rigaku Oxford Diffraction *CrysAlis^{Pro} software system*, version 1.171.40.78a; Rigaku Corporation: Wroclaw, Poland, **2020**.
16. Sheldrick, G. M., *SHELXT* – Integrated space-group and crystal-structure determination. *Acta Crystallogr. Sect. A* **2015**, *71*, 3-8.
17. Sheldrick, G. M., Crystal structure refinement with *SHELXL*. *Acta Crystallogr. Sect. C* **2015**, *71*, 3-8.

18. Dolomanov, O. V.; Bourhis, L. J.; Gildea, R. J.; Howard, J. A. K.; Puschmann, H., *OLEX2: a complete structure solution, refinement and analysis program. J. Appl. Crystallogr.* **2009**, *42*, 339-341.

19. Müller, P., Practical suggestions for better crystal structures. *Crystallogr. Rev.* **2009**, *15*, 57-83.

Chapter 4

Derivatives of a Modular Water-Soluble Iron-Porphyrin Complex for the Sequestration of Carbon Monoxide

4.1 Introduction

Chapter 2 explored a synthetic iron porphyrin with a bis-pocket motif to act as a potential CO poisoning antidote. Taking inspiration from a previously reported bis-pocket heme model from the Suslick group, I synthesized a water-soluble iron porphyrin with a similar bis-pocket architecture. I demonstrated that this complex could not only bind CO but bind it with a higher affinity than hemoglobin. I also showed that the complex could sequester CO from CO-poisoned red blood cells. The synthetic approach was intentionally designed to be modular to allow for rapid derivatization, which in turn can allow a class of compounds to quickly progress through structure-activity-relationship (SAR) studies.¹ Chapter 3 then demonstrated the synthetic feasibility of derivatizing the modular scaffold.

The purpose of this chapter is to combine the proof-of-concept molecule from Chapter 2 with the synthetic advancements of Chapter 3 and start to investigate the properties of derivatives with a drug discovery mindset. A preliminary SAR investigation will be

described, with an emphasis on some of the properties that were noted in Chapter 2 (Figure 4.1). The synthetic usefulness of this scaffold's designed modularity will be demonstrated by synthesizing a small library of derivatives. This chapter will then explore how changes in the bis-pocket motif of our potential CO poisoning antidotes

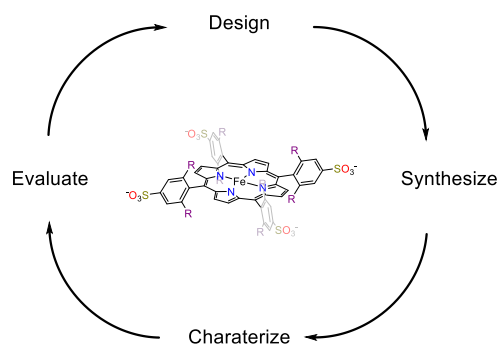


Figure 4.1. Diagram of a SAR cycle.

affect solubility, CO binding, and stability. Finally, it will be shown that a derivative of **2.12** from Chapter 2 still maintains the ability to sequester CO from COHb

4.1 Results and Discussion

Synthesis

To begin, a handful of derivatives were targeted that would allow investigation into any potential steric and electronic trends that could emerge as the bis-pocket motif of the platform is systematically changed. Bulkier groups were added to potentially affect the stability of our CO-bound species. Polarity was modulated to change the overall solubility of our derivatives.

To synthesize these derivatives, the methodologies previously discussed in Chapter 3 were employed. I began by synthesizing 5,10,15,20-tetrakis(2,6-dibromo-4-(trimethylsilyl)phenyl)porphyrin. As demonstrated in the earlier chapters, the bromine atoms acted as synthetic handles for the bis-pocket motif to be installed via a Suzuki coupling reaction. By incorporating the bis-pocket motif after macrocyclization of the porphyrin, I was able to greatly improve the yield over previously reported methodologies.² This also facilitated late-stage derivatization, crucial when trying to investigate SAR. Free base porphyrins **3.2a**, **3.2b**, **3.2d**, **3.2e**, **3.2h**, **3.2i**, **3.2k**, **3.2q** were synthesized as described in Chapter 3. Refluxing the free base porphyrin in 1,2,4-TCB with FeCl₂ and lutidine allowed iron to be inserted into these derivatives (Figure 4.2). I targeted eight derivatives that would encompass changes in sterics and electronics. Adding methyl groups would increase bulk to

potentially affect stability and act as electron donors (**4.3b**, **4.3c**). Incorporation of electron-withdrawing groups, like fluorine, would complement the insight gained

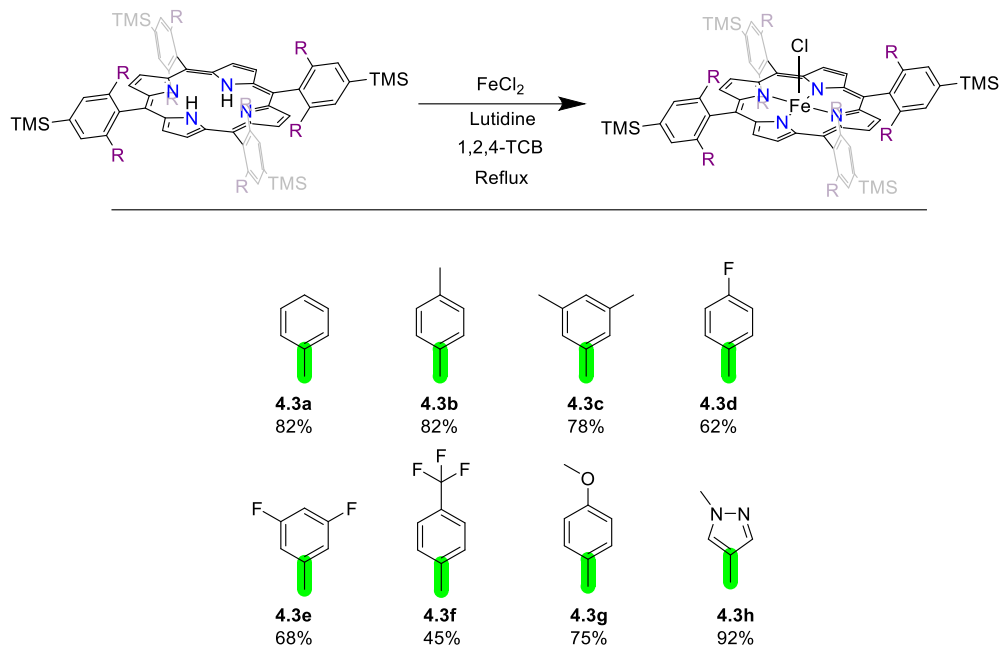


Figure 4.2. Metalation of the target derivatives. Yields shown are isolated yields.

from methyl addition (**4.3d**, **4.3e**, **4.3f**). The strongly electron-donating nature of **4.3g** would allow for comparison to the strong electron-withdrawing effect imparted by **4.3f**. Finally, **4.3h** was added primarily because it was noted in Chapter 2 that the corresponding porphyrin had markedly increased solubility in polar solvents during its purification. Compound **4.3h** will also allow insight into the effects of introducing heterocycles to the CO binding pocket.

To impart water solubility, the derivatives from Figure 4.2 were then sulfonated with trimethylsilyl chlorosulfonate as described in Chapter 3 (Figure 4.3). Unlike Chapter 3, the counter cation was not exchanged to sodium in order to

simplify generating this library of derivatives. The derivatives were studied as the triethylammonium salts obtained directly from purification via reverse phase

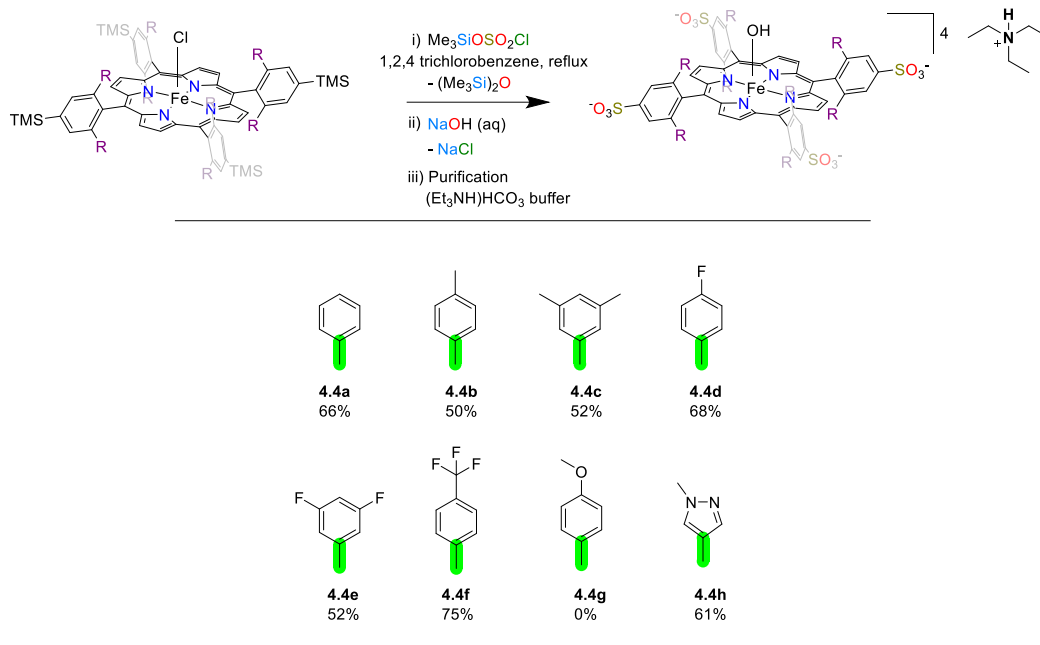
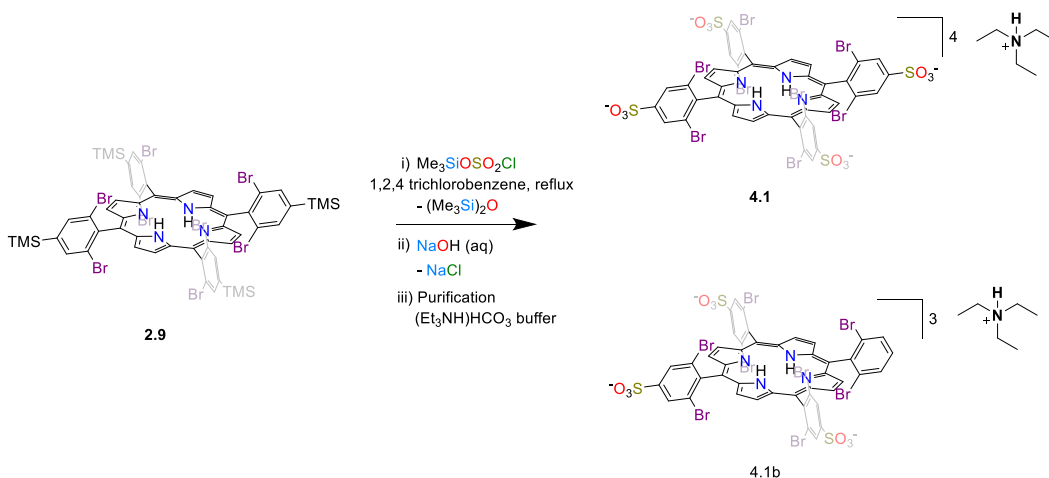


Figure 4.3. Sulfonation of the target derivatives. Yields shown are isolated yields.

chromatography, rather than being subjected to a subsequent salt metathesis followed by extensive desalting via dialysis. The influence of the counterion will be investigated in future biological work, but by holding the counterion constant across the derivatives explored here, the systematic influence of different substituents can still be explored. Of the derivatives from Figure 4.2, only **4.3g** was unsuccessfully sulfonated in this manner. Varying the sulfonation reaction conditions, by changing equivalents of sulfonating agent, time, or temperature, always resulted in over-sulfonation of **4.3g** as determined by mass spectrometric analysis. Using 1 equiv or less of sulfonating agent resulted in not all TMS groups being converted to sulfonates,

and more than 1 equiv would lead to extra sulfonate groups, most likely adding to the methoxy-substituted aryl rings. I hypothesize that over-sulfonation is likely due to the electron-rich nature of the methoxy group. To address the over-sulfonation, I decided that rearranging the order of the synthetic steps might allow the synthesis of the desired product and avoid over-sulfonation. I hypothesized that if I performed the Suzuki couplings after sulfonation, I could avoid the undesired reactions with trimethylsilyl chlorosulfonate. I started by sulfonating 5,10,15,20-tetrakis(2,6-dibromo-4-(trimethylsilyl)phenyl)porphyrin (**2.9**). Treating this material with trimethylsilyl chlorosulfonate in CCl_4 , as described in Chapter 2,



Scheme 4.1. Sulfonation of **4.1**.

resulted in two major products. The desired product **4.1** was formed 1:1 with an impurity as determined by HPLC. Collecting the impurity allowed me to determine by NMR spectroscopy that loss of one TMS was the major side-product **4.1b** (Scheme 4.1). Changes to the equivalents of the sulfonating agent did not increase the yield of desired product. Fortunately, simply changing the solvent to 1,2,4-TCB and

increasing the temperature allowed the desired compound to be formed as the major product (90% by HPLC) and isolated in a 75% yield. The previously reported isolation of the sulfonated iron porphyrin relied on reverse-phase chromatography. Unfortunately, under the conditions of water/MeCN with 0.1% TFA, the products would streak on the column, impeding purification. Purification using a 1% triethylammonium bicarbonate buffer instead of a TFA additive, however, led to sharp chromatography bands and great separation from impurities. This resulted in a sulfonated porphyrin with triethylammonium counterions, which had the added benefit of permitting quantification on the counter cations by NMR spectroscopy. In the previous method, in contrast, the amount of sodium counterion cannot be assessed in such a ready fashion. It is important to note that in subsequent reactions, the triethylammonium counterions did not alter or impede further chemistry on compound **4.1**.

To create bis-pocket porphyrins from **4.1**, I decided to first attempt the Suzuki coupling conditions from Chapter 2 that utilized diglyme and water as the solvents. Compound **4.1** was dissolved in a 1:1 mixture of water and diglyme containing Pd(dppf)Cl₂, Cs₂CO₃, and phenylboronic acid. The mixture was sparged with N₂ and refluxed for 16 h. While I was able to confirm the formation of the desired product **4.2a** (Figure 4.4) by ¹H NMR, these conditions produced a porphyrinic impurity that I could not separate, resulting in a product of 90% purity as determined by ¹H NMR. This led to the need to find better Suzuki coupling conditions for **4.1**. Simply substituting the base, as was done in Chapter 3, showed no improvement in product

isolation. Altering the solvents alone also had little effect. However, by exchanging the solvents to toluene/water in combination with using diisopropylethylamine (DIPEA) as the base, I was able to acquire the desired compounds in high yields and purity (Figure 4.4). Again, demonstrating the synthetic usefulness of this methodology as highlighted in Chapter 3. I utilized this methodology to synthesize five derivatives of **4.1**. Compounds **4.2a** and **4.2f** were targeted in order to synthesize **4.4a** and **4.4c** with the new synthetic route. Comparison of the samples of **4.4a** and **4.4c** obtained using the two different routes will ensure that both strategies do in fact lead to the same desired outcome. Compound **4.2b** was required for the synthesis of **4.4g**. Lastly, compounds **4.2c** and **4.2e** were synthesized in order to demonstrate that this new synthetic methodology tolerates a wide range of coupling partners.

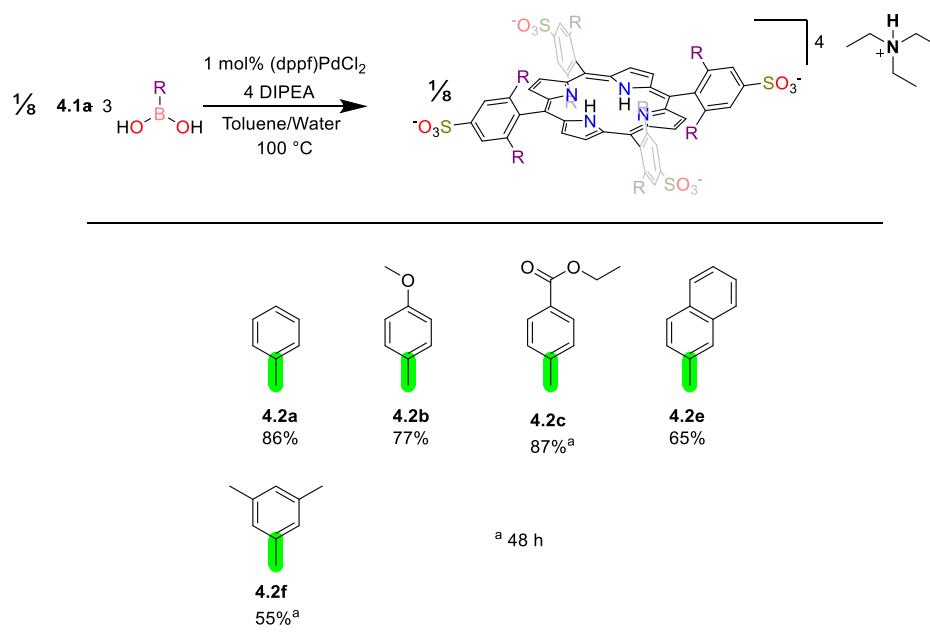


Figure 4.4. Suzuki coupling with **4.1** and various boronic acids. Yields shown are isolated yields.

With the desired sulfonated free base porphyrins in hand, a new metalation procedure needed to be developed. The previously discussed metalation conditions from Chapter 3 no longer worked because **4.2a-4.2f** have no solubility in 1,2,4-TCB. To address this, I attempted the reaction with the more polar high-boiling point solvents DMF, DMSO, diglyme, and ethylene glycol. I found that only ethylene glycol gave conversion to the desired metalated porphyrins. Ethylene glycol was very effective in dissolving these compounds and iron chloride. Insertion of iron occurred cleanly and rapidly, reaching completion in less than 30 min for the less sterically

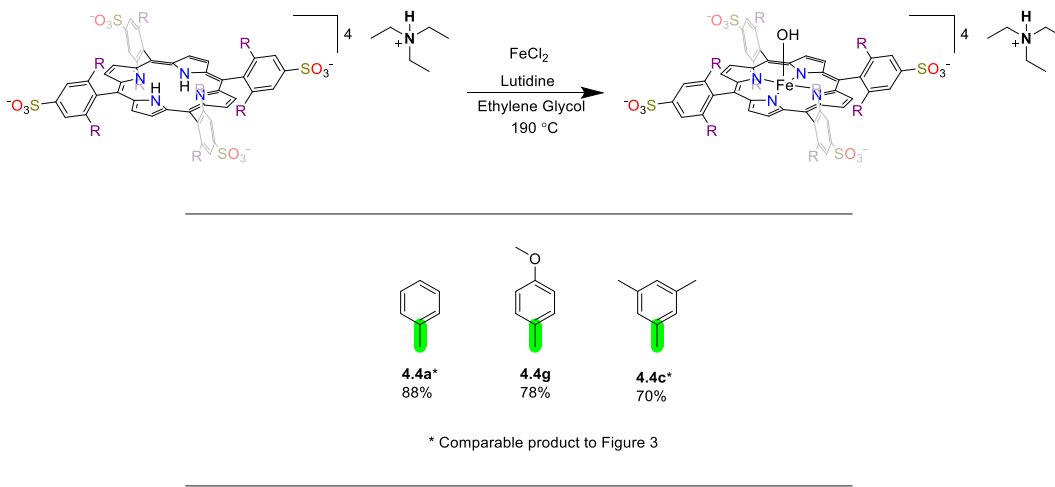


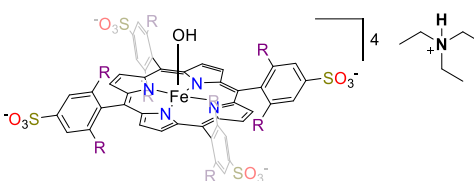
Figure 4.5. Metalation of sulfonated derivatives. Yields shown are isolated yields.

encumbered derivatives, **4.2a** and **4.2b** (Figure 4.5). UV-vis spectroscopy, HPLC, and mass spectrometry confirmed that metalation of **3.2a** gave **4.4a** and **2.2f** gave **4.4c**. In both cases, the material obtained was consistent with the material resulting from the synthetic route in Figure 4.2. This new synthetic pathway allowed for the synthesis of

derivative **4.4g**, which was previously unobtainable due to its electron-rich nature, leading to over sulfonation with the previous methodology.

Solubility

To begin testing trends in physical properties of these derivatives, I decided to first determine how changes to the pockets affected the overall solubility of these molecules. To 1-5 mg of each derivative was added 5-20 μ l of water. All solutions were heated at 90 °C for 1 h and allowed to rest at room temperature overnight to create a saturated solution of each derivative. The samples were centrifuged, and a UV-vis spectrum was collected of each supernatant. Using molar extinction coefficients, the solubility was determined. Due to the intensity of color for these samples, it was difficult to definitively ascertain whether saturation had occurred or not, i.e. solid could not be easily observed at the bottom of the microcentrifuge tubes. For those that could be determined, there was clearly an impact on solubility when a lipophilic group was added to the 4 position, as in **4.4b** and **4.4f** (Figure 4.6). To compare relative solubility and polarity, I instead turned to HPLC retention times (RT) to observe trends. The eight chosen derivatives were individually injected onto an HPLC column with the same 10 min solvent ramp for each, starting at 0% water containing 1% triethylammonium bicarbonate and ending at 100% MeCN. The RT of these molecules, tabulated in Figure 4.6, are affected by polarity and solubility, along with other factors.³⁻⁴ Here trends are consistent with the lipophilicity of the aryl groups that are installed. As more lipophilicity is added, the RT increases, as seen in the change



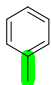
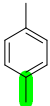
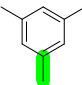
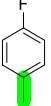
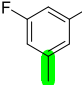
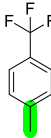
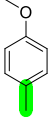
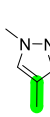
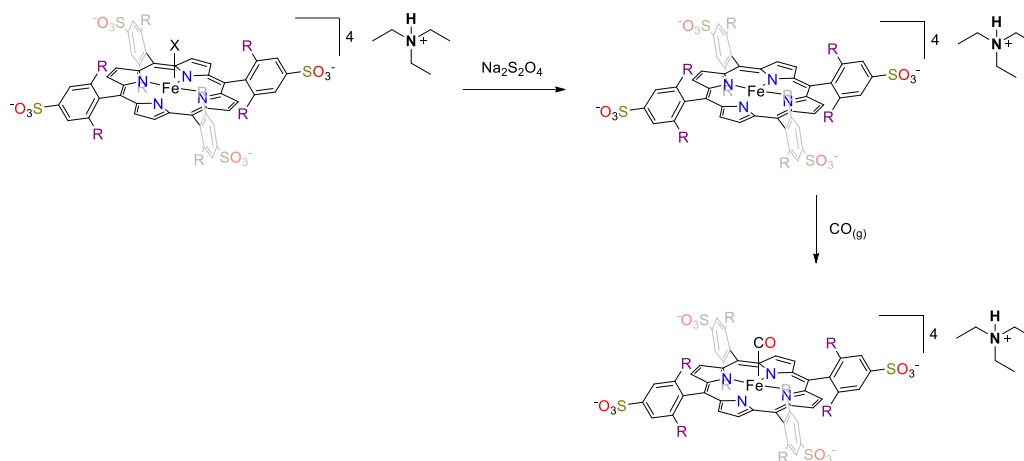
	4.4a	4.4b	4.4c	4.4d	4.4e	4.4f	4.4g	4.4h
R=								
RT(min)	4.25	4.60	4.97	4.25	4.43	4.90	4.06	2.76
conc. mol/L	>0.01	0.0052	>0.01	>0.02	>0.01	0.00027	>0.01	>0.03

Figure 4.6. RT and approximate solubilities of target derivatives.

from **4.4a** to **4.4b** to **4.4c**. When polar groups or heterocycles are incorporated, **4g** and **4h**, there are dramatic reductions in RT. There is an interesting dependence on substitution pattern. If a lipophilic group is placed in the 4 position of the aryl rings comprising the pockets, there is a noticeable reduction in water solubility (**4.4b** and **4.4f**), but the 3 and 5 positions seem to allow lipophilicity addition without solubility loss (e.g., **4.4c** and **4.4e**). Some of the derivatives, like **4.4c**, also require the initial addition of heat to help with dissolution. Once dissolved and allowed to cool to room temperature the derivative stays dissolved, and no precipitation was noted for weeks.

CO Binding

With the methodology to synthesize all the derivatives established, the ability of each derivative to bind CO needed to be confirmed. As demonstrated in Chapter 2, each derivative was dissolved in PBS followed by the addition of sodium dithionite to



Scheme 4.2. Generation of the Fe(II)CO species.

effect the reduction of Fe(III) to Fe(II) and a UV-vis spectrum was acquired (Figure 4.7). CO was then briefly bubbled through the solution to generate the CO bound species and another UV-vis spectrum was acquired (Scheme 4.2). The general changes in the UV-vis spectra were consistent within the series of derivatives and with compound **2.12** from Chapter 2. The spectral shifts are demonstrated in Figure 4.7 for

4.4h. Adding sodium

dithionite to a solution of Compound **4.4h** ($\lambda_{\text{max}} = 427 \text{ nm}$ in PBS, pH 7.4) reduces the compound to afford an Fe(II) complex. The Soret band red shifts to 439 nm upon reduction of **4.4h** (Figure 4.7). A

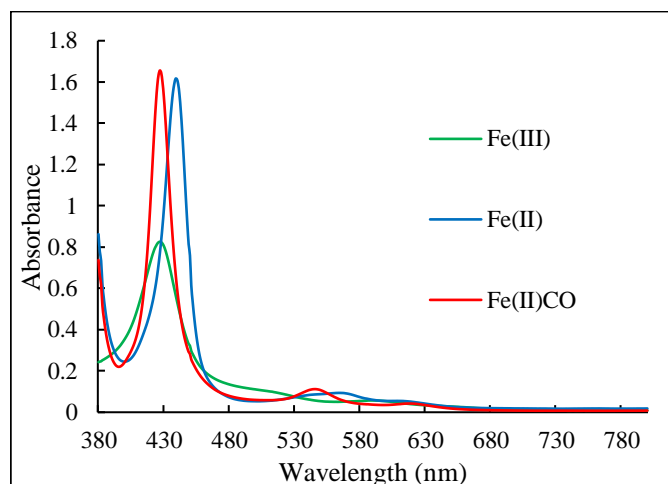


Figure 4.7. Electronic absorption spectra of Fe(III) **4.4h**, Fe(II) **4.4h**, and Fe(II)CO **4.4h**

red shift in the Soret is consistent with the literature as discussed in Chapter 2.⁵ UV-vis of reduced **4.4h** treated with CO shows a Soret band at 427 nm in PBS (Figure 4.7); this blue shift is consistent with formation of an Fe(II)CO complex.² All the other derivatives also show the same red shift upon reduction, and blue shift upon binding CO (C.11-C.17). The Soret bands for these derivatives fall within a similar range of 430-450nm, except that of **4.4h** at 427 nm. Notably, **4.4h** is the only derivative not featuring a decorated phenyl ring. Also, most of the derivatives have similar shaped Soret bands, with a few notable exceptions. Compounds **4.4c**, **4.4e**, and **4.4f** have Soret bands that are composed of multiple peaks (C.13, C.15, C.16). These changes in the Soret bands suggest that the structural makeup of the bis-pocket motif may have some impact on either the binding of CO or the composition and number of ligands bound to the iron center. For example, the split Soret of **4.4f** and shape of the Q bands, could suggest that this compound binds more than one CO under 1 atm of CO (C.16).⁶ Further work on the CO partial pressure dependence of these spectral changes will be needed to understand these differences.

The capability of these derivatives to bind CO was also assessed by IR spectroscopy. In the same fashion as **2.12** in Chapter 2, an IR spectrum for each of the reduced and CO bound derivatives was collected. In a 1.5 mL microcentrifuge tube, each derivative was dissolved in water and degassed with nitrogen. CO was bubbled through the solution followed by the addition of sodium dithionite. This immediately generated a vibrant red solution consistent with the color change that was observed when generating a Fe(II)CO species in Chapter 2. To this solution was added

tetraphenylphosphonium chloride to induce precipitation of the carbonyl-bound derivative. The mixture was centrifuged, and the supernatant was removed. The precipitate was mixed with KBr and pressed to form a pellet. An IR spectrum was collected for each derivative and the CO stretching frequency of the bound carbonyl was tabulated (Figure 4.8). The IR spectrum of each derivative showed a distinct carbonyl stretching frequency near 1970 cm^{-1} , indicating they all were capable of binding CO.⁷⁻⁸ Little variation in stretching frequency was observed and no trends in sterics or electronics could be determined. The minor variation in CO stretching frequency could indicate that all derivatives bind CO with the same strength or simply that the makeup of the pocket, for these derivatives, plays little role in the nature of the Fe-CO bonding interaction.⁷

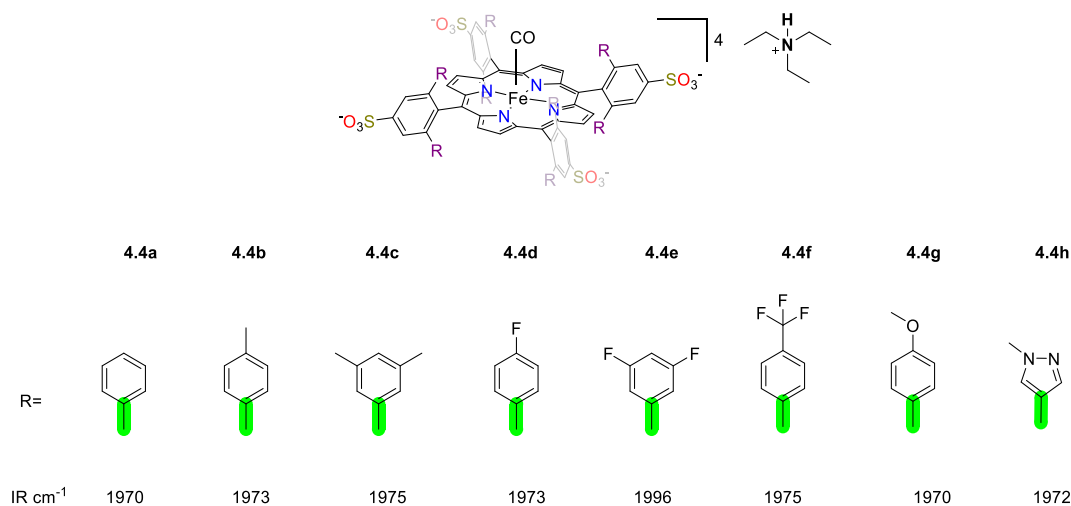


Figure 4.8. CO stretching frequencies for the Fe(II)CO species of each derivative.

After demonstrating the capability to bind CO, the series of derivatives was tested to determine trends in oxidative stability. To test stability, I modified a

procedure reported by the Kitagishi group.⁹ A stock solution, at a concentration of 1 mg/mL, of each derivative in PBS was prepared. These solutions were sparged with nitrogen to remove any dissolved oxygen and then bubbled with CO for 30 s. To each solution was added 5 mg of sodium dithionite, generating the Fe(II)CO bound species for each derivative. A 5 μ L aliquot of each derivative was subsequently added to a cuvette containing 1 mL of air-equilibrated PBS. Upon addition, any residual sodium dithionite was immediately consumed by dissolved oxygen and periodic UV-vis scans were collected to

monitor the oxidation of the Fe(II)CO species in solution. Using this method, all derivatives except **4.4b** and **4.4c** were immediately oxidized to the Fe(III) species.

This experiment more accurately gives the

stability of the CO-bound species compared to the method used in Chapter 2. In

Chapter 2, air was bubbled through the cuvette containing excess sodium dithionite

until no more sodium dithionite was observed, giving half-lives of approximately 120

min for **2.13**. Using the method presented in this chapter, the synthesized **2.13** made

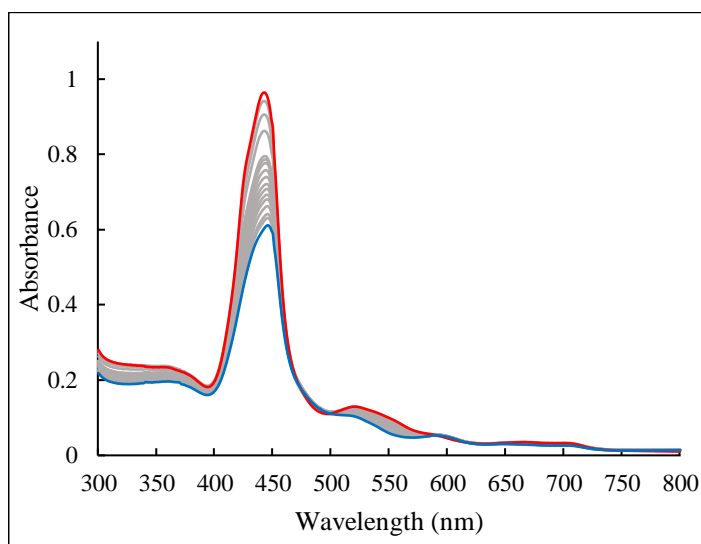


Figure 4.9. Stability of the Fe(II)CO complex of **4.4c** in PBS (pH 7.4). Spectra were acquired at 2 h intervals until no more change in absorbance was observed.

from **4.4a**, showed a half-life shorter than the spectral acquisition time. I hypothesize that the experiment from Chapter 2 is observing the dissolution of oxygen from the atmosphere into the cuvette and then oxidation of the compound. While most derivatives showed rapid oxidation using this new experimental approach, **4.4c** had a measurable half-life. The Fe(II)CO species formed from **4.4c** demonstrated an impressive approximate half-life of 8 h (Figure 4.9). From these data it appears that introducing significant lipophilic steric bulk at the 3 and 5 positions of the pocket-forming aryl rings does impart oxidative stability. The crystal structure of **4.3c** (from **3.4f** in Chapter 2) shows that when an atom is occupying space in a pocket on one face of the porphyrin, the pocket on the other face tightens and has a smaller void volume, due to steric strain. This could be the contributing factor to the increased stability of the Fe(II)CO species of **4.4c**. When CO is bound, the other face of the

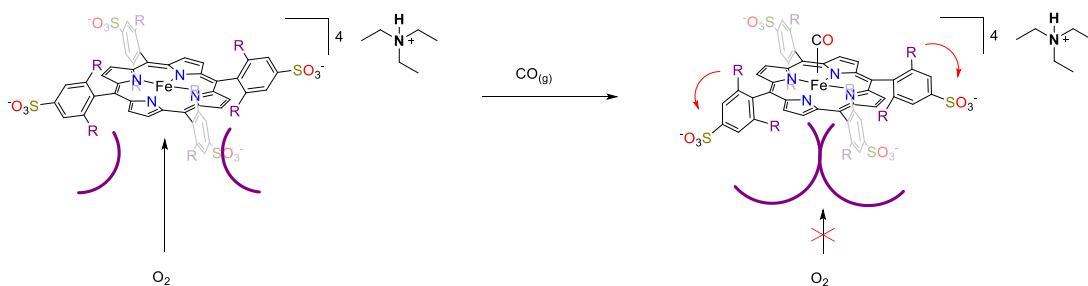


Figure 4.10. Diagram of steric bulk inhibiting oxidation. Exaggerated canting of *meso* rings depicting pocket shift.

porphyrin becomes protected from autooxidation by the bulky aryl rings (Figure 4.10).

Finally, to further stress the potential for these derivatives to act as CO poisoning antidotes, **4.4h** was chosen to demonstrate that even though it is a

derivative of **2.12** from Chapter 2, it retains the ability to sequester CO from COHb. Reduced **4.4h** was titrated into a solution of COHb as discussed in Chapter 2. As shown in Figure 4.11, the Soret from COHb at 419 nm is replaced with a Soret at 427 nm. This new band is the overlap of deoxyhemoglobin (436 nm) and the

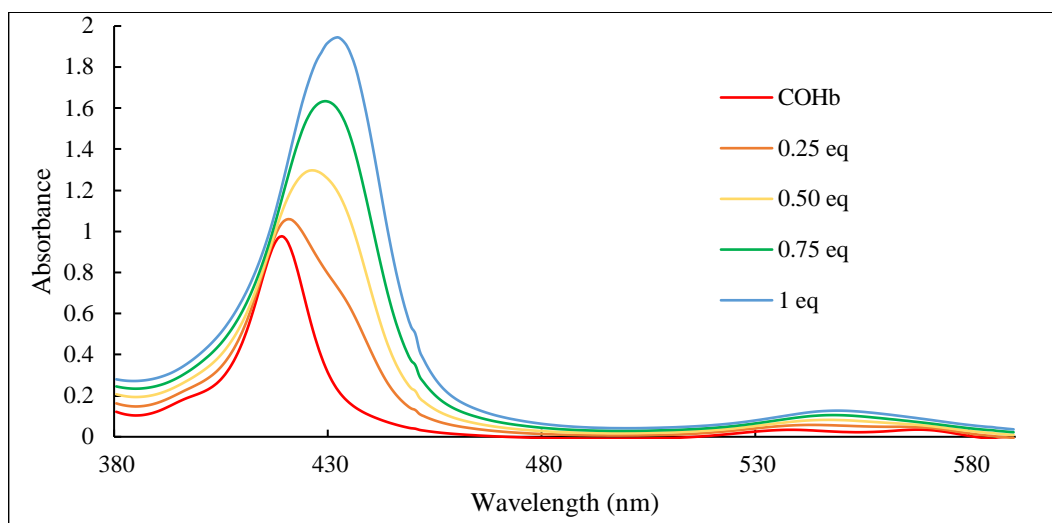


Figure 4.11. Titration of bovine COHb (2.5 μM) with **4.4h** in PBS (pH 7.4, 5.7 mM $\text{Na}_2\text{S}_2\text{O}_4$).

Fe(II)CO species of **4.4h** (Figure 4.7). The characteristic two Q bands of COHb are also transformed into one band at 550 nm, characteristic of deoxyhemoglobin.¹⁰

4.3 Conclusion

This chapter has demonstrated the effectiveness of the modular nature of this porphyrin platform to allow for quick and efficient derivatization. A small library of eight derivatives was synthesized and a new synthetic route was used to synthesize water-soluble bis-pocket iron porphyrin complexes with electron-rich aryl rings. All derivatives maintained the ability to bind CO and **4.4h** showed that derivatization can

be performed without removing the ability to sequester CO from COHb. This curated library of derivatives allowed trends in biologically important properties to be discussed. Both solubility and stability were significantly affected by the structural make-up of the pockets on this scaffold. Using the knowledge gained from this first round of SAR, new derivatives will be targeted that will maintain the properties that impart water solubility, such as the inclusion of heterocycles and hydrogen-bond-donating and -accepting functional groups. This can be combined with the structural motifs that impart oxidative stability, such as steric bulk that cages the open face of the Fe(II)CO species, inhibiting oxidation. This work should prove useful in the rapid advancement of derivatives of this scaffold to uncover a small molecule CO poisoning antidote.

4. 4 Experimental Methods

General considerations. All reactions were performed under N₂ unless otherwise specified. Glassware was oven dried prior to use. All solvents and reagents are commercially available and used as received unless otherwise stated. Compounds **2.9**, **3.2a**, **3.2b**, **3.2d**, **3.2e**, **3.2h**, **3.2i**, **3.2k**, and **3.2q** were prepared as previously described.^{2,11} Suzuki-Miyaura reactions were performed in Chemglass 20-mL reaction vials fitted with pressure relief caps and heated on a hot plate fitted with a Chemglass 4-place pie wedge for 20-mL scintillation vials. For the purification of **4.4a**, **4.4b**, **4.4c**, **4.4d**, **4.4e**, **4.4f**, **4.4g**, **4.4h**, **4.2a**, **4.2b**, **4.2c**, **4.2e**, and **4.2f**, an Isolera Prime Biotage fitted with a Sfär C18 column was employed. A solution of 1%

triethylammonium bicarbonate in water was generated by dissolving 40 mL of triethylamine in 4 L of ultra-pure (UP) water ($>18 \text{ M}\Omega \text{ cm}$) followed by the addition of 150 g of dry ice. Analytical HPLC was performed on a Shimadzu Prominence-I LC-2030 Plus fitted with a Phenomenex Luna silica $5 \mu\text{m}$ 100 \AA column ($250 \times 10 \text{ mm}$). Organic solutions were concentrated under reduced pressure on a Buchi Rotavapor R-100. CDCl_3 and $\text{DMSO-}d_6$ were purchased from Cambridge Isotope Laboratories and used as received. ^1H , $^{13}\text{C}\{^1\text{H}\}$, and $^{19}\text{F}\{^1\text{H}\}$ NMR spectra were recorded on a Bruker Avance III HD 500 NMR spectrometer equipped with a multinuclear Smart Probe. Signals in the ^1H and ^{13}C NMR spectra are reported in ppm as chemical shifts from tetramethylsilane. NMR signals were referenced using the CHCl_3 (^1H , 7.26 ppm), $\text{DMSO-}d_5$ (^1H , 2.50 ppm), or CDCl_3 (^{13}C , 77.0 ppm) solvent signals. The following abbreviations were used to explain the multiplicities: s = singlet, d = doublet, t = triplet, q = quartet, m = multiplet, sext = sextet. Solution phase magnetic moments were measured using a modified Evans method.¹² UV-visible absorption spectra were measured on a VWR UV-6300PC dual-beam spectrophotometer. MALDI mass spectra were acquired using timsControl v 1.1.19 on a timsTOF fleX mass spectrometer (Bruker Scientific, Billerica, MA) over the mass range 1000–2500 Da. In positive reflectron mode, laser power was set to 20%, and laser application was set to MS Dried Droplet. In negative reflectron mode, laser power was set to 30%, and laser application was set to MS Dried Droplet. Compounds were dissolved in DCM or MeOH and 1 μL was mixed with 1 μL of matrix (50:50 α -cyano-4-hydroxycinnamic acid:2,5-dihydroxybenzoic acid in a

solution of 70:30 ACN:H₂O with 0.1% trifluoroacetic acid). Samples were spotted on a stainless steel MSP 96 spot target plate and allowed to air dry. For each compound, 1000 laser shots at 2000 Hz were delivered in a random walk across the spot. Data were subsequently analyzed in DataAnalysis v 5.3 (Bruker Scientific, Billerica, MA). The aqueous solubility of **4.4a-4.4h** was assessed by adding sufficient solid to a minimal volume of water such that a portion of solid remained undissolved at room temperature, centrifuging the mixture, removing an aliquot from the supernatant, and determining the concentration of the compound in the aliquot using UV-vis spectroscopy.

Synthesis of 4.1 Triethylammonium 5,10,15,20-tetrakis(2,6-dibromo-4-(sulfonate)phenyl)porphyrin. Compound **2.9** (300 mg, 0.1967 mmol) and 12 equiv of trimethylsilyl chlorosulfonate (0.36 mL, 0.1589 mmol) were dissolved in 1,2,4-TCB (10 mL) in a 20-mL reaction vial fitted with a pressure release cap. The reaction was sealed and incubated at 140 °C for 30 min. The reaction was removed from heat and quenched with 5 mL of 1 M NaOH (aq) and stirred vigorously for 10 min. The crude mixture was diluted with methanol and passed through a pad of silica with 1:1 DCM/MeOH. The filtrate was concentrated under reduced pressure and purified by reverse phase flash column chromatography using a ramp to 95% acetonitrile in water with 1% triethylammonium bicarbonate. The eluted product was concentrated under reduced pressure and **4.1** was isolated as a purple solid (297 mg, 77%). ¹H NMR (500 MHz, DMSO-*d*₆) δ 8.72 (s, 8H), 8.26 (s, 8H), 3.08 (q, J = 7.1 Hz, 24H), 1.16 (t, J =

7.2 Hz, 36H), -2.67 (s, 2H); $^{13}\text{C}\{^1\text{H}\}$ NMR (126 MHz, DMSO- d_6) δ 152.22, 141.72, 129.06, 127.35, 118.39, 46.27, 9.14. UV/vis (MeOH) λ_{abs} (log ϵ): 370 (sh), 418 (5.67), 449 (sh), 513 (4.46), 541 (sh), 591 (4.07); HPLC (C18 Silica, water 1% triethylammonium bicarbonate buffer/ACN = 5 min ramp to 100% ACN, flow rate = 1.5 mL/min, λ = 400 nm) t_{R} = 2.41 min (99%).

Synthesis of 4.2a Triethylammonium 5,10,15,20-tetrakis(2,6-di(phenyl)-4-(sulfonate)phenyl)porphyrin. Compound **4.1** (90 mg, 0.0547 mmol), 3 mol% per carbon-bromine bond of palladium catalyst (0.0131 mmol), 32 equiv of phenylboronic acid (1.751 mmol), and 32 equiv of diisopropylethylamine (1.751 mmol) were dissolved in a mixture of toluene (2 mL) and DI water (2 mL) in a 20-mL reaction vial fitted with a pressure relief cap. The mixture was sparged with N_2 for 5 min, then sealed and brought to 100 °C on a hot plate and stirred for 20 h. The crude reaction mixture was dry loaded onto silica and purified by normal phase flash chromatography. The eluted product was concentrated under reduced pressure and purified by reverse phase flash column chromatography using a ramp to 95% acetonitrile in water with 1% triethylammonium bicarbonate. The eluted product was concentrated under reduced pressure and **4.2a** was isolated as a purple solid (92 mg, 86%). ^1H NMR (500 MHz, DMSO- d_6) δ 8.41 (s, 8H), 7.85 (s, 8H), 6.51 (d, J = 7.5 Hz, 16H), 6.42 (t, J = 7.4 Hz, 9H), 6.28 (t, J = 7.7 Hz, 16H), 3.11 (q, J = 7.3 Hz, 25H), 1.18 (t, J = 7.3 Hz, 39H), -3.68 (s, 2H). $^{13}\text{C}\{^1\text{H}\}$ NMR (126 MHz, DMSO- d_6) δ 148.91, 144.83, 141.64, 138.09, 128.97, 127.19, 126.10, 126.07, 115.95, 46.28, 40.51,

40.34, 40.17, 40.01, 39.84, 39.67, 39.51, 9.14. UV/vis (MeOH) λ_{abs} (log ϵ): 415 (sh), 435 (4.56), 530 (3.24), 565 (2.74), 607 (2.74), 665 (2.36).

Synthesis of 4.2b Triethylammonium 5,10,15,20-tetrakis(2,6-di(4-methoxyphenyl)-4-(sulfonate)phenyl)porphyrin. Compound **4.1** (100 mg, 0.0608 mmol), 3 mol% per carbon-bromine bond of palladium catalyst (0.0146 mmol), 32 equiv of 4-methoxyphenylboronic acid (1.945 mmol), and 32 equiv of diisopropylethylamine (1.945 mmol) were dissolved in a mixture of toluene (2 mL) and DI water (2 mL) in a 20-mL reaction vial fitted with a pressure relief cap. The mixture was sparged with N₂ for 5 min, then sealed and brought to 100 °C on a hot plate and stirred for 20 h. The crude reaction mixture was dry loaded onto silica and purified by normal phase flash chromatography. The eluted product was concentrated under reduced pressure and purified by reverse phase flash column chromatography using a ramp to 95% acetonitrile in water with 1% triethylammonium bicarbonate. The eluted product was concentrated under reduced pressure and **4.2b** was isolated as a purple solid (102 mg, 77%). ¹H NMR (500 MHz, DMSO-*d*₆) δ 8.37 (s, 8H), 7.80 (s, 8H), 6.38 (d, *J* = 8.8 Hz, 16H), 5.83 (d, *J* = 8.9 Hz, 16H), 3.18 – 3.04 (m, 48H), 1.18 (t, *J* = 7.3 Hz, 36H), -3.50 (s, 2H) (Residual methanol is obscuring counterion peaks). ¹³C{¹H} NMR (126 MHz, DMSO-*d*₆) δ 157.29, 148.78, 144.53, 138.28, 134.12, 130.14, 125.95, 116.30, 112.59, 54.69, 46.28, 40.50, 40.34, 40.17, 40.00, 39.84, 39.67, 39.50, 9.13. UV/vis (MeOH) λ_{abs} (log ϵ): 419 (sh), 440 (4.66), 533 (3.34), 569 (3.03), 609 (2.84), 669 (2.48).

Synthesis of 4.2c Triethylammonium 5,10,15,20-tetrakis(2,6-di(4-ethoxycarbonylphenyl)-4-(sulfonate)phenyl)porphyrin. Compound **4.1** (90 mg, 0.0547 mmol), 3 mol% per carbon-bromine bond of palladium catalyst (0.0131 mmol), 32 equiv of 4-ethoxycarbonylphenylboronic acid (1.751 mmol), and 32 equiv of diisopropylethylamine (1.751 mmol) were dissolved in a mixture of toluene (2 mL) and DI water (2 mL) in a 20-mL reaction vial fitted with a pressure relief cap. The mixture was sparged with N₂ for 5 min, then sealed and brought to 100 °C on a hot plate and stirred for 48 h. The crude reaction mixture was dry loaded onto silica and purified by normal phase flash chromatography. The eluted product was concentrated under reduced pressure and purified by reverse phase flash column chromatography using a ramp to 95% acetonitrile in water with 1% triethylammonium bicarbonate. The eluted product was concentrated under reduced pressure and **4.2c** was isolated as a purple solid (120 mg, 87%). ¹H NMR (500 MHz, DMSO-*d*₆) δ 8.33 (s, 8H), 7.95 (s, 8H), 6.87 (d, J = 8.6 Hz, 16H), 6.46 (d, J = 8.2 Hz, 16H), 3.81 (q, J = 7.1 Hz, 16H), 3.06 (q, J = 7.2 Hz, 27H), 1.17 (t, J = 7.3 Hz, 44H), 0.85 (t, J = 7.1 Hz, 25H), -3.59 (s, 2H). ¹³C{¹H} NMR (126 MHz, DMSO-*d*₆) δ 165.20, 149.31, 146.21, 144.46, 137.67, 129.51, 128.05, 127.84, 126.92, 115.18, 60.52, 46.21, 39.93, 14.02, 9.17. UV/vis (MeOH) λ_{abs} (log ε): 382 (sh), 439 (5.46), 496 (sh), 532 (4.18), 568 (3.91), 608 (3.81), 667 (3.63).

Synthesis of 4.2e Triethylammonium 5,10,15,20-tetrakis(2,6-di(2-naphthyl)-4-(sulfonate)phenyl)porphyrin. Compound **4.1** (90 mg, 0.0547 mmol), 3 mol% per carbon-bromine bond of palladium catalyst (0.0131 mmol), 32 equiv of 2-naphthylboronic acid (1.7508 mmol), and 32 equiv of diisopropylethylamine (1.7508 mmol) were dissolved in a mixture of toluene (2 mL) and DI water (2 mL) in a 20-mL reaction vial fitted with a pressure relief cap. The mixture was sparged with N₂ for 5 min, then sealed and brought to 100 °C on a hot plate and stirred for 20 h. The crude reaction mixture was dry loaded onto silica and purified by normal phase flash chromatography. The eluted product was concentrated under reduced pressure and purified by reverse phase flash column chromatography using a ramp to 95% acetonitrile in water with 1% triethylammonium bicarbonate. The eluted product was concentrated under reduced pressure and **4.2e** was isolated as a purple solid (84 mg, 65%). ¹H NMR (500 MHz, DMSO-*d*₆) δ 8.48 (s, 8H), 7.89 (s, 8H), 7.59 (s, 8H), 7.26 – 7.07 (m, 33H), 5.59 (d, J = 8.6 Hz, 8H), 5.27 (d, J = 8.7 Hz, 8H), 3.10 (q, J = 7.1 Hz, 25H), 1.18 (t, J = 7.3 Hz, 39H), -3.82 (s, 2H). ¹³C{¹H} NMR (126 MHz, DMSO-*d*₆) δ 149.05, 144.84, 139.36, 138.20, 132.49, 130.88, 127.96, 127.67, 127.32, 126.66, 126.12, 125.91, 125.79, 115.77, 46.27, 40.50, 40.34, 40.17, 40.00, 39.84, 39.67, 39.50, 9.17. UV/vis (MeOH) λ_{abs} (log ε): 339 (sh), 441 (5.34), 534 (4.14), 568 (3.88), 606 (3.85), 632 (sh), 667 (3.66), 679 (sh), 701 (sh).

Synthesis of 4.2f Triethylammonium 5,10,15,20-tetrakis(2,6-di(3,5-dimethylphenyl)-4-(sulfonate)phenyl)porphyrin. Compound **4.1** (100 mg, 0.0547

mmol), 3 mol% per carbon-bromine bond of palladium catalyst (0.0131 mmol), 32 equiv of 3,5-dimethylphenylboronic acid (1.751 mmol), and 32 equiv of diisopropylethylamine (1.751 mmol) were dissolved in a mixture of toluene (2 mL) and DI water (2 mL) in a 20-mL reaction vial fitted with a pressure relief cap. The mixture was sparged with N₂ for 5 min, then sealed and brought to 100 °C on a hot plate and stirred for 48 h. The crude reaction mixture was dry loaded onto silica and purified by normal phase flash chromatography. The eluted product was concentrated under reduced pressure and purified by reverse phase flash column chromatography using a ramp to 95% acetonitrile in water with 1% triethylammonium bicarbonate. The eluted product was concentrated under reduced pressure and **4.2f** was isolated as a purple solid (65 mg, 55%). ¹H NMR (500 MHz, DMSO-*d*₆) δ 8.43 (s, 8H), 7.78 (s, 8H), 6.11 (s, 16H), 5.92 (s, 8H), 3.10 (q, J = 7.3 Hz, 24H), 1.18 (t, J = 7.3 Hz, 36H), 1.08 (s, 48H), -3.09 (s, 2H). ¹³C{¹H} NMR (126 MHz, DMS-*d*₆) δ 148.51, 145.15, 141.67, 137.71, 135.70, 127.71, 126.95, 126.63, 116.27, 46.28, 40.49, 40.32, 40.15, 39.99, 39.82, 39.65, 39.49, 20.56, 9.15. UV/vis (MeOH) λ_{abs} (log ε): 417 (sh), 436 (4.82), 531 (3.35), 565 (2.78), 611 (2.55), 668 (1.79)

Synthesis of 4.3a 5,10,15,20-tetrakis(2,6-diphenyl-4-

(trimethylsilyl)phenyl)porphyrinatochloroiron(III). Compound **3.2a** (73 mg, 0.0483 mmol), 10 equiv of 2,6-lutidine (0.483 mmol), and 100 equiv of FeCl₂ (4.83 mmol) were dissolved in 1,2,4-TCB (5 mL) under an aerobic atmosphere in a 20-mL reaction vial fitted with a pressure relief cap. The reaction mixture was sealed and

heated to 213 °C for 1 h on a hot plate fitted with a Chemglass 4-place pie wedge for 20-mL scintillation vials. The crude reaction mixture was diluted with hexanes, loaded onto a silica column, and purified by normal phase flash chromatography. The product was eluted in a 1:1 solvent mixture of hexanes:chloroform and concentrated under reduced pressure to yield the isolated product as deep purple crystals (63 mg, 82%). Characterization was consistent with previously reported data (Chapter 2).

Synthesis of 4.3b 5,10,15,20-tetrakis(2,6-di(4-methylphenyl)-4-(trimethylsilyl)phenyl)porphyrinatochloroiron(III). Compound **3.2e** (220 mg, 0.1356 mmol), 10 equiv of 2,6-lutidine (1.356 mmol), and 100 equiv of FeCl₂ (13.5635 mmol) were dissolved in 1,2,4-TCB (5 mL) under an aerobic atmosphere in a 20-mL reaction vial fitted with a pressure relief cap. The reaction mixture was sealed and heated to 213 °C for 1 h on a hot plate fitted with a Chemglass 4-place pie wedge for 20-mL scintillation vials. The crude reaction mixture was diluted with hexanes, loaded onto a silica column, and purified by normal phase flash chromatography. The product was eluted in a 1:1 solvent mixture of hexanes:chloroform and concentrated under reduced pressure to yield the isolated product as deep purple crystals (190 mg, 82%).; UV/vis (CHCl₃) λ_{abs} (log ε): 363 (sh), 447 (5.08), 524 (4.12), 589 (3.65), 708 (3.66).; HPLC (Silica, hexane/DCM = 12 min ramp to 100% DCM, flow rate = 3.0 mL/min, λ = 400 nm) t_R = 6.07 min (94%)

Synthesis of 4.3c 5,10,15,20-tetrakis(2,6-di(3,5-dimethylphenyl)-4-(trimethylsilyl)phenyl)porphyrinatochloroiron(III). Compound **3.2d** (110 mg, 0.0634 mmol), 10 equiv of 2,6-lutidine (0.634 mmol), and 100 equiv of FeCl₂ (6.3401 mmol) were dissolved in 1,2,4-TCB (5 mL) under an aerobic atmosphere in a 20-mL reaction vial fitted with a pressure relief cap. The reaction mixture was sealed and heated to 213 °C for 3 h on a hot plate fitted with a Chemglass 4-place pie wedge for 20-mL scintillation vials. The crude reaction mixture was diluted with hexanes, loaded onto a silica column, and purified by normal phase flash chromatography. The product was eluted in a 1:1 solvent mixture of hexanes:chloroform and concentrated under reduced pressure to yield the isolated product as deep purple crystals (90 mg, 78%). Characterization was consistent with previously reported synthesis (Chapter 2).

Synthesis of 4.3d 5,10,15,20-tetrakis(2,6-di(4-fluorophenyl)-4-(trimethylsilyl)phenyl)porphyrinatochloroiron(III). Compound **3.2h** (260 mg, 0.1572 mmol), 10 equiv of 2,6-lutidine (1.572 mmol), and 100 equiv of FeCl₂ (15.7195 mmol) were dissolved in 1,2,4-TCB (5 mL) under an aerobic atmosphere in a 20-mL reaction vial fitted with a pressure relief cap. The reaction mixture was sealed and heated to 213 °C for 1 h on a hot plate fitted with a Chemglass 4-place pie wedge for 20-mL scintillation vials. The crude reaction mixture was diluted with hexanes, loaded onto a silica column, and purified by normal phase flash chromatography. The product was eluted in a 1:1 solvent mixture of hexanes:chloroform and concentrated under reduced pressure to yield the isolated

product as deep purple crystals (170 mg, 62%); UV/vis (CHCl₃) λ_{abs} (log ϵ): 360 (sh), 446 (5.00), 521 (4.11), 585 (3.64), 707 (3.56); HPLC (Silica, hexane/DCM = 12 min ramp to 100% DCM, flow rate = 3.0 mL/min, λ = 400 nm) t_{R} = 6.95 min (99%)

Synthesis of 4.3e 5,10,15,20-tetrakis(2,6-di(3,5-difluorophenyl)-4-

(trimethylsilyl)phenyl)porphyrinatochloroiron(III). Compound **3.2b** (175 mg, 0.0973 mmol), 10 equiv of 2,6-lutidine (0.9733 mmol), and 100 equiv of FeCl₂ (9.733 mmol) were dissolved in 1,2,4-TCB (10 mL) under an aerobic atmosphere in a 20-mL reaction vial fitted with a pressure relief cap. The reaction mixture was sealed and heated to 213 °C for 1.5 h on a hot plate fitted with a Chemglass 4-place pie wedge for 20-mL scintillation vials. The crude reaction mixture was diluted with hexanes, loaded onto a silica column, and purified by normal phase flash chromatography. The product was eluted in a 1:1 solvent mixture of hexanes:chloroform and concentrated under reduced pressure to yield the isolated product as deep purple crystals (125 mg, 68%). UV/vis (CHCl₃) λ_{abs} (log ϵ): 359 (sh), 442 (5.13), 515 (4.13), 579 (3.74), 695 (3.66).; HPLC (Silica, hexane/DCM = 12 min ramp to 100% DCM, flow rate = 3.0 mL/min, λ = 400 nm) t_{R} = 6.63 min (99%).

Synthesis of 4.3f 5,10,15,20-tetrakis(2,6-di(4-trifluoromethylphenyl)-4-

(trimethylsilyl)phenyl)porphyrinatochloroiron(III). Compound **3.2i** (156 mg, 0.0759 mmol), 10 equiv of 2,6-lutidine (0.759 mmol), and 100 equiv of FeCl₂ (7.596 mmol) were dissolved in 1,2,4-TCB (5 mL) under an aerobic atmosphere in a 20-mL

reaction vial fitted with a pressure relief cap. The reaction mixture was sealed and heated to 213 °C for 3 h on a hot plate fitted with a Chemglass 4-place pie wedge for 20-mL scintillation vials. The crude reaction mixture was diluted with hexanes, loaded onto a silica column, and purified by normal phase flash chromatography. The product was eluted in a 1:1 solvent mixture of hexanes:chloroform and concentrated under reduced pressure to yield the isolated product as deep purple crystals (73 mg, 45%). UV/vis (CHCl₃) λ_{abs} (log ϵ): 370 (sh), 444 (4.96), 522 (3.99), 702 (3.43); HPLC (Silica, hexane/DCM = 12 min ramp to 100% DCM, flow rate = 3.0 mL/min, λ = 400 nm) t_{R} = 6.11 min (99%)

Synthesis of 4.3g 5,10,15,20-tetrakis(2,6-di(4-methoxyphenyl)-4-(trimethylsilyl)phenyl)porphyrinatochloroiron(III). Compound **3.2k** (63 mg, 0.036 mmol), 10 equiv of 2,6-lutidine (0.36 mmol), and 100 equiv of FeCl₂ (3.6 mmol) were dissolved in 1,2,4-TCB (5 mL) under an aerobic atmosphere in a 20-mL reaction vial fitted with a pressure relief cap. The reaction mixture was sealed and heated to 213 °C for 1.5 h on a hot plate fitted with a Chemglass 4-place pie wedge for 20-mL scintillation vials. The crude reaction mixture was diluted with hexanes, loaded onto a silica column, and purified by normal phase flash chromatography. The product was eluted in a 9:1 solvent mixture of chloroform:MeOH and concentrated under reduced pressure to yield the isolated product as deep purple crystals (50 mg, 75%). UV/vis (CHCl₃) λ_{abs} (log ϵ): 377 (sh), 450 (5.01), 525 (4.09), 592 (3.58), 713

(3.54); HPLC (Silica, DCM/MeOH = 8 min ramp to 100% MeOH, flow rate = 3.0 mL/min, $\lambda = 400$ nm) $t_R = 3.90$ min (90%).

Synthesis of 4.3h 5,10,15,20-tetrakis(2,6-di(*N*-methylpyrazolyl)-4-

(trimethylsilyl)phenyl)porphyrinatochloroiron(III). Compound **3.2q** (155 mg,

0.1005 mmol), 10 equiv of 2,6-lutidine (1.0045 mmol), and 100 equiv of FeCl₂ (10.0454 mmol) were dissolved in 1,2,4-TCB (5 mL) under an aerobic atmosphere in a 20-mL reaction vial fitted with a pressure relief cap. The reaction mixture was sealed and heated to 213 °C for 1 h on a hot plate fitted with a Chemglass 4-place pie wedge for 20-mL scintillation vials. The crude reaction mixture was diluted with hexanes, loaded onto a silica column, and purified by normal phase flash chromatography. The product was eluted in a 1:1 solvent mixture of chloroform:MeOH and concentrated under reduced pressure to yield the isolated product as deep purple crystals (150 mg, 92%); UV/vis (CHCl₃) λ_{abs} (log ϵ): 434 (4.74), 520 (3.94), 591 (3.47), 707 (3.35); HPLC (Silica, DCM/MeOH = 8 min ramp to 100% MeOH, flow rate = 3.0 mL/min, $\lambda = 400$ nm) $t_R = 5.77$ min (94%).

Synthesis of 4.4a Triethylammonium 5,10,15,20-tetrakis(2,6-di(phenyl)-4-

(sulfonate)phenyl)porphyrinatohydroxoiron(III). Compound **4.3a** (50 mg, 0.0313

mmol) and 12 equiv of trimethylsilyl chlorosulfonate (0.0576 mL, 0.3752 mmol) were dissolved in CCl₄ (5 mL) in a 20-mL reaction vial fitted with a pressure release cap. The reaction was sealed and incubated at 75 °C for 1 h. The reaction was

removed from heat and quenched with 2 mL of 1 M NaOH (aq) and stirred vigorously for 10 min. The crude mixture was diluted with methanol and passed through a pad of silica with 1:1 DCM/MeOH. The filtrate was concentrated under reduced pressure and purified by reverse phase flash column chromatography using a ramp to 95% acetonitrile in water with 1% triethylammonium bicarbonate. The eluted product was concentrated under reduced pressure and **4.4a** was isolated as a purple solid (42 mg, 66%). UV/vis (H₂O) λ_{abs} (log ϵ): 340 (4.49), 435 (5.09), 500 (sh), 609 (sh); HRMS (MALDI) m/z : [M-4(C₆H₁₆N)Cl+3H]⁻ Calcd for C₉₂H₅₉FeN₄O₁₂S₄⁻ 1595.2367; Found 1595.2281; HPLC (C18 Silica, water 1% triethylammonium bicarbonate buffer/ACN = 5 min ramp to 100% ACN, flow rate = 1.5 mL/min, λ = 400 nm) t_{R} = 2.18 min (99%).

Synthesis of 4.4b Triethylammonium 5,10,15,20-tetrakis(2,6-di(4-methylphenyl)-4-(sulfonate)phenyl)porphyrinatohydroxoiron(III). Compound **4.3b** (100 mg, 0.0584 mmol) and 12 equiv of trimethylsilyl chlorosulfonate (0.1076 mL, 0.7009 mmol) were dissolved in CCl₄ (5 mL) in a 20-mL reaction vial fitted with a pressure release cap. The reaction was sealed and incubated at 75 °C for 1 h. The reaction was removed from heat and quenched with 2 mL of 1 M NaOH (aq) and stirred vigorously for 10 min. The crude mixture was diluted with methanol and passed through a pad of silica with 1:1 DCM/MeOH. The filtrate was concentrated under reduced pressure and purified by reverse phase flash column chromatography using a ramp to 95% acetonitrile in water with 1% triethylammonium bicarbonate. The eluted

product was concentrated under reduced pressure and **4.4b** was isolated as a purple solid (62 mg, 50%). UV/vis (H₂O) λ_{abs} (log ϵ): 339 (4.39), 442 (4.94), 600 (sh); HRMS (MALDI) m/z : [M-4(C₆H₁₆N)Cl+3H]⁻ Calcd for C₁₀₀H₇₅FeN₄O₁₂S₄⁻ 1707.3619; Found 1707.3469; HPLC (C18 Silica, water 1% triethylammonium bicarbonate buffer/ACN = 5 min ramp to 100% ACN, flow rate = 1.5 mL/min, λ = 400 nm) t_{R} = 2.39 min (99%).

Synthesis of 4.4c Triethylammonium 5,10,15,20-tetrakis(2,6-di(3,5-dimethylphenyl)-4-(sulfonate)phenyl)porphyrinatohydroxoiron(III). Compound **4.3c** (100 mg, 0.0584 mmol) and 12 equiv of trimethylsilyl chlorosulfonate (0.1076 mL, 0.7009 mmol) were dissolved in CCl₄ (5 mL) in a 20-mL reaction vial fitted with a pressure release cap. The reaction was sealed and incubated at 75 °C for 1 h. The reaction was removed from heat and quenched with 2 mL of 1 M NaOH (aq) and stirred vigorously for 10 min. The crude mixture was diluted with methanol and passed through a pad of silica with 1:1 DCM/MeOH. The filtrate was concentrated under reduced pressure and purified by reverse phase flash column chromatography using a ramp to 95% acetonitrile in water with 1% triethylammonium bicarbonate. The eluted product was concentrated under reduced pressure and **4.4c** was isolated as a purple solid (65 mg, 52%). UV/vis (H₂O) λ_{abs} (log ϵ): 446 (4.91), 599 (4.09), 641 (sh); HRMS (MALDI) m/z : [M-4(C₆H₁₆N)Cl+3H]⁻ Calcd for C₁₀₈H₉₁FeN₄O₁₂S₄⁻ 1819.4871; Found 1819.4738; HPLC (C18 Silica, water 1% triethylammonium

bicarbonate buffer/ACN = 5 min ramp to 100% ACN, flow rate = 1.5 mL/min, λ = 400 nm) t_R = 2.62 min (99%).

Synthesis of 4.4d Triethylammonium 5,10,15,20-tetrakis(2,6-di(4-fluorophenyl)-4-(sulfonate)phenyl)porphyrinatohydroxoiron(III). Compound **4.3d** (100 mg, 0.0584 mmol) and 12 equiv of trimethylsilyl chlorosulfonate (0.1076 mL, 0.7009 mmol) were dissolved in CCl₄ (5 mL) in a 20-mL reaction vial fitted with a pressure release cap. The reaction was sealed and incubated at 75 °C for 1 h. The reaction was removed from heat and quenched with 2 mL of 1 M NaOH (aq) and stirred vigorously for 10 min. The crude mixture was diluted with methanol and passed through a pad of silica with 1:1 DCM/MeOH. The filtrate was concentrated under reduced pressure and purified by reverse phase flash column chromatography using a ramp to 95% acetonitrile in water with 1% triethylammonium bicarbonate. The eluted product was concentrated under reduced pressure and **4.4d** was isolated as a purple solid (85 mg, 68%). UV/vis (H₂O) λ_{abs} (log ϵ): 339 (4.48), 435 (5.03), 609 (sh); HRMS (MALDI) m/z : [M-4(C₆H₁₆N)Cl+3H]⁻ Calcd for C₉₂H₅₁F₈FeN₄O₁₂S₄⁻ 1739.1613; Found 1739.1508; HPLC (C18 Silica, water 1% triethylammonium bicarbonate buffer/ACN = 12 min ramp to 100% ACN, flow rate = 1.5 mL/min, λ = 400 nm) t_R = 2.25 min (99%).

Synthesis of 4.4e Triethylammonium 5,10,15,20-tetrakis(2,6-di(3,5-difluorophenyl)-4-(sulfonate)phenyl)porphyrinatohydroxoiron(III). Compound

4.3e (100 mg, 0.0584 mmol) and 12 equiv of trimethylsilyl chlorosulfonate (0.1076 mL, 0.7009 mmol) were dissolved in CCl₄ (5 mL) in a 20-mL reaction vial fitted with a pressure release cap. The reaction was sealed and incubated at 75 °C for 1 h. The reaction was removed from heat and quenched with 2 mL of 1 M NaOH (aq) and stirred vigorously for 10 min. The crude mixture was diluted with methanol and passed through a pad of silica with 1:1 DCM/MeOH. The filtrate was concentrated under reduced pressure and purified by reverse phase flash column chromatography using a ramp to 95% acetonitrile in water with 1% triethylammonium bicarbonate. The eluted product was concentrated under reduced pressure and **4.4e** was isolated as a purple solid (64 mg, 52%). UV/vis (H₂O) λ_{abs} (log ϵ): 329 (4.25), 432 (4.79), 472 (sh), 591 (4.11); HRMS (MALDI) m/z : [M-4(C₆H₁₆N)Cl+3H]⁻ Calcd for C₉₂H₄₃F₁₆FeN₄O₁₂S₄⁻ 1883.0860; Found 1883.0765; HPLC (C18 Silica, water 1% triethylammonium bicarbonate buffer/ACN = 5 min ramp to 100% ACN, flow rate = 1.5 mL/min, λ = 400 nm) t_{R} = 2.32 min (99%).

Synthesis of 4.4f Triethylammonium 5,10,15,20-tetrakis(2,6-di(4-trifluoromethylphenyl)-4-(sulfonate)phenyl)porphyrinatohydroxoiron(III).

Compound **4.3f** (100 mg, 0.0584 mmol) and 12 equiv of trimethylsilyl chlorosulfonate (0.1076 mL, 0.7009 mmol) were dissolved in CCl₄ (5 mL) in a 20-mL reaction vial fitted with a pressure release cap. The reaction was sealed and incubated at 75 °C for 1 h. The reaction was removed from heat and quenched with 2 mL of 1 M NaOH (aq) and stirred vigorously for 10 min. The crude mixture was

diluted with methanol and passed through a pad of silica with 1:1 DCM/MeOH. The filtrate was concentrated under reduced pressure and purified by reverse phase flash column chromatography using a ramp to 95% acetonitrile in water with 1% triethylammonium bicarbonate. The eluted product was concentrated under reduced pressure and **4.4f** was isolated as a purple solid (90 mg, 75%). UV/vis (H₂O) λ_{abs} (log ϵ): 330 (4.44), 433 (5.03), 590 (4.34), 633 (sh); HRMS (MALDI) m/z : [M-4(C₆H₁₆N)Cl+3H]⁻ Calcd for C₁₀₀H₅₁F₂₄FeN₄O₁₂S₄⁻ 2139.1358; Found 2139.1294; HPLC (C18 Silica, water 1% triethylammonium bicarbonate buffer/ACN = 5 min ramp to 100% ACN, flow rate = 1.5 mL/min, λ = 400 nm) t_{R} = 2.52 min (99%).

Synthesis of 4.4h Triethylammonium 5,10,15,20-tetrakis(2,6-di(*N*-methylpyrazolyl)-4-(sulfonate)phenyl)porphyrinatohydroxoiron(III). Compound **4.3h** (30 mg, 0.0184 mmol) and 12 equiv of trimethylsilyl chlorosulfonate (0.0339 mL, 0.2206 mmol) were dissolved in CCl₄ (3 mL) and ACN (2 mL) in a 20-mL reaction vial fitted with a pressure release cap. The reaction was sealed and incubated at 75 °C for 1 h. The reaction was removed from heat and quenched with 2 mL of 1 M NaOH (aq) and stirred vigorously for 10 min. The crude mixture was diluted with methanol and passed through a pad of silica with 1:1 DCM/MeOH. The filtrate was concentrated under reduced pressure and purified by reverse phase flash column chromatography using a ramp to 95% acetonitrile in water with 1% triethylammonium bicarbonate. The eluted product was concentrated under reduced pressure and **4.4h** was isolated as a purple solid (23 mg, 61%). UV/vis (H₂O) λ_{abs} (log

ϵ): 342 (4.48), 429 (5.01), 512 (sh), 591 (3.95); HRMS (MALDI) m/z : $[M-4(C_6H_{16}N)+3H]^-$ Calcd for $C_{73}H_{57}ClFeN_{18}O_{12}S_4^-$ 1596.2330; Found 1596.2325; HPLC (C18 Silica, water 1% triethylammonium bicarbonate buffer/ACN = 5 min ramp to 100% ACN, flow rate = 1.5 mL/min, λ = 400 nm) t_R = 1.63 min (99%).

Alternate Synthesis of 4.4a* Triethylammonium 5,10,15,20-tetrakis(2,6-di(phenyl)-4-(sulfonate)phenyl)porphyrinatohydroxoiron(III). Compound **4.2a** (25 mg, 0.0128 mmol), 10 equiv of 2,6-lutidine (0.1284 mmol), and 100 equiv of $FeCl_2$ (1.284 mmol) were dissolved in ethylene glycol (2 mL) under an aerobic atmosphere in a 20-mL reaction vial fitted with a pressure relief cap. The reaction mixture was sealed and heated to 190 °C for 30 min on a hot plate fitted with a Chemglass 4-place pie wedge for 20-mL scintillation vials. The crude mixture was diluted with methanol and passed through a pad of silica with 1:1 DCM/MeOH. The filtrate was concentrated under reduced pressure and purified by reverse phase flash column chromatography using a ramp to 95% acetonitrile in water with 1% triethylammonium bicarbonate. The eluted product was concentrated under reduced pressure and **4.4a** was isolated as a purple solid (23 mg, 88%). Characterization was consistent with previous methodology synthesis.

Synthesis of 4.4g Triethylammonium 5,10,15,20-tetrakis(2,6-di(4-methoxyphenyl)-4-(sulfonate)phenyl)porphyrinatohydroxoiron(III). Compound **4.2b** (100 mg, 0.0457 mmol), 10 equiv of 2,6-lutidine (0.4572 mmol), and 100 equiv

of FeCl₂ (4.5725 mmol) were dissolved in ethylene glycol (5 mL) under an aerobic atmosphere in a 20-mL reaction vial fitted with a pressure relief cap. The reaction mixture was sealed and heated to 190 °C for 30 min on a hot plate fitted with a Chemglass 4-place pie wedge for 20-mL scintillation vials. The crude mixture was diluted with methanol and passed through a pad of silica with 1:1 DCM/MeOH. The filtrate was concentrated under reduced pressure and purified by reverse phase flash column chromatography using a ramp to 95% acetonitrile in water with 1% triethylammonium bicarbonate. The eluted product was concentrated under reduced pressure and **4.4g** was isolated as a purple solid (77 mg, 78%). UV/vis (H₂O) λ_{abs} (log ε): 340 (4.44), 441 (4.93), 548 (sh), 599 (3.94); HRMS (MALDI) *m/z*: [M-4(C₆H₁₆N)Cl+3H]⁻ Calcd for C₁₀₀H₇₅FeN₄O₂₀S₄⁻ 1835.3212; Found 1835.3118; HPLC (C18 Silica, water 1% triethylammonium bicarbonate buffer/ACN = 5 min ramp to 100% ACN, flow rate = 1.5 mL/min, λ = 400 nm) t_R = 2.17 min (99%).

Alternate Synthesis of 4.4c* Triethylammonium 5,10,15,20-tetrakis(2,6-di(3,5-dimethylphenyl)-4-(sulfonate)phenyl)porphyrinatohydroxoiron(III). Compound **4.2f** (25 mg, 0.0114 mmol), 10 equiv of 2,6-lutidine (0.1138 mmol), and 100 equiv of FeCl₂ (1.1384 mmol) were dissolved in ethylene glycol (2 mL) under an aerobic atmosphere in a 20-mL reaction vial fitted with a pressure relief cap. The reaction mixture was sealed and heated to 190 °C for 1 h on a hot plate fitted with a Chemglass 4-place pie wedge for 20-mL scintillation vials. The crude mixture was diluted with methanol and passed through a pad of silica with 1:1 DCM/MeOH. The

filtrate was concentrated under reduced pressure and purified by reverse phase flash column chromatography using a ramp to 95% acetonitrile in water with 1% triethylammonium bicarbonate. The eluted product was concentrated under reduced pressure and **4.4c** was isolated as a purple solid (18 mg, 70%). Characterization was consistent with previous methodology synthesis.

4.5 References

1. Hughes, J. P.; Rees, S.; Kalindjian, S. B.; Philpott, K. L., Principles of early drug discovery. *Br. J. Pharmacol.* **2011**, *162*, 1239-1249.
2. Droege, D. G.; Johnstone, T. C., A water-soluble iron-porphyrin complex capable of rescuing CO-poisoned red blood cells. *Chem. Commun.* **2022**, *58*, 2722-2725.
3. Namjesnik-Dejanovic, K.; Cabaniss, S. E., Reverse-Phase HPLC Method for Measuring Polarity Distributions of Natural Organic Matter. *Environ. Sci. Technol.* **2003**, *38*, 1108-1114.
4. Dong, M. W., 9 - How to be more successful with HPLC analysis: Practical aspects in HPLC operation. In *Handbook of Pharmaceutical Analysis by HPLC*, 2005; pp 255-271.
5. Kano, K.; Kitagishi, H.; Koderu, M.; Hirota, S., Dioxygen Binding to a Simple Myoglobin Model in Aqueous Solution. *Angew. Chem., Int. Ed.* **2005**, *44*, 435-438.
6. Wayland, B. B.; Mehne, L. F.; Swartz, J., Mono- and biscarbonyl complexes of iron(II) tetraphenylporphyrin. *J. Am. Chem. Soc.* **1978**, *100*, 2379-2383.
7. Collman, J. P.; Brauman, J. I.; Halbert, T. R.; Suslick, K. S., Nature of O₂ and CO binding to metalloporphyrins and heme proteins. *Proc. Natl. Acad. Sci. U.S.A.* **1976**, *73*, 3333-3337.
8. Moore, J. N.; Hansen, P. A.; Hochstrasser, R. M., Iron-carbonyl bond geometries of carboxymyoglobin and carboxyhemoglobin in solution determined by picosecond time-resolved infrared spectroscopy. *Proc. Natl. Acad. Sci. U.S.A.* **1988**, *85*, 5062-5066.

9. Mao, Q.; Zhao, X.; Kiriya, A.; Negi, S.; Fukuda, Y.; Yoshioka, H.; Kawaguchi, A. T.; Motterlini, R.; Foresti, R.; Kitagishi, H., A synthetic porphyrin as an effective dual antidote against carbon monoxide and cyanide poisoning. *Proc. Natl. Acad. Sci. U.S.A.* **2023**, *120*.
10. Azarov, I.; Wang, L.; Rose, J. J.; Xu, Q.; Huang, X. N.; Belanger, A.; Wang, Y.; Guo, L.; Liu, C.; Ucer, K. B.; McTiernan, C. F.; O'Donnell, C. P.; Shiva, S.; Tejero, J.; Kim-Shapiro, D. B.; Gladwin, M. T., Five-coordinate H64Q neuroglobin as a ligand-trap antidote for carbon monoxide poisoning. *Sci. Transl. Med.* **2016**, *8*, 368ra173.
11. Droege, D. G.; Parker, A. L.; Milligan, G. M.; Jenkins, R.; Johnstone, T. C., Synthesis and Functionalization of Challenging meso-Substituted Aryl Bis-pocket Porphyrins Accessed via Suzuki–Miyaura Cross-Coupling. *J. Org. Chem.* **2022**, *87*, 11783-11795.
12. Schubert, E. M., Utilizing the Evans method with a superconducting NMR spectrometer in the undergraduate laboratory. *J. Chem. Educ.* **1992**, *69*, *1*, 62.

Appendix A: Supplementary Experimental Data for Chapter 2

Published in part Droege, D. G.; Johnstone, T. C. *Chem. Commun.* **2022**, 58, 2722–
2725

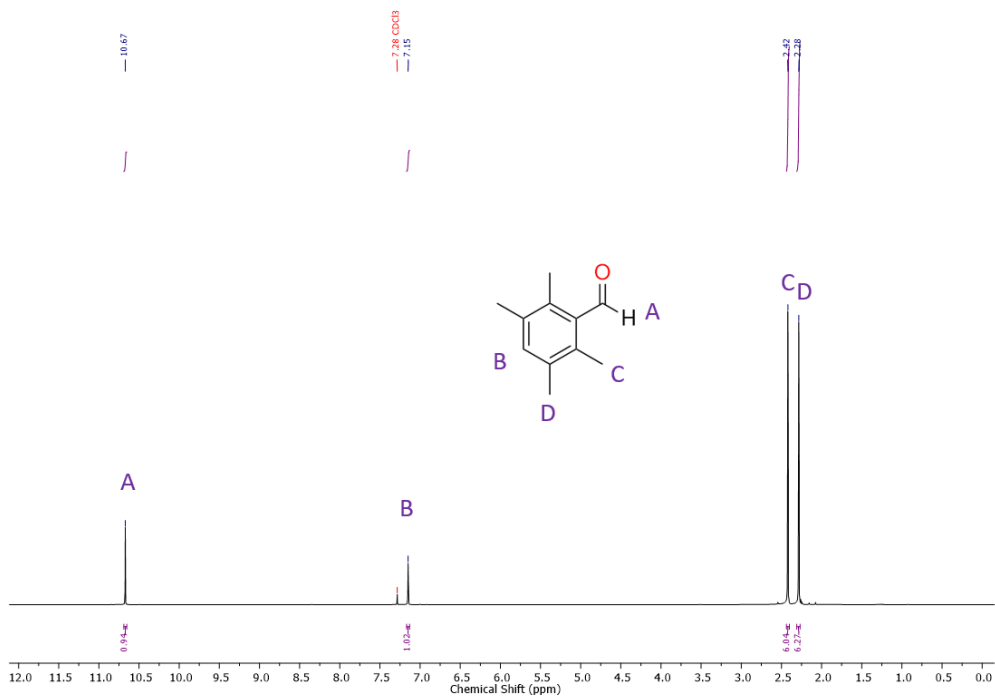


Figure A.1. ^1H NMR spectrum (500 MHz, CDCl_3) of **2.2**.

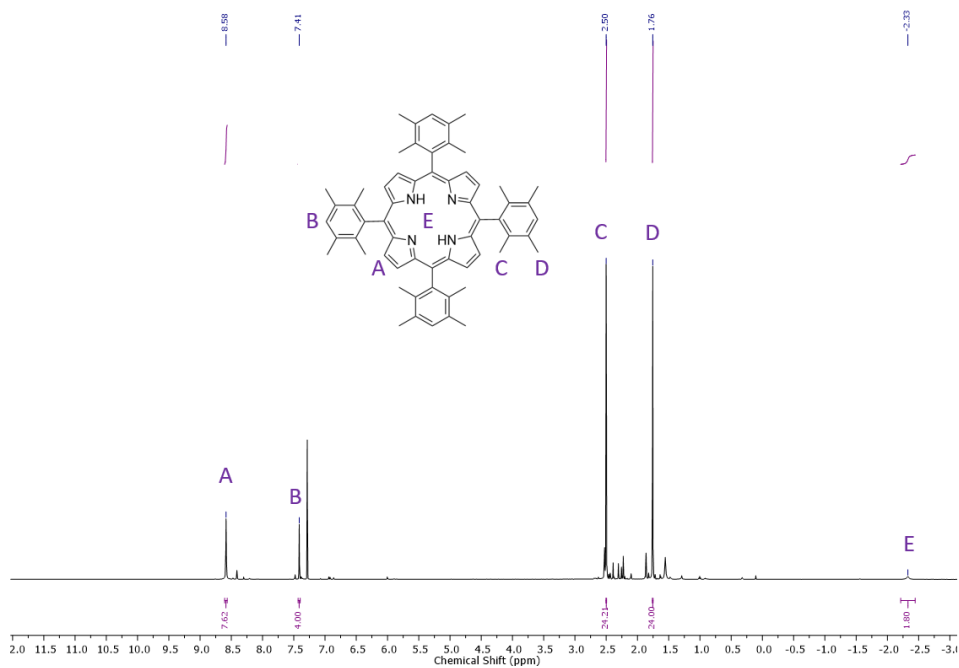


Figure A.2. ^1H NMR spectrum (500 MHz, CDCl_3) of **2.3**.

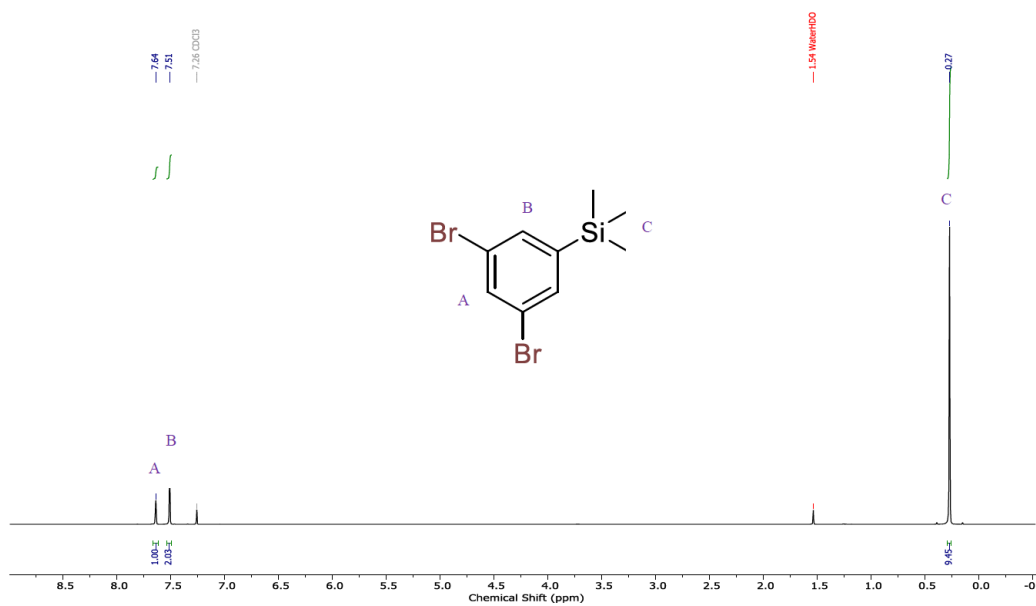


Figure A.5. ¹H NMR spectrum (500 MHz, CDCl₃) of 2.7.

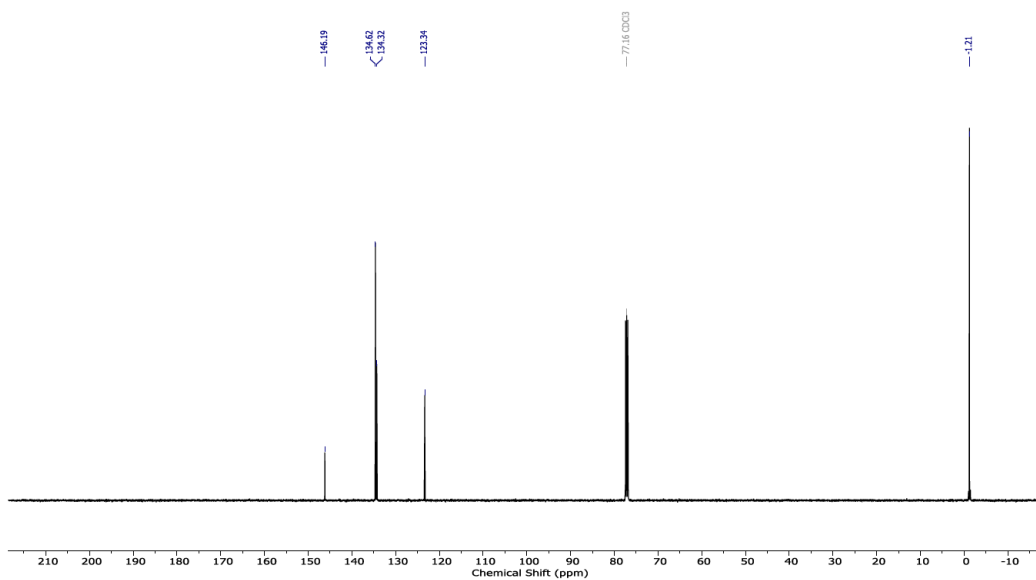


Figure A.6. ¹³C{¹H} NMR spectrum (126 MHz, CDCl₃) of 2.7.

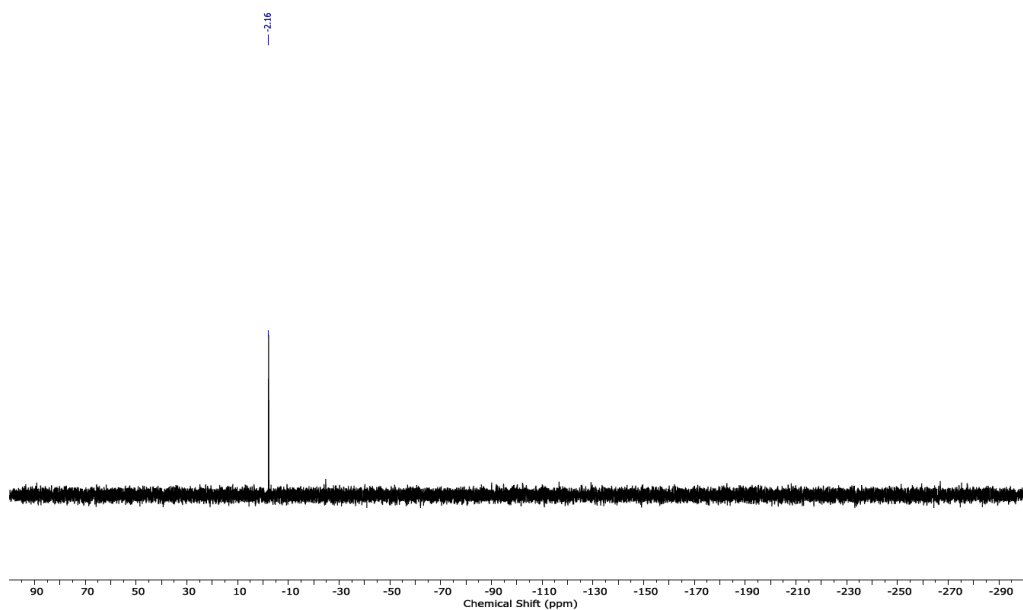


Figure A.7. $^{29}\text{Si}\{^1\text{H}\}$ NMR spectrum (99 MHz, CDCl_3) of **2.7**.

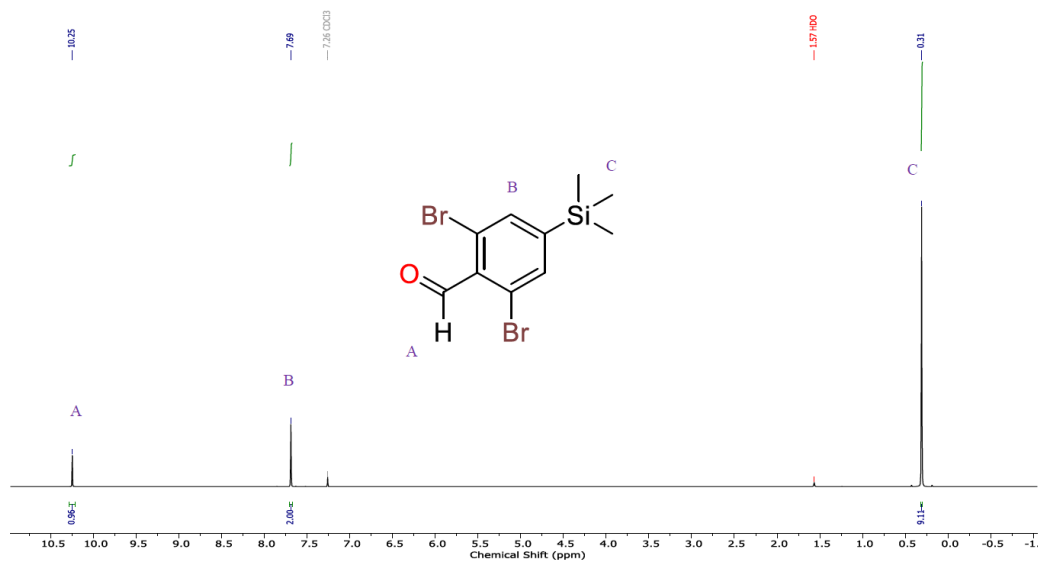


Figure A.8. ^1H NMR spectrum (500 MHz, CDCl_3) of **2.8**.

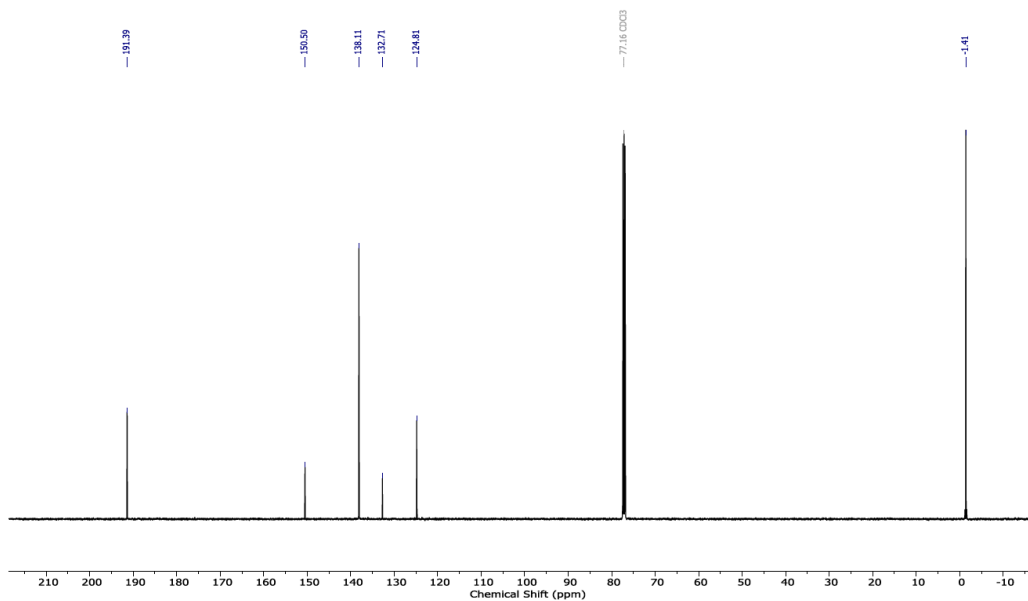


Figure A.9. $^{13}\text{C}\{^1\text{H}\}$ NMR spectrum (126 MHz, CDCl_3) of **2.8**.

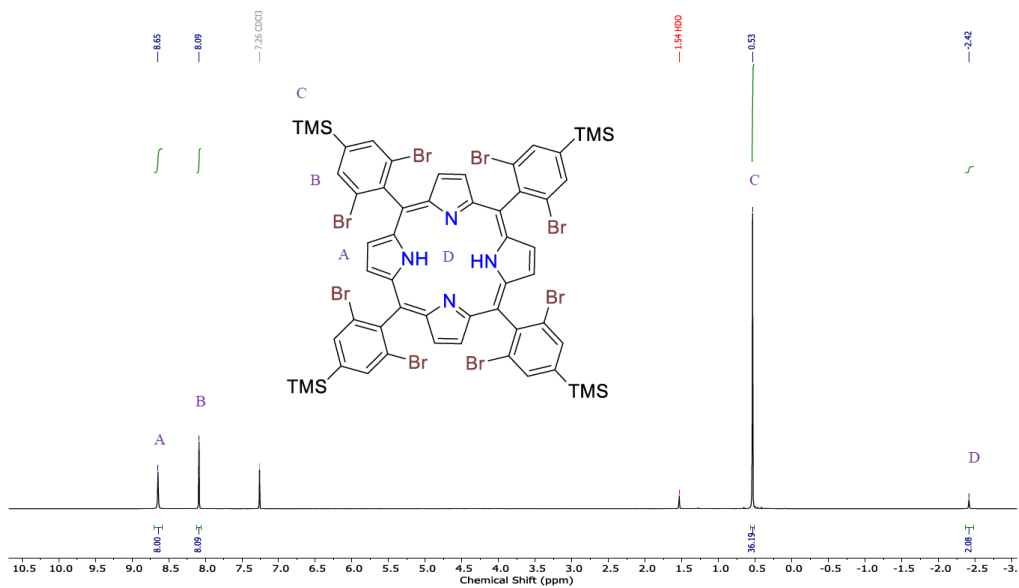


Figure A.10. ^1H NMR spectrum (500 MHz, CDCl_3) of **2.9**.

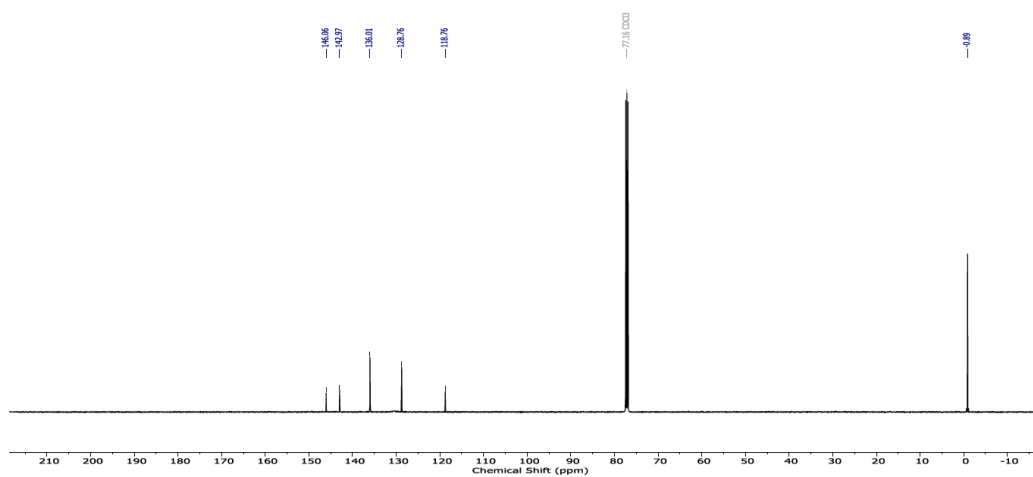


Figure A.11. $^{13}\text{C}\{^1\text{H}\}$ NMR spectrum (126 MHz, CDCl_3) of **2.9**.

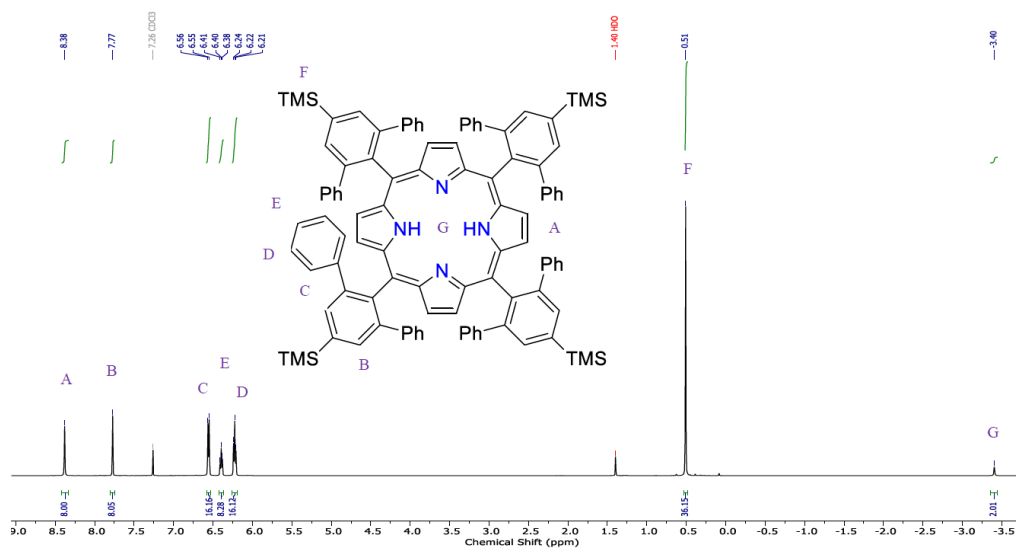


Figure A.12. ^1H NMR spectrum (500 MHz, CDCl_3) of **2.10**.

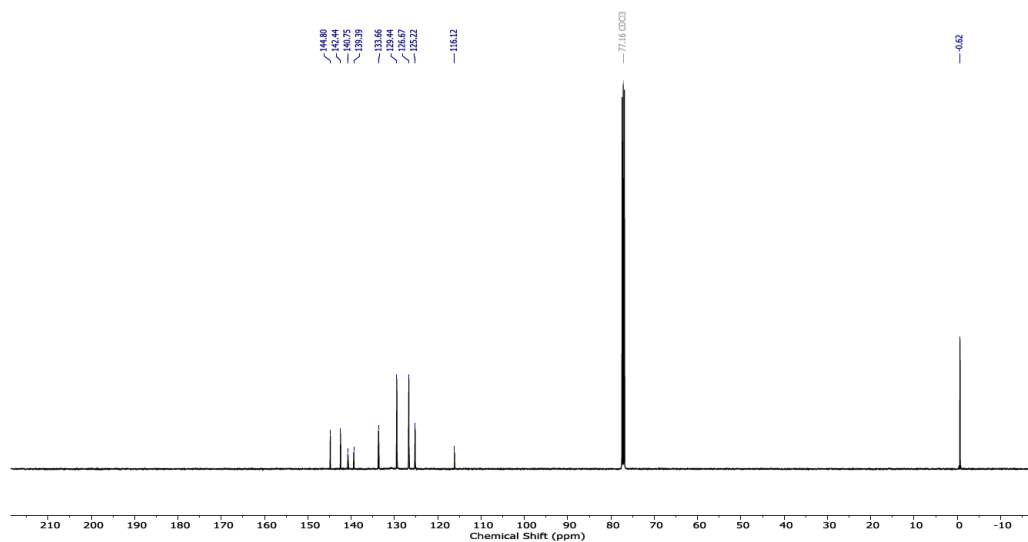


Figure A.13. $^{13}\text{C}\{^1\text{H}\}$ NMR spectrum (126 MHz, CDCl_3) of **2.10**.

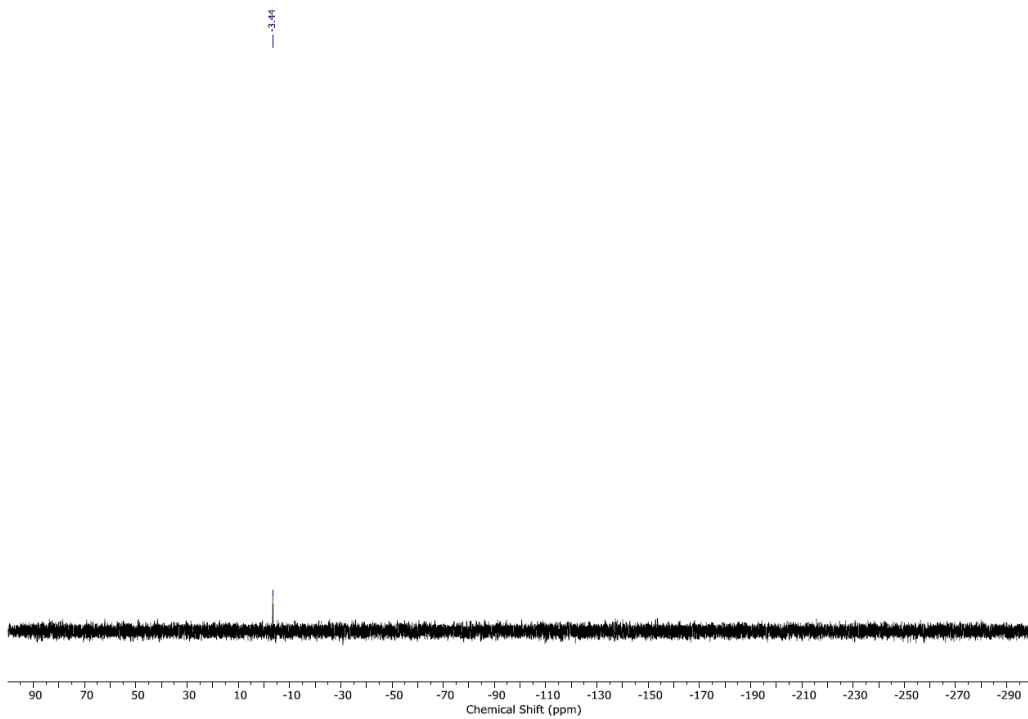


Figure A.14. $^{29}\text{Si}\{^1\text{H}\}$ NMR spectrum (99 MHz, CDCl_3) of **2.10**.

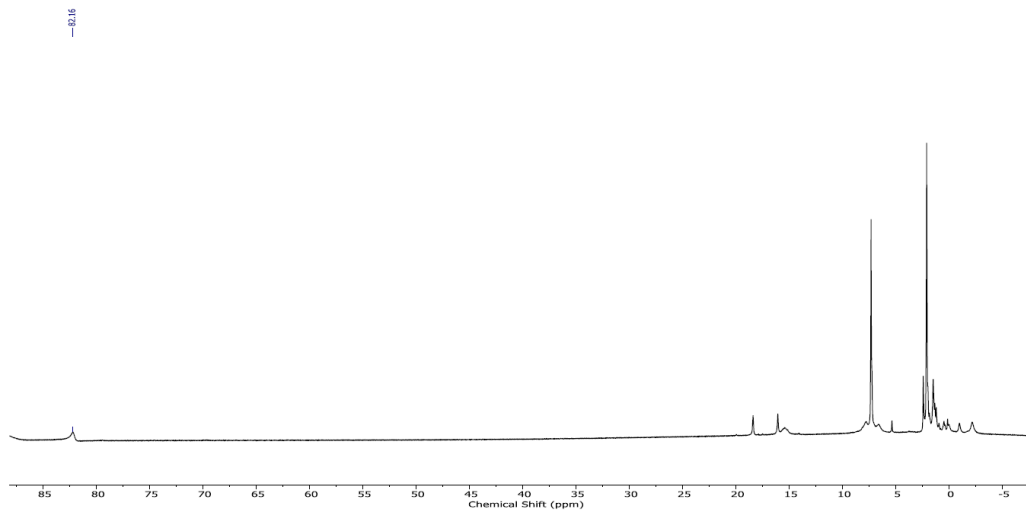


Figure A.15. ^1H NMR spectrum (500 MHz, CDCl_3) of **2.11**. NB: this substance is paramagnetic.

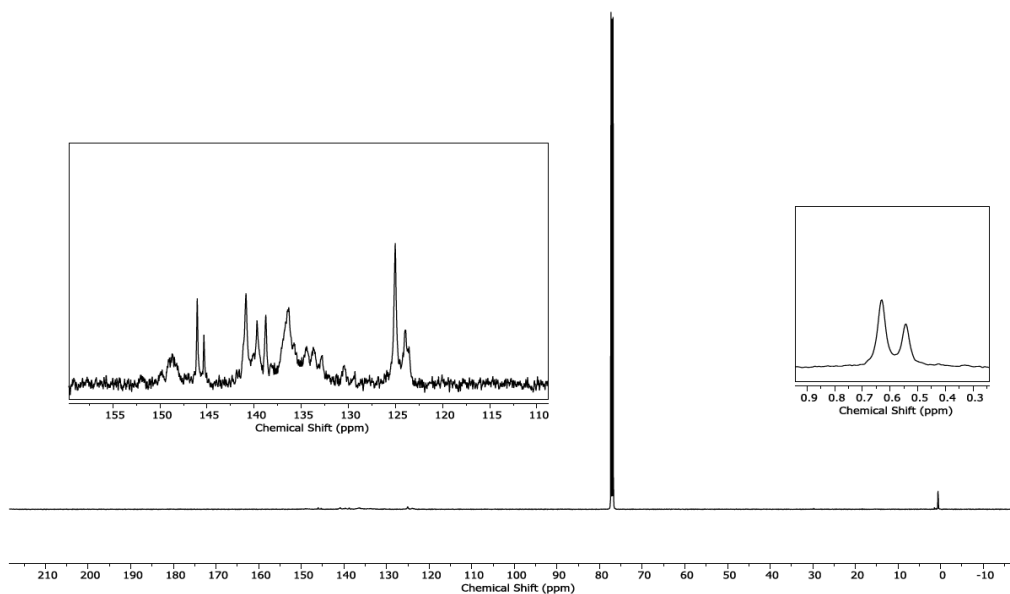


Figure A.16. $^{13}\text{C}\{^1\text{H}\}$ NMR spectrum (500 MHz, CDCl_3) of **2.11**. NB: this substance is paramagnetic.

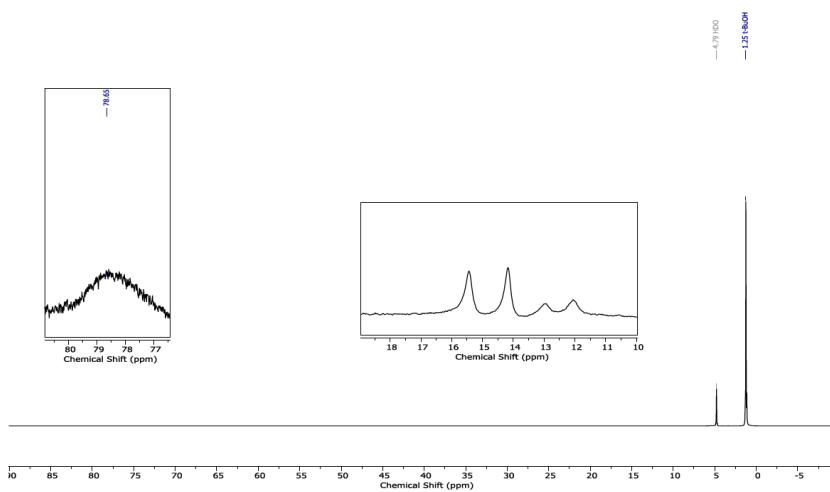


Figure A.17. ^1H NMR spectrum (500 MHz, D_2O , 10% $^t\text{BuOH}$) of the sample used for Evans' method μ_{eff} determination of **2.12**. NB: this substance is paramagnetic.

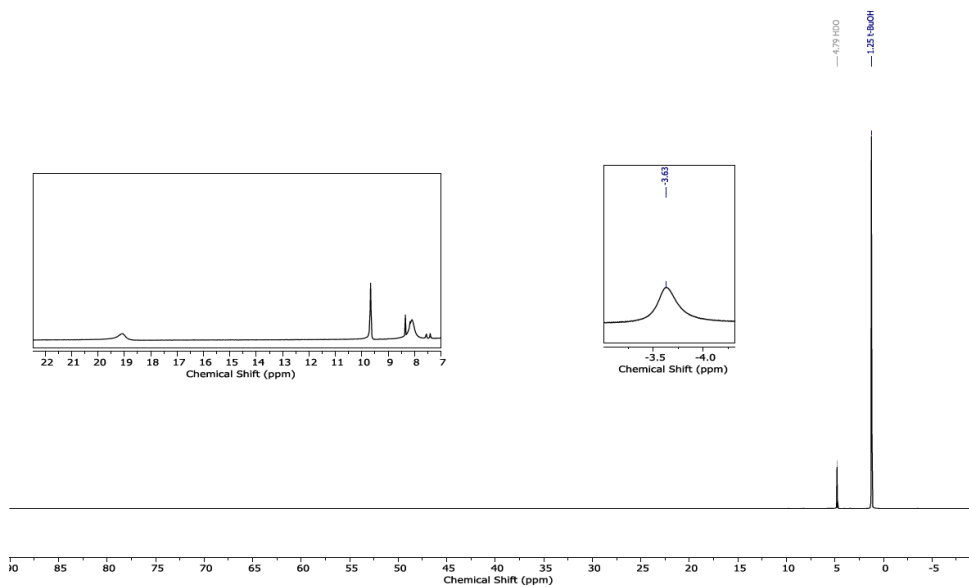


Figure A.18. ^1H NMR spectrum (500 MHz, PBS-d , 10% $^t\text{BuOH}$) of the sample used for Evans' method μ_{eff} determination of reduced **2.12**. NB: this substance is paramagnetic.

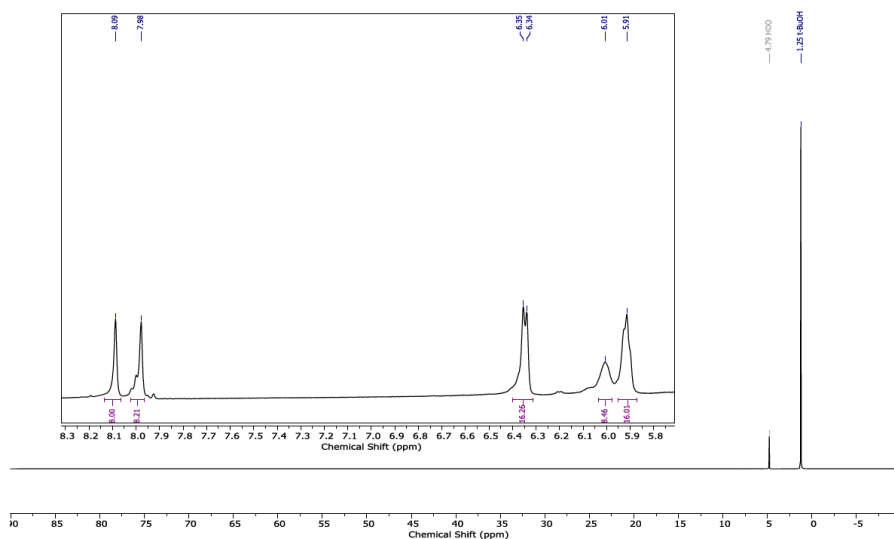


Figure A.19. ¹H NMR spectrum (500 MHz, PBS-*d*, 10% ¹BuOH) of the sample used for Evans' method μ_{eff} determination of **2.13**.

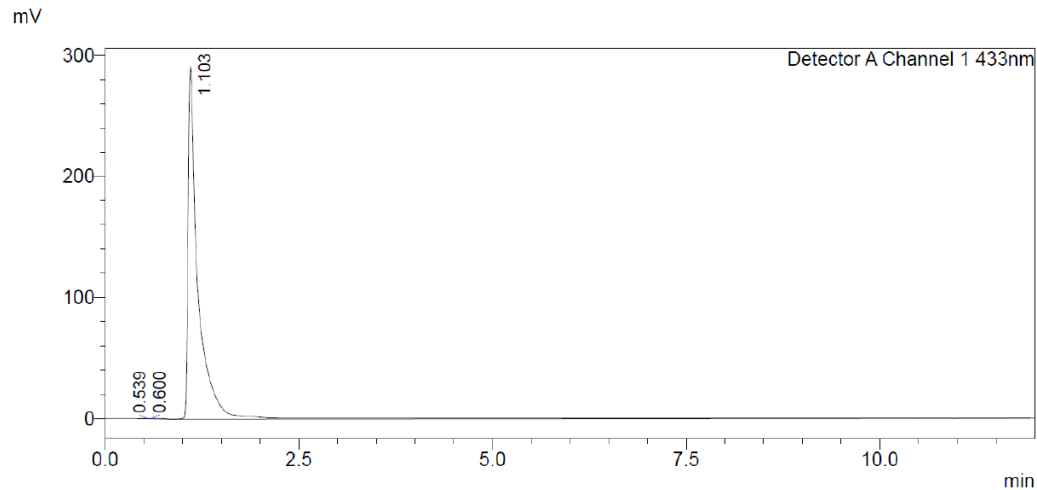


Figure A.20. HPLC chromatogram of **2.12**. Absorbance is measured at 433 nm and the analyte was eluted with a H₂O/MeCN (0.01% TFA) gradient of 0-95% MeCN over 15 min.

Table A.1. Refinement Details for High-Resolution Crystal Structures

Compound	2.10·2MeCN	2.11·DCM·MeCN	2.12_{DMSO}·4DCM
Formula	C ₁₀₈ H ₁₀₀ N ₆ Si ₄	C ₁₀₇ H ₉₈ Cl ₂ FeN ₅ OSi ₄	C ₁₁₁ H ₉₉ Cl ₂₁ FeN ₄ Na ₃ O ₁₈ S ₁₀
FW	1594.29	1709.01	2966.81
T (K)	100.0(1)	100.0(1)	100.0(1)
λ (Å)	1.54184	1.54184	1.54184
Crystal System	Triclinic	Monoclinic	Triclinic
Space group	<i>P1</i>	<i>P2₁/c</i>	<i>P1</i>
<i>a</i> (Å)	13.1696(2)	16.3187(2)	14.03520(10)
<i>b</i> (Å)	13.5821(2)	12.8480(2)	14.48810(10)
<i>c</i> (Å)	16.0892(2)	23.5087(2)	16.95090(10)
α (°)	89.2370(10)		72.6450(10)
β (°)	71.1150(10)	106.80000(10)	80.2710(10)
γ (°)	61.112(2)		88.616(2)
Volume (Å ³)	2348.33	4718.53(10)	86.7770(10)
<i>Z</i>	1	2	1
ρ _{calc} (Mg/m ³)	1.127	1.203	1.519
Size (mm ³)	0.25×0.19×0.05	0.31×0.17×0.05	0.15×0.08×0.08
θ range (°)	2.95-67.07	2.79-76.74	2.77-67.08
Total data	89543	67527	95102
Unique data	8389	8417	11584
Parameters	540	588	831
Completeness (%)	100	99.9	99.9
<i>R</i> _{int} (%)	4.46	3.59	3.48
<i>R</i> ₁ (% , I > 2σ)	3.38	6.48	5.73
<i>R</i> ₁ (% , all data)	3.57	6.90	5.90
<i>wR</i> ₂ (% , I > 2σ)	8.59	18.16	15.81
<i>wR</i> ₂ (% , all data)	8.72	18.47	15.95
<i>S</i>	1.041	1.065	1.037

Table A.2. Crystallographic Parameters for Low-Resolution Crystal Structure of **2.12**

Compound	2.12
T (K)	100.0(1)
λ (Å)	1.54184
Crystal System	Tetragonal
Space group	$P4_2/n$
a (Å)	23.1879(2)
c (Å)	24.2311(3)
Volume (Å ³)	13028.5(2)
Z	4

Appendix B: Supplementary Experimental Data for Chapter 3

Published in part Daniel G. Droege, A. Leila Parker, Griffin M. Milligan, Robert Jenkins, and Timothy C. Johnstone, *J. Org. Chem.* **2022**, *87*, 11783–11795

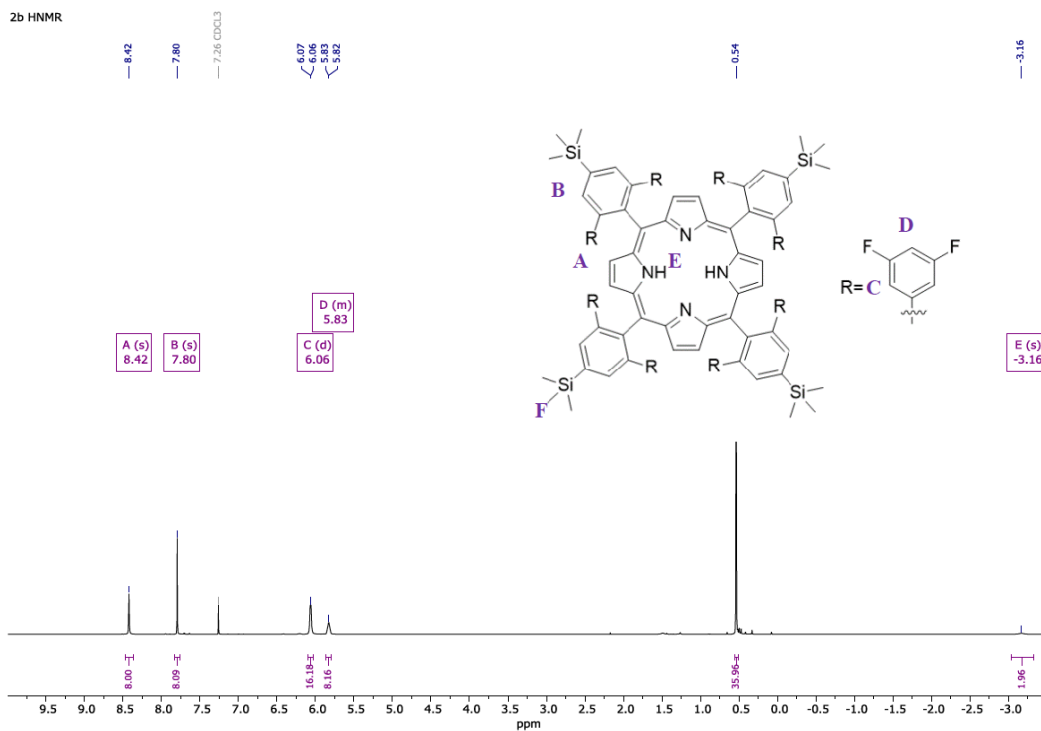


Figure B.1. ¹H NMR spectrum (500 MHz, CDCl₃) of **3.2b**.

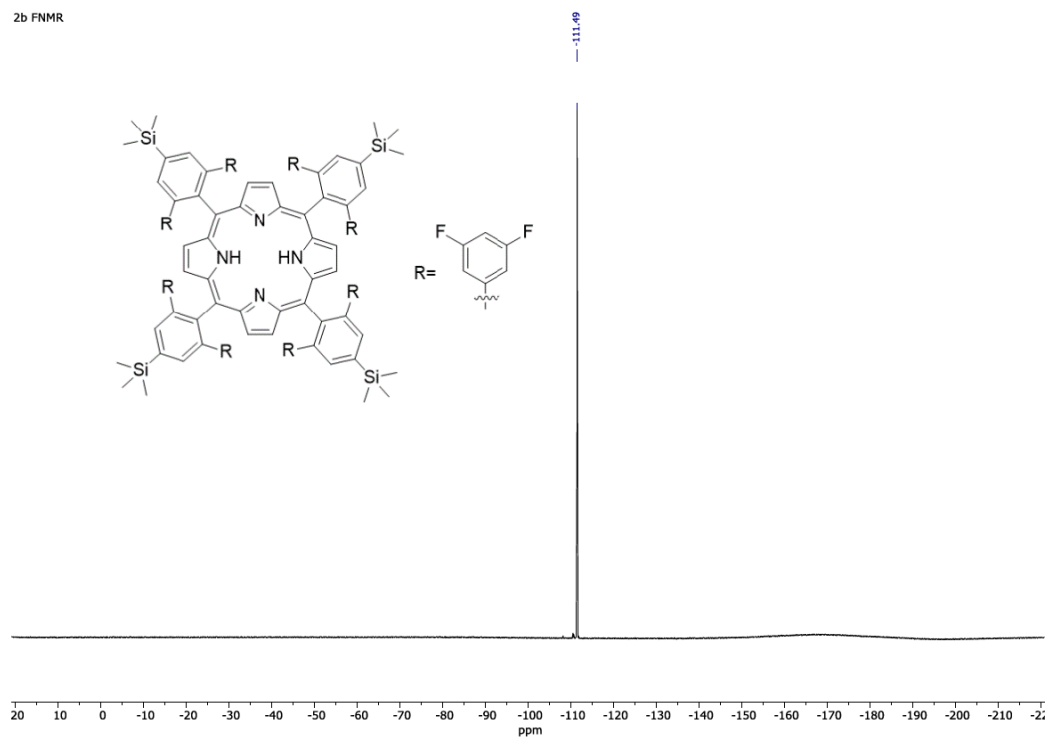


Figure B.2. ¹⁹F{¹H} NMR spectrum (470 MHz, CDCl₃) of **3.2b**.

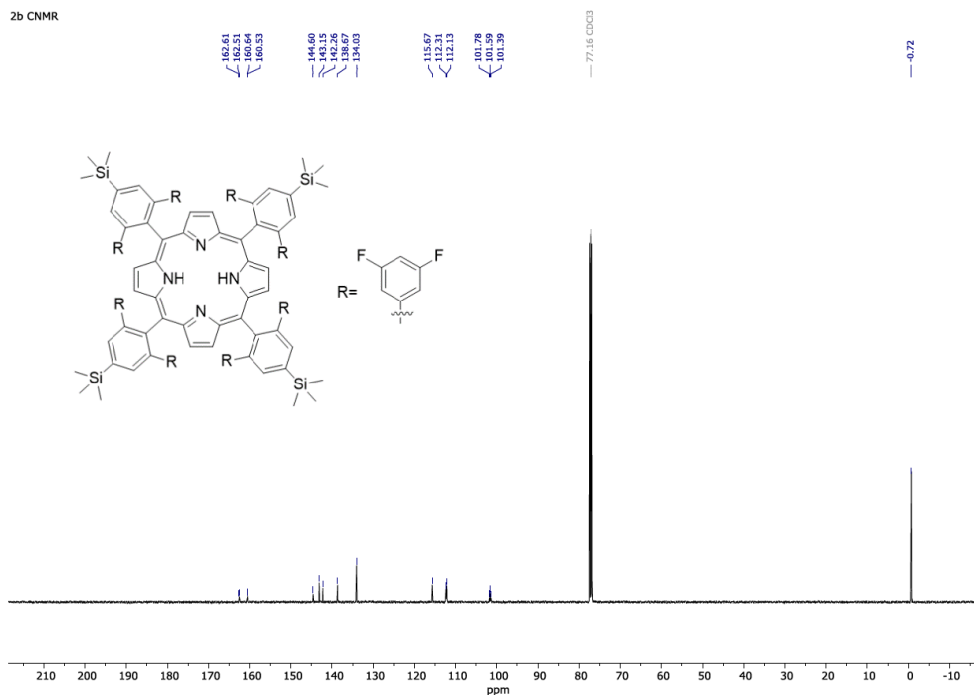


Figure B.3. $^{13}\text{C}\{^1\text{H}\}$ NMR spectrum (126 MHz, CDCl_3) of **3.2b**.

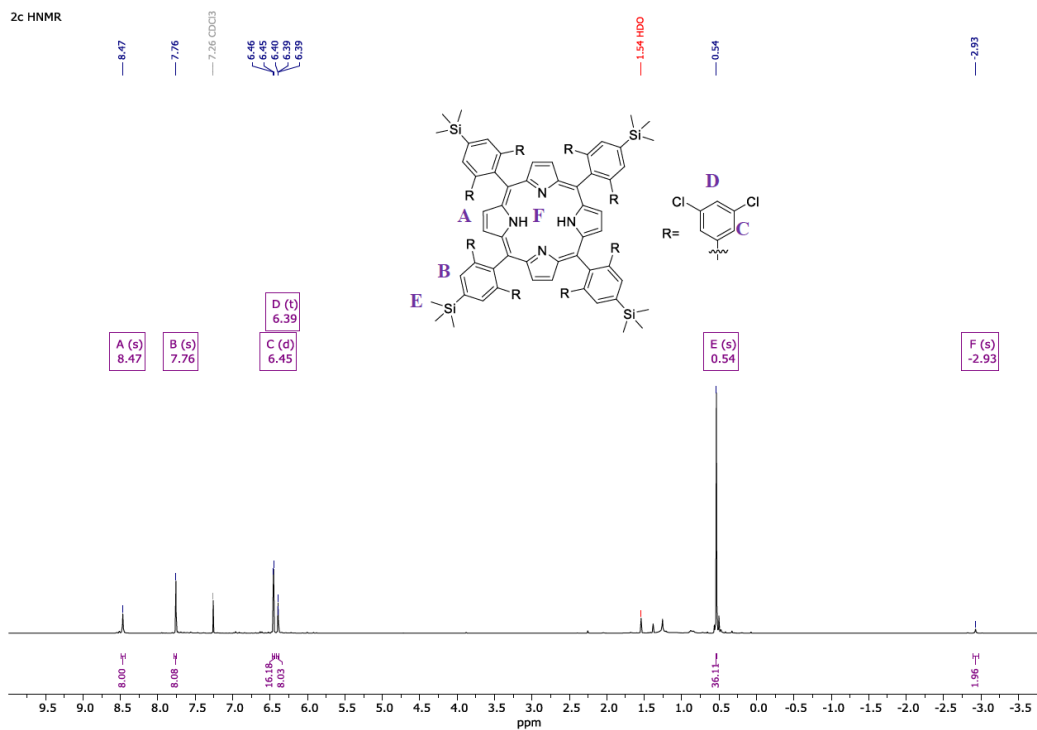


Figure B.4. ^1H NMR spectrum (500 MHz, CDCl_3) of **3.2c**.

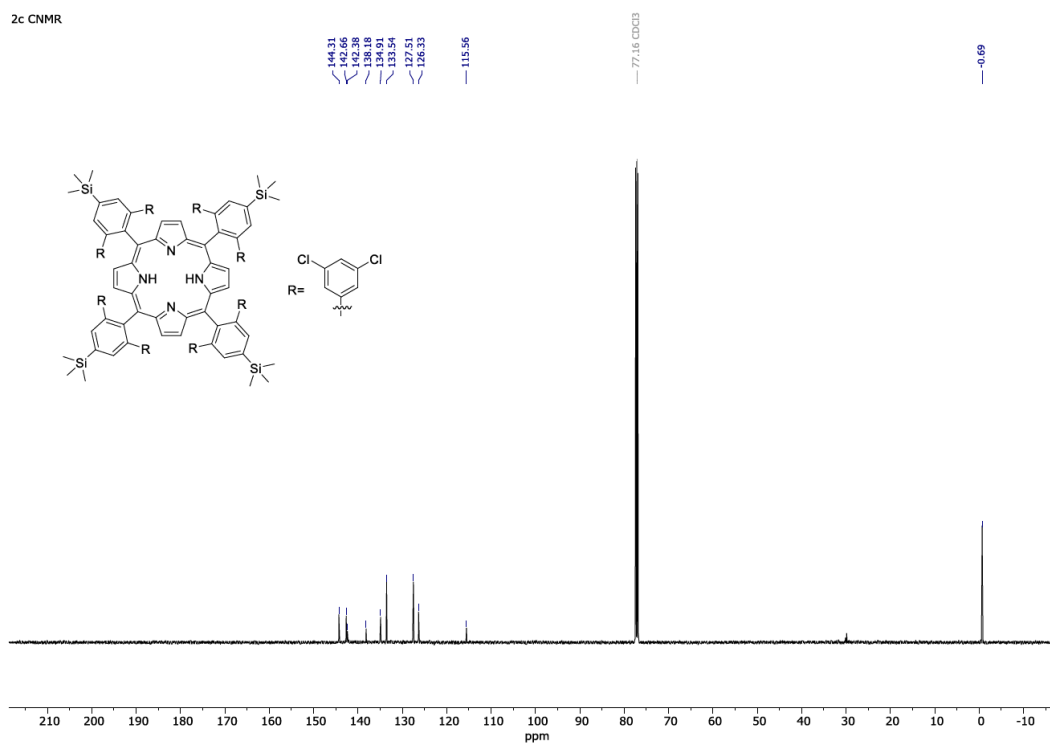


Figure B.5. $^{13}\text{C}\{^1\text{H}\}$ NMR spectrum (126 MHz, CDCl_3) of **3.2c**.

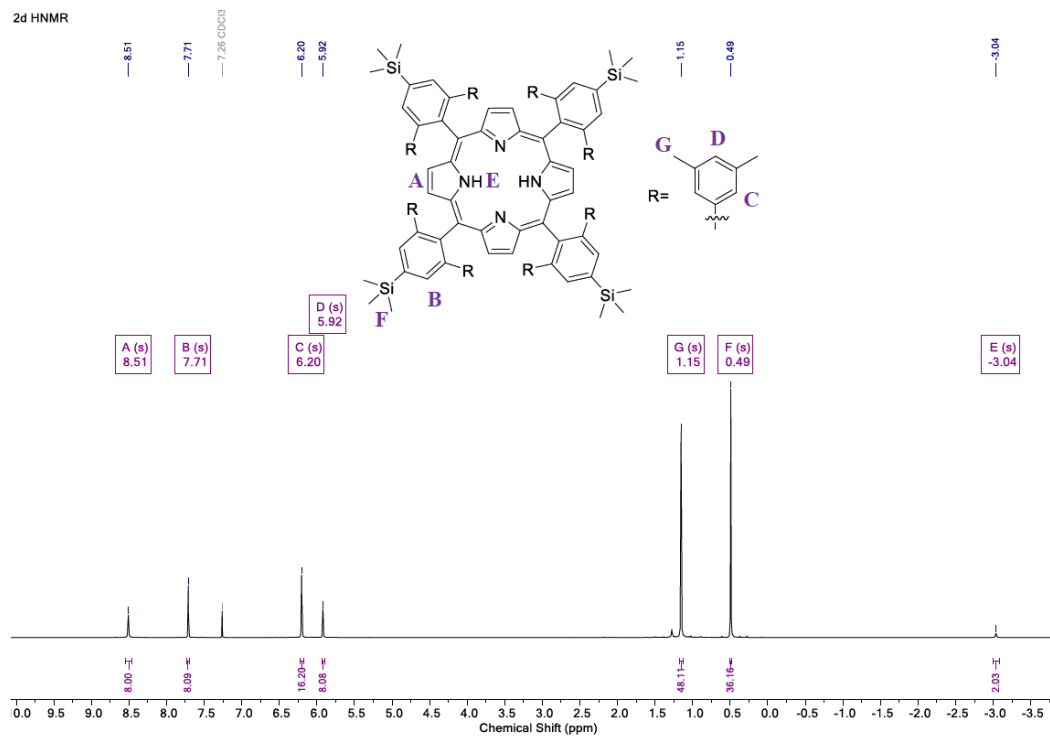


Figure B.6. ^1H NMR spectrum (500 MHz, CDCl_3) of **3.2d**.

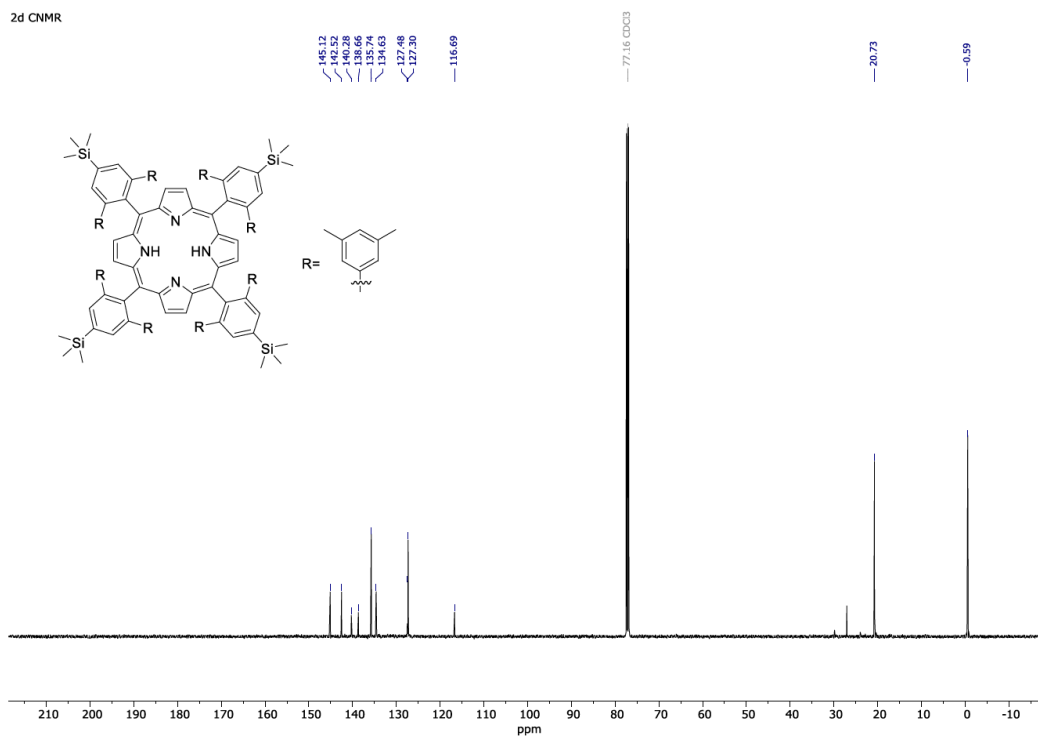


Figure B.7. $^{13}\text{C}\{^1\text{H}\}$ NMR spectrum (126 MHz, CDCl_3) of **3.2d**.

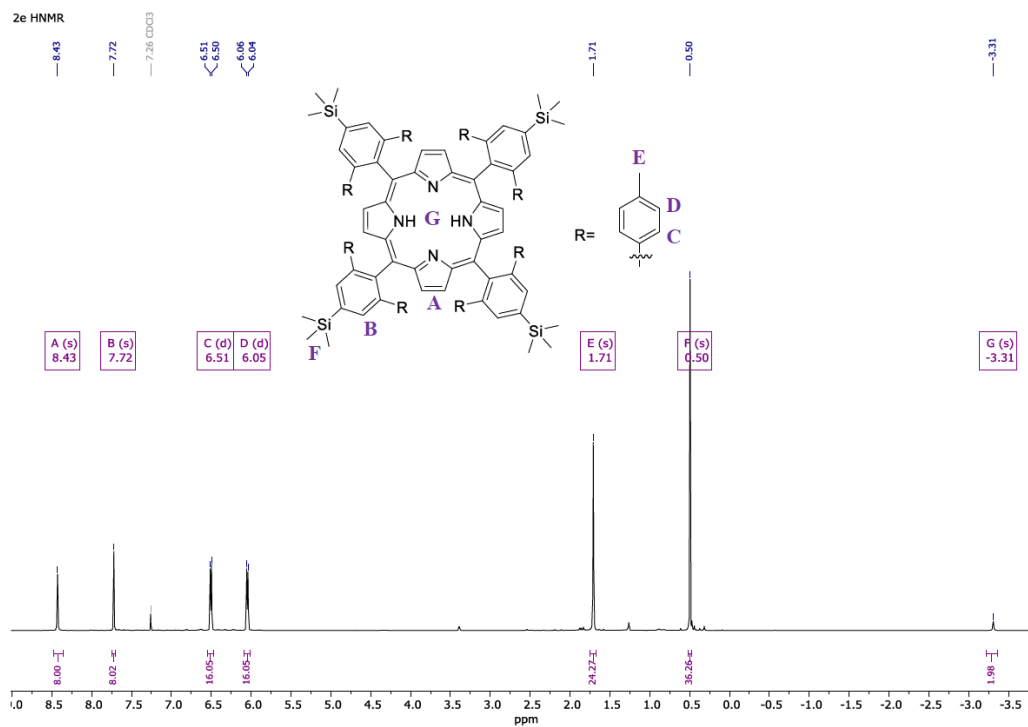


Figure B.8. ^1H NMR spectrum (500 MHz, CDCl_3) of **3.2e**.

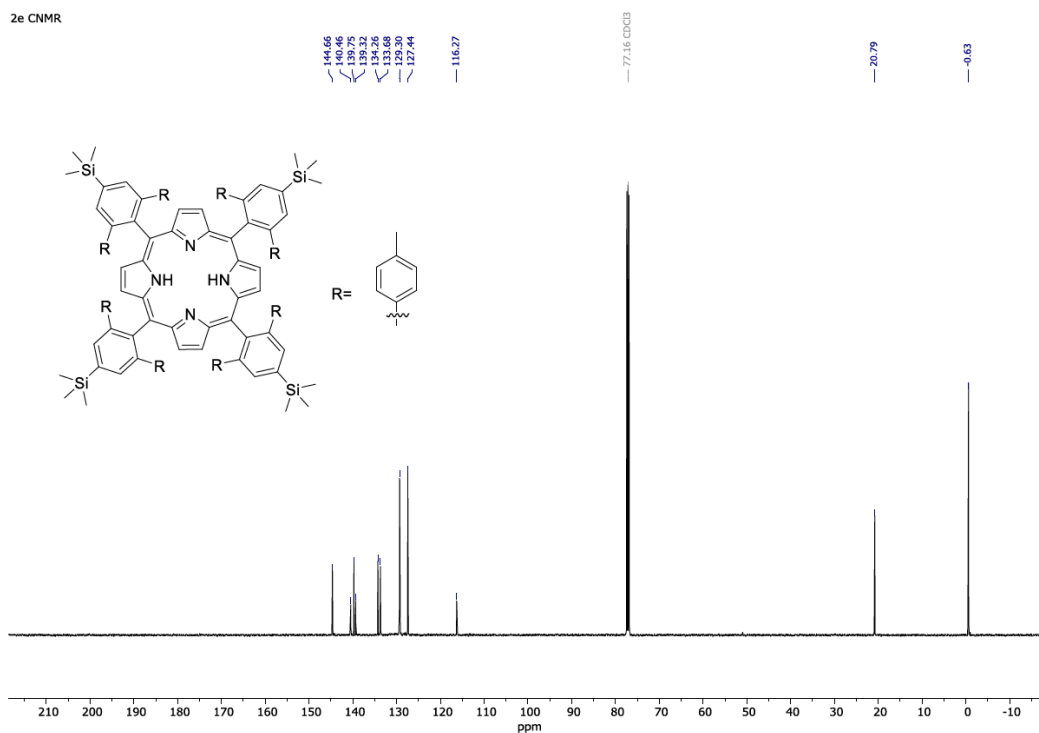


Figure B.9. $^{13}\text{C}\{^1\text{H}\}$ NMR spectrum (126 MHz, CDCl_3) of **3.2e**.

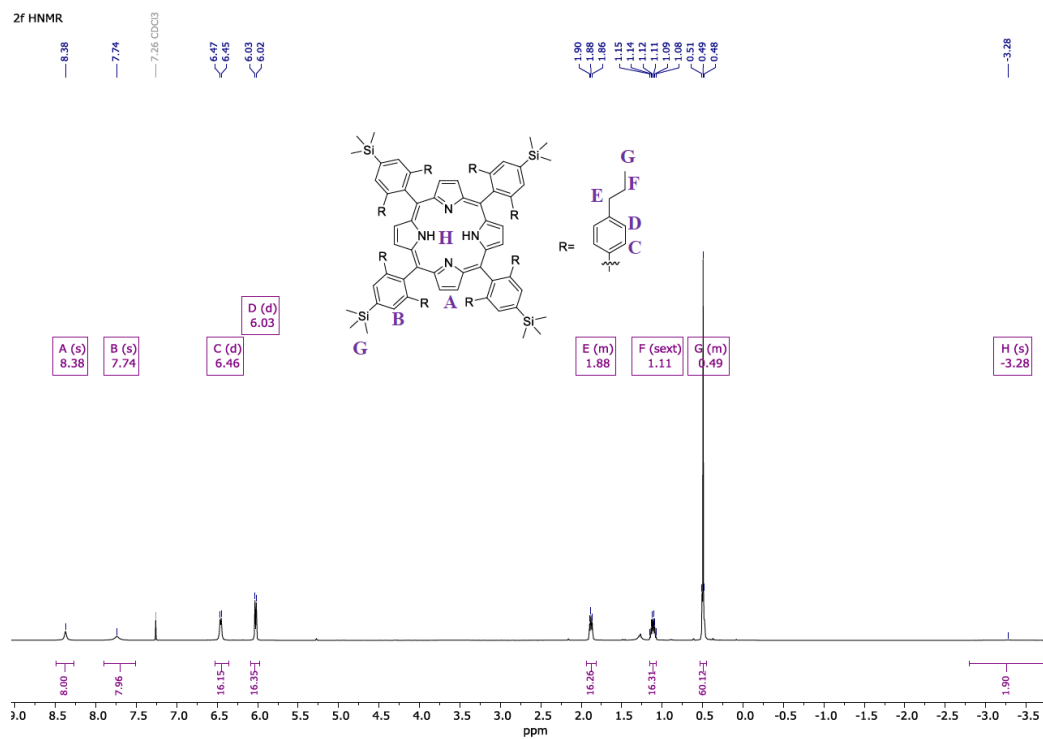


Figure B.10. ^1H NMR spectrum (500 MHz, CDCl_3) of **3.2f**.

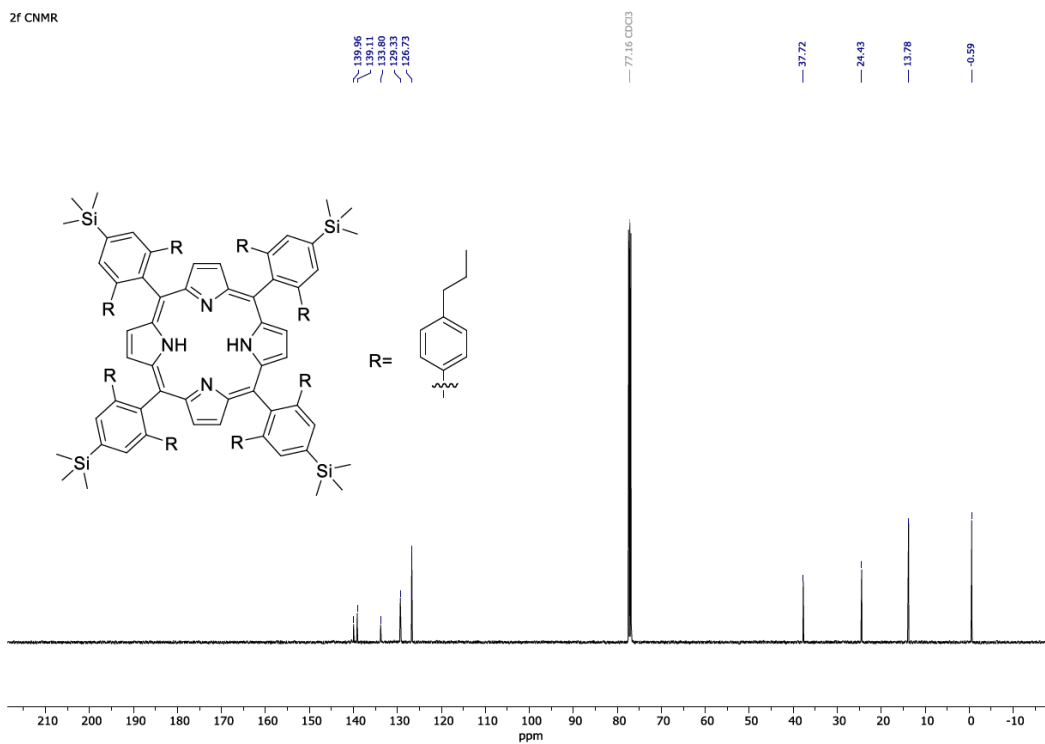


Figure B.11. ¹³C{¹H} NMR spectrum (126 MHz, CDCl₃) of **3.2f**.

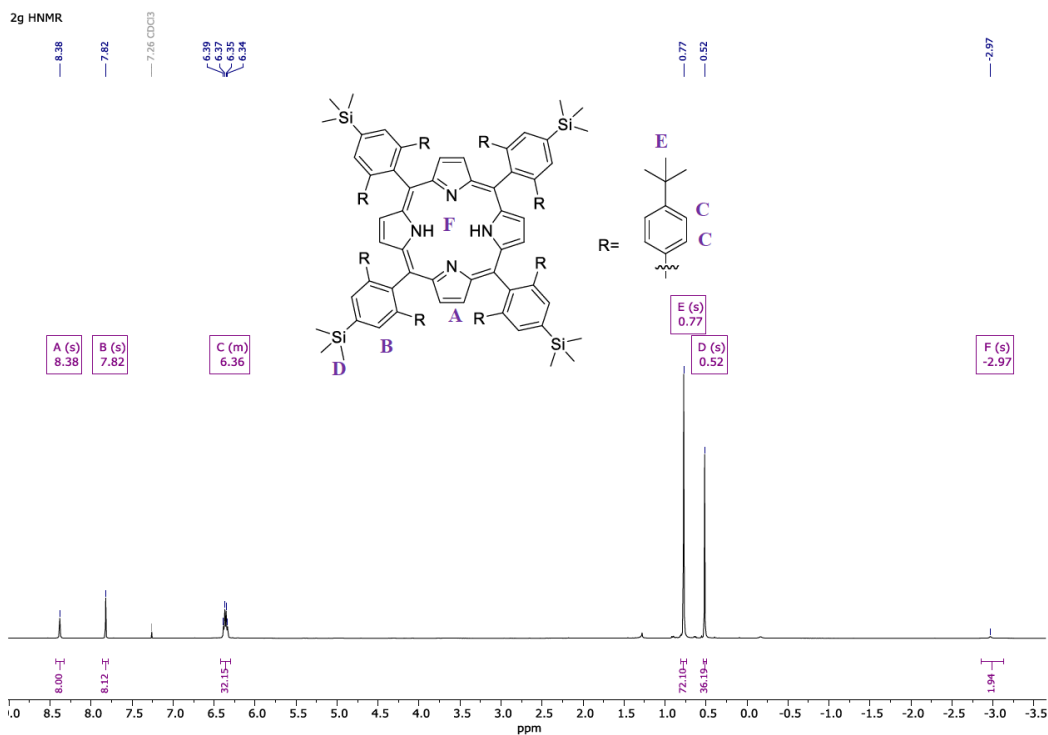


Figure B.12. ¹H NMR spectrum (500 MHz, CDCl₃) of **3.2g**.

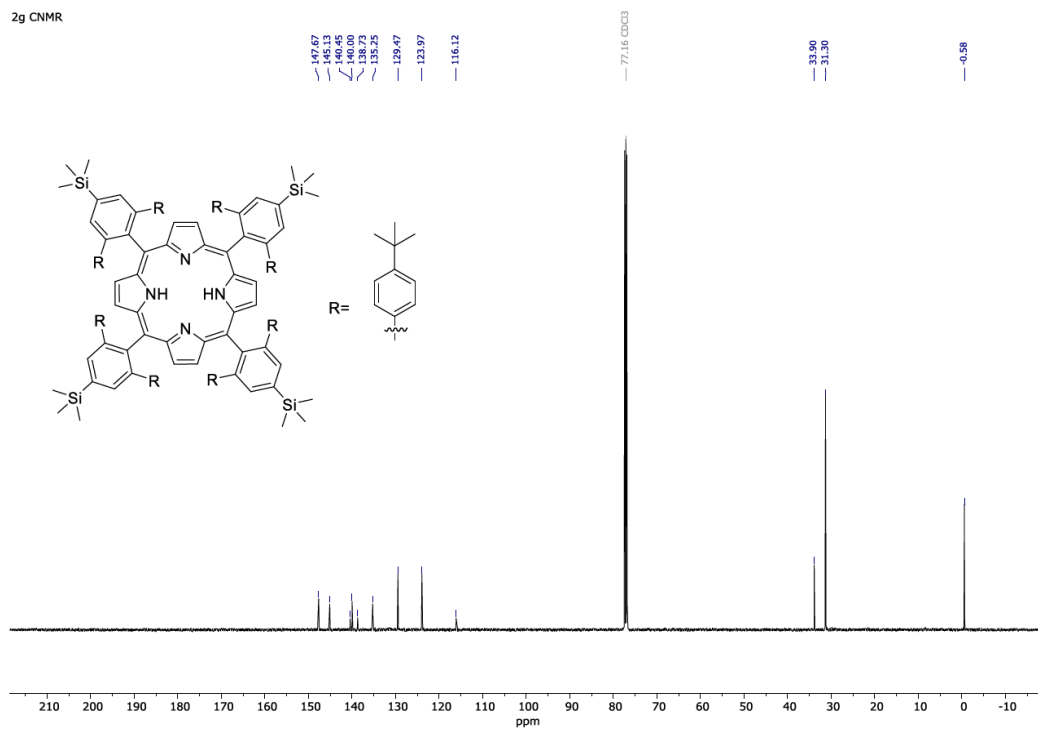


Figure B.13. $^{13}\text{C}\{^1\text{H}\}$ NMR spectrum (126 MHz, CDCl₃) of **3.2g**.

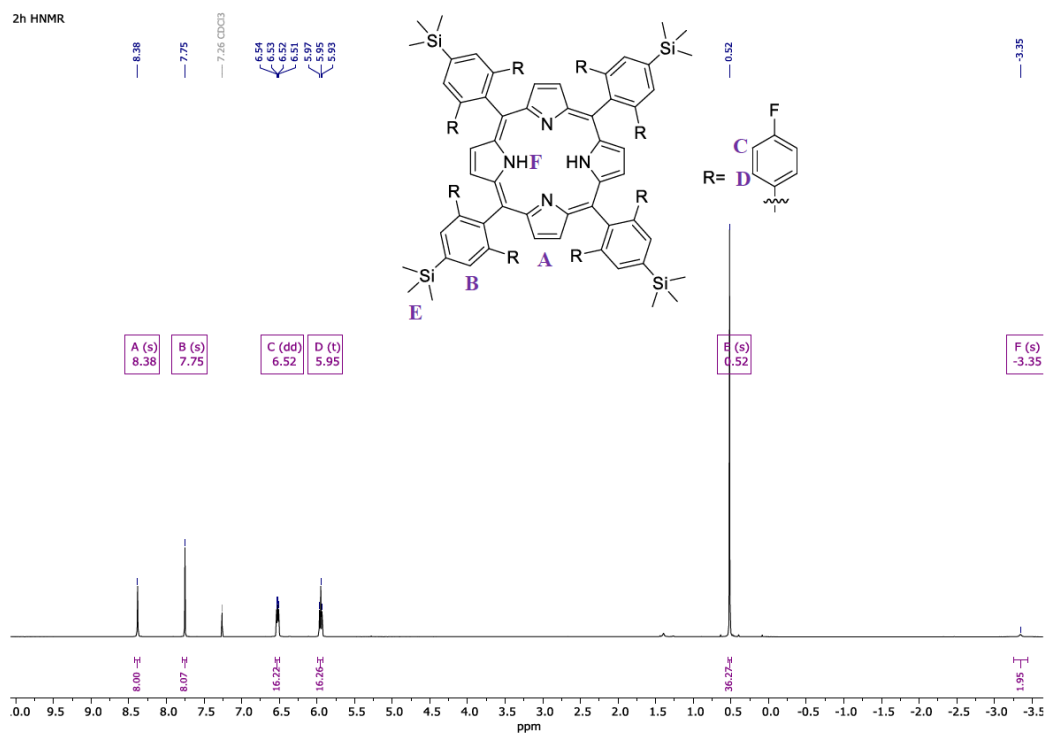


Figure B.14. ^1H NMR spectrum (500 MHz, CDCl₃) of **3.2h**.

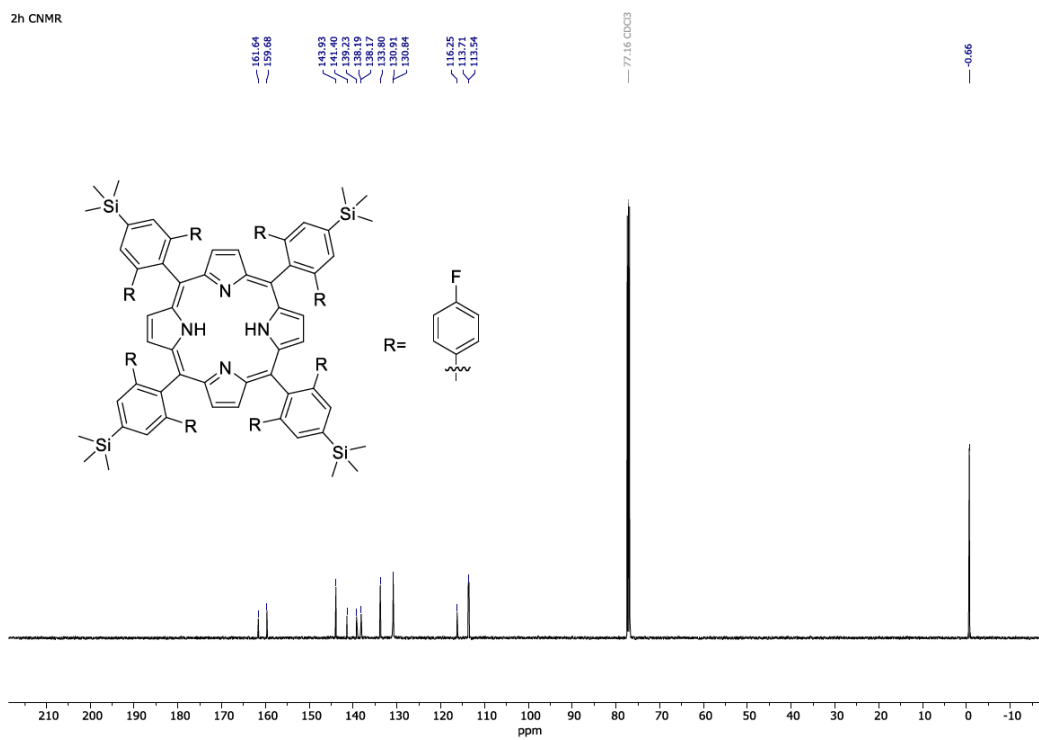


Figure B.15. $^{13}\text{C}\{^1\text{H}\}$ NMR spectrum (126 MHz, CDCl_3) of **3.2h**.

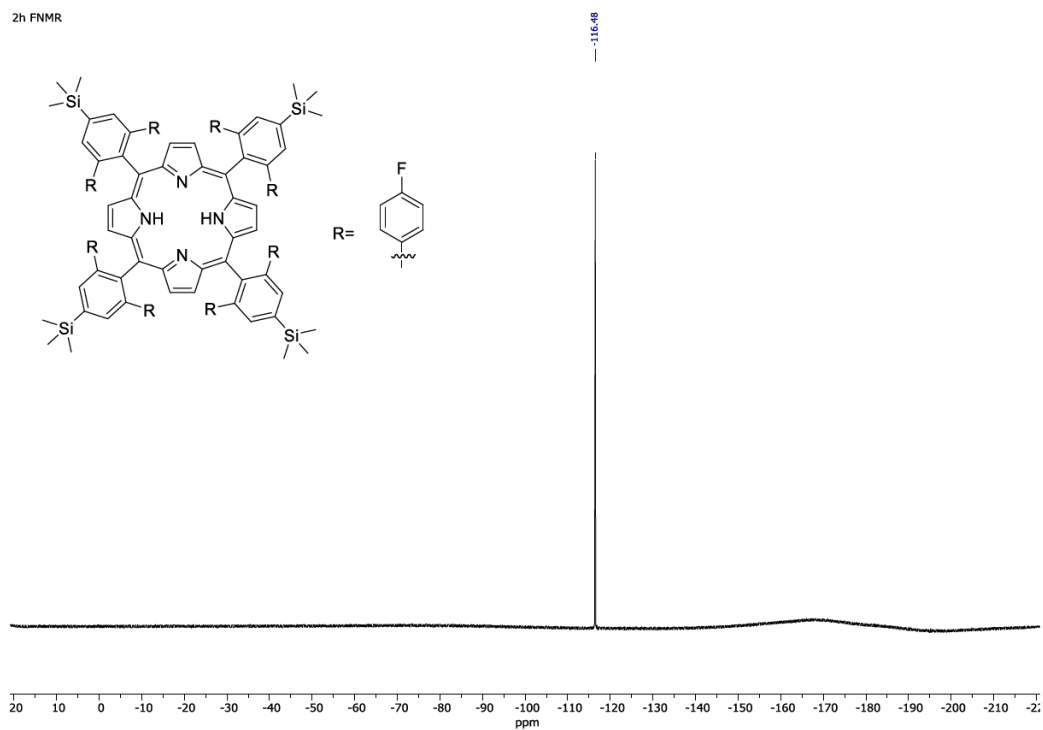


Figure B.16. $^{19}\text{F}\{^1\text{H}\}$ NMR spectrum (470 MHz, CDCl_3) of **3.2h**.

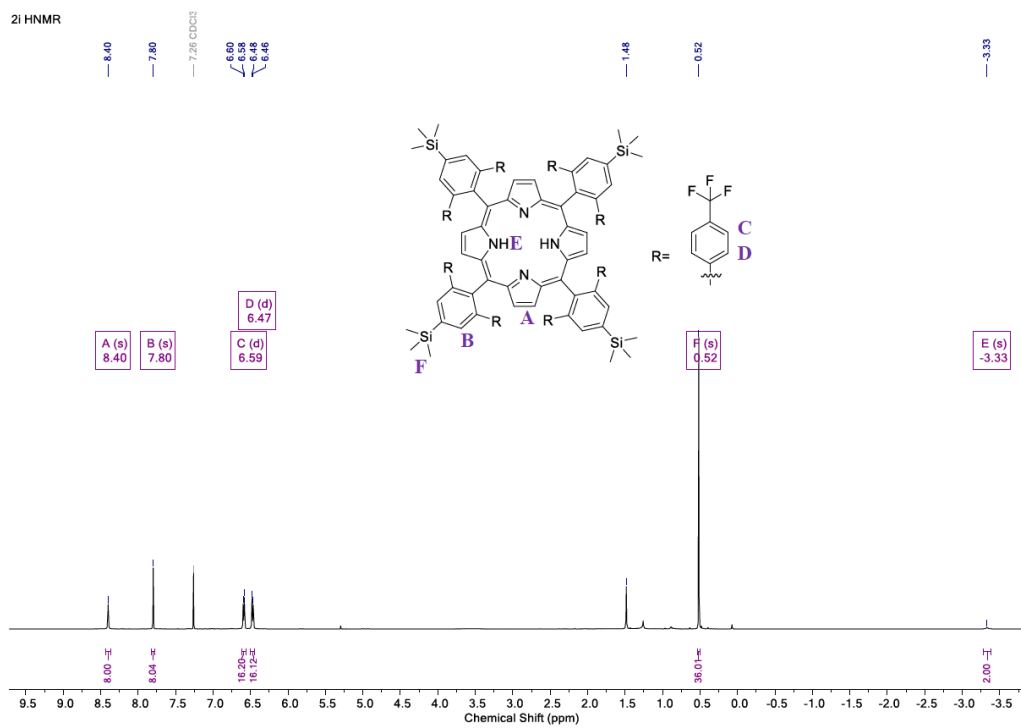


Figure B.17. ^1H NMR spectrum (500 MHz, CDCl_3) of **3.2i**.

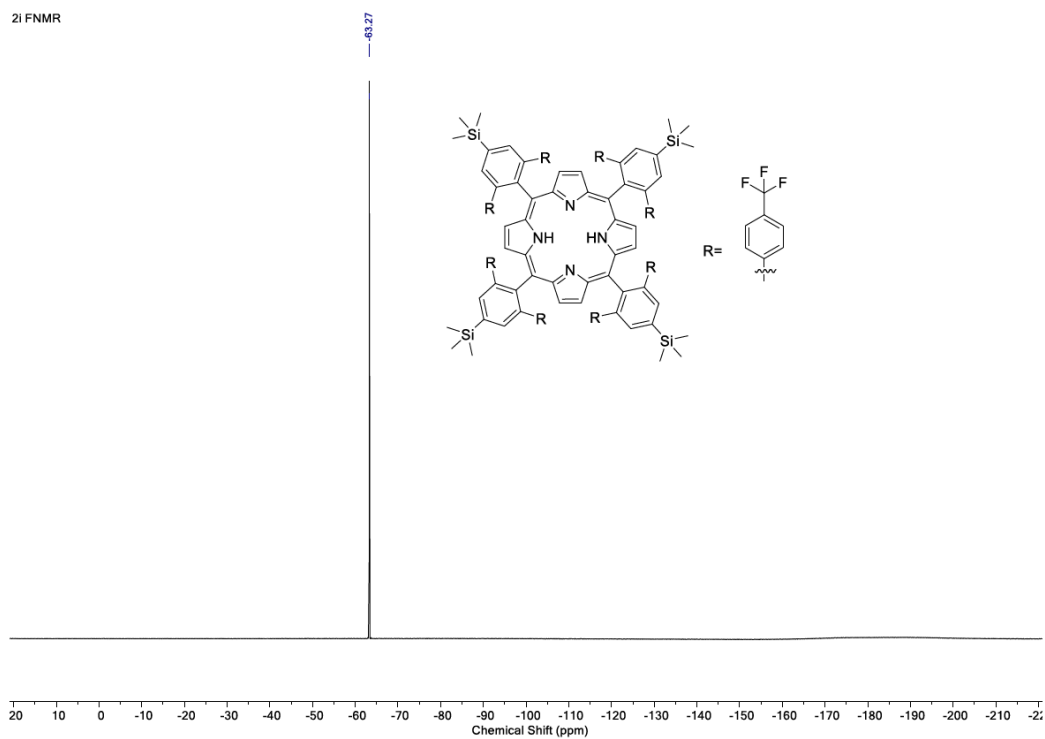


Figure B.18. $^{19}\text{F}\{^1\text{H}\}$ NMR spectrum (470 MHz, CDCl_3) of **3.2i**.

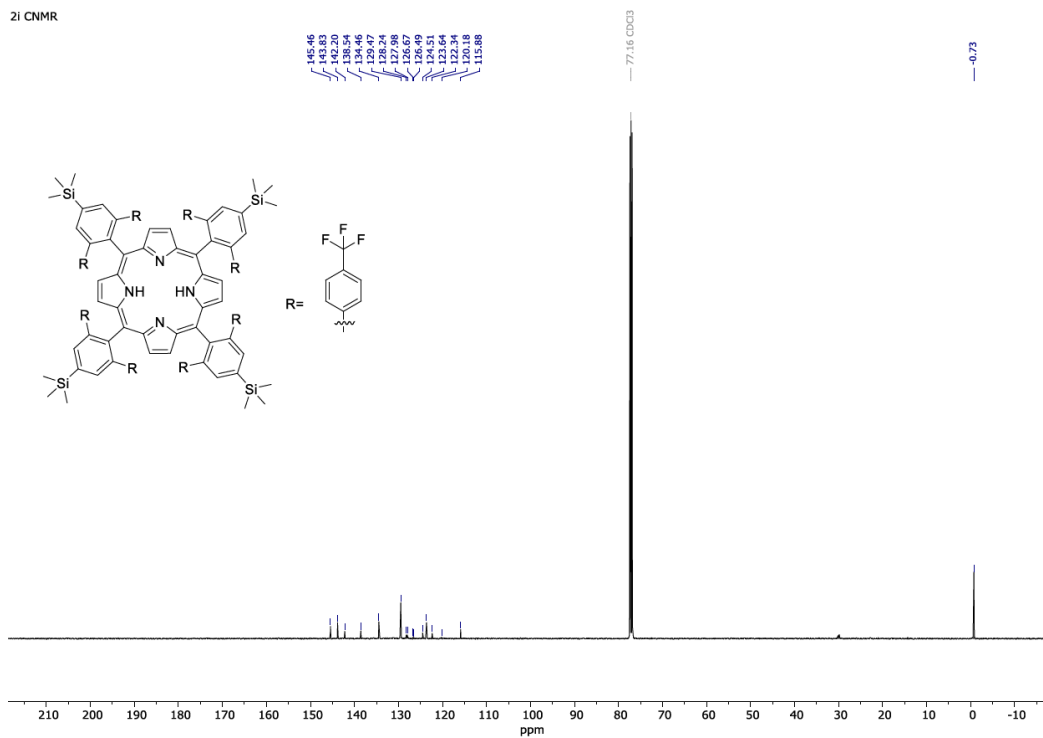


Figure B.19. $^{13}\text{C}\{^1\text{H}\}$ NMR spectrum (126 MHz, CDCl_3) of 3.2i.

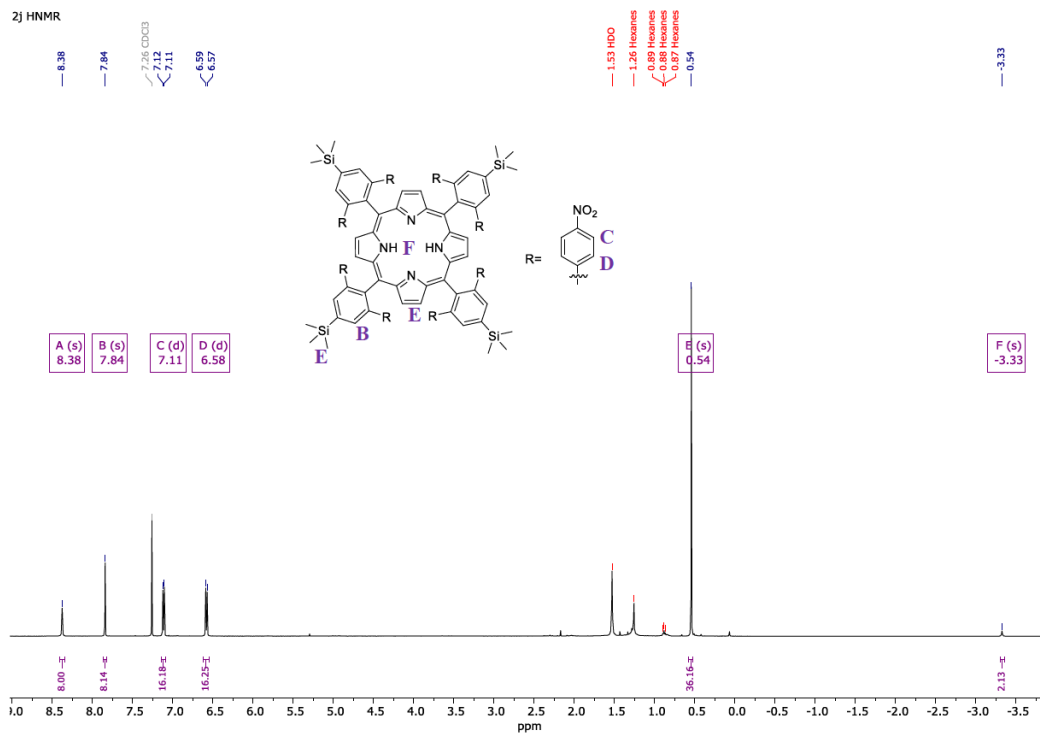


Figure B.20. ^1H NMR spectrum (500 MHz, CDCl_3) of 3.2j.

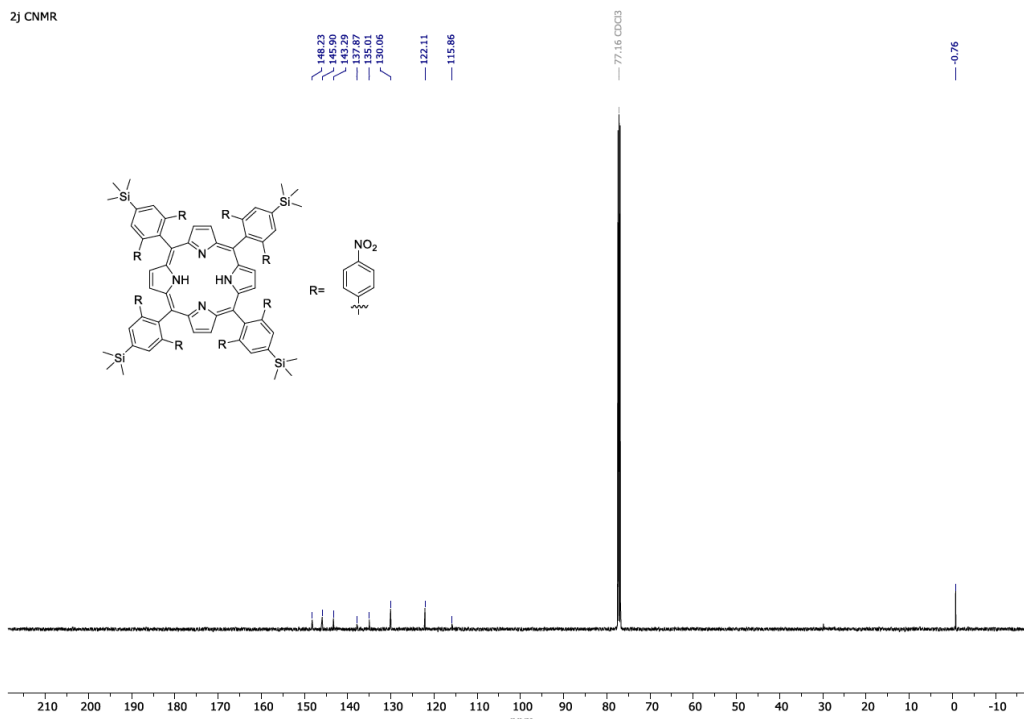


Figure B.21. $^{13}\text{C}\{^1\text{H}\}$ NMR spectrum (126 MHz, CDCl_3) of **3.2j**.

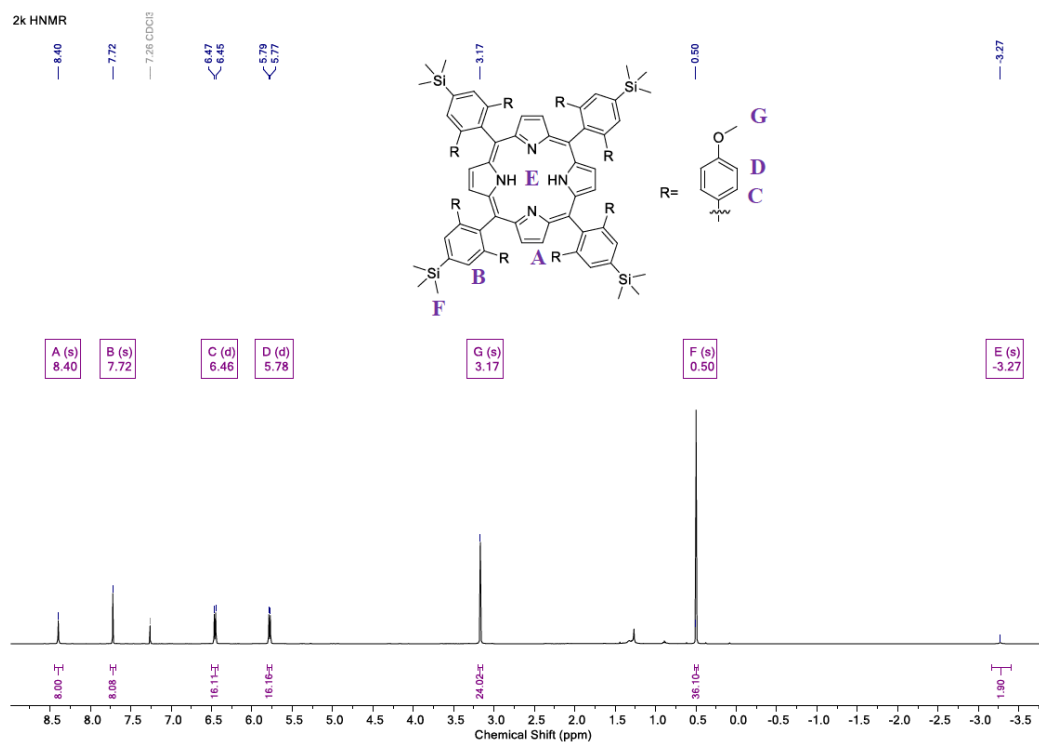


Figure B.22. ^1H NMR spectrum (500 MHz, CDCl_3) of **3.2k**.

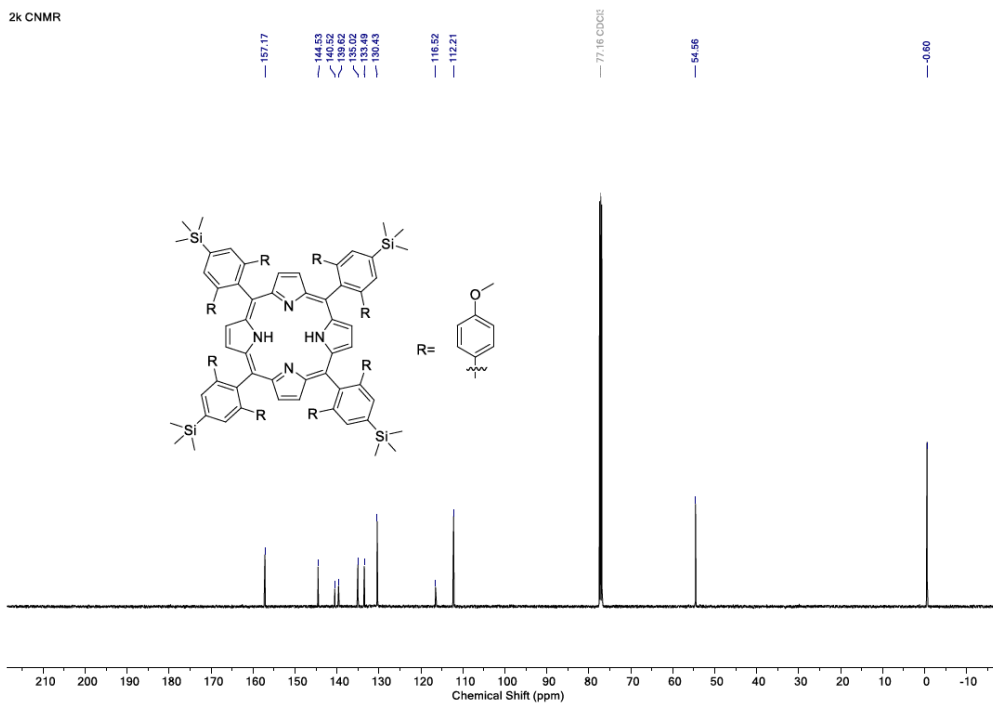


Figure B.23. $^{13}\text{C}\{^1\text{H}\}$ NMR spectrum (126 MHz, CDCl_3) of **3.2k**.

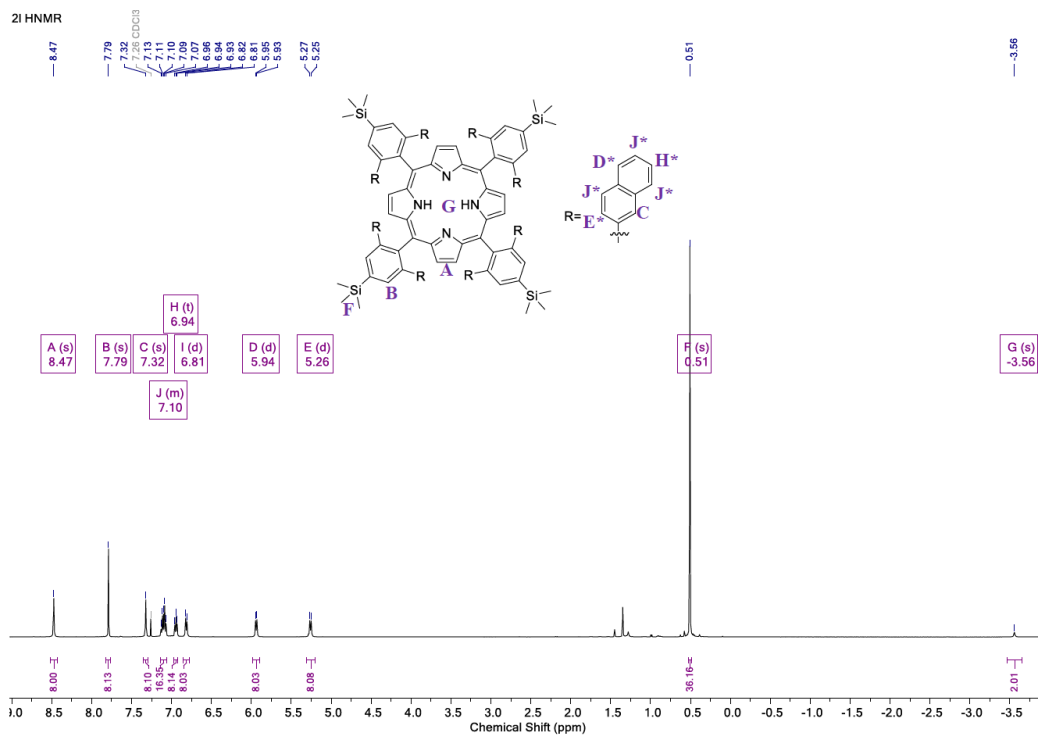


Figure B.24. ^1H NMR spectrum (500 MHz, CDCl_3) (* tentative assignment) of **3.2l**.

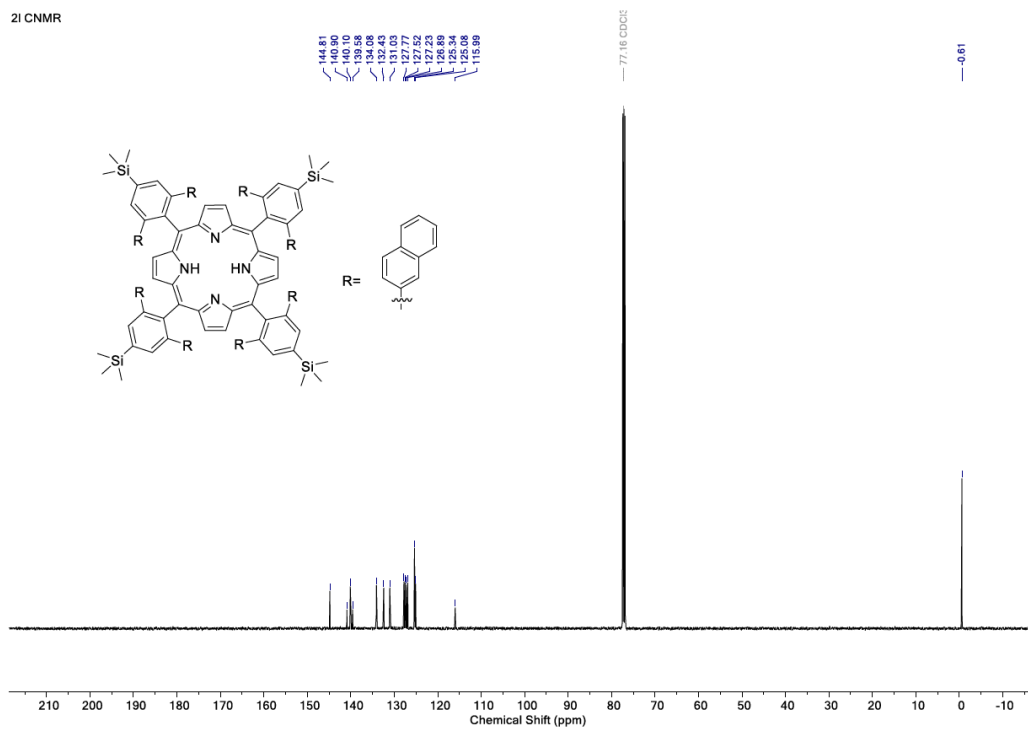


Figure B.25. $^{13}\text{C}\{^1\text{H}\}$ NMR spectrum (126 MHz, CDCl_3) of **3.2l**.

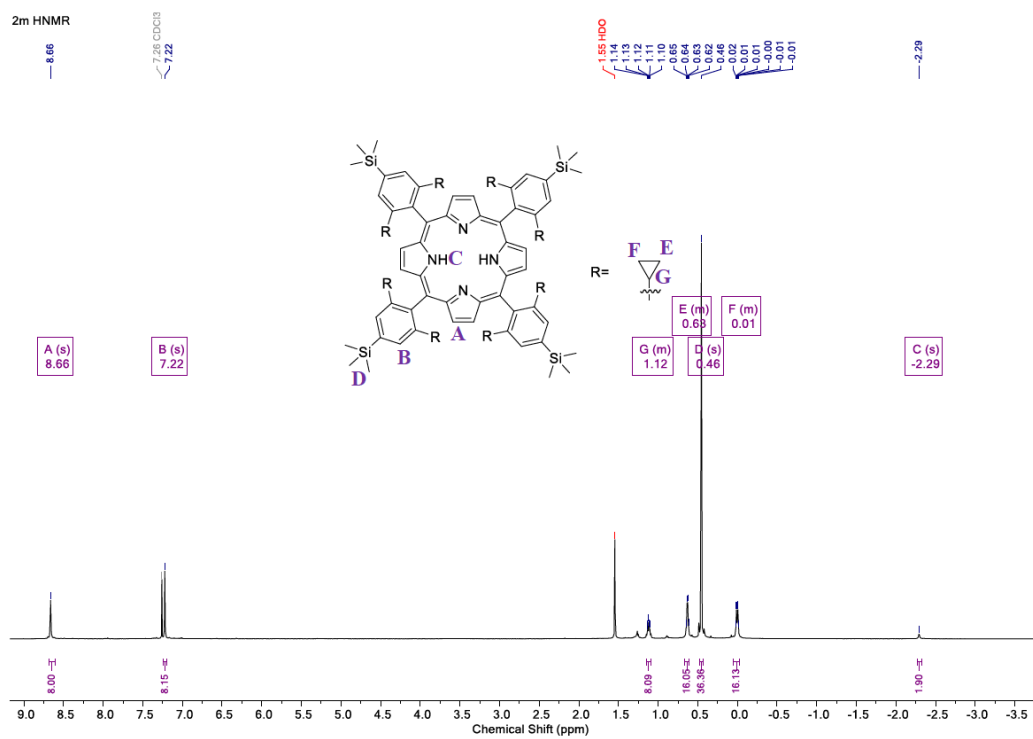


Figure B.26. ^1H NMR spectrum (500 MHz, CDCl_3) of **3.2m**.

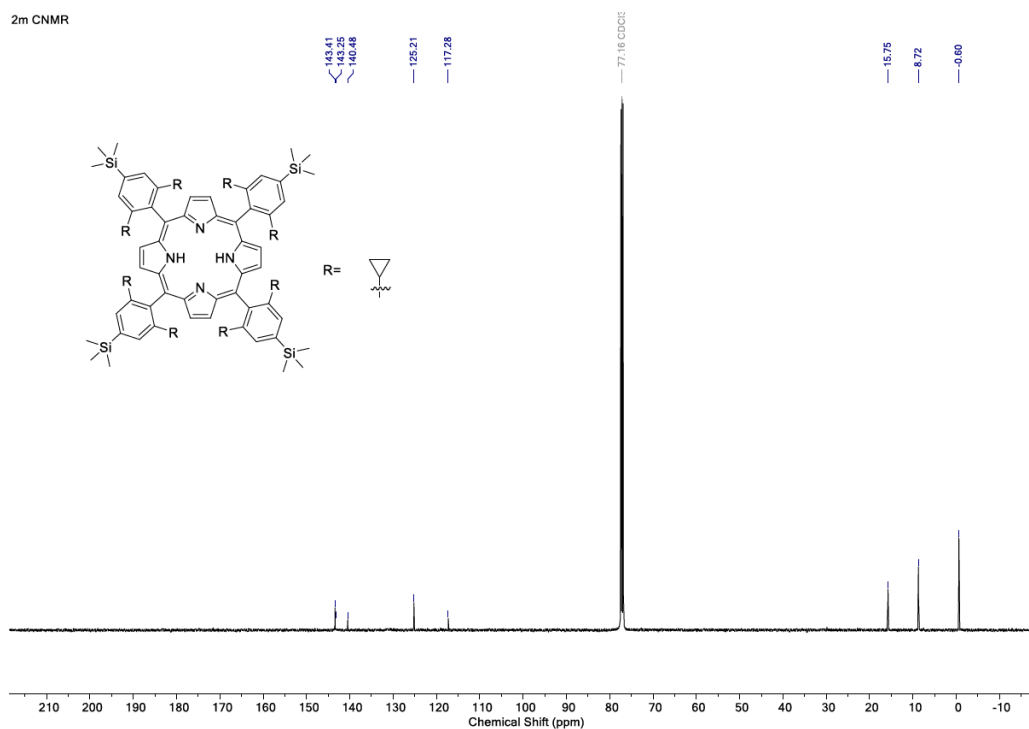


Figure B.27. $^{13}\text{C}\{^1\text{H}\}$ NMR spectrum (126 MHz, CDCl_3) of **3.2m**.

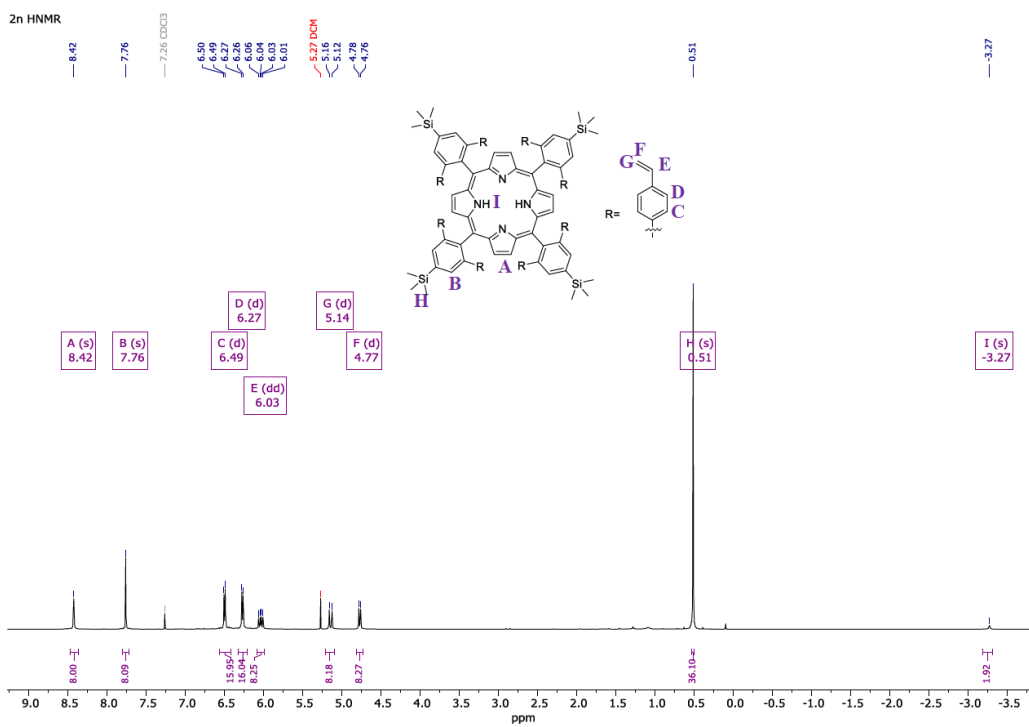


Figure B.28. ^1H NMR spectrum (500 MHz, CDCl_3) of **3.2n**.

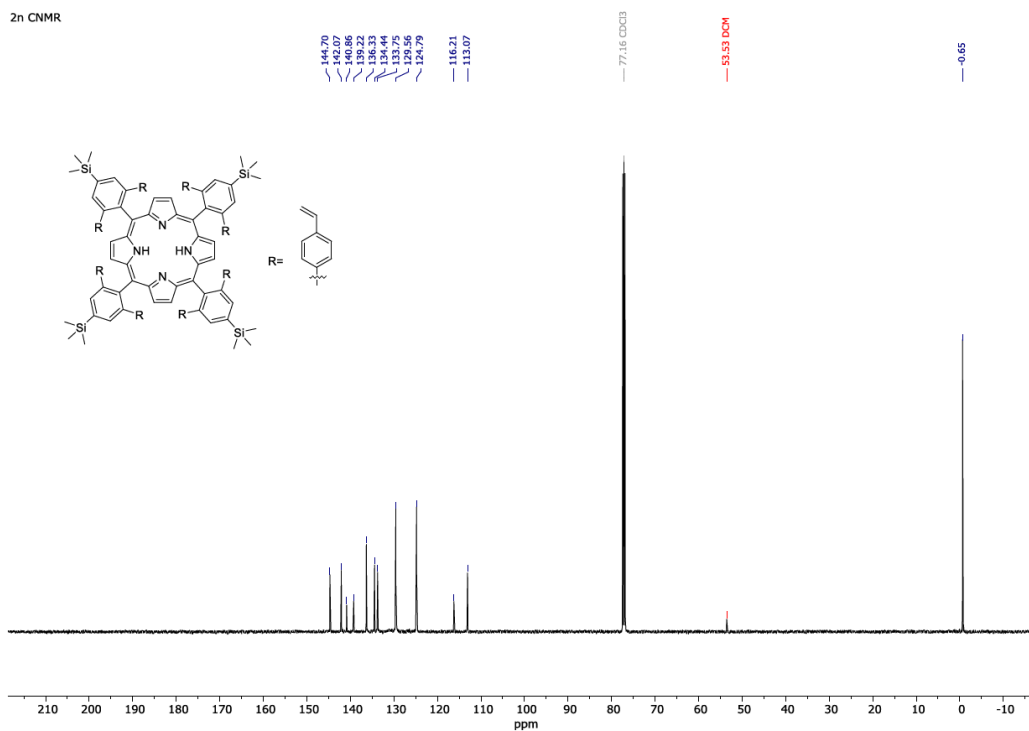


Figure B.29. $^{13}\text{C}\{^1\text{H}\}$ NMR spectrum (126 MHz, CDCl₃) of **3.2n**.

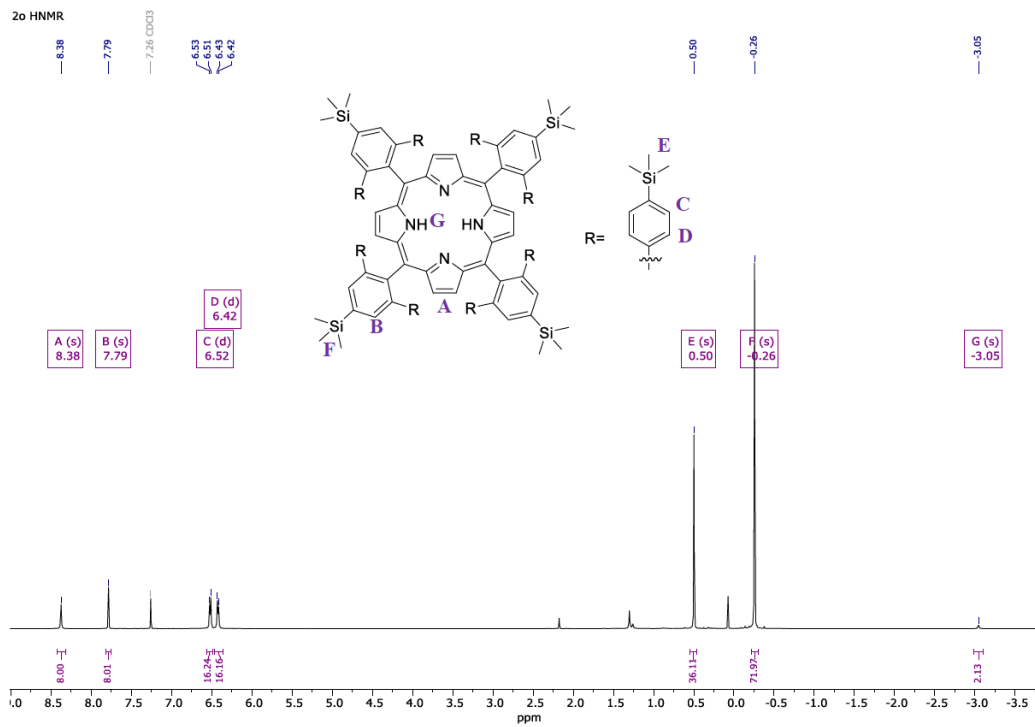


Figure B.30. ^1H NMR spectrum (500 MHz, CDCl₃) of **3.2o**.

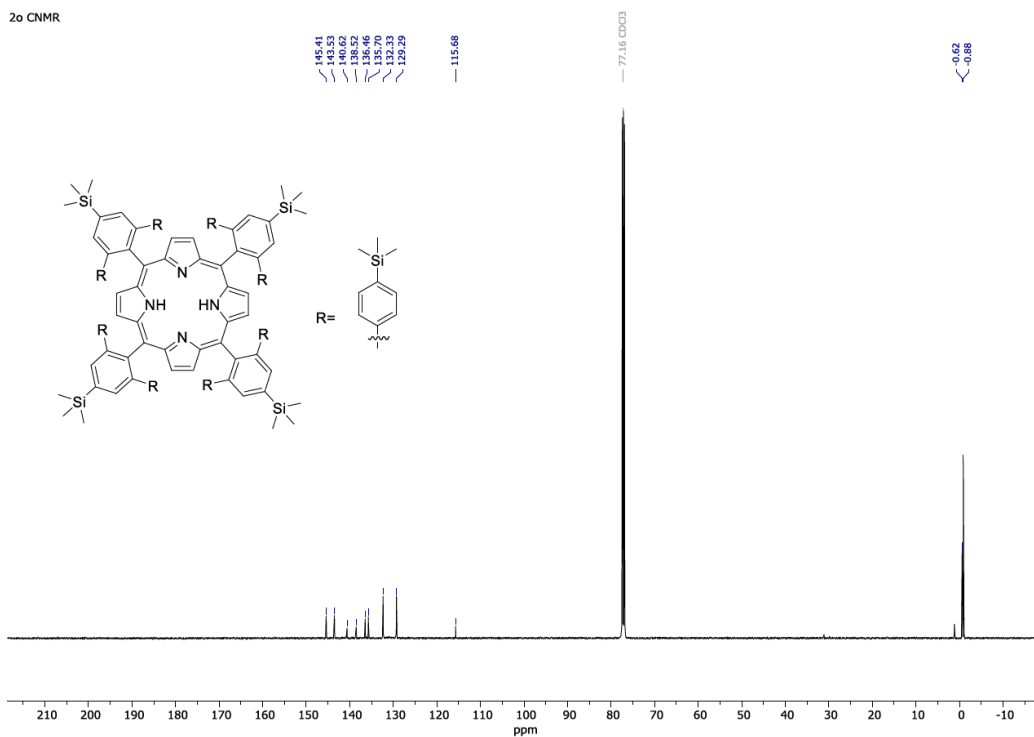


Figure B.31. ¹³C{¹H} NMR spectrum (126 MHz, CDCl₃) of **3.2o**.

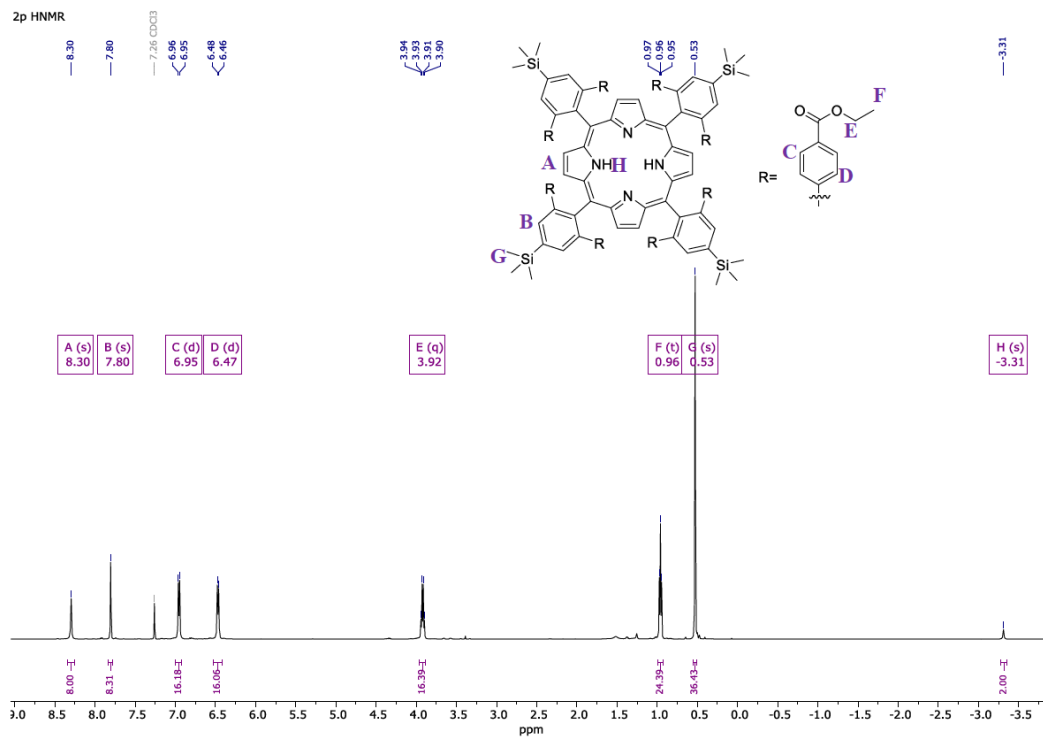


Figure B.32. ¹H NMR spectrum (500 MHz, CDCl₃) of **3.2p**.

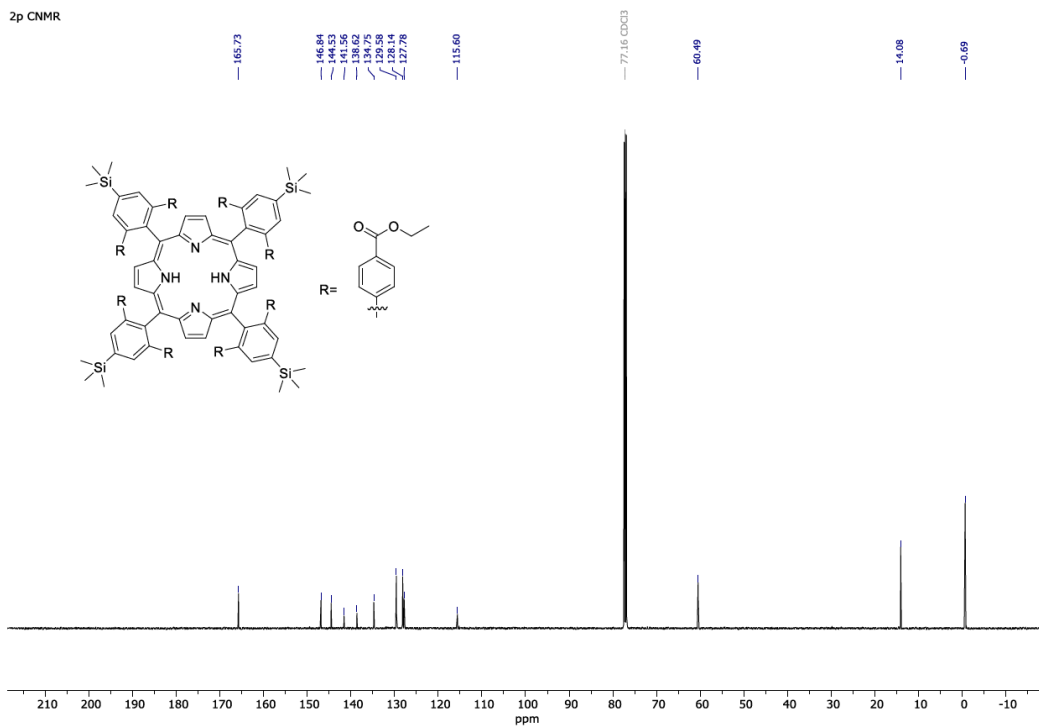


Figure B.33. $^{13}\text{C}\{^1\text{H}\}$ NMR spectrum (126 MHz, CDCl₃) of **3.2p**.

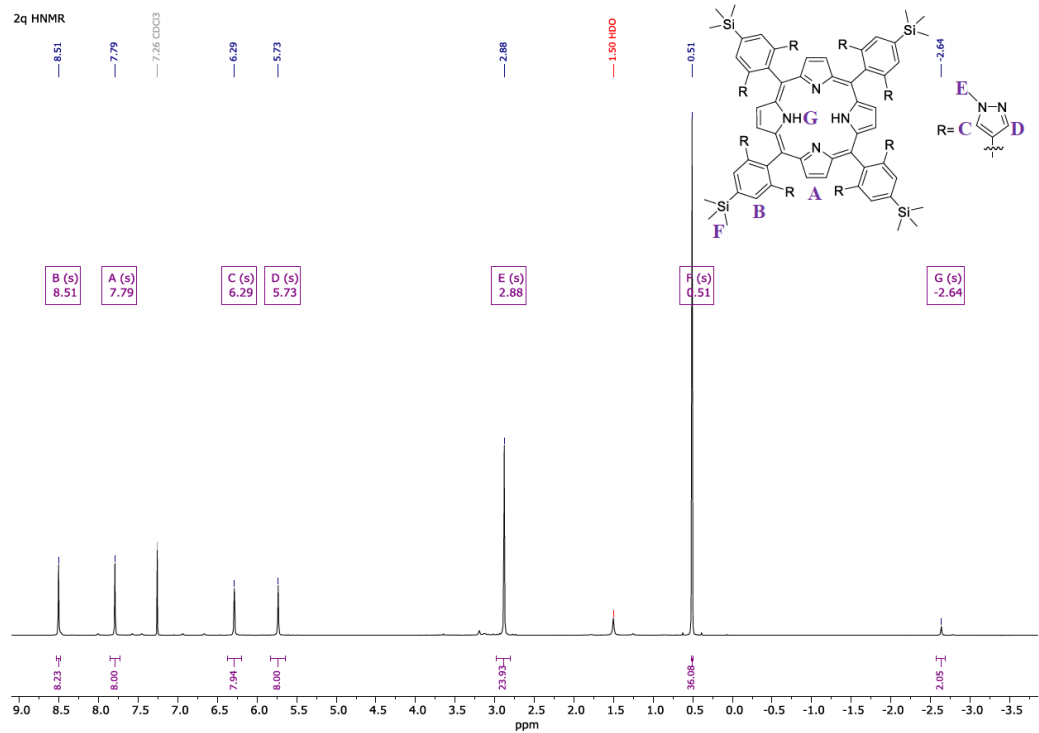


Figure B.34. ^1H NMR spectrum (500 MHz, CDCl₃) of **3.2q**.

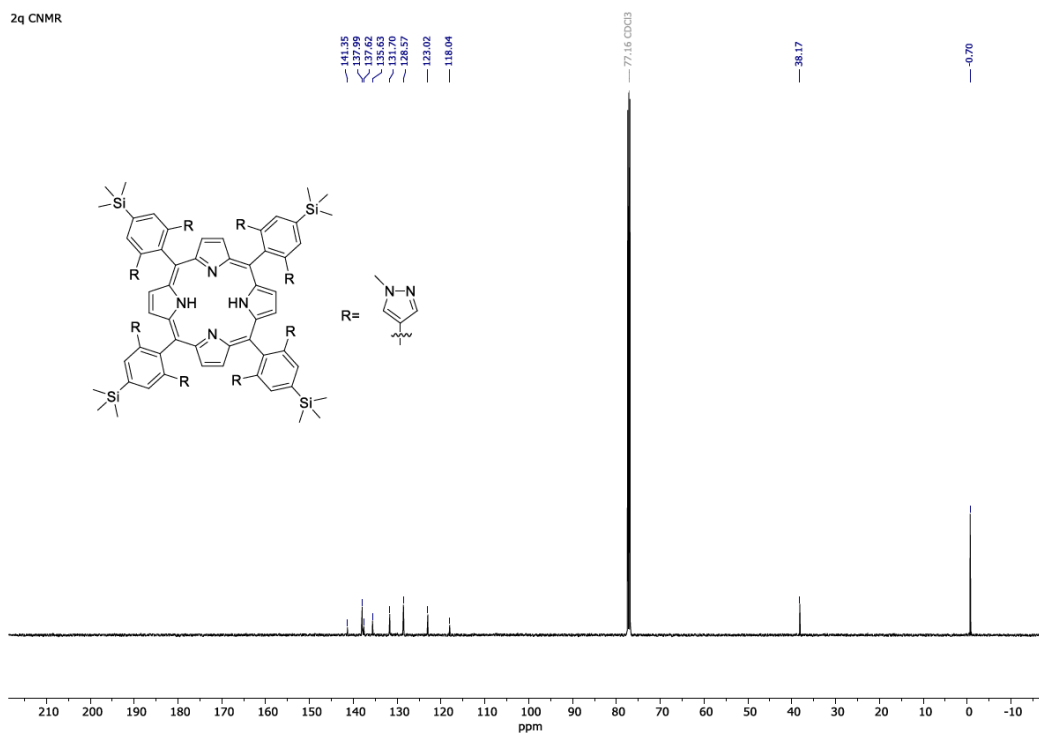


Figure B.35. $^{13}\text{C}\{^1\text{H}\}$ NMR spectrum (126 MHz, CDCl_3) of **3.2q**.

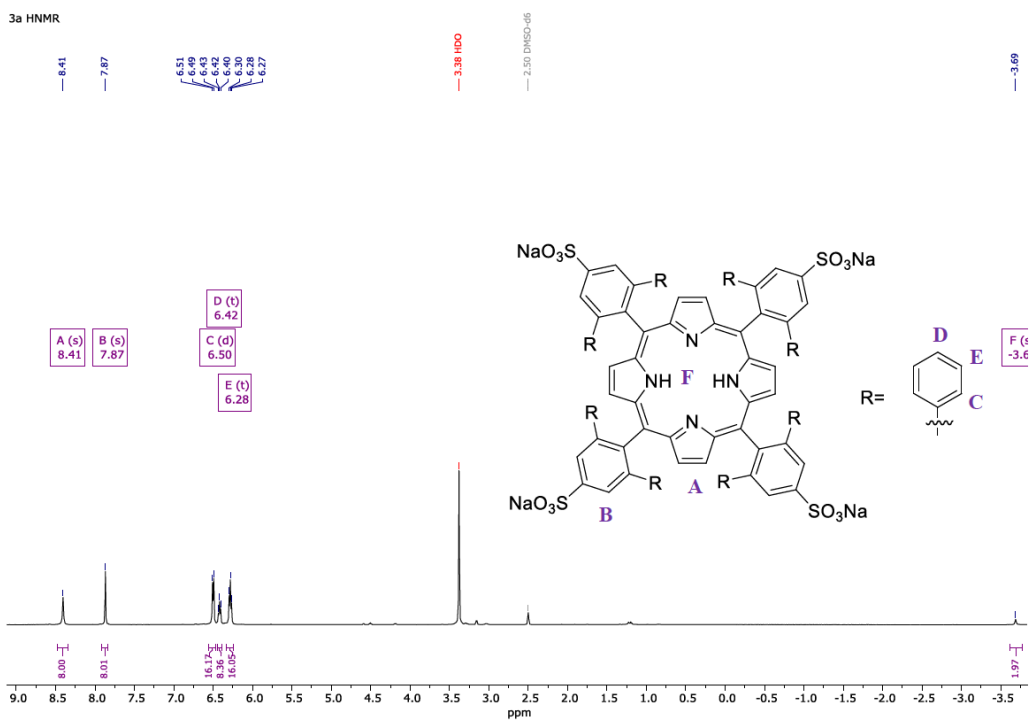


Figure B.36. ^1H NMR spectrum (500 MHz, $\text{DMSO-}d_6$) of **3.3a**.

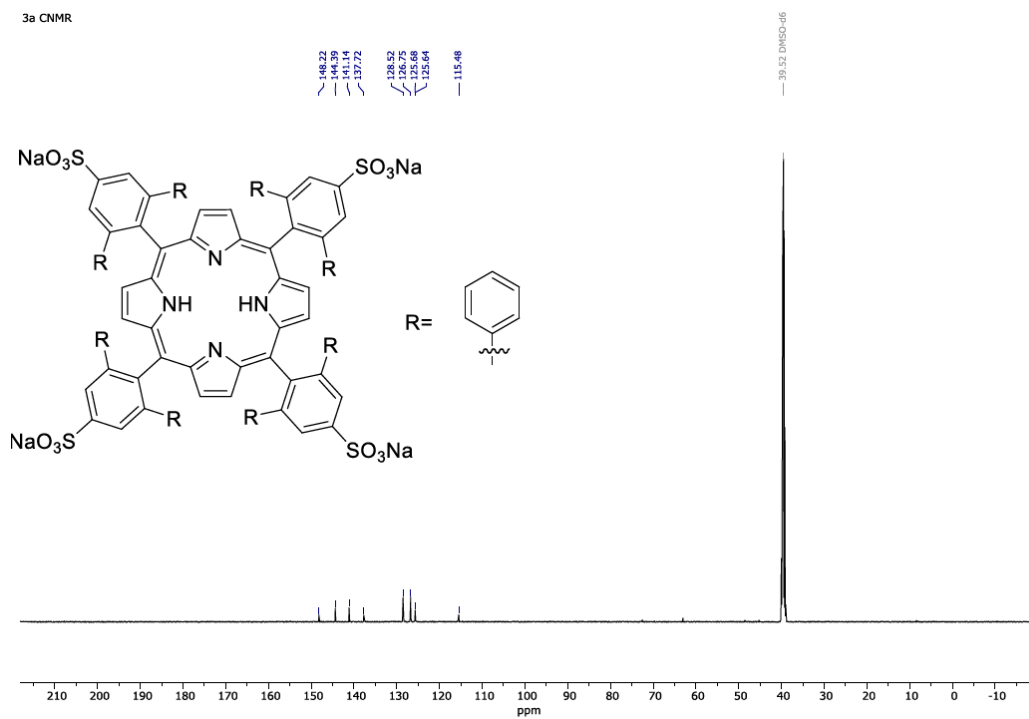


Figure B.37. $^{13}\text{C}\{^1\text{H}\}$ NMR spectrum (126 MHz, DMSO- d_6) of **3.3a**.

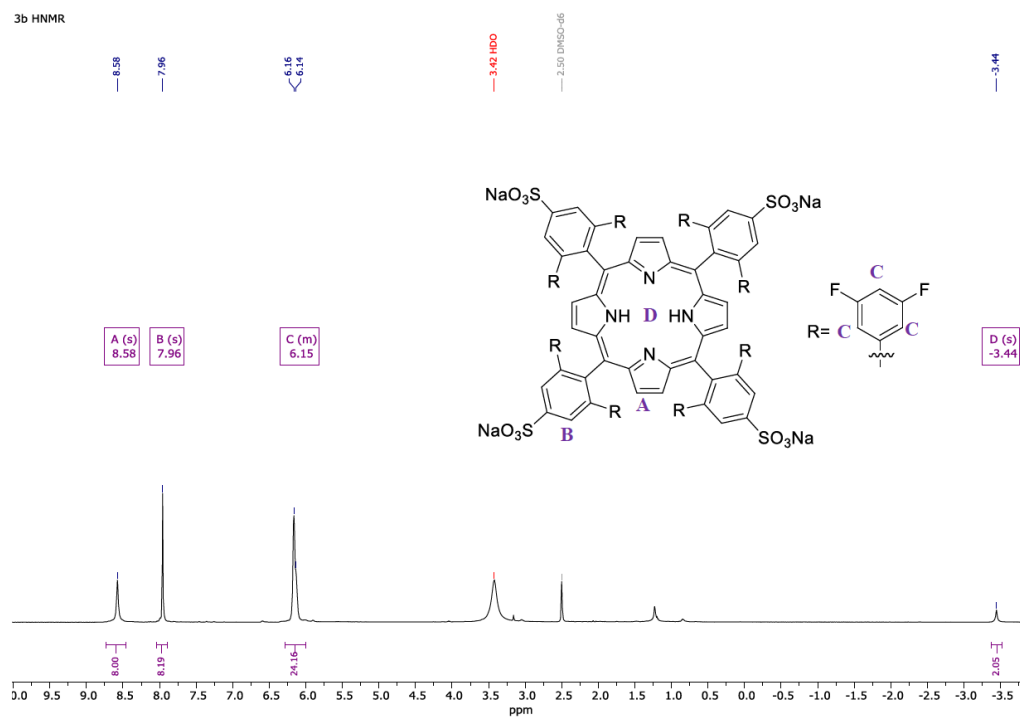


Figure B.38. ^1H NMR spectrum (500 MHz, DMSO- d_6) of **3.3b**.

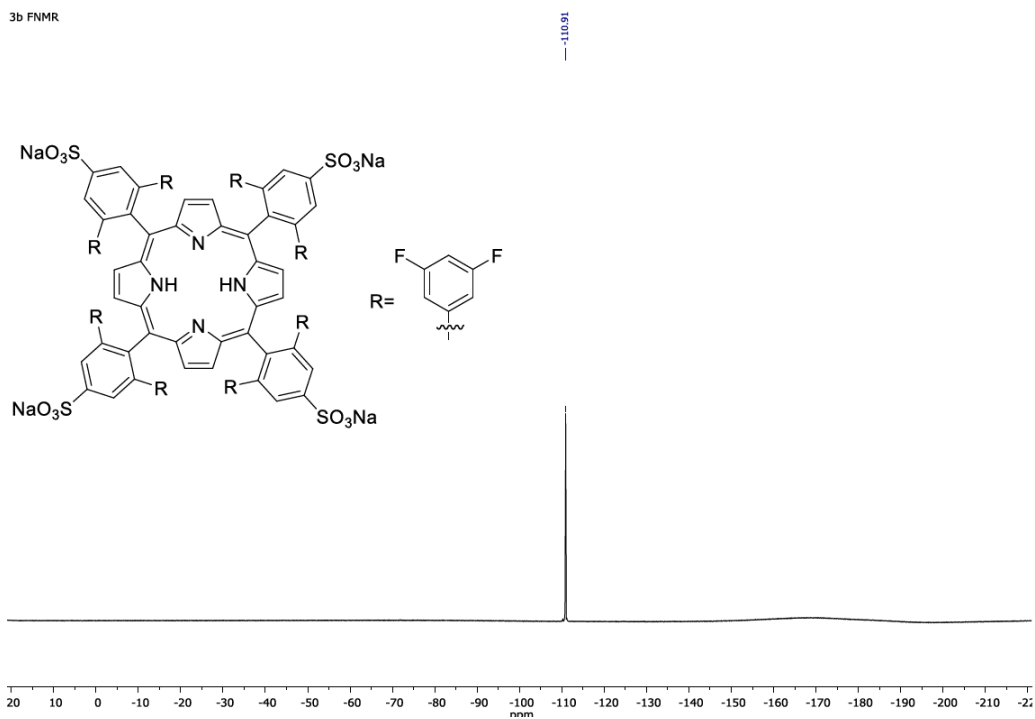


Figure B.39. $^{19}\text{F}\{^1\text{H}\}$ NMR spectrum (470 MHz, $\text{DMSO-}d_6$) of **3.3b**.

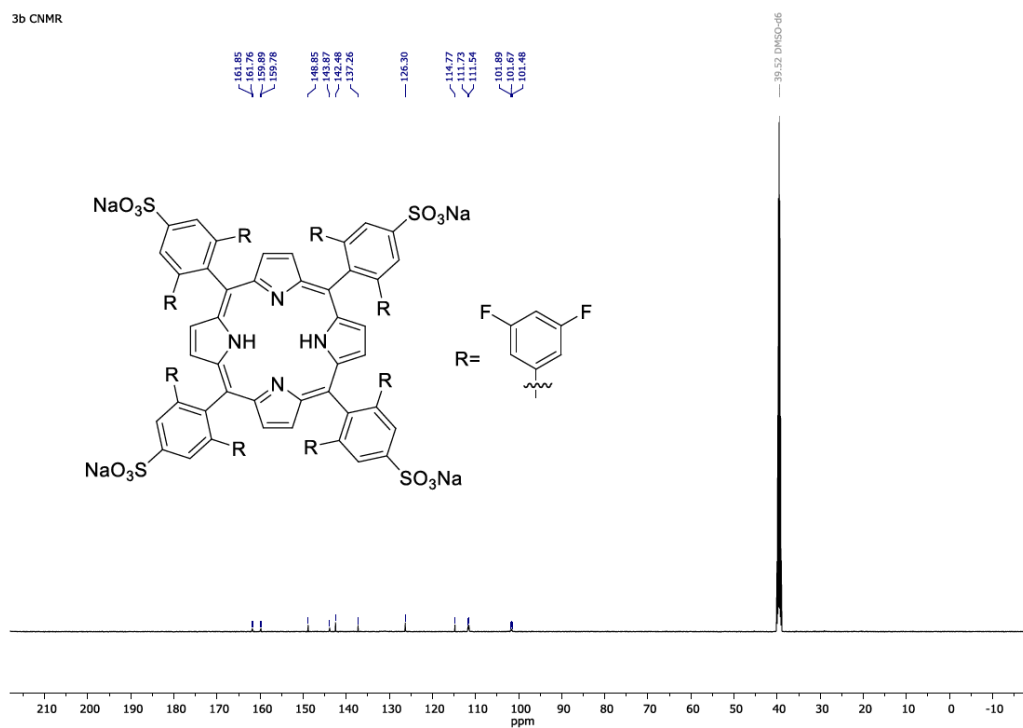


Figure B.40. $^{13}\text{C}\{^1\text{H}\}$ NMR spectrum (126 MHz, $\text{DMSO-}d_6$) of **3.3b**.

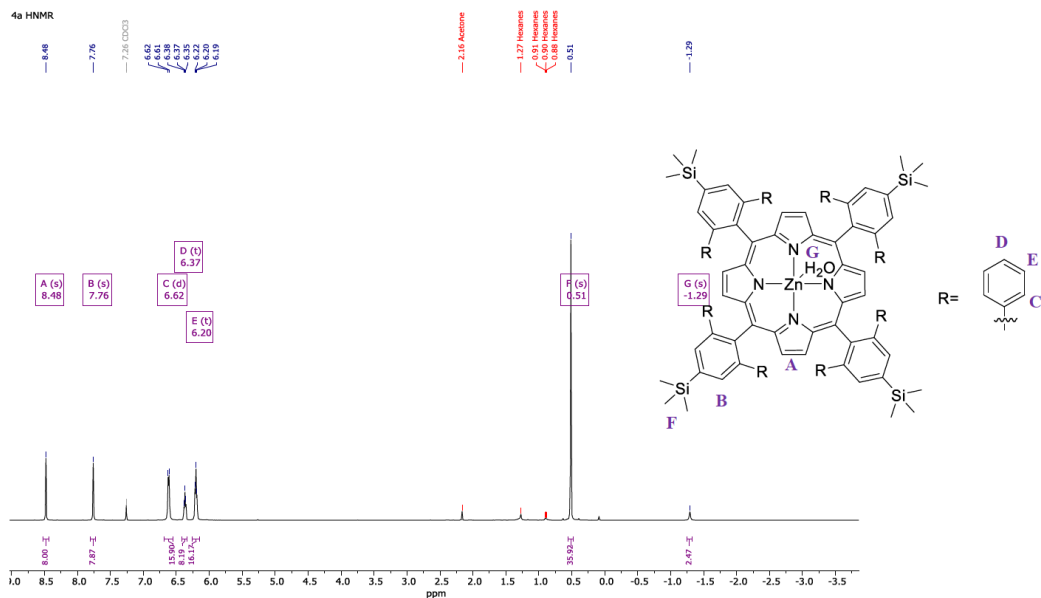


Figure B.41. ^1H NMR spectrum (500 MHz, CDCl_3) of **3.4a**.

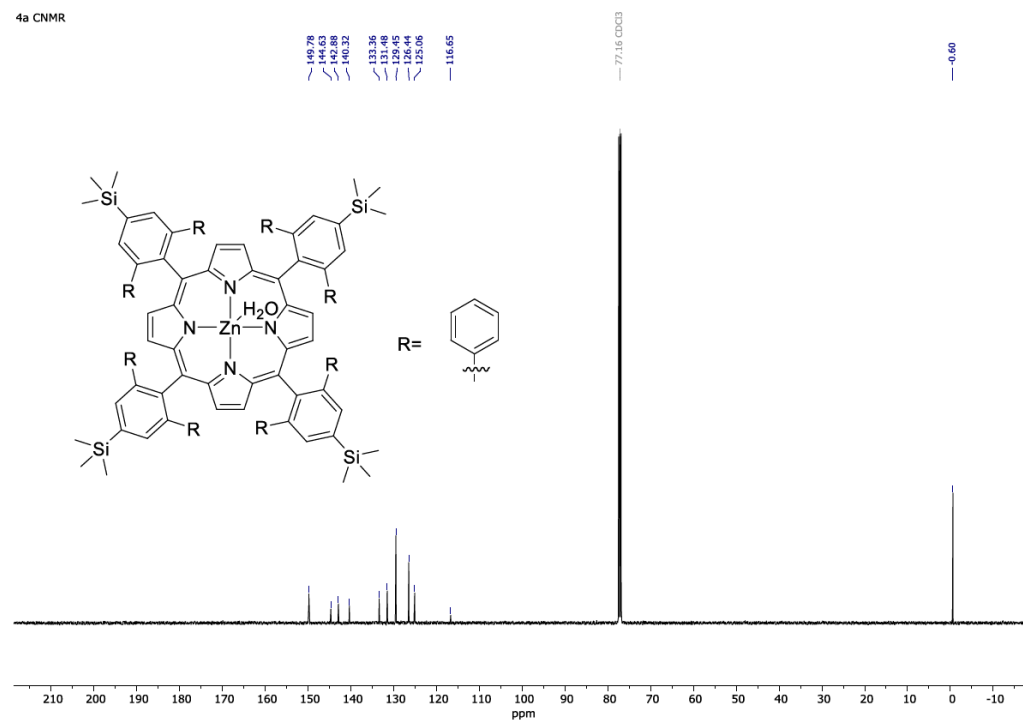


Figure B.42. $^{13}\text{C}\{^1\text{H}\}$ NMR spectrum (126 MHz, CDCl_3) of **3.4a**.

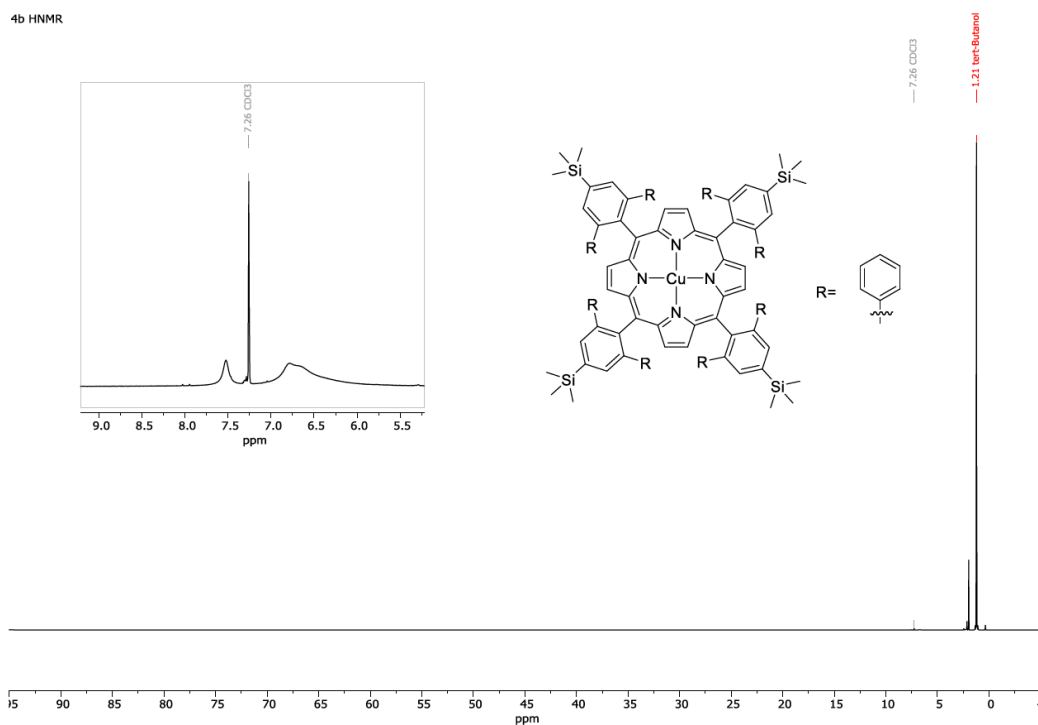


Figure B.43. ¹H NMR spectrum (500 MHz, CDCl₃) (n.b. paramagnetic) of **3.4b**.

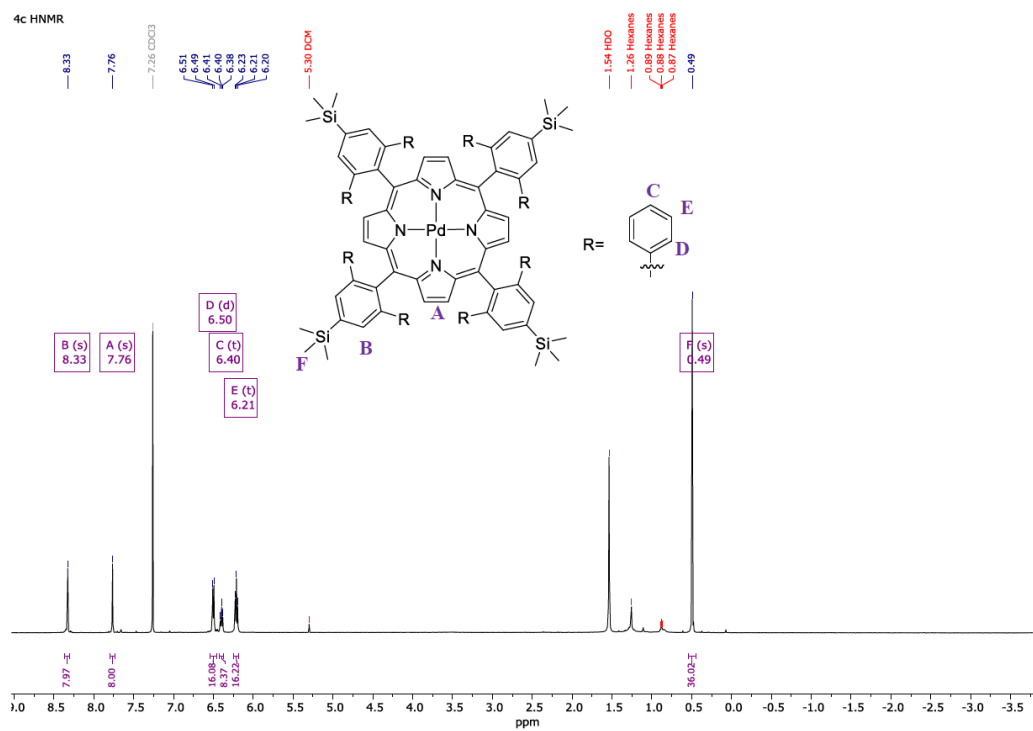


Figure B.44. ¹H NMR spectrum (500 MHz, CDCl₃) of **3.4c**.

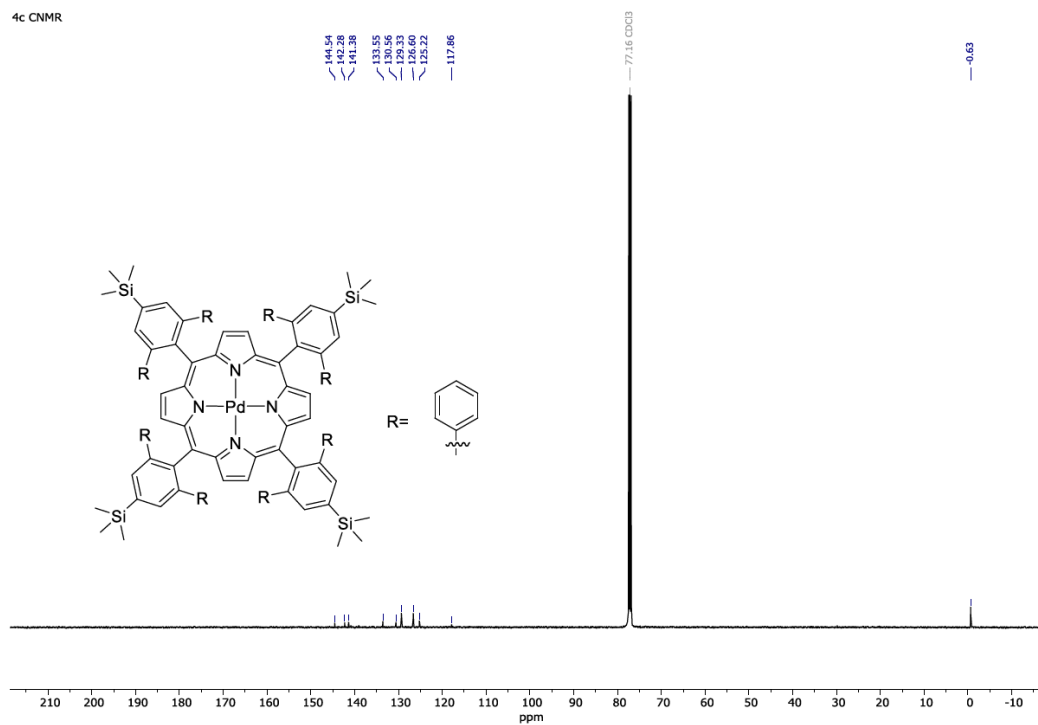


Figure B.45. $^{13}\text{C}\{^1\text{H}\}$ NMR spectrum (126 MHz, CDCl_3) of **3.4c**.

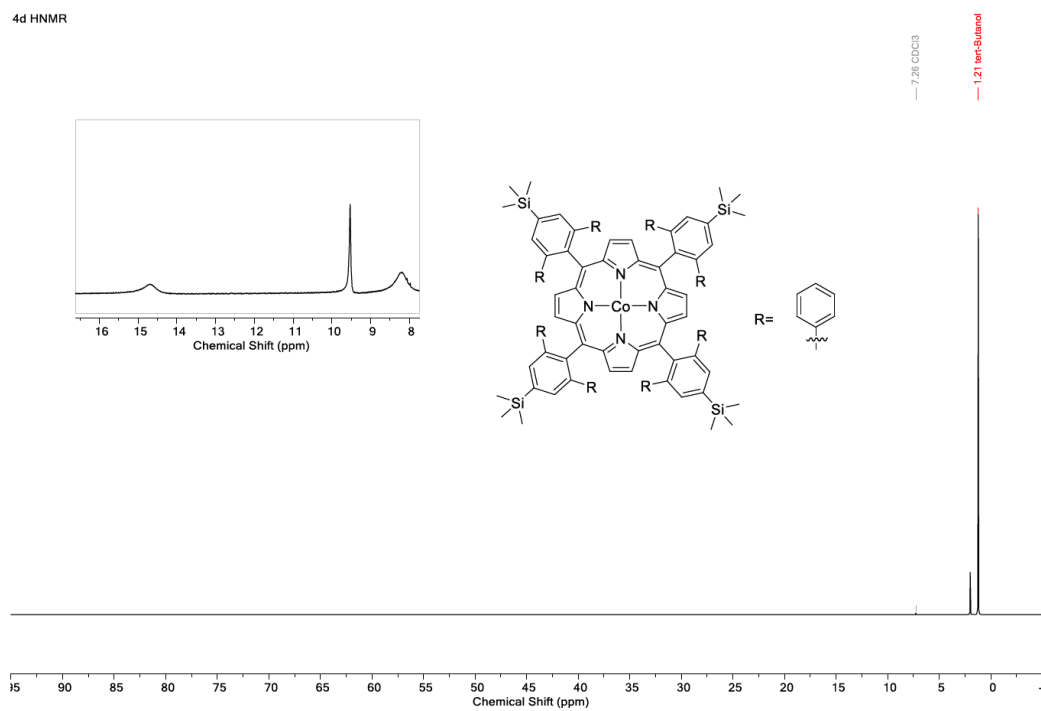
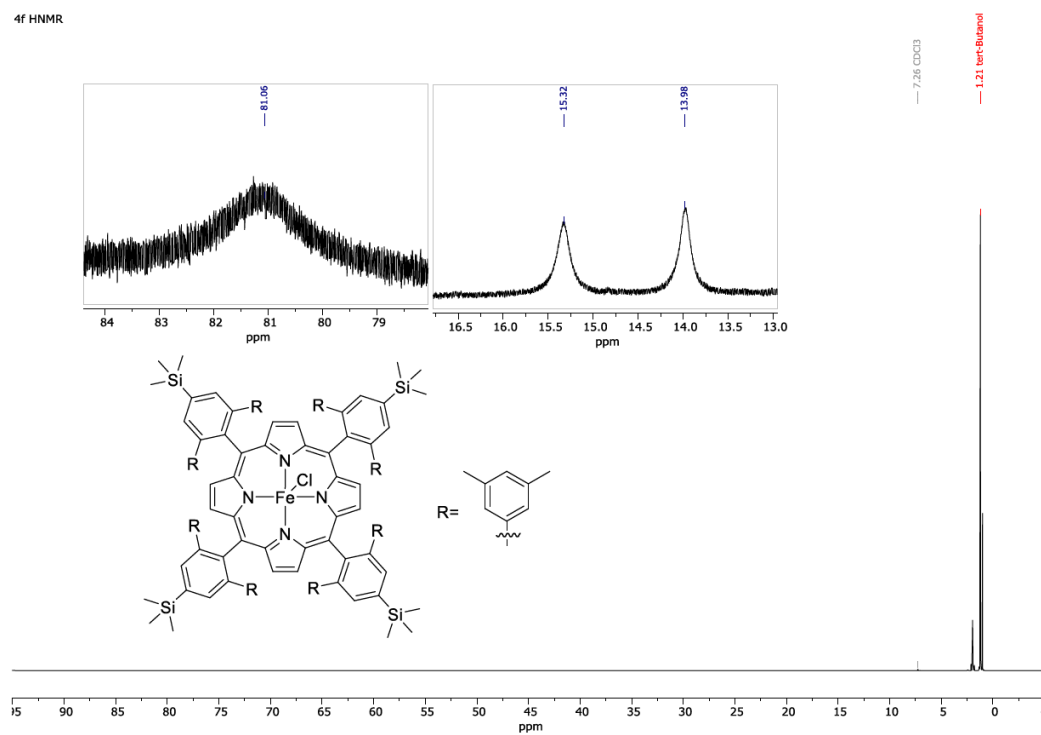
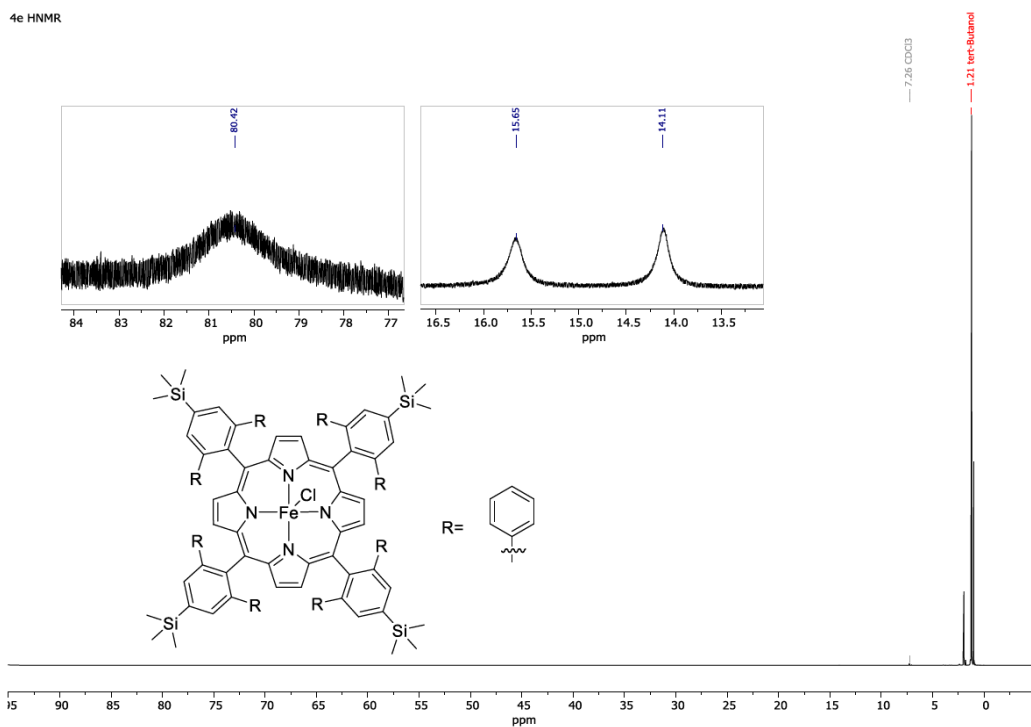


Figure B.46. ^1H NMR spectrum (500 MHz, CDCl_3) (n.b. paramagnetic) of **3.4d**.



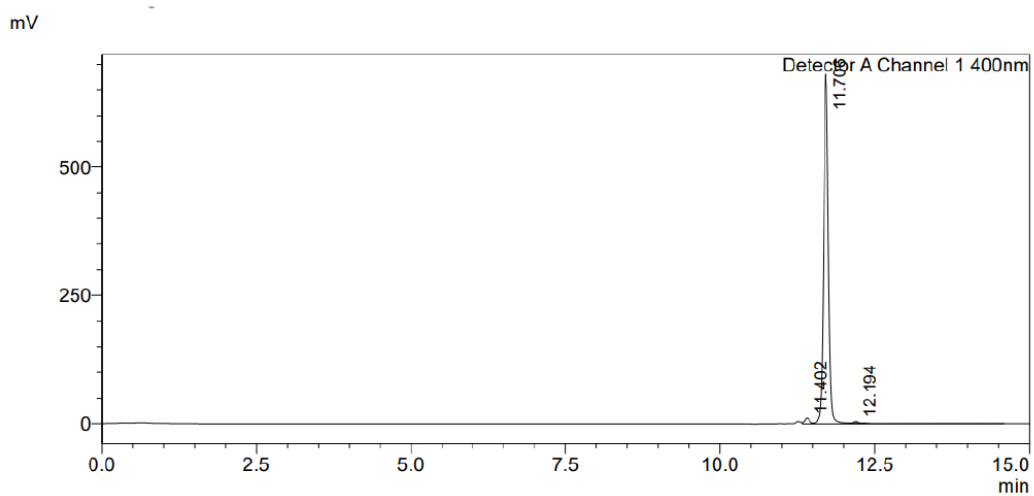


Figure B.49. HPLC chromatogram of **3.4b** confirming >95% purity. Absorbance is measured at 400 nm and the analyte was eluted with a Hexane/DCM gradient of 0-100% DCM over 15 min.

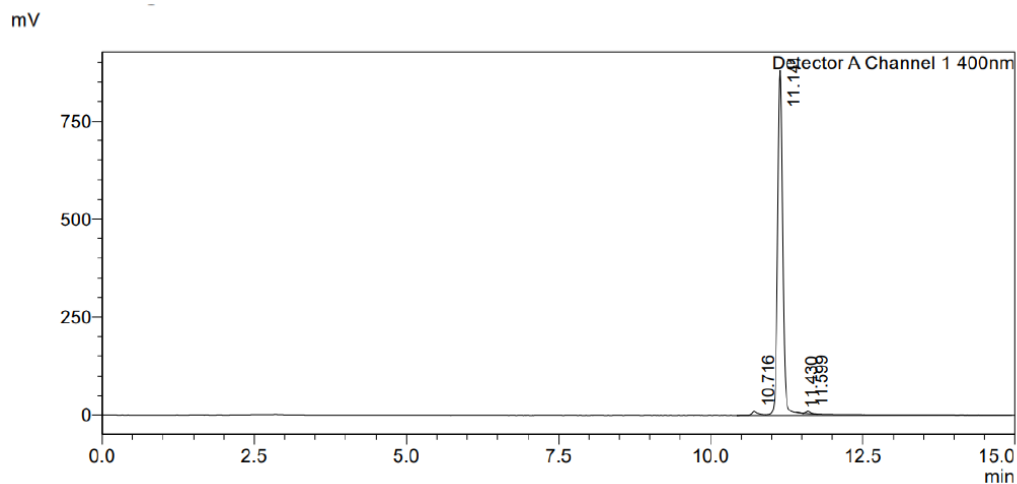


Figure B.50. HPLC chromatogram of **3.4d** confirming >97% purity. Absorbance is measured at 400 nm and the analyte was eluted with a Hexane/DCM gradient of 0-100% DCM over 15 min.

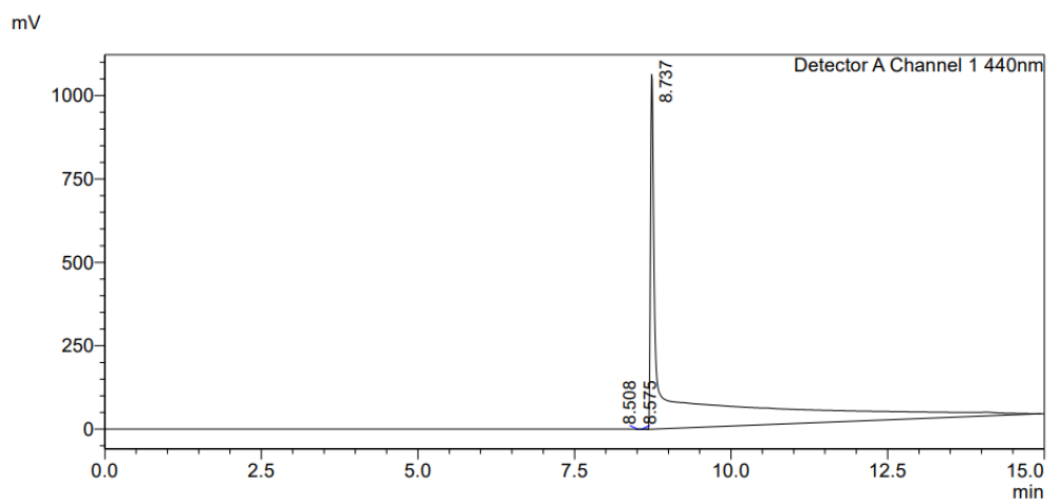


Figure B.51. HPLC chromatogram of **3.4e** confirming >97% purity. Absorbance is measured at 440 nm and the analyte was eluted with a Hexane/DCM gradient of 0-100% DCM over 15 min.

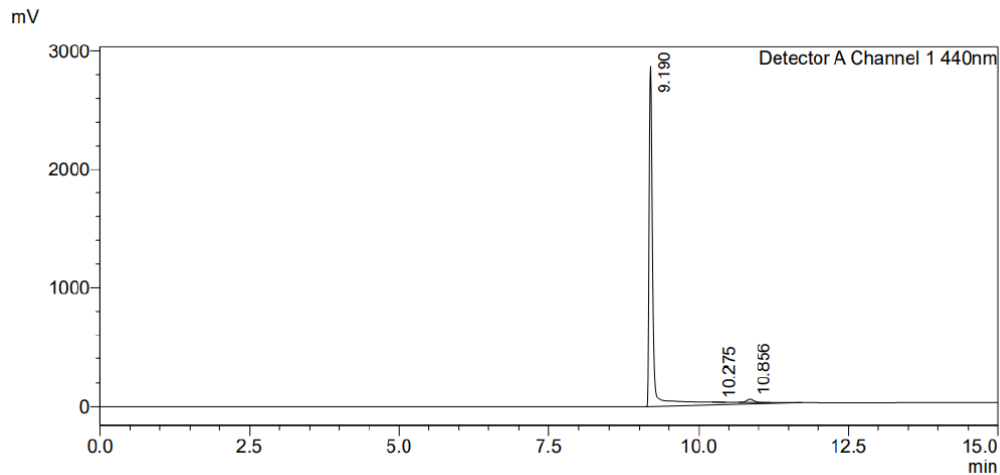


Figure B.52. HPLC chromatogram of **3.4f** confirming >97% purity. Absorbance is measured at 440 nm and the analyte was eluted with a Hexane/DCM gradient of 0-100% DCM over 15 min.

Table B.1. Crystallographic Refinement Details.

Compound	3.2b·2MeCN	3.2c·MeCN·1.5CHCl₃	3.2d·MeCN·3C₆H₃Cl₃
Formula	C ₁₀₈ H ₈₄ F ₁₆ N ₆ Si ₄	C _{107.5} H _{82.5} Cl _{20.5} N ₅ Si ₄	C ₁₄₀ H ₁₃₈ Cl ₉ N ₅ Si ₄
FW	1882.17	2283.37	2321.96
T (K)	100.0(11)	99.99(10)	100.01(10)
λ (Å)	1.54184	1.54184	1.54184
Crystal System	Triclinic	Monoclinic	Monoclinic
Space group	<i>P</i> 1	<i>I</i> 2/ <i>a</i>	<i>P</i> 2 ₁ / <i>n</i>
<i>a</i> (Å)	12.5909(2)	23.2819(2)	16.53020(10)
<i>b</i> (Å)	13.6056(2)	19.67030(10)	40.0808(3)
<i>c</i> (Å)	17.3122(2)	47.5453(3)	19.68380(10)
α (°)	103.7060(10)	90	90
β (°)	106.6640(10)	92.3390(10)	97.4540(10)
γ (°)	106.8540(2)	90	90
Volume (Å ³)	2548.03(7)	21755.8(3)	12931.17(14)
<i>Z</i>	1	8	4
Size (mm ³)	0.16×0.07×0.04	0.41×0.31×0.03	0.16×0.11×0.06
θ range (°)	2.843-67.078	2.942-67.077	2.518-67.079
Total data	34597	138551	175824
Unique data	9086	19392	23102
Parameters	610	1307	1599
Completeness (%)	99.9	99.9	100.0
<i>R</i> _{int} (%)	2.90	4.61	4.19
<i>R</i> ₁ (% , <i>I</i> > 2σ)	3.69	6.39	7.74
<i>R</i> ₁ (% , all data)	4.14	6.90	8.05
<i>wR</i> ₂ (% , <i>I</i> > 2σ)	9.60	18.20	20.51
<i>wR</i> ₂ (% , all data)	9.87	18.72	20.70
<i>S</i>	1.028	1.033	1.158

Table B.2. Crystallographic Refinement Details.

Compound	3.2e·MeCN·C₇H₈	3.2f·2MeCN	3.2h·2MeCN·C₇H₅N
Formula	C ₁₂₃ H ₁₂₄ N ₆ Si ₄	C ₁₃₂ H ₁₄₈ N ₆ Si ₄	C ₁₁₅ H ₉₇ F ₈ N ₇ Si ₄
FW	1798.63	1930.92	1841.35
T (K)	100.6(10)	100.00(11)	101(1)
λ (Å)	1.54184	1.54184	1.54184
Crystal System	Monoclinic	Triclinic	Monoclinic
Space group	<i>P</i> 2 ₁ / <i>c</i>	<i>P</i> 1	<i>P</i> 2 ₁ / <i>c</i>
<i>a</i> (Å)	16.34530(10)	13.3916(5)	17.9444(2)
<i>b</i> (Å)	29.9212(2)	15.4829(7)	14.42580(10)
<i>c</i> (Å)	23.1963(2)	16.1203(6)	23.4254(2)
α (°)	90	67.333(4)	90
β (°)	107.5830(10)	72.696(3)	110.6190(10)
γ (°)	90	87.191(3)	90
Volume (Å ³)	10814.62(15)	2936.5(2)	5675.51(10)
<i>Z</i>	4	1	2
Size (mm ³)	0.13×0.08×0.07	0.88×0.18×0.05	0.29×0.17×0.05
θ range (°)	2.485-67.079	3.117-67.067	2.631-67.078
Total data	171800	38820	106189
Unique data	19313	10456	10128
Parameters	1281	732	646
Completeness (%)	100	99.9	99.9
<i>R</i> _{int} (%)	3.28	5.87	3.90
<i>R</i> ₁ (% , I > 2 σ)	4.51	5.63	5.65
<i>R</i> ₁ (% , all data)	4.79	6.59	5.86
<i>wR</i> ₂ (% , I > 2 σ)	11.01	15.16	15.41
<i>wR</i> ₂ (% , all data)	11.16	15.97	15.57
<i>S</i>	1.114	1.033	1.047

Table B.3. Crystallographic Refinement Details.

Compound	3.2i·CHCl₃	3.2k·2MeCN·CHCl₃	3.2l·2MeCN
Formula	C ₁₁₃ H ₈₇ Cl ₃ F ₂₄ N ₄ Si ₄	C ₁₁₇ H ₁₁₇ Cl ₃ N ₆ O ₈ Si ₄	C ₁₄₀ H ₁₁₆ N ₆ Si ₄
FW	2175.57	1953.87	1994.74
T (K)	99.99(10)	100.0(13)	99.98(15)
λ (Å)	1.54184	1.54184	1.54184
Crystal System	Monoclinic	Triclinic	Monoclinic
Space group	<i>P2₁/n</i>	<i>P1</i>	<i>P2₁/c</i>
<i>a</i> (Å)	18.7167(2)	11.9189(2)	16.6762(3)
<i>b</i> (Å)	23.8213(2)	15.7967(3)	23.8081(4)
<i>c</i> (Å)	26.6679(3)	16.5347(3)	30.0004(3)
α (°)	90	101.9810(10)	90
β (°)	93.2670(10)	108.897(2)	91.4430(10)
γ (°)	90	107.1330(10)	90
Volume (Å ³)	11870.7(2)	2651.88(9)	11907.2(3)
<i>Z</i>	4	1	4
Size (mm ³)	0.22×0.1×0.06	0.23×0.09×0.06	0.23×0.15×0.03
θ range (°)	2.489-67.077	2.998-67.078	2.369-67.078
Total data	167793	35890	95662
Unique data	21182	9457	21185
Parameters	1510	651	1598
Completeness (%)	100.0	99.9	99.6
<i>R</i> _{int} (%)	4.76	3.42	3.62
<i>R</i> ₁ (% , I > 2σ)	6.51	6.01	6.76
<i>R</i> ₁ (% , all data)	7.53	6.66	8.32
<i>wR</i> ₂ (% , I > 2σ)	16.97	16.44	18.24
<i>wR</i> ₂ (% , all data)	17.69	16.97	19.37
<i>S</i>	1.029	1.042	1.022

Table B.4. Crystallographic Refinement Details.

Compound	3.2m	3.2o·5MeCN	3.2p
Formula	C ₈₀ H ₉₄ N ₄ Si ₄	C ₁₃₈ H ₁₇₃ N ₉ Si ₁₂	C ₁₂₈ H ₁₂₆ N ₄ O ₁₆ Si ₄
FW	1223.95	2294.92	2088.68
T (K)	99.99(14)	100.01(10)	100.01(10)
λ (Å)	1.54184	1.54184	1.54184
Crystal System	Triclinic	Monoclinic	Monoclinic
Space group	<i>P</i> 1	<i>P</i> 2 ₁ / <i>n</i>	<i>I</i> 2/ <i>a</i>
<i>a</i> (Å)	14.3294(2)	23.9843(2)	22.8311(2)
<i>b</i> (Å)	16.7136(3)	24.2555(2)	24.7546(3)
<i>c</i> (Å)	18.2148(2)	27.5665(2)	23.6019(4)
α (°)	103.3400(10)	90	90
β (°)	90.2160(10)	90.8630(10)	98.1630(10)
γ (°)	100.0870(10)	90	90
Volume (Å ³)	4174.61(11)	16035.0(2)	13204.0(3)
<i>Z</i>	2	4	4
Size (mm ³)	0.29×0.08×0.03	0.81×0.6×0.27	0.29×0.25×0.18
θ range (°)	2.496-67.075	2.424-67.080	2.601-67.073
Total data	56459	218940	11799
Unique data	14868	28618	11799
Parameters	897	1681	878
Completeness (%)	99.8	99.9	100.0
<i>R</i> _{int} (%)	4.38	5.03	N/A ^a
<i>R</i> ₁ (% , <i>I</i> > 2 σ)	8.19	6.82	10.13
<i>R</i> ₁ (% , all data)	8.84	7.44	10.63
<i>wR</i> ₂ (% , <i>I</i> > 2 σ)	20.86	18.58	30.79
<i>wR</i> ₂ (% , all data)	21.25	19.11	31.29
<i>S</i>	1.091	1.024	1.049

^a Non-merohedral twin

Table B.5. Crystallographic Refinement Details.

Compound	3.2q ·½Et ₂ O	3.3b ·5C ₆ H ₁₄ O ₃	3.4a ·MeCN·H ₂ O
Formula	C ₉₀ H ₉₉ N ₂₀ O _{0.50} Si ₄	C ₁₂₂ H ₁₁₂ F ₁₆ N ₄ Na ₄ O ₂₇ S ₄	C ₁₀₆ H ₉₇ N ₅ OSi ₄ Zn
FW	1581.25	2590.35	1634.61
T (K)	100.0(3)	100.01(11)	100.0(10)
λ (Å)	1.54184	1.54184	1.54184
Crystal System	Triclinic	Monoclinic	Triclinic
Space group	<i>P</i> 1	<i>C</i> 2/ <i>m</i>	<i>P</i> 1
<i>a</i> (Å)	15.5214(3)	13.5375(2)	13.1539(2)
<i>b</i> (Å)	16.8377(3)	32.1685(4)	13.6553(2)
<i>c</i> (Å)	19.6805(3)	14.4984(2)	16.1176(3)
α (°)	104.498(2)	90	73.1390(10)
β (°)	91.652(2)	90.9620(10)	70.611(2)
γ (°)	92.538(2)	90	61.251(2)
Volume (Å ³)	4970.49	6312.89(15)	2364.30(8)
<i>Z</i>	2	2	1
Size (mm ³)	0.27×0.05×0.04	0.15×0.08×0.07	0.1×0.06×0.03
θ range (°)	2.321-67.077	2.747-67.067	2.943-67.078
Total data	64662	39300	69421
Unique data	17671	5750	8457
Parameters	1121	537	552
Completeness (%)	99.5	100.0	100
<i>R</i> _{int} (%)	6.26	4.87	3.58
<i>R</i> ₁ (% , I > 2σ)	6.63	4.88	5.65
<i>R</i> ₁ (% , all data)	7.46	5.22	5.95
<i>wR</i> ₂ (% , I > 2σ)	18.38	13.17	14.83
<i>wR</i> ₂ (% , all data)	19.22	13.43	15.04
<i>S</i>	1.041	1.050	1.115

Table B.6. Crystallographic Refinement Details.

Compound	3.4b·2MeCN	3.4c·2MeCN	3.4d·2MeCN
Formula	C ₁₀₈ H ₉₈ CuN ₆ Si ₄	C ₁₀₈ H ₉₈ N ₆ PdSi ₄	C ₁₀₈ H ₉₈ CoN ₆ Si ₄
FW	1655.82	1698.68	1651.21
T (K)	100.0(10)	99.9(2)	101(2)
λ (Å)	1.54184	1.54184	1.54184
Crystal System	Triclinic	Triclinic	Triclinic
Space group	<i>P</i> 1	<i>P</i> 1	<i>P</i> 1
<i>a</i> (Å)	13.1905(2)	13.2012(3)	13.1816(2)
<i>b</i> (Å)	13.6409(3)	13.6615(3)	13.6278(2)
<i>c</i> (Å)	16.0599(2)	16.0477(3)	16.0608(2)
α (°)	72.320(2)	72.357(2)	72.3800(10)
β (°)	71.031(2)	70.882(2)	70.9320(10)
γ (°)	61.419(2)	61.519(2)	61.282(2)
Volume (Å ³)	2361.21(9)	2365.70(10)	2354.14(7)
<i>Z</i>	1	1	1
Size (mm ³)	0.15×0.07×0.02	0.42×0.16×0.04	0.1×0.08×0.03
θ range (°)	2.957-67.073	2.961-67.080	2.957-67.076
Total data	66105	63611	31966
Unique data	8428	8428	8410
Parameters	545	545	545
Completeness (%)	99.9	99.6	99.9
<i>R</i> _{int} (%)	4.61	5.48	3.01
<i>R</i> ₁ (% , <i>I</i> > 2 σ)	3.60	3.87	3.30
<i>R</i> ₁ (% , all data)	4.14	4.05	3.42
<i>wR</i> ₂ (% , <i>I</i> > 2 σ)	9.38	10.30	7.76
<i>wR</i> ₂ (% , all data)	9.70	10.45	7.82
<i>S</i>	1.035	1.047	1.023

Table B.7. Crystallographic Refinement Details.

Compound	3.4e ·MeCN·CHCl ₃	3.4f ·½C ₇ H ₈
Formula	C ₁₀₇ H ₉₆ Cl ₄ FeN ₅ Si ₄	C _{123.5} H ₁₂₈ ClFeN ₄ Si ₄
FW	1761.89	1871.95
T (K)	100.0(10)	100.0(12)
λ (Å)	1.54184	1.54184
Crystal System	Triclinic	Monoclinic
Space group	<i>P</i> 1	<i>P</i> 2 ₁ / <i>n</i>
<i>a</i> (Å)	12.8777(3)	13.85030(10)
<i>b</i> (Å)	16.3497(4)	31.0859(3)
<i>c</i> (Å)	23.5222(4)	26.2645(3)
α (°)	106.739(2)	90
β (°)	90.100(2)	90.4670(10)
γ (°)	90.228(2)	90
Volume (Å ³)	4742.60(19)	11307.78(19)
<i>Z</i>	2	4
Size (mm ³)	0.21×0.09×0.05	0.07×0.05×0.03
θ range (°)	2.822-67.081	2.843-67.071
Total data	61182	143167
Unique data	16845	20048
Parameters	1158	1520
Completeness (%)	99.4	99.2
<i>R</i> _{int} (%)	4.20	5.84
<i>R</i> ₁ (% , I > 2σ)	11.82	7.60
<i>R</i> ₁ (% , all data)	12.45	9.08
<i>wR</i> ₂ (% , I > 2σ)	26.22	18.59
<i>wR</i> ₂ (% , all data)	26.51	19.27
<i>S</i>	1.222	1.126

Table B.8. Pocket Volumes.

Compound	Pocket Volume \AA^3 (^a)	Pocket Volume (top, bottom) \AA^3
3.2a	22 (11)	
3.2b	23.25(12)	
3.2c	34.75	(28.5, 6.25)
3.2d	12.5	(9, 3.5)
3.2e	19.25(10)	
3.2f	34.75(17.3)	
3.2h	25.0(12.5)	
3.2i	13.0	(7.625, 5.375)
3.2k	31.75(16)	
3.2l	20.875(11)	
3.2m	44.5(22)	
3.2o	23.875(12.1)	
3.2p	16.25	(10.75, 5.5)
3.2q	10.25	Only top pocket
3.3b	7.75 (3.875)	

^a average volume across both pockets.

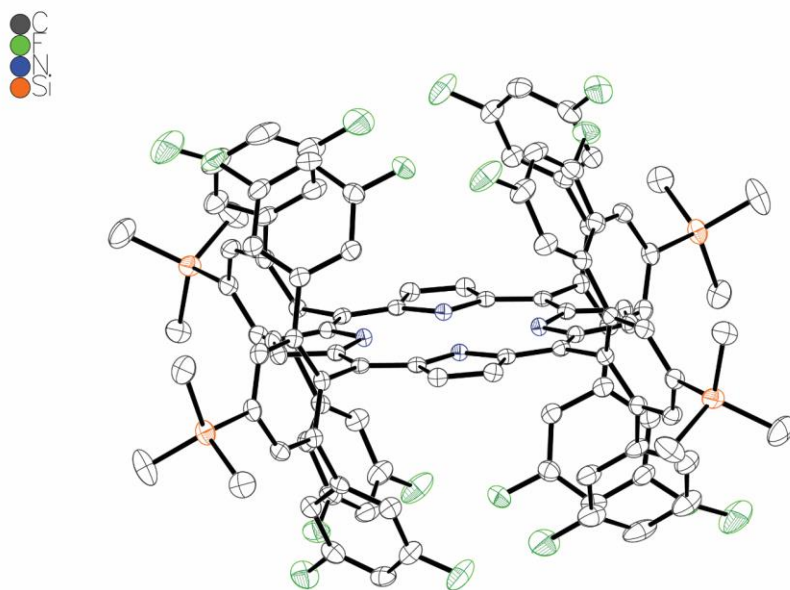


Figure B.53. Thermal ellipsoid plot (50% ellipsoids) of the crystal structure of **3.2b**.

H atoms and solvent omitted for clarity.

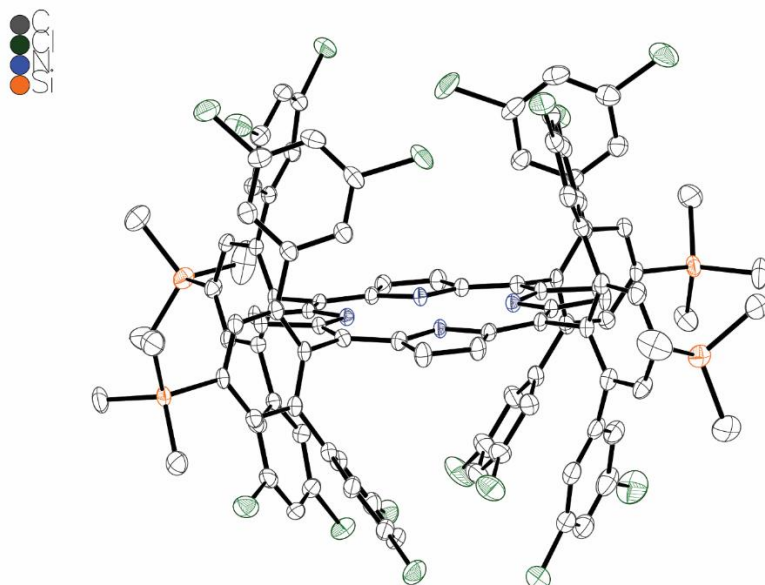


Figure B.54. Thermal ellipsoid plot (50% ellipsoids) of the crystal structure of **3.2c**.

H atoms and solvent omitted for clarity.

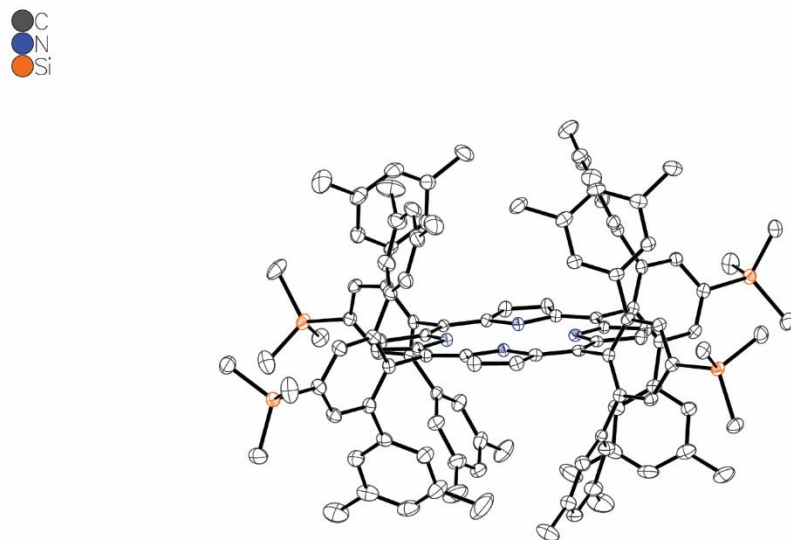


Figure B.55. Thermal ellipsoid plot (50% ellipsoids) of the crystal structure of **3.2d**.

H atoms and solvent omitted for clarity.

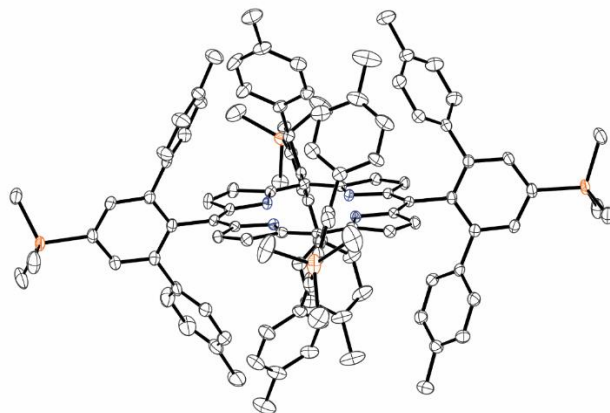


Figure B.56. Thermal ellipsoid plot (50% ellipsoids) of the crystal structure of **3.2e**.

H atoms, solvent, and minor components of the disorder omitted for clarity.

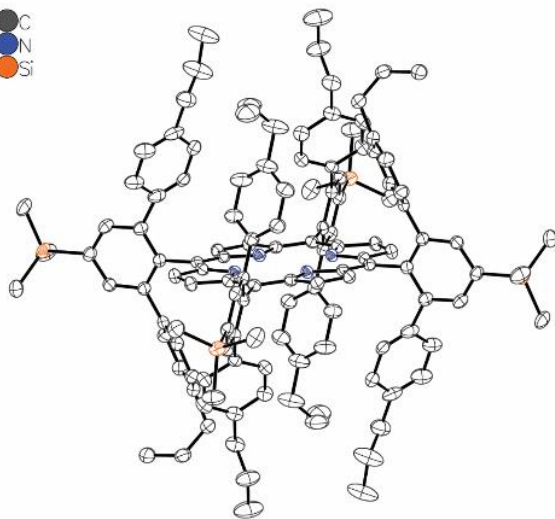


Figure B.57. Thermal ellipsoid plot (50% ellipsoids) of the crystal structure of **3.2f**.

H atoms, solvent, and minor components of the disorder omitted for clarity.

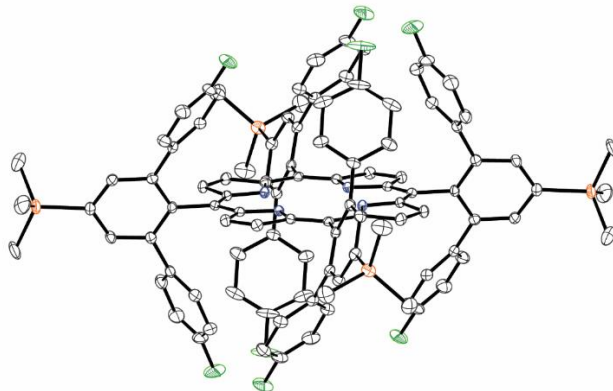


Figure B.58. Thermal ellipsoid plot (50% ellipsoids) of the crystal structure of **3.2h**.
H atoms and solvent omitted for clarity.

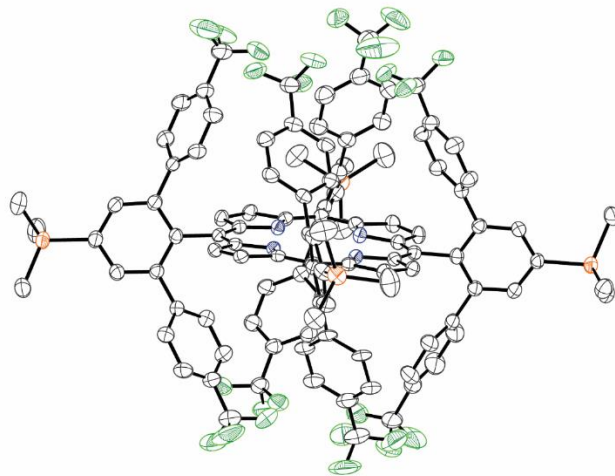


Figure B.59. Thermal ellipsoid plot (50% ellipsoids) of the crystal structure of **3.2i**.
H atoms, solvent, and minor components of the disorder omitted for clarity.

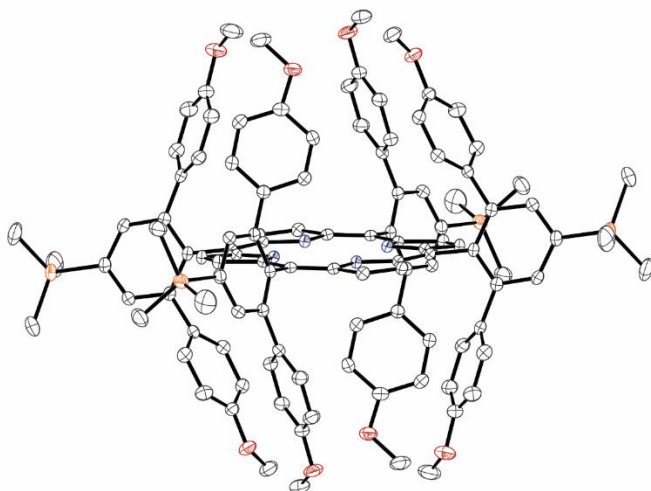


Figure B.60. Thermal ellipsoid plot (50% ellipsoids) of the crystal structure of **3.2k**.

H atoms and solvent omitted for clarity.

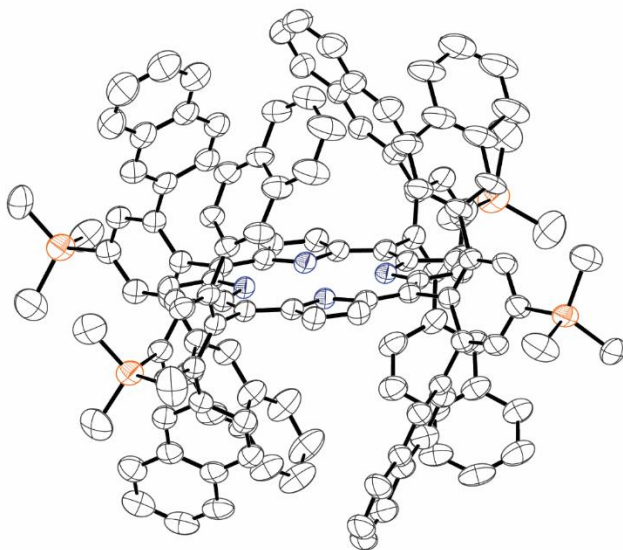


Figure B.61. Thermal ellipsoid plot (50% ellipsoids) of the crystal structure of **3.2l**.

H atoms, solvent, and minor components of the disorder omitted for clarity.

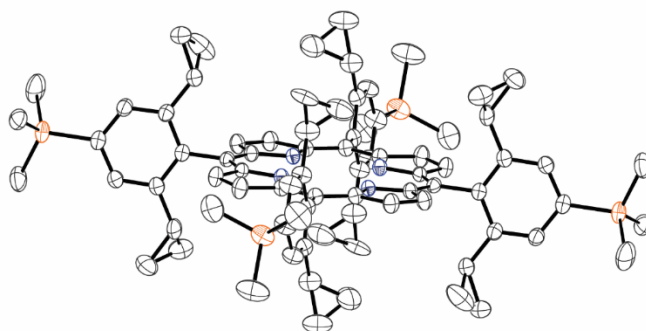


Figure B.62. Thermal ellipsoid plot (50% ellipsoids) of the crystal structure of **3.2m**.
H atoms, solvent, and minor components of the disorder omitted for clarity.

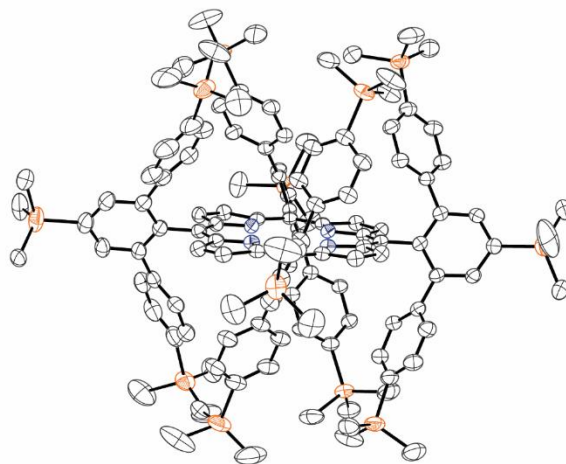


Figure B.63. Thermal ellipsoid plot (50% ellipsoids) of the crystal structure of **3.2o**.
H atoms, solvent, and minor components of the disorder omitted for clarity.

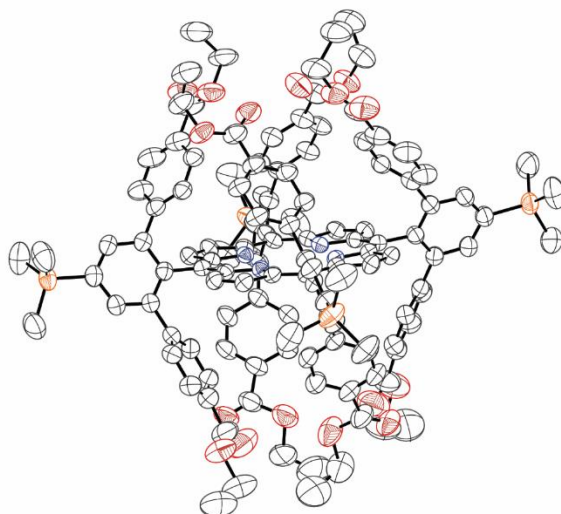


Figure B.64. Thermal ellipsoid plot (50% ellipsoids) of the crystal structure of **3.2p**.

H atoms, solvent, and minor components of the disorder omitted for clarity.

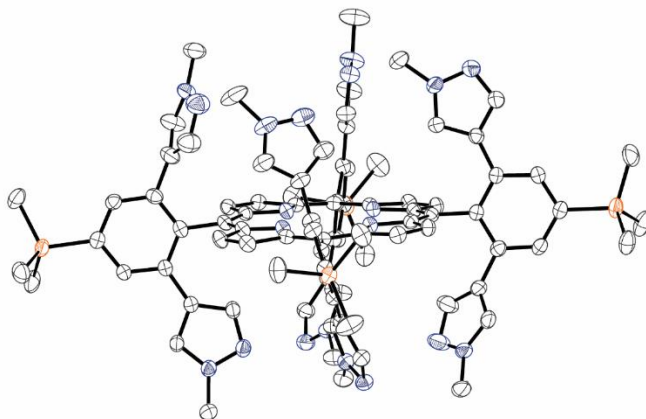


Figure B.65. Thermal ellipsoid plot (50% ellipsoids) of the crystal structure of **3.2q**.

H atoms, solvent, and minor components of the disorder omitted for clarity.

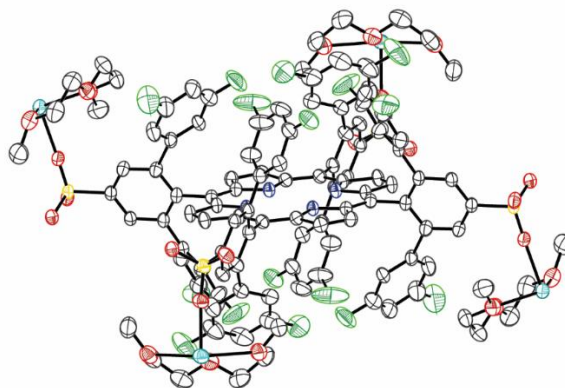


Figure B.66. Thermal ellipsoid plot (50% ellipsoids) of the crystal structure of **3.3b**.

H atoms, solvent, and minor components of the disorder omitted for clarity.

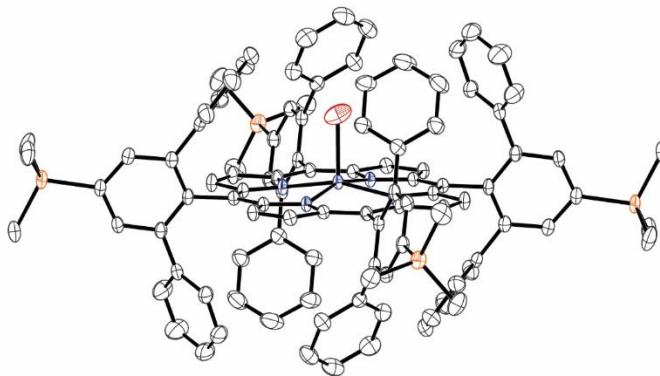


Figure B.67. Thermal ellipsoid plot (50% ellipsoids) of the crystal structure of **3.4a**.

H atoms, solvent, and minor components of the disorder omitted for clarity.

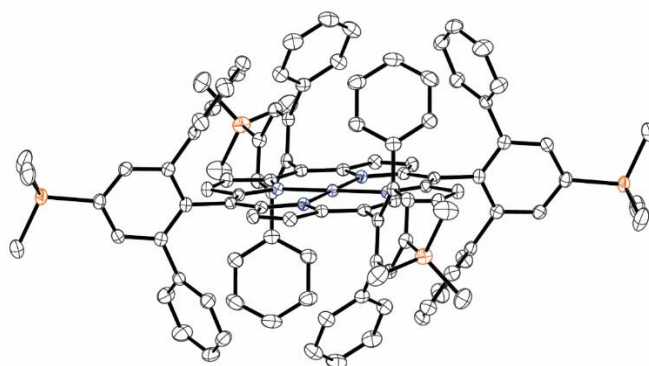


Figure B.68. Thermal ellipsoid plot (50% ellipsoids) of the crystal structure of **3.4b**.

H atoms and solvent omitted for clarity.

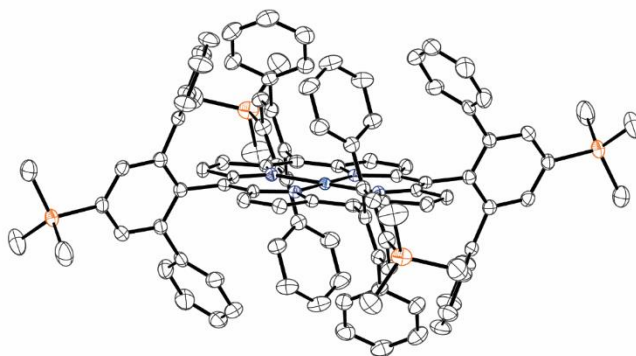


Figure B.69. Thermal ellipsoid plot (50% ellipsoids) of the crystal structure of **3.4c**.

H atoms and solvent omitted for clarity.

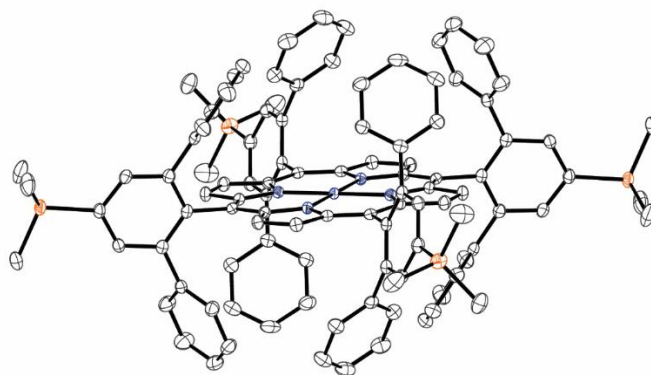


Figure B.70. Thermal ellipsoid plot (50% ellipsoids) of the crystal structure of **3.4d**.

H atoms and solvent omitted for clarity.

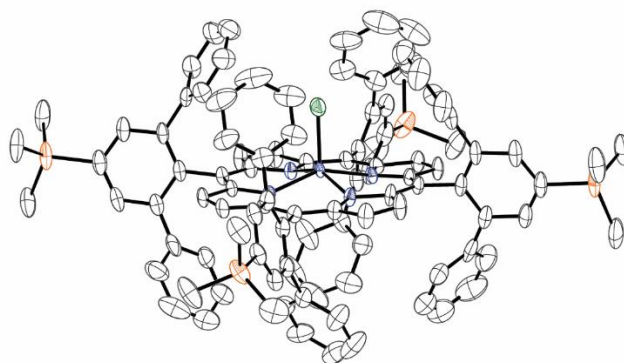


Figure B.71. Thermal ellipsoid plot (50% ellipsoids) of the crystal structure of **3.4e**.

H atoms, solvent, and minor components of the disorder omitted for clarity.

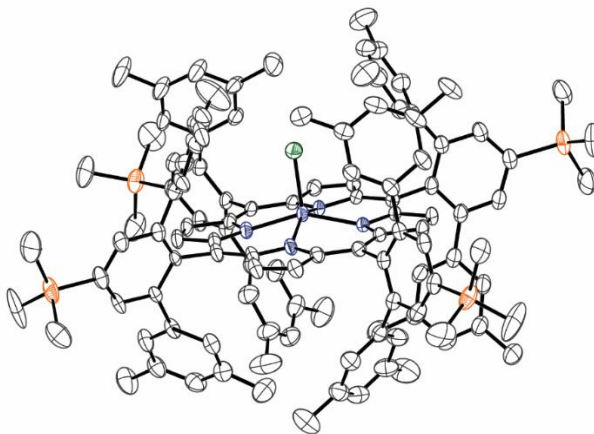


Figure B.72. Thermal ellipsoid plot (50% ellipsoids) of the crystal structure of **3.4f**.

H atoms, solvent, and minor components of the disorder omitted for clarity.

Appendix C: Supplementary Experimental Data for Chapter 4

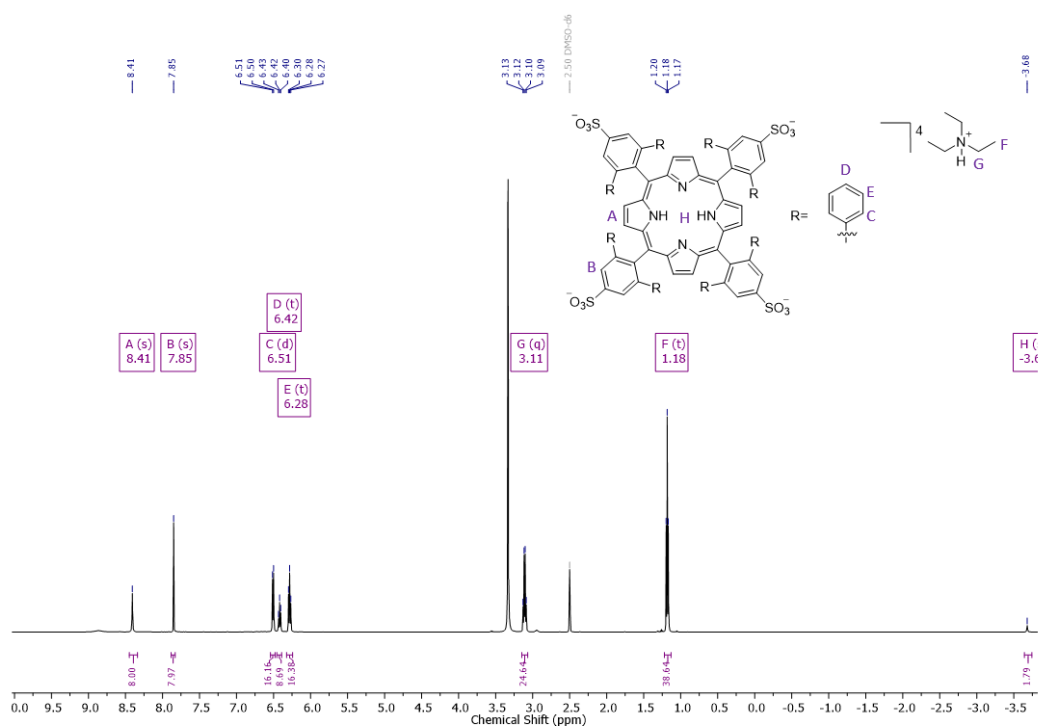


Figure C.1. ^1H NMR spectrum (500 MHz, $\text{DMSO-}d_6$) of **4.2a**

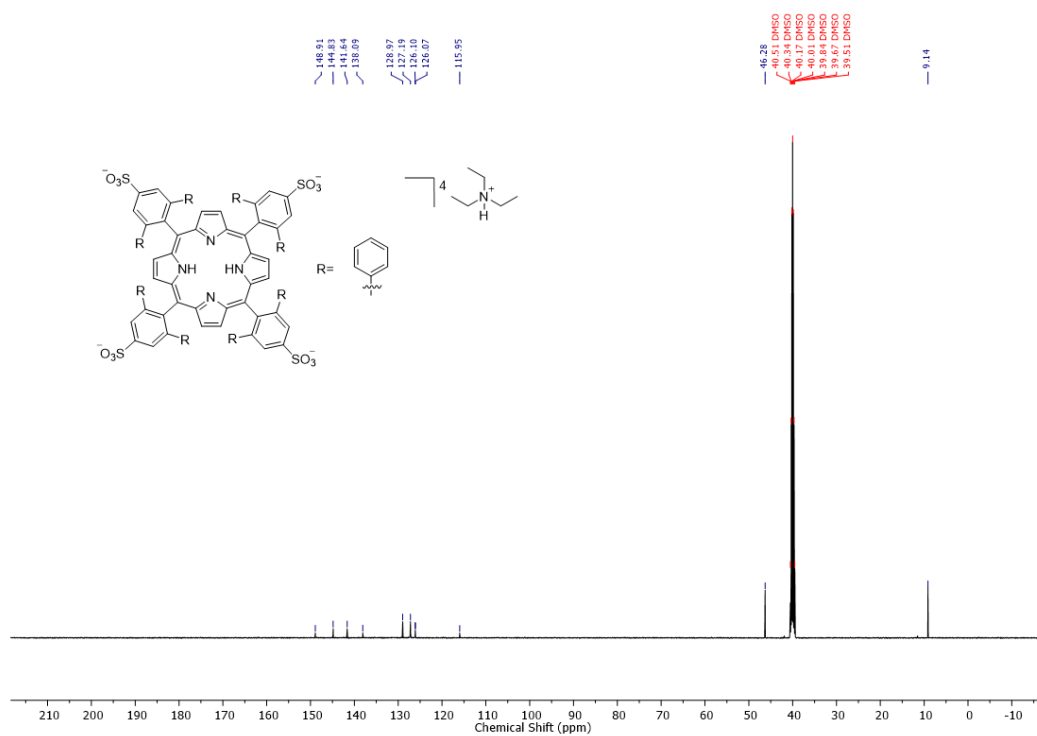


Figure C.2. $^{13}\text{C}\{^1\text{H}\}$ NMR spectrum (126 MHz, $\text{DMSO-}d_6$) of **4.2a**

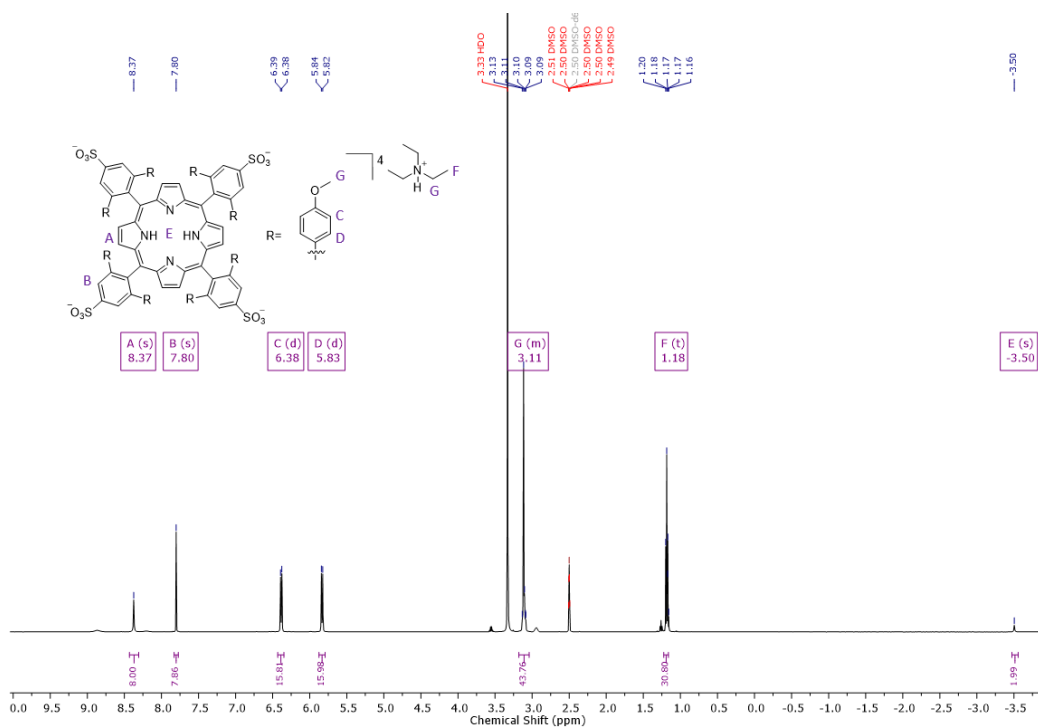


Figure C.3. ^1H NMR spectrum (500 MHz, $\text{DMSO-}d_6$) of **4.2b**

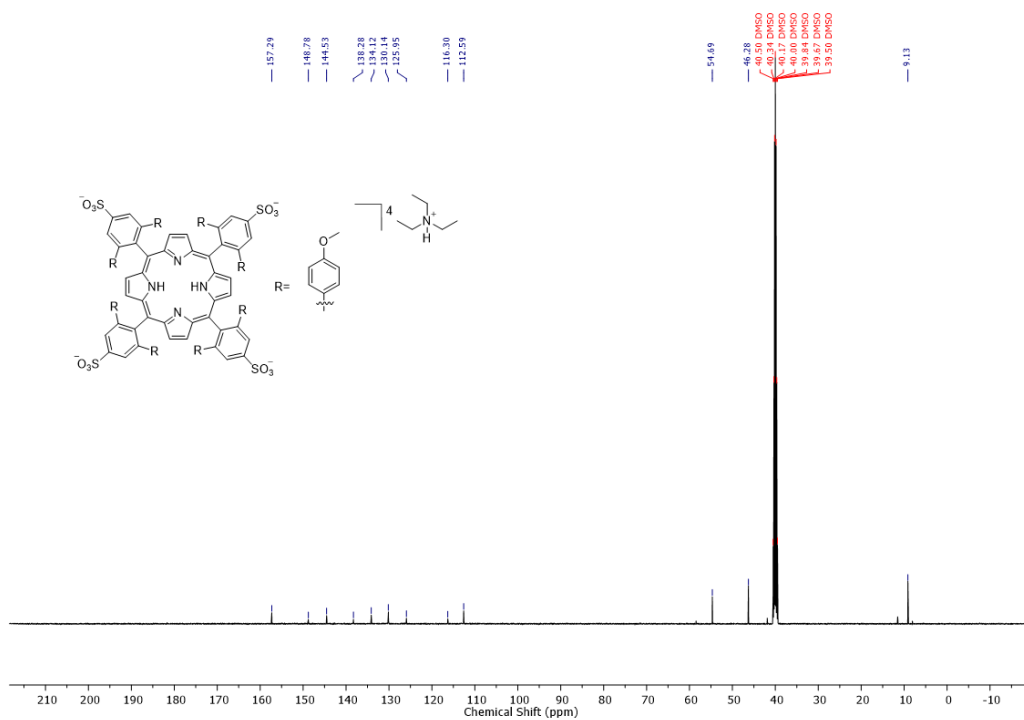


Figure C.4. $^{13}\text{C}\{^1\text{H}\}$ NMR spectrum (126 MHz, $\text{DMSO-}d_6$) of **4.2b**

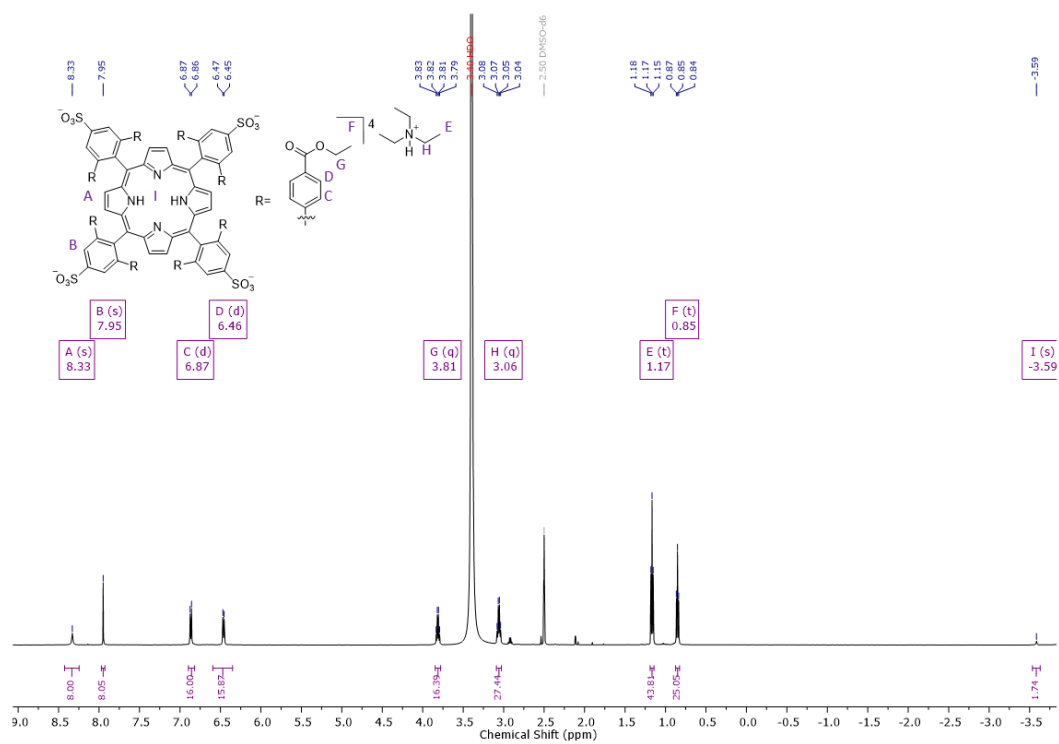


Figure C.5. ^1H NMR spectrum (500 MHz, DMSO- d_6) of 4.2c

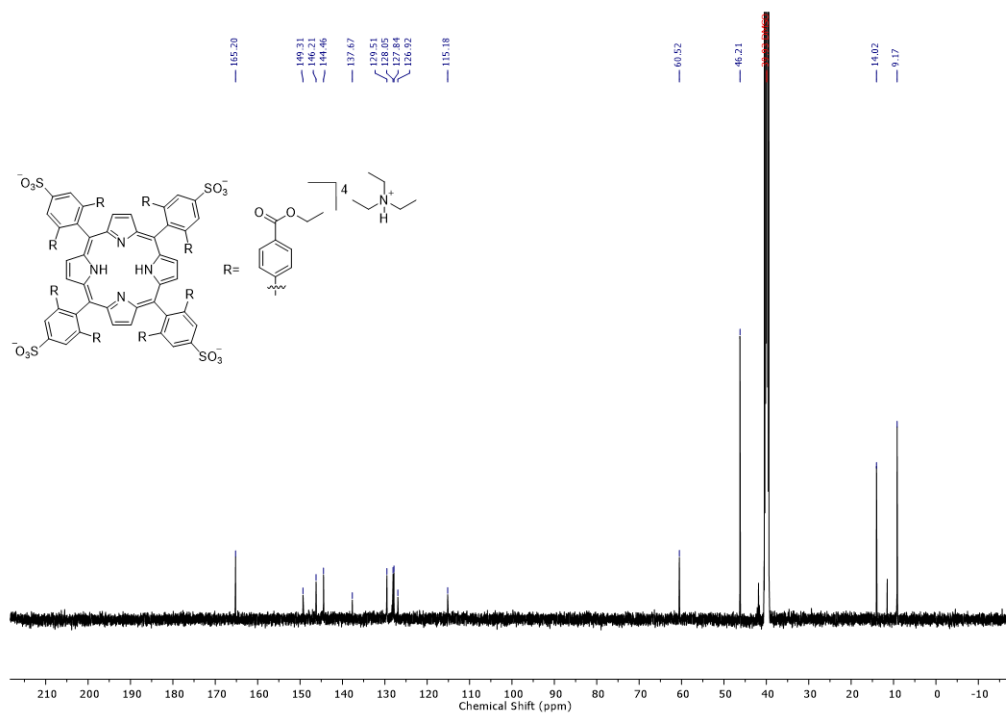


Figure C.6. $^{13}\text{C}\{^1\text{H}\}$ NMR spectrum (126 MHz, DMSO- d_6) of 4.2c

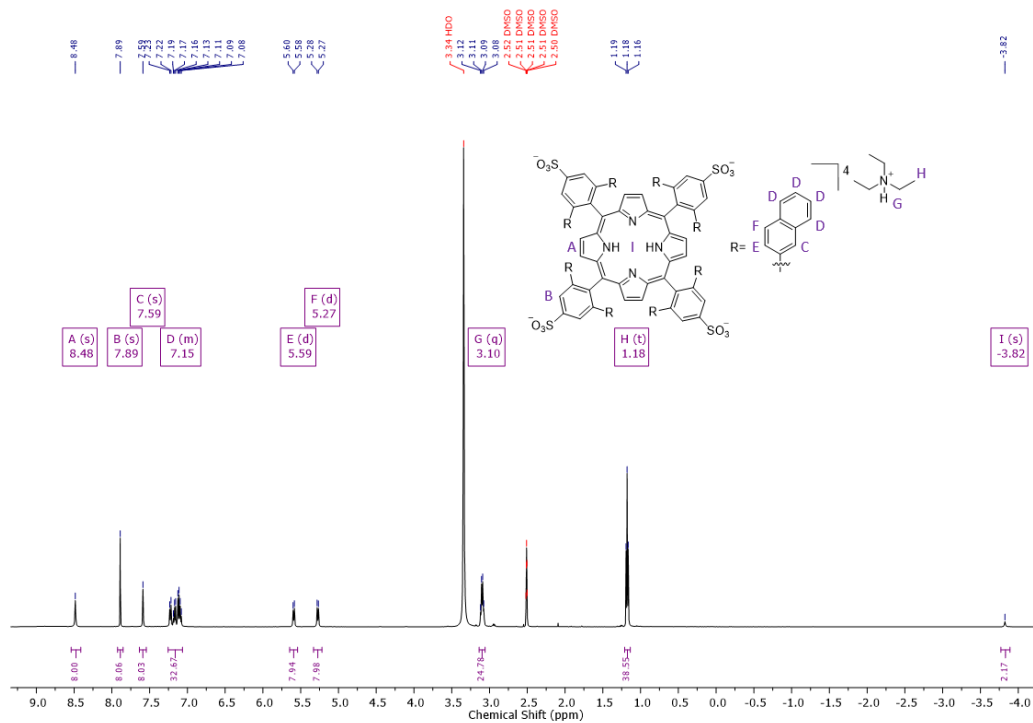


Figure C.7. ^1H NMR spectrum (500 MHz, $\text{DMSO-}d_6$) of **4.2e**

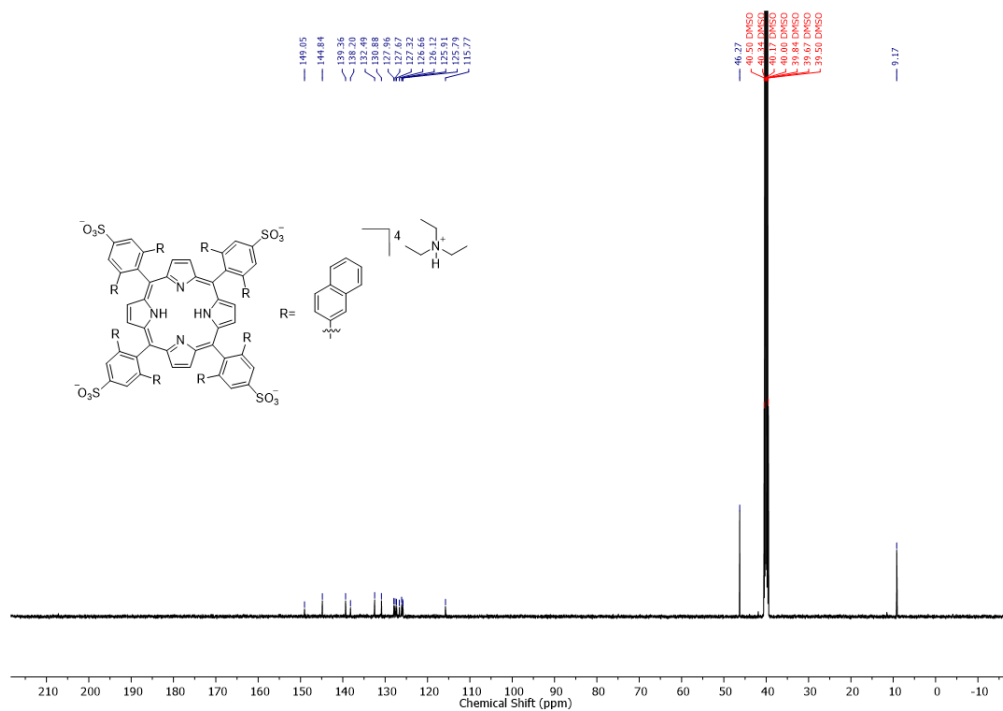


Figure C.8. $^{13}\text{C}\{^1\text{H}\}$ NMR spectrum (126 MHz, $\text{DMSO-}d_6$) of **4.2e**

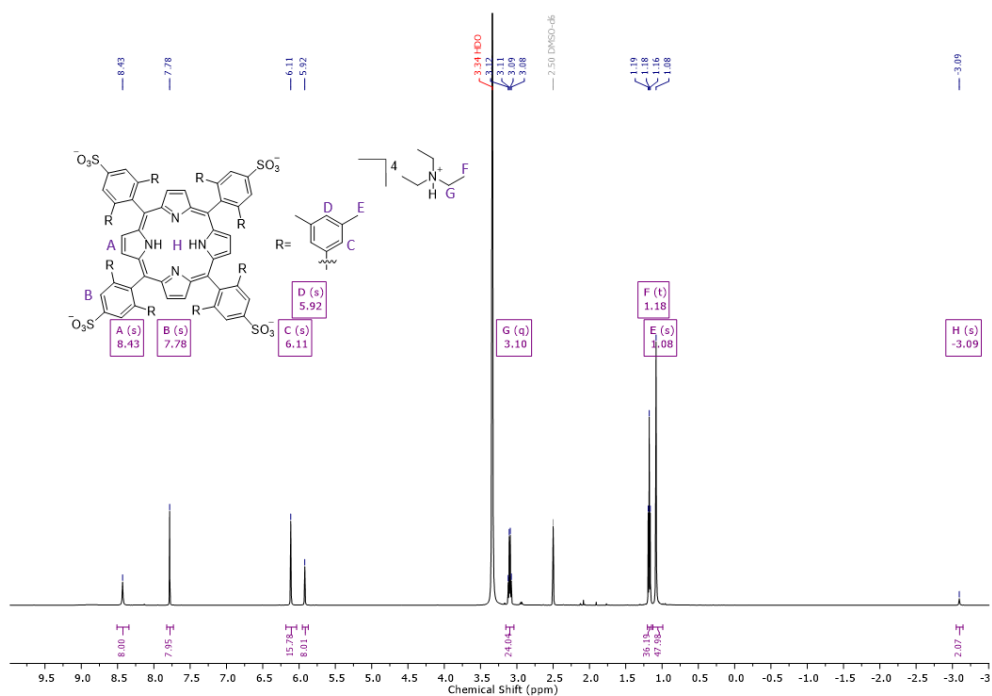


Figure C.9. ^1H NMR spectrum (500 MHz, $\text{DMSO-}d_6$) of **4.2f**

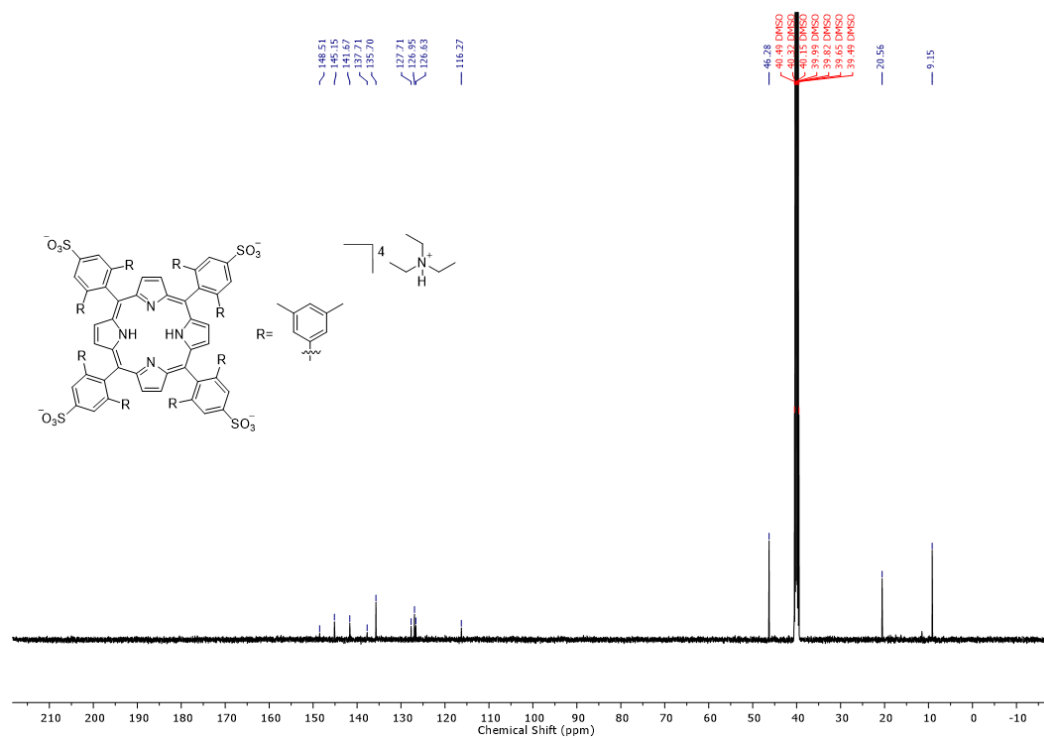


Figure C.10. $^{13}\text{C}\{^1\text{H}\}$ NMR spectrum (126 MHz (500 MHz), $\text{DMSO-}d_6$) of **4.2f**

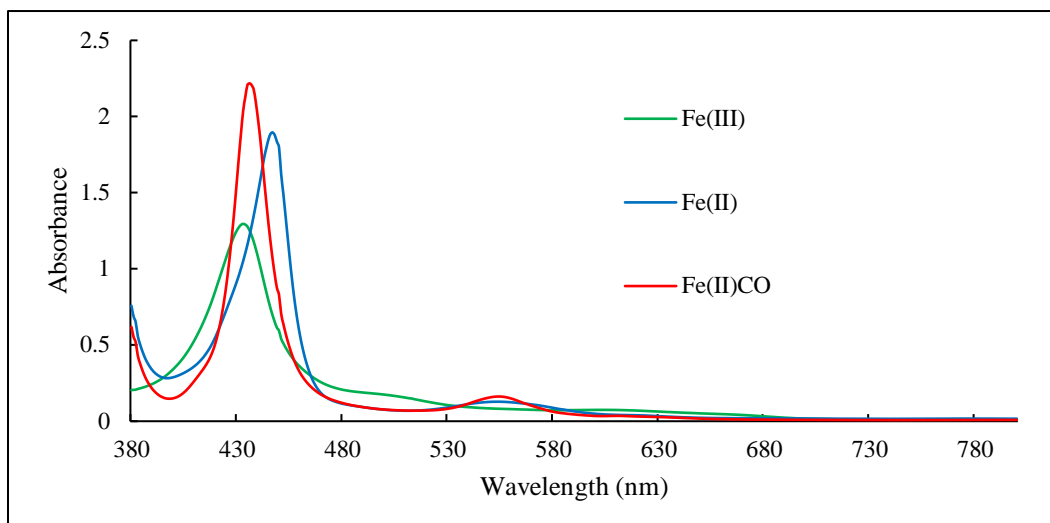


Figure C.11. Electronic absorption spectra of Fe(III) **4.4a**, Fe(II) **4.4a**, and Fe(II)CO **4.4a** (PBS, pH 7.4).

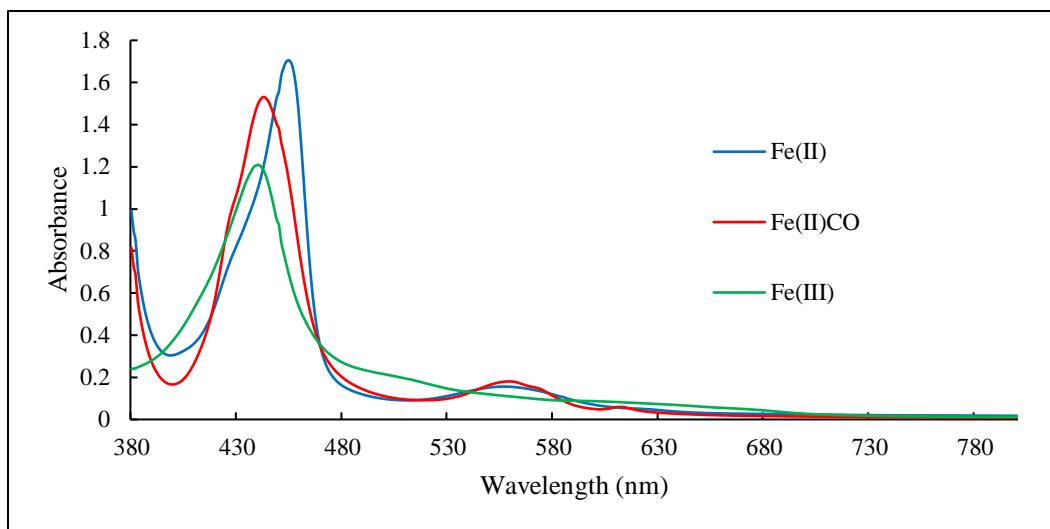


Figure C.12. Electronic absorption spectra of Fe(III) **4.4b**, Fe(II) **4.4b**, and Fe(II)CO **4.4b** (PBS, pH 7.4).

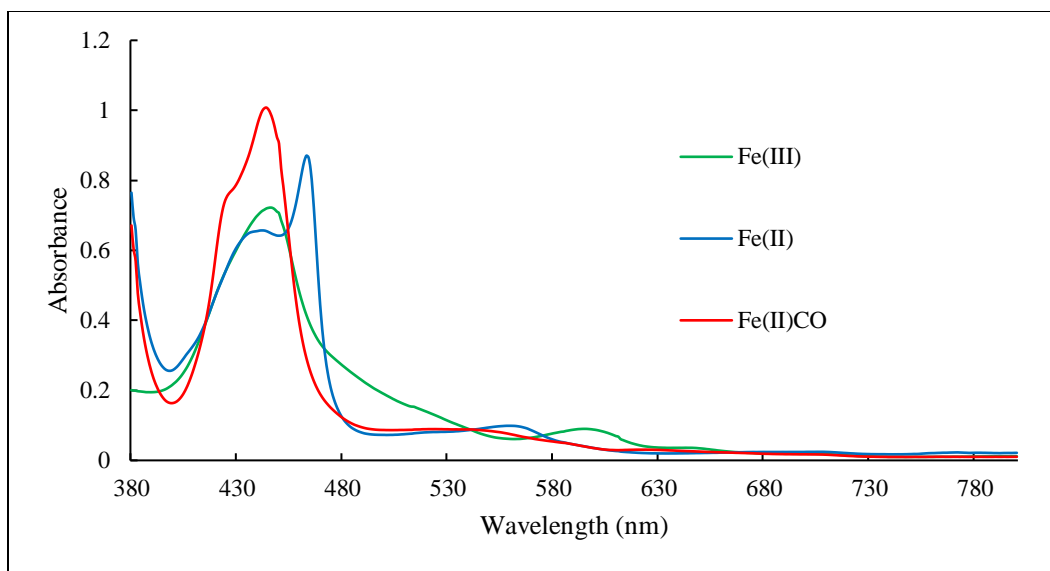


Figure C.13. Electronic absorption spectra of Fe(III) **4.4c**, Fe(II) **4.4c**, and Fe(II)CO **4.4c** (PBS, pH 7.4).

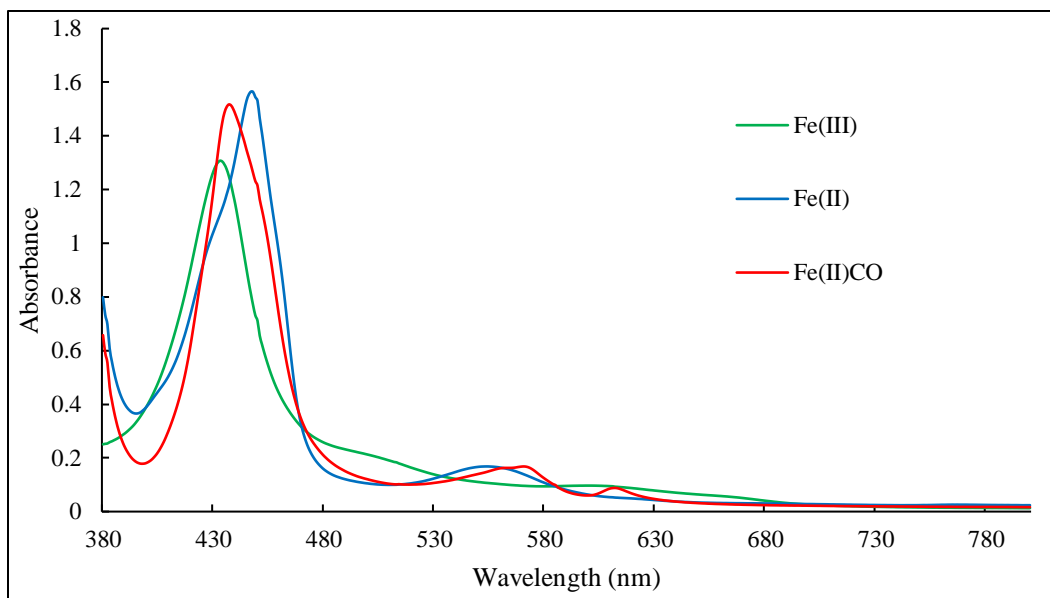


Figure C.14. Electronic absorption spectra of Fe(III) **4.4d**, Fe(II) **4.4d**, and Fe(II)CO **4.4d** (PBS, pH 7.4).

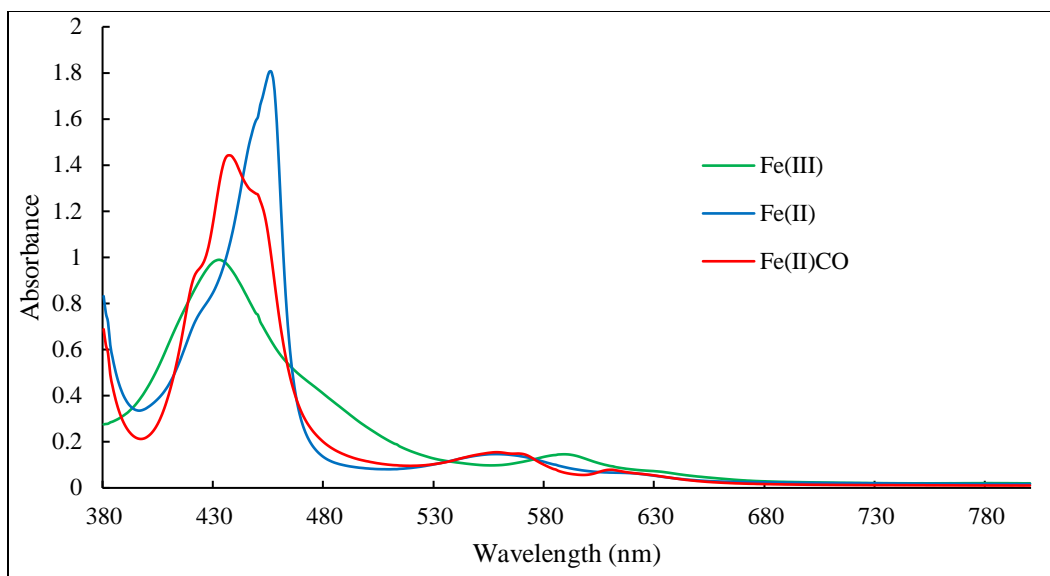


Figure C.15. Electronic absorption spectra of Fe(III) **4.4e**, Fe(II) **4.4e**, and Fe(II)CO **4.4e** (PBS, pH 7.4).

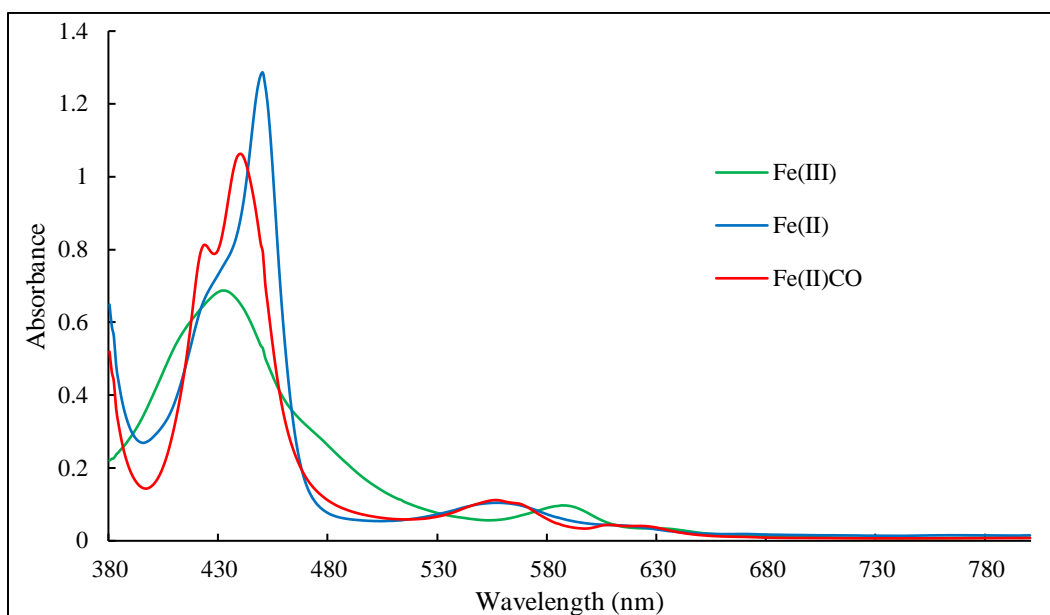


Figure C.16. Electronic absorption spectra of Fe(III) **4.4f**, Fe(II) **4.4f**, and Fe(II)CO **4.4f** (PBS, pH 7.4).

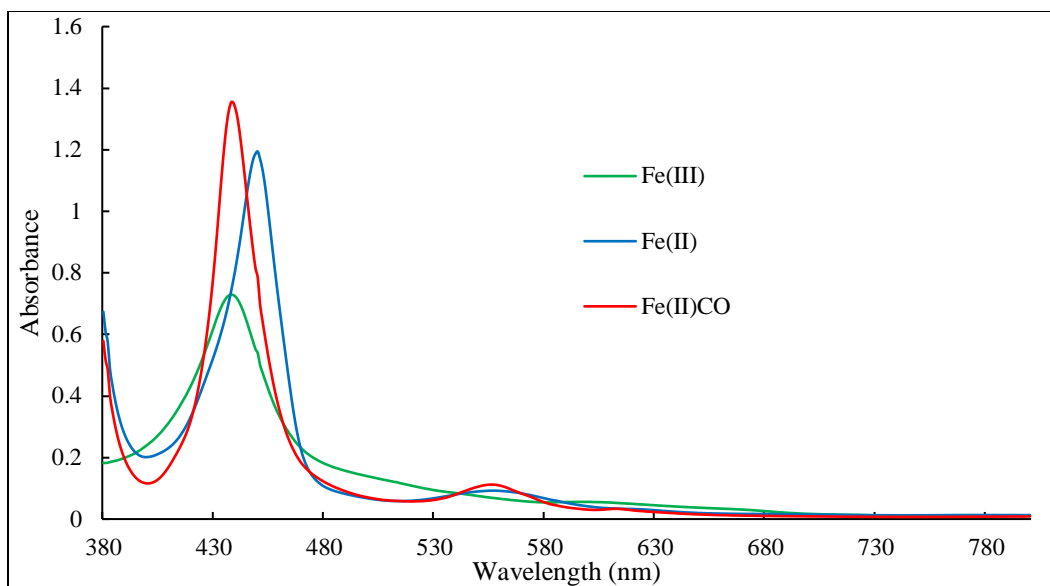


Figure C.17. Electronic absorption spectra of Fe(III) **4.4g**, Fe(II) **4.4g**, and Fe(II)CO **4.4g** (PBS, pH 7.4).

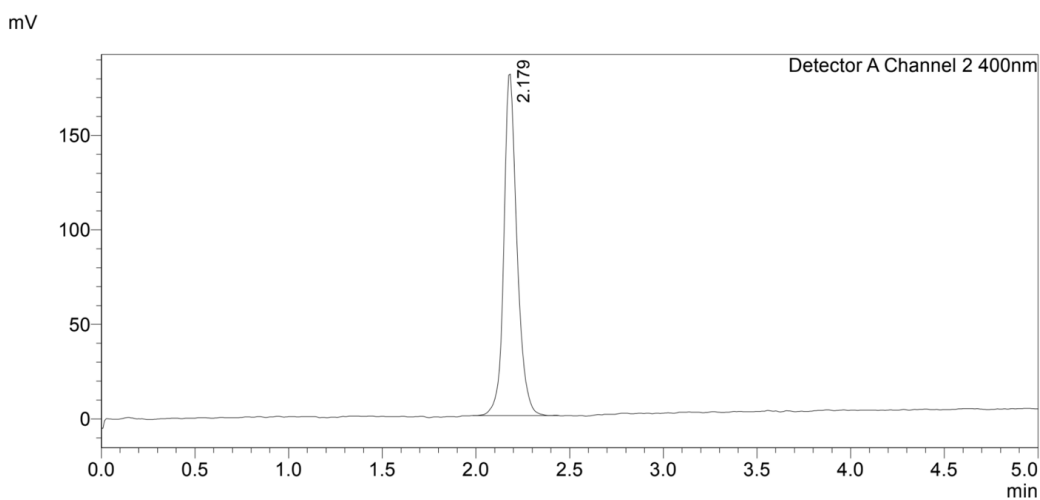


Figure C.18. HPLC chromatogram of **4.4a** confirming >99% purity. Absorbance is measured at 400 nm and the analyte was eluted with a H₂O(1% triethylammonium bicarbonate)/MeCN gradient of 0-100% MeCN over 5 min.

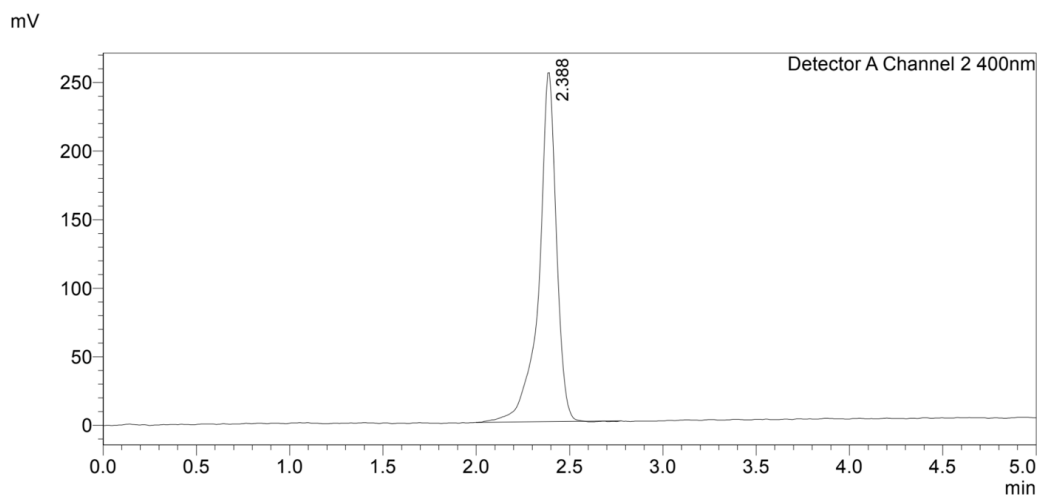


Figure C.19. HPLC chromatogram of **4.4b** confirming >99% purity. Absorbance is measured at 400 nm and the analyte was eluted with a H₂O(1% triethylammonium bicarbonate)/MeCN gradient of 0-100% MeCN over 5 min.

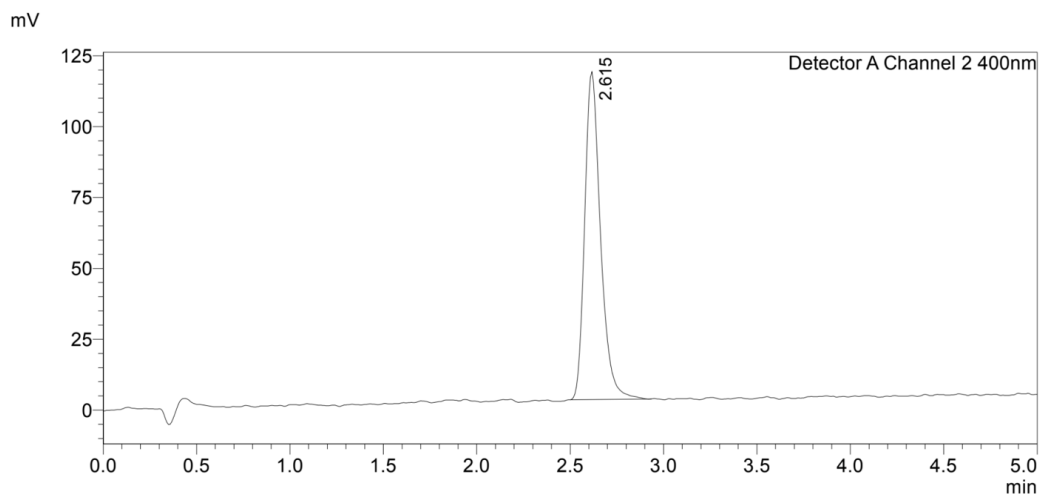


Figure C.20. HPLC chromatogram of **4.4c** confirming >99% purity. Absorbance is measured at 400 nm and the analyte was eluted with a H₂O(1% triethylammonium bicarbonate)/ MeCN gradient of 0-100% MeCN over 5 min.

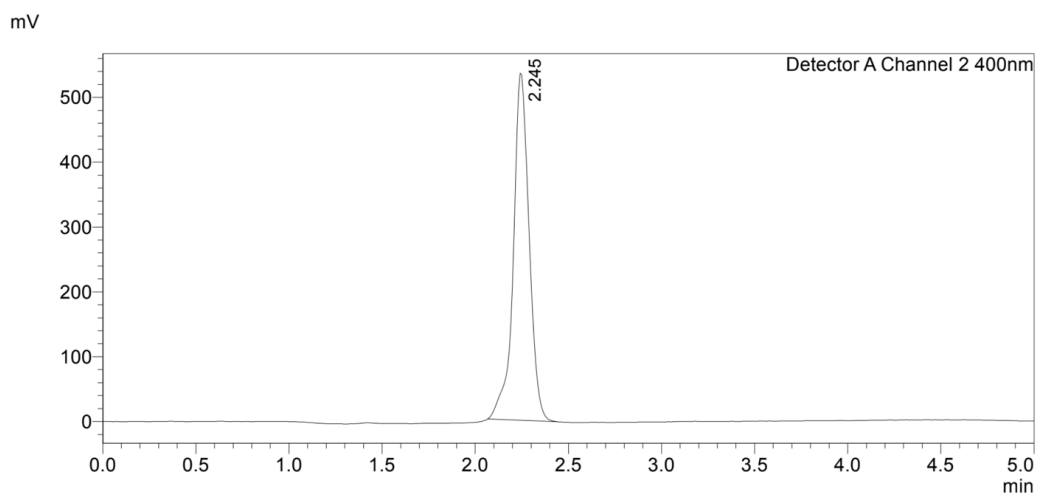


Figure C.21. HPLC chromatogram of **4.4d** confirming >99% purity. Absorbance is measured at 400 nm and the analyte was eluted with a H₂O(1% triethylammonium bicarbonate)/ MeCN gradient of 0-100% MeCN over 5 min.

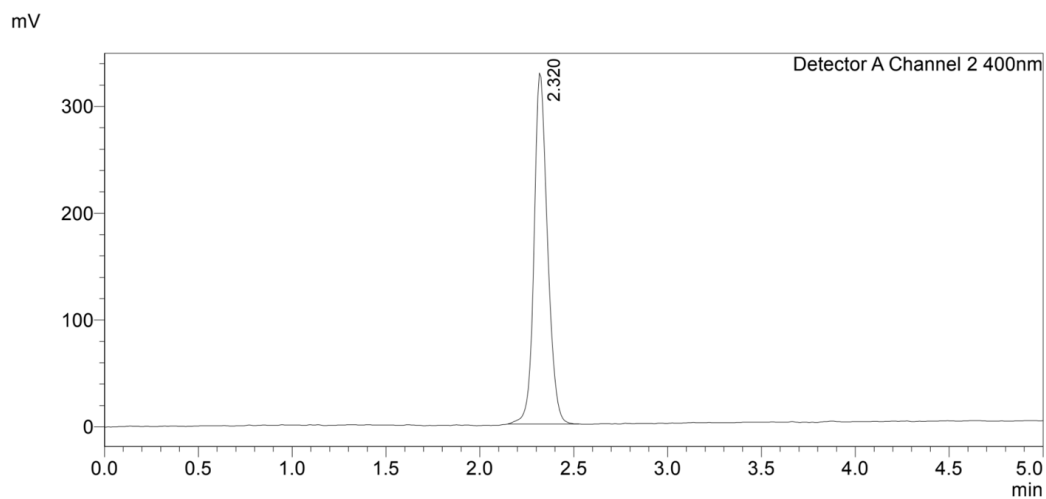


Figure C.22. HPLC chromatogram of **4.4e** confirming >99% purity. Absorbance is measured at 400 nm and the analyte was eluted with a H₂O(1% triethylammonium bicarbonate)/ MeCN gradient of 0-100% MeCN over 5 min.

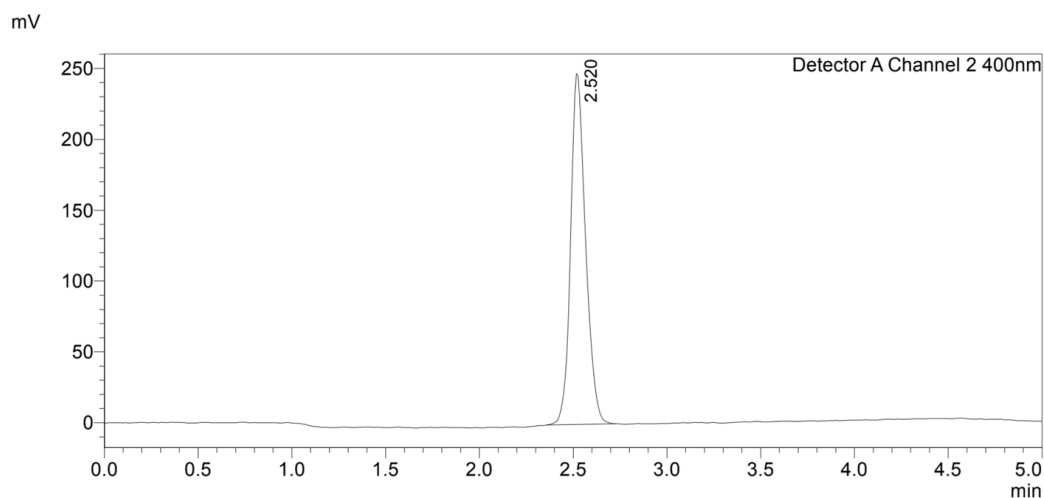


Figure C.23. HPLC chromatogram of **4.4f** confirming >99% purity. Absorbance is measured at 400 nm and the analyte was eluted with a H₂O(1% triethylammonium bicarbonate)/ MeCN gradient of 0-100% MeCN over 5 min.

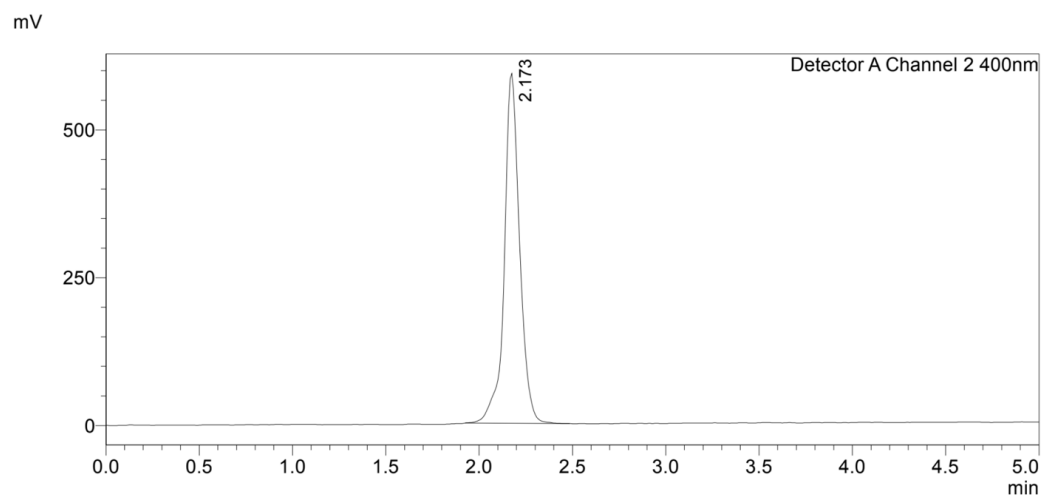


Figure C.24. HPLC chromatogram of **4.4g** confirming >99% purity. Absorbance is measured at 400 nm and the analyte was eluted with a H₂O(1% triethylammonium bicarbonate)/ MeCN gradient of 0-100% MeCN over 5 min.

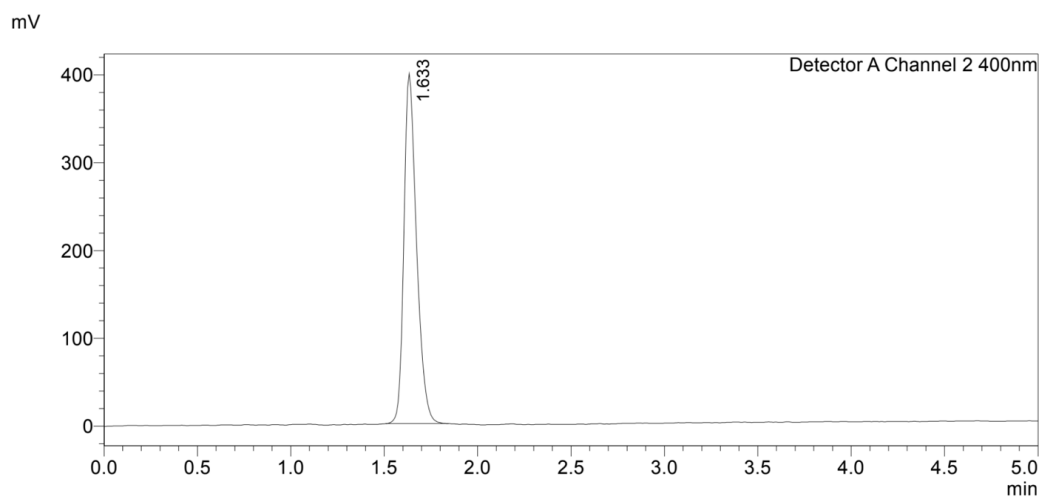


Figure C.25. HPLC chromatogram of **4.4h** confirming >99% purity. Absorbance is measured at 400 nm and the analyte was eluted with a H₂O(1% triethylammonium bicarbonate)/ MeCN gradient of 0-100% MeCN over 5 min.

Bibliography

Adler, A. D.; Longo, F. R.; Finarelli, J. D.; Goldmacher, J.; Assour, J.; Korsakoff, L., A Simplified Synthesis for *meso*-Tetraphenylporphine. *J. Org. Chem.* **1967**, *32*, 476-476.

Azarov, I.; Wang, L.; Rose, J. J.; Xu, Q.; Huang, X. N.; Belanger, A.; Wang, Y.; Guo, L.; Liu, C.; Ucer, K. B.; McTiernan, C. F.; O'Donnell, C. P.; Shiva, S.; Tejero, J.; Kim-Shapiro, D. B.; Gladwin, M. T., Five-coordinate H64Q neuroglobin as a ligand-trap antidote for carbon monoxide poisoning. *Sci. Transl. Med.* **2016**, *8*, 368ra173.

Boaz, N. C.; Bell, S. R.; Groves, J. T., Ferryl Protonation in Oxoiron(IV) Porphyrins and Its Role in Oxygen Transfer. *J. Am. Chem. Soc.* **2015**, *137*, 2875-2885.

Brune, B.; Ullrich, V., Inhibition of platelet aggregation by carbon monoxide is mediated by activation of guanylate cyclase. *Mol. Pharmacol.* **1987**, *32*, 497-504.

Chakraborty, I.; Carrington, S. J.; Mascharak, P. K., Design Strategies To Improve the Sensitivity of Photoactive Metal Carbonyl Complexes (photoCORMs) to Visible Light and Their Potential as CO-Donors to Biological Targets. *Acc. Chem. Res.* **2014**, *47*, 2603-2611.

Chakraborty, I.; Carrington, S. J.; Roseman, G.; Mascharak, P. K., Synthesis, Structures, and CO Release Capacity of a Family of Water-Soluble PhotoCORMs: Assessment of the Biocompatibility and Their Phototoxicity toward Human Breast Cancer Cells. *Inorg. Chem.* **2017**, *56*, 1534-1545.

Collman, J. P., Synthetic models for the oxygen-binding hemoproteins. *Acc. Chem. Res.* **1977**, *10*, 265-272.

Collman, J. P.; Brauman, J. I.; Doxsee, K. M., Carbon monoxide binding to iron porphyrins. *Proc. Natl. Acad. Sci. U.S.A.* **1979**, *76*, 6035-6039.

Collman, J. P.; Brauman, J. I.; Halbert, T. R.; Suslick, K. S., Nature of O₂ and CO binding to metalloporphyrins and heme proteins. *Proc. Natl. Acad. Sci. U.S.A.* **1976**, *73*, 3333-3337.

Collman, J. P.; Gagne, R. R.; Halbert, T. R.; Marchon, J.-C.; Reed, C. A., Reversible oxygen adduct formation in ferrous complexes derived from a "picket fence" porphyrin. A model for oxymyoglobin. *J. Am. Chem. Soc.* **1973**, *95*, 7868-7870.

Collman, J. P.; Gagne, R. R.; Reed, C.; Halbert, T. R.; Lang, G.; Robinson, W. T., "Picket fence porphyrins." Synthetic models for oxygen binding hemoproteins. *J. Am. Chem. Soc.* **1975**, *97*, 1427-1439.

- Collman, J. P.; Hoard, J. L.; Kim, N.; Lang, G.; Reed, C. A., Synthesis, Stereochemistry, and Structure-Related Properties of $\alpha,\beta,\gamma,\delta$ -Tetraphenylporphinatoiron(II). *J. Am. Chem. Soc.* **1975**, *97*, 2676-2681.
- Dewilde, S.; Kiger, L.; Burmester, T.; Hankeln, T.; Baudin-Creuzat, V.; Aerts, T.; Marden, M. C.; Caubergs, R.; Moens, L., Biochemical characterization and ligand binding properties of neuroglobin, a novel member of the globin family. *J. Biol. Chem.* **2001**, *276*, 38949-55.
- Dolomanov, O. V.; Bourhis, L. J.; Gildea, R. J.; Howard, J. A. K.; Puschmann, H., *OLEX2*: a complete structure solution, refinement and analysis program. *J. Appl. Crystallogr.* **2009**, *42*, 339-341.
- Dong, M. W., 9 - How to be more successful with HPLC analysis: Practical aspects in HPLC operation. In *Handbook of Pharmaceutical Analysis by HPLC*, 2005; pp 255-271.
- Droege, D. G.; Johnstone, T. C., A water-soluble iron-porphyrin complex capable of rescuing CO-poisoned red blood cells. *Chem. Commun.* **2022**, *58*, 2722-2725.
- Droege, D. G.; Parker, A. L.; Milligan, G. M.; Jenkins, R.; Johnstone, T. C., Synthesis and Functionalization of Challenging meso-Substituted Aryl Bis-pocket Porphyrins Accessed via Suzuki–Miyaura Cross-Coupling. *J. Org. Chem.* **2022**, *87*, 11783-11795.
- Durrant, J. D.; Votapka, L.; Sørensen, J.; Amaro, R. E., POVME 2.0: An Enhanced Tool for Determining Pocket Shape and Volume Characteristics. *J. Chem. Theory Comput.* **2014**, *10*, 5047-5056.
- Esfandiari bayat, Z.; Rahiminezhad, H.; Zakavi, S., Solvent effects on catalytic activity of manganese porphyrins with cationic, anionic and uncharged *meso* substituents: Indirect evidence on the nature of active oxidant species. *Appl. Organomet. Chem.* **2019**, *33*, e4678.
- Farhang, M.; Akbarzadeh, A. R.; Rabbani, M.; Ghadiri, A. M., A retrospective-prospective review of Suzuki–Miyaura reaction: From cross-coupling reaction to pharmaceutical industry applications. *Polyhedron* **2022**, *227*, 116124.
- Fleischer, E. B.; Palmer, J. M.; Srivastava, T. S.; Chatterjee, A., Thermodynamic and Kinetic Properties of an Iron-Porphyrin System. *J. Am. Chem. Soc.* **1971**, *93*, 3162-3167.

Goldbaum, L. R.; Ramirez, R. G.; Absalon, K. B., What is the mechanism of carbon monoxide toxicity? *Aviat. Space. Environ. Med.* **1975**, *46*, 1289-91.

Gouterman, M., Study of the Effects of Substitution on the Absorption Spectra of Porphin. *J. Chem. Phys.* **1959**, *30*, 1139-1161.

Guillerm, V.; Weseliński, Ł. J.; Alkordi, M.; Mohideen, M. I. H.; Belmabkhout, Y.; Cairns, A. J.; Eddaoudi, M., Porous organic polymers with anchored aldehydes: a new platform for post-synthetic amine functionalization en route for enhanced CO₂ adsorption properties. *Chem. Commun.* **2014**, *50*, 1937-1940.

Haldane, J., The Relation of the Action of Carbonic Oxide to Oxygen Tension. *J. Physiol.* **1895**, *18*, 201-217.

Hampson, N. B.; Piantadosi, C. A.; Thom, S. R.; Weaver, L. K., Practice Recommendations in the Diagnosis, Management, and Prevention of Carbon Monoxide Poisoning. *Am. J. Respir. Crit. Care Med.* **2012**, *186*, 1095-1101.

Hopper, C. P.; Zambrana, P. N.; Goebel, U.; Wollborn, J., A brief history of carbon monoxide and its therapeutic origins. *Nitric Oxide* **2021**, *111-112*, 45-63.

Hu, C.; Noll, B. C.; Schulz, C. E.; Scheidt, W. R., Four-Coordinate Iron(II) Porphyrinates: Electronic Configuration Change by Intermolecular Interaction. *Inorg. Chem.* **2007**, *46*, 619-621.

Hughes, J. P.; Rees, S.; Kalindjian, S. B.; Philpott, K. L., Principles of early drug discovery. *Br. J. Pharmacol.* **2011**, *162*, 1239-1249.

Kano, K.; Kitagishi, H.; Kodera, M.; Hirota, S., Dioxygen Binding to a Simple Myoglobin Model in Aqueous Solution. *Angew. Chem., Int. Ed.* **2005**, *44*, 435-438.

Kitagishi, H.; Mao, Q.; Kitamura, N.; Kita, T., HemoCD as a Totally Synthetic Artificial Oxygen Carrier: Improvements in the Synthesis and O₂/CO Discrimination. *Artif. Organs* **2017**, *41*, 372-380.

La Mar, G. N.; Walker, F. A., Dynamics of Axial Ligation in Metalloporphyrins. I. Imidazole Exchange in Low-Spin Ferric Porphyrins. *J. Am. Chem. Soc.* **1972**, *94*, 8607-8608.

Lima, C. F. R. A. C.; Rodrigues, A. S. M. C.; Silva, V. L. M.; Silva, A. M. S.; Santos, L. M. N. B. F., Role of the Base and Control of Selectivity in the Suzuki-Miyaura Cross-Coupling Reaction. *ChemCatChem* **2014**, 1291-1302.

- Lin, C.-H.; Tour, J., Hydrogen-Bond-Assisted π -Stacking of Shape-Persistent Cyclophanes. *J. Org. Chem.* **2002**, *67*, 7761-7768.
- Lindsey, J. S.; Wagner, R. W., Investigation of the Synthesis of Ortho-Substituted Tetraphenylporphyrins. *J. Org. Chem.* **1989**, *54*, 828-836.
- Lindsey, J. S.; Wagner, R. W., Investigation of the Synthesis of Ortho-Substituted Tetraphenylporphyrins. *J. Org. Chem.* **1989**, *54*, 828-836.
- Littke, A. F.; Fu, G. C., Palladium-Catalyzed Coupling Reactions of Aryl Chlorides. *Angew. Chem., Int. Ed.* **2002**, *41*, 4176-4211.
- Luciano, M.; Brückner, C., Modifications of Porphyrins and Hydroporphyrins for Their Solubilization in Aqueous Media. *Molecules* **2017**, *22*, 980.
- Maluenda, I.; Navarro, O., Recent Developments in the Suzuki-Miyaura Reaction: 2010–2014. *Molecules* **2015**, *20*, 7528-7557.
- Mao, Q.; Das, P. K.; Le Gac, S.; Boitrel, B.; Dorcet, V.; Oohora, K.; Hayashi, T.; Kitagishi, H., Functional Myoglobin Model Composed of a Strapped Porphyrin/Cyclodextrin Supramolecular Complex with an Overhanging COOH That Increases O₂/CO Binding Selectivity in Aqueous Solution. *Inorg. Chem.* **2021**, *60*, 12392-12404.
- Mao, Q.; Zhao, X.; Kiriya, A.; Negi, S.; Fukuda, Y.; Yoshioka, H.; Kawaguchi, A. T.; Motterlini, R.; Foresti, R.; Kitagishi, H., A synthetic porphyrin as an effective dual antidote against carbon monoxide and cyanide poisoning. *Proc. Natl. Acad. Sci. U.S.A.* **2023**, *120*, 9.
- Matsu-ura, M.; Tani, F.; Naruta, Y., Formation and Characterization of Carbon Monoxide Adducts of Iron “Twin Coronet” Porphyrins. Extremely Low CO Affinity and a Strong Negative Polar Effect on Bound CO. *J. Am. Chem. Soc.* **2002**, *124*, 1941-1950.
- Miyaura, N.; Yanagi, T.; Suzuki, A., The Palladium-Catalyzed Cross-Coupling Reaction of Phenylboronic Acid with Haloarenes in the Presence of Bases. *Synth. Commun.* **2006**, *11*, 513-519.
- Momenteau, M.; Loock, B., ‘Basket handle’ porphyrins: new synthetic iron(II) complexes for oxygen binding. *J. Mol. Catal.* **1980**, *7*, 315-320.
- Moore, J. N.; Hansen, P. A.; Hochstrasser, R. M., Iron-carbonyl bond geometries of carboxymyoglobin and carboxyhemoglobin in solution determined by picosecond

time-resolved infrared spectroscopy. *Proc. Natl. Acad. Sci. U.S.A.* **1988**, *85*, 5062-5066.

Motterlini, R.; Foresti, R., Biological signaling by carbon monoxide and carbon monoxide-releasing molecules. *Am. J. Physiol.: Cell Physiol.* **2017**, *312*, C302-C313.

Motterlini, R.; Otterbein, L. E., The therapeutic potential of carbon monoxide. *Nat. Rev. Drug Discov.* **2010**, *9*, 728-743.

Müller, P., Practical suggestions for better crystal structures. *Crystallogr. Rev.* **2009**, *15*, 57-83.

Namjesnik-Dejanovic, K.; Cabaniss, S. E., Reverse-Phase HPLC Method for Measuring Polarity Distributions of Natural Organic Matter. *Environ. Sci. Technol.* **2003**, *38*, 1108-1114.

Pettersen, E. F.; Goddard, T. D.; Huang, C. C.; Meng, E. C.; Couch, G. S.; Croll, T. I.; Morris, J. H.; Ferrin, T. E., UCSF ChimeraX: Structure visualization for researchers, educators, and developers. *Protein Sci.* **2020**, *30*, 70-82.

Pisarek, S.; Maximova, K.; Gryko, D., Strategies toward the synthesis of amphiphilic porphyrins. *Tetrahedron* **2014**, *70*, 6685-6715.

Priestley, J., XIX. Observations on different kinds of air. *Phil. Trans. R. Soc.* **1772**, *62*, 147-264.

Rigaku Oxford Diffraction *CrysAlis^{Pro}* software system, version 1.171.40.78a; Rigaku Corporation: Wroclaw, Poland, **2020**.

Roderique, J. D.; Josef, C. S.; Feldman, M. J.; Spiess, B. D., A modern literature review of carbon monoxide poisoning theories, therapies, and potential targets for therapy advancement. *Toxicology* **2015**, *334*, 45-58.

Rose, E. J.; Venkatasubramanian, P. N.; Swartz, J. C.; Jones, R. D.; Basolo, F.; Hoffman, B. M., Carbon monoxide binding kinetics in "capped" porphyrin compounds. *Proc. Natl. Acad. Sci. U.S.A.* **1982**, *79*, 5742-5745.

Rothmund, P., Formation of Porphyrins from Pyrrole and Aldehydes. *J. Am. Chem. Soc.* **1935**, *57*, 2010-2011.

Schubert, E. M., Utilizing the Evans method with a superconducting NMR spectrometer in the undergraduate laboratory. *J. Chem. Educ.* **1992**, *69*, 1, 62.

- Sheldrick, G. M., *SHELXT* – Integrated space-group and crystal-structure determination. *Acta Crystallogr. Sect. A* **2015**, *71*, 3-8.
- Sheldrick, G. M., Crystal structure refinement with *SHELXL*. *Acta Crystallogr. Sect. C* **2015**, *71*, 3-8.
- Sircar, K.; Clower, J.; Shin, M. k.; Bailey, C.; King, M.; Yip, F., Carbon monoxide poisoning deaths in the United States, 1999 to 2012. *Am. J. Emerg. Med.* **2015**, *33*, 1140-1145.
- Suslick, K. S.; Fox, M. M., A Bis-Pocket Porphyrin. *J. Am. Chem. Soc.* **1983**, *105*, 3507-3510.
- Suslick, K. S.; Fox, M. M.; Reinert, T. R., Influences on carbon monoxide and dioxygen binding to iron(II) porphyrins. *J. Am. Chem. Soc.* **1984**, *106*, 4522-4525.
- Untereiner, A. A.; Wu, L.; Wang, R., The Role of Carbon Monoxide as a Gasotransmitter in Cardiovascular and Metabolic Regulation. In *Gasotransmitters: Physiology and Pathophysiology*, **2012**; pp 37-70.
- Varma, D. R.; Mulay, S.; Chemtob, S., Carbon Monoxide: From Public Health Risk to Painless Killer. In *Handbook of Toxicology of Chemical Warfare Agents*, **2009**; pp 271-292.
- Walker, F. A., NMR and EPR Spectroscopy of Paramagnetic Metalloporphyrins and Heme Proteins. In *Handbook of Porphyrin Science (Volume 6)*, **2010**; pp 1-337.
- Wayland, B. B.; Mehne, L. F.; Swartz, J., Mono- and biscarbonyl complexes of iron(II) tetraphenylporphyrin. *J. Am. Chem. Soc.* **1978**, *100*, 2379-2383.
- Weaver, L. K., Clinical practice. Carbon monoxide poisoning. *N. Engl. J. Med.* **2009**, *360*, 1217-25.
- Yang, N. J.; Hinner, M. J., Getting Across the Cell Membrane: An Overview for Small Molecules, Peptides, and Proteins. In *Site-Specific Protein Labeling*, **2015**; pp 29-53.
- Ye, B.-H.; Naruta, Y., A novel method for the synthesis of regiospecifically sulfonated porphyrin monomers and dimers. *Tetrahedron* **2003**, *59*, 3593-3601.